THE UNIVERSITY
of EDINBURGH

Impacts of variable renewable generation on thermal power plant operating regimes

Robert Alasdair Wilson Bruce

Doctor of Philosophy

THE UNIVERSITY OF EDINBURGH

2015

To you as a reader.

Lay summary

Large amounts of renewable energy sources, such as wind power, are likely to cause fundamental and structural changes to the operation of future power systems. In the United Kingdom, large amounts of wind generation is expected to be deployed to contribute towards renewable energy and carbon dioxide (CO_2) emission targets. Wind generation has low marginal costs, limited predictability, and typically displaces more expensive thermal power plants, with higher marginal costs, potentially changing flexibility and reserve requirements. New low-carbon power plants, such as CO_2 capture and storage and nuclear, may impact power system flexibility and ramping capabilities. Low-carbon power systems are therefore likely to be required to manage increased levels of variability and uncertainty at operational timescales.

This work uses high-resolution wind data for UK wind sites. The locations of existing and proposed wind farms are used to produce plausible and internally consistent wind deployment scenarios that represent the spatial distribution of future UK wind capacity. Historic electricity demand and wind output data are used to assess both demand and wind variability. An electricity system dispatch model is developed to evaluate how power plants are likely to operate in the future with large proportions of wind power. A number of metrics are then used to assess the operating profiles of thermal power plants. A sensitivity analysis investigates the impacts of part-load efficiency losses, ramp rates, minimum up/down times, and start-up/shut-down costs on power plant operating regimes and flexibility requirements. The interactions between a portfolio of energy storage units and flexible CO_2 capture units are then explored.

This multi-disciplinary research presents a detailed assessment of operational flexibility requirements, highlighting the non-linear impacts of increasing wind capacity. The methodological framework presented here uses onshore and offshore wind data but is expected to provide useful insights for other power systems.

Abstract

The integration of variable renewable energy sources (VRE) is likely to cause fundamental and structural changes to the operation of future power systems. In the United Kingdom (UK), large amounts of price-insensitive and variable-output wind generation is expected to be deployed to contribute towards renewable energy and carbon dioxide (CO_2) emission targets. Wind generation, with near-zero marginal costs, limited predictability, and a limited ability to provide upward dispatch, displaces price-setting thermal power plants, with higher marginal costs, changing flexibility and reserve requirements. New-build, commercial-scale, and low-carbon generation capacity, such as CO_2 capture and storage (CCS) and nuclear, may impact power system flexibility and ramping capabilities. Low-carbon generation portfolios with price-sensitive thermal power plants and energy storage are therefore likely to be required to manage increased levels of variability and uncertainty at operational timescales.

This work builds on a high-resolution wind reanalysis dataset of UK wind sites. The locations of existing and proposed wind farms are used to produce plausible and internally consistent wind deployment scenarios that represent the spatial distribution of future UK wind capacity. Temporally consistent electricity demand data is used to characterise and assess demand-wind variability and net demand ramp events. A unit commitment and economic dispatch (UCED) model is developed to evaluate the likely operating regimes of thermal power plants and CCS-equipped units across a range of future UK wind scenarios. Security constraints for reserve and power plant operating constraints, such as power output limits, ramp rates, minimum up/down times, and start-up times, ensure the operational feasibility of dispatch schedules. The load factors, time spent at different loads, and the ramping and start-up requirements of thermal power plants are assessed. CO_2 duration curves are developed to assess the impacts of increasing wind capacity on the distribution of CO_2 emissions. A sensitivity analysis investigates the impacts of part-load efficiency losses, ramp rates, minimum up/down times, and start-up/shut-down costs on power plant operating regimes and flexibility requirements. The interactions between a portfolio of energy storage units and flexible CO_2 capture units are then explored.

This multi-disciplinary research presents a temporally-explicit and detailed assessment of operational flexibility requirements at full 8760 hour resolution, highlighting the non-linear impacts of increasing wind capacity. The methodological framework presented here uses high spatial- and temporal-resolution wind data but is expected to provide useful insights for other VRE-based power systems to mitigate the implications of inadequate flexibility.

Acknowledgements

This thesis would not have been possible without the help and invaluable support of my supervisors: Dr. Hannah Chalmers, Prof. Gareth P. Harrison and Prof. Jon Gibbins. I also thank my colleagues at the School of Engineering at the University of Edinburgh. In particular, I would like to thank Sam Hawkins who provided the wind speed reanalysis dataset and Edward Barbour for his help and advice on energy storage.

I would like to thank the staff at SSE plc. for making this Ph.D. possible. In particular, I would like to thank both Ricky Chaggar and Jeremy Carey for their supervision. I would also like to thank Sorcha Schnittger, the CCPilot100+ plant team, Alan McFadden and the Energy Portfolio Management team for their help during my internships at SSE plc.

I would like to thank the UKCCSRC for funding my International Exchange to the UK-China (Guangdong) CCUS Centre in Guangzhou, China. I would also like to thank Dr. Jia Li, Dr. Xi Liang and colleagues at the UK-China (Guangdong) CCUS Centre and the Guangdong Electric Design Institute for their guidance and hospitality.

Financial support for this research was provided by the Energy Technology Partnership in Scotland and SSE plc.

Declaration

I declare that this thesis was composed by myself, that the work contained is my own except where explicitly stated otherwise in the text, and that this work has not been submitted for any other degree or professional qualification except as specified.

Robert Alasdair Wilson Bruce

Contents

List of figures

List of tables

List of publications

The work described in this thesis has been reported in the following publications:

1. A. R. W. Bruce, G. P. Harrison, J. Gibbins, and H. Chalmers, "Operational flexibility of future generation portfolios using high spatial- and temporal-resolution wind data," *IEEE Transactions on Sustainable Energy*, 2015. DOI: 10.1109/TSTE.2015.2497704

2. A. R. W. Bruce, G. P. Harrison, J. Gibbins, and H. Chalmers, "Assessing operating regimes of CCS power plants in high wind and energy storage scenarios," *Energy Procedia*, vol. 63, pp. 7529-7540, Elsevier, 2014. DOI: 10.1016/j.egypro.2014.11.789

3. A. R. W. Bruce, G. P. Harrison, J. Gibbins, and H. Chalmers, "Impacts of wind and energy storage on future thermal power plant operating regimes," In *EI Energy Systems Conference 2014*, London, UK.

4. A. R. W. Bruce, G. P. Harrison, J. Gibbins, and H. Chalmers, "Reviewing case study examples of energy storage capabilities to uncover practical outcomes in terms of ease and efficiency," In *3rd Annual Power Plant Flexibility and Optimization Conference 2013*, Amsterdam, Netherlands.

Nomenclature

ACS	Average cold spell
ACSWP	Average cold spell winter peak
AGR	Advanced gas-cooled reactor
ASC	Advanced supercritical
BM	Balancing mechanism
BWR	Boiling water reactor
BSC	Balancing and settlement code
CC	Capacity credit
CCGT	Combined cycle gas turbine
CCR	CO_2 capture ready
CCS	CO_2 capture and storage
CF	Capacity factor
CfD	Contracts for difference
CO_2	Carbon dioxide
COPT	Capacity outage probability table
CPF	Carbon price floor
DECC	Department of Energy and Climate Change
DP	Dynamic programming
ELCC	Effective load carrying capability
EFC	Effective firm capacity
EOP	Electricity output penalty
EPR	European pressurised reactor
EPS	Emissions performance standard
EMR	Electricity market reform
EU	European Union
EEU	Expected energy unserved
FIT	Feed-in tariff
FOR	Forced outage rate
FPN	Final physical notification
GB	Great Britain
GHG	Greenhouse gas
GT	Gas turbine
GW	Giga-watt
GWh	Giga-watt hour

IEA	International Energy Agency
IEAGHG	International Energy Agency greenhouse gas
IGCC	Integrated gasification combined cycle
kW	Kilo-watt
kWh	Kilo-watt hour
LCOE	Levelised cost of electricity
LOEE	Loss of energy expectation
LOLD	Loss of load duration
LOLE	Loss of load expectation
LOLF	Loss of load frequency
LOLP	Loss of load probability
LP	Linear programming
MEA	Monoethanolamine
MIP	Mixed-integer programming
MILP	Mixed-integer linear programming
MPa	Mega Pascals
MW	Mega-watt
MWh	Mega-watt hour
NO_X	Nitrous oxides
NPV	Net present value
OCGT	Open cycle gas turbine
OFGEM	Office for gas and electricity markets
O&M	Operating and maintenance
Pa	Pascals
PCC	Post-combustion capture
PV	Photo voltaic
PWR	Pressurised water reactor
R&D	Research and development
RO	Renewable obligation
ROC	Renewable obligation certificate
SBP	System buy price
SCUC	Security constrained unit commitment
SSP	System sell price
SO_2	Sulphur dioxide
SO	System operator
SRMC	Short-run marginal cost
UC	Unit commitment
UK	United Kingdom
US	United States

USA	United States of America
USC	Ultra supercritical
USC-PC	Ultra supercritical pulverised coal
VOLL	Value of lost load
VRE	Variable renewable energy sources
WACC	Weighted average cost of capital

Chapter 1

Introduction

1.1 Background

Global surface temperatures since 1850 have increased due to anthropogenic climate change and the increase in atmospheric carbon dioxide (CO_2) [Solomon *et al.*, 2007]. The utilisation of fossil fuels in the electricity sector has contributed to the release of CO_2 and other greenhouse gases (GHGs). This has caused many policy makers and energy stakeholders to implement CO_2 reduction policies. For example, in 2007 the European Union (EU) implemented a binding target to source 20% of the EU's total energy consumption from renewables by 2020 and reduce EU GHG emissions by 20% from 1990 levels [EU, 2009; DECC, 2013a]. The prevailing view is that the electricity sector may have to decarbonise significantly more than 20% in order to electrify other sectors of the economy, such as heat and transport.

The three main proposed low-carbon electricity generation technologies are renewables, fossil fueled power plants equipped with CO_2 capture and storage (CCS), and nuclear. These generation technologies will have to interact together to generate a reliable source of power to meet a varying demand profile. However, these generation technologies are intrinsically different. For example, variable renewable energy sources (VRE), such as wind and photovoltaics (PV), are typically characterised by near-zero variable operating costs, locational dependency, limited predictability, and a limited ability to provide upward dispatch [Perez-Arriaga and Batlle, 2012].

Onshore and offshore wind power is likely to provide the dominant share of renewable generation in the United Kingdom (UK) in the short- to medium-term [DECC, 2013a]. Whilst solar generation is diurnal, peaking during the day when electricity demand is relatively high, wind generation is far more variable and uncertain. The large-scale deployment of wind generation capacity will displace thermal power plants with higher variable operating costs, fundamentally changing the structure of traditional centralised power systems. This will impact the economics and operating characteristics of thermal power plants which provide the bulk of power system flexibility by ramping to meet net demand variations. Energy storage, interconnectors, and demand-side management can also be utilised to provide operational flexibility.

Thermal power plants to be built in the near future are likely to be operational in 2050 and

onwards. It is therefore important that in the next infrastructure investment cycle thermal power plants are designed and operated to meet future flexibility requirements. This requires first understanding the potential variability and uncertainty from a geographically diverse portfolio of onshore and offshore wind.

It is also likely that a significant amount of fossil fueled power plants will have to be either installed with CCS when it is commissioned or retrofitted with post-combustion capture at a later stage [DECC, 2013a]. In addition, CCS-equipped power plants may also need to be sufficiently flexible to manage the increased variability and uncertainty from wind power. However, the potential operating regimes and flexibility of CCS-equipped power plants are relatively unknown. The impacts of variable renewable generation, in particular onshore and offshore wind, on thermal power plant operating regimes are therefore an important consideration in future power systems.

It is also important to understand how changes in thermal power plant technical characteristics, such as ramp rates or part-load losses, effect the power system. This is also likely to lead to new thermal power plant operating regimes and start-up/shut-down requirements, as thermal units adjust to meet net demand variations. The concept of 'flexibility' does not include temporal irreversibilities such as start-up and shut-downs which can significantly impact short-term dispatch decisions.

1.2 Research questions and scope

Increased volumes of onshore and offshore wind generation are likely to increase the variability and uncertainty in net demand, increasing the need for conventional power plants and CCS-equipped power plants to provide operational flexibility and reserve services. In addition, wind output varies significantly between years and so understanding the impacts of inter-annual variations in wind output is important for power plant operating regimes and long-term system planning.

This thesis focuses on characterising and developing methods to assess the impacts of increased wind generation on power system costs and CO_2 emissions, as well as investigating generation flexibility. In particular, this thesis aims to improve the understanding of thermal power plant operating regimes and operational flexibility in power systems with large proportions of wind, energy storage and CCS-equipped power plants.

A unit commitment and economic dispatch (UCED) model is developed to assess the operating regimes of thermal power plants, CCS-equipped power plants and energy storage units to meet variations in wind output and demand. This is done by performing simulations of power system operation over multiple years to evaluate the impacts of varying demand and wind profiles on power plant operation. Ensuring sufficient reserve and flexibility requirements with

large proportions of onshore and offshore wind requires modelling the temporal variations in wind output over operational time-scales. This is done by utilising a high-resolution wind resource dataset which is employed in this thesis to produce credible estimates of wind power production. Time-series of wind power outputs are then used to understand the likely changes to the operating regimes of power plant with and without CO_2 capture and storage.

In this context, the main research objectives are:

- determine more realistic wind generation outputs for a portfolio of onshore and offshore wind farms in GB;
- identify the potential variability and uncertainty of the future GB wind portfolio as a prerequisite for understanding power system flexibility;
- assess the impacts of increasing wind capacity on system costs and CO_2 emissions;
- assess the impacts of inter-annual wind output and demand variations on system costs and CO_2 emissions;
- assess the marginal impacts of increasing wind generation capacity on CO_2 emissions;
- evaluate the potential operating regimes of thermal power plants in portfolios with large amounts of wind;
- quantify the ramping and start-up requirements for thermal power plants with increasing amounts of wind capacity;
- evaluate power system flexibility and identify the key flexibility parameters and characteristics of future thermal power plants with CCS;
- evaluate the impacts of adjusting thermal power plant ramp rates, minimum up/down times, start-up and shut-down costs, and part-load losses on system costs and CO_2 emissions;
- examine the impacts of flexible CO_2 capture and storage on system costs and power system operation; and
- assess the optimal charge/discharge strategies for a portfolio of energy storage units.

1.3 Original contribution

This multi-disciplinary work draws on perspectives from a range of fields including energy systems, electrical and mechanical engineering and economics. Although this focused assessment uses GB as a case study, the methodologies presented in this work could be applied to other power systems and technologies.

A useful contribution to the energy systems literature is Bruce *et al.* [2014], which presented an assessment of power plant operating regimes with CCS using high-resolution wind data. This thesis extends the analysis and methodology presented in this paper by further developing the underpinning UCED model and considers a broader range of input data and case studies. The following results can be considered an original contribution to knowledge:

- the development of wind portfolios for GB of increasing wind capacities that reflect the evolving spatial distribution of onshore and offshore wind turbines into the future;
- the assessment of wind and net demand variability at hourly, daily, seasonal and annual time-scales to understand the potential future generation flexibility requirements of the power system;
- the development of a unit commitment and economic dispatch (UCED) model with flexible CO_2 capture power plants and energy storage units to study thermal power plant operating regimes with large proportions of wind;
- CO_2 emissions analysis of an assumed thermal generation portfolio and the development of CO_2 emission duration curves to evaluate the impacts of increasing amounts of wind capacity on the distribution of CO_2 emissions;
- the assessment of the marginal impacts of wind and demand on CO_2 emissions with increasing wind capacity; and
- the evaluation of future CCS operating patterns and the potential variations in flow rates of captured CO_2.

1.4 Thesis overview

This thesis is composed of seven chapters whose contents are summarised below.

Chapter 2 provides a background of the existing electricity system in GB and gives an overview of the recent electricity market reform. A number of impacts of renewables on power system operation are presented. The challenges of power system modelling and the sources of flexibility in power systems is discussed. The flexibility characteristics of thermal power plants and energy storage units to balance large amounts of wind power is then discussed. The potential flexibility of CCS-equipped thermal power plants is then introduced. The reserve and response requirements of wind-based power systems is outlined and the method to simulate wind forecast errors is given. A literature review of recent power system integration studies and a comprehensive review of unit commitment models for future power systems is then presented.

Chapter 3 then gives a detailed overview of the wind resource in GB and the advanced wind speed reanalysis dataset employed in this work. The engineering fundamentals of modern wind turbines is then presented and the methodological process to transform wind speeds into wind power outputs using aggregate power curves is detailed. This is supported by a comprehensive validation of the simulated wind power outputs using a number of publicly available data sources.

Chapter 4 then outlines the process of characterising and developing future GB wind scenarios. These realistic and plausible wind capacity scenarios are developed at existing and future

GB wind sites and then analysed in terms of capacity factors and variability. A sensitivity analysis is performed on the technical availability of the assumed onshore and offshore wind fleets. A temporal analysis of net demand variability is then performed using weather-corrected electricity demand and wind output data to understand the variability challenge.

Chapter 5 provides a detailed description of the unit commitment and economic dispatch (UCED) model with flexible CO_2 capture power plants and energy storage. Security constraints for reserve requirements and the technical operating parameters of thermal power plants (ramp up/down rates, minimum up/down times, power output limits, start-up times etc.) are described. A test system is then introduced to demonstrate the ability of the UCED model to dispatch thermal power plants and CCS-equipped units to meet demand and provide reserve requirements.

Chapter 6 introduces a base case generation portfolio of thermal power plants that is used to investigate the operating regimes of thermal units with increasing wind capacity. The non-linear impacts of increasing wind capacity and inter-annual variations in wind output and demand are highlighted in terms of system costs and CO_2 emissions. The marginal impacts of demand and wind output on CO_2 emissions is then investigated. The impacts on power plant load factors, time spent at different loads, and start-up and ramping requirements are evaluated across a range of wind capacity scenarios. Power plant operating characteristics such as part-load efficiency losses, ramp rates, minimum up/down times, and start-up/shut-down costs are adjusted to understand and quantify the impacts on system costs and flexibility. The interactions between energy storage and flexible CO_2 capture power plants is then explored. Finally, the impacts of CO_2 capture plant bypass on system costs are assessed.

Chapter 7 discusses the results and conclusions and suggests improvements for future work.

The thesis also contains several appendices with additional data sources and results.

Appendix A contains a complete list of the onshore and offshore wind sites available in the wind reanalysis dataset.

Appendix B shows the temporal distributions of capacity factors for the onshore and offshore wind portfolios for the years 2000 and 2010.

Appendix C provides additional input data and technical information for the IEEE RTS-96 test system used in Chapter 5.

Appendix D provides additional input data and technical information for the generation portfolio used in Chapter 6.

Chapter 2

Future power systems

2.1 Introduction

In order to understand the operating regimes of thermal power plants in future power systems, it is first essential to understand the structure of existing and future power systems. This chapter introduces and outlines the fundamental engineering principles of modern electricity systems and the potential impacts of weather-variable renewables. Then, power generation technologies such as thermal power plants with and without CO_2 capture and storage (CCS) and other sources of power system flexibility are briefly discussed. An overview of the increase reserve and response requirements to accommodate increasing wind generation is then presented. A literature review of recent renewable integration studies and modelling techniques is then given before a discussion of the proposed work.

The aim of this chapter is therefore to:

- outline existing and power system structures and basic operating principles;
- introduce power system flexibility and the various sources of flexibility;
- discuss the short-term optimisation problem and outline methods of quantifying flexibility in VRE-based power systems;
- outline the response, reserve and inertia requirements of power systems;
- provide an up-to-date literature review and discuss various types of power system models and their applications; and
- introduce the unit commitment (UC) problem.

2.2 Power systems

2.2.1 Introduction

Great Britain (GB) has a liberalised electricity market involving suppliers and generators. In GB, the transmission system is operated by National Grid Electricity Transmission (NGET). The electricity and gas markets in GB are regulated by the Gas and Electricity Markets Authority which operates through the Office of Gas and Electricity Markets (Ofgem). The GB

market operates under the British Electricity Transmission Trading Arrangements (BETTA) which came into effect in 2005. A detailed overview of the market structure and arrangements under BETTA can be found in National Grid [2011b].

Suppliers purchase electricity in the wholesale market and then sell it to consumers. These suppliers of electricity operate in a competitive market where consumers are able to choose electricity suppliers to provide them with electricity. Bilateral contracts are traded between suppliers, generators, traders and consumers in half-hourly blocks up to 1 hour before real-time (gate closure) [National Grid, 2011b]. Market players have the option to participate in the forwards/futures contract market and short-term bilateral market. At gate closure all market participants must provide contract volumes and Final Physical Notifications (FPNs) to National Grid the system operator (SO).

The forwards/futures contract markets operates typically from 24 hours to several years ahead of real-time [National Grid, 2011b]. Generators and suppliers can enter contracts to deliver or take at an agreed price in the future. These agreed contract prices are not disclosed to the public.

Power exchanges are used typically 24 hours ahead of real-time to adjust contract positions. Energy companies will use power exchanges to balance their contractual electricity traded positions for their generation portfolios. A time-weighted average price for each half-hourly trading block is typically published by power exchanges (for example APX Power UK [APX, 2015]).

The Balancing Mechanism (BM) is then used to balance both demand and supply at half-hourly time periods. The Balancing and Settlement Code (BSC) is administered by Elexon [2001], and operates through a system of bids and offers. The SO accepts bid/offer submissions in order to balance the system close to real-time. BM generator units make offers to increase generation or reduce demand. BM units also make bids to reduce generation or increase demand. The National Grid as the SO acts as the sole counter party.

Any imbalances between market participants contractual electricity traded positions (at gate closure) and the physical power flow is then determined. The System Sell Price (SSP) is paid *to* BSC trading parties who had a net surplus and the System Buy Price (SBP) is paid *by* BSC trading parties who had a net deficit of energy. The SSP and SBP is calculated by the SO for each trading block and is reported in Elexon [2015].

The National Grid as the SO has been appointed as the delivery body for the Electricity Market Reform (EMR) [National Grid, 2014a], which is discussed in more detail in the next section.

2.2.2 Impact of renewables

There is a consensus in th United Kingdom (UK) and European Union (EU) that increasing proportions of renewables are needed to help mitigate the impacts of climate-change and achieve decarbonisation of the energy sectors. The proportion of electricity demand met through variable-output renewable energy sources (VRE) such as wind and solar photovoltaics (PV) are expected to increase in the UK [DECC, 2013a] and in Europe [EC, 2009]. VRE generation technologies are characterised by very low short-run marginal costs (SRMC)[1]. VRE generation fluctuates according to the availability of the renewable resource and displaces conventional thermal power plants with higher short-run marginal costs [IEA, 2011]. The integration of large proportions of VRE is therefore likely to cause fundamental and structural changes to power systems and thermal power plant operating regimes.

Net demand

The demand for electricity D_t less any wind generation W_t gives the net demand at time t:

$$D_t^{\text{net}} = D_t - W_t \tag{2.1}$$

Figure 2.1 shows a typical demand profile and net demand D_t^{net} for one week in winter. There are several consecutive days of high demand followed by a typically weekend demand profile. With 30 GW of wind capacity, the demand to be met by non-wind capacity (net demand) falls significantly. There is also a large increase in wind generation that coincides with low demand over the weekend. This causes net demand to fall to very low levels. This is likely to push down market prices to very low levels and cause many thermal plants that are not providing ancillary services to shut-down [Poyry, 2009].

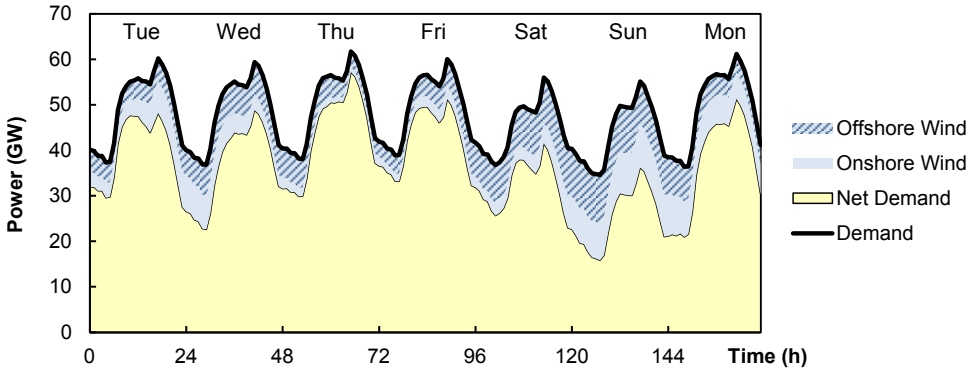

Figure 2.1: Time-series of demand, wind, and net demand for a typical week in winter.

Net demand is also more likely to be much more volatile than the existing demand profile, with

1. The short-run marginal cost (SRMC) is the change in short-run total cost for an extremely small change in output.

extreme wind periods causing large power swings. The ramping requirements of the thermal generation portfolio are therefore also likely to increase, putting strain on older and less flexible generation assets [IEA, 2011].

Short-run marginal costs

Power plants in a generation portfolio form a supply curve and are traditionally dispatched in ascending order of price which reflects the SRMC, see Figure 2.2. The supply curve is also referred to as the merit-order which ranges from the least expensive plant to the most expensive. A range of power generation technologies make up the supply curve including nuclear, coal, combined cycle gas turbine (CCGT), and open cycle gas turbine (OCGT). The demand curve is relatively steep which represents the relative price inelasticity of demand [Poyry, 2010]. That is, a large change in price will have little impact of demand. However, small changes in supply can have very large changes in price. VRE, which typically have near-zero SRMC, can be treated as a negative demand and so shifts the supply curve to the left. Therefore, when net demand (demand net VRE) falls or VRE increases, a new price is determined by market dynamics which is typically lower than the original price [Poyry, 2010]. This is referred to as the merit-order effect. Figure 2.3 shows the impact of energy storage on net demand and SRMC.

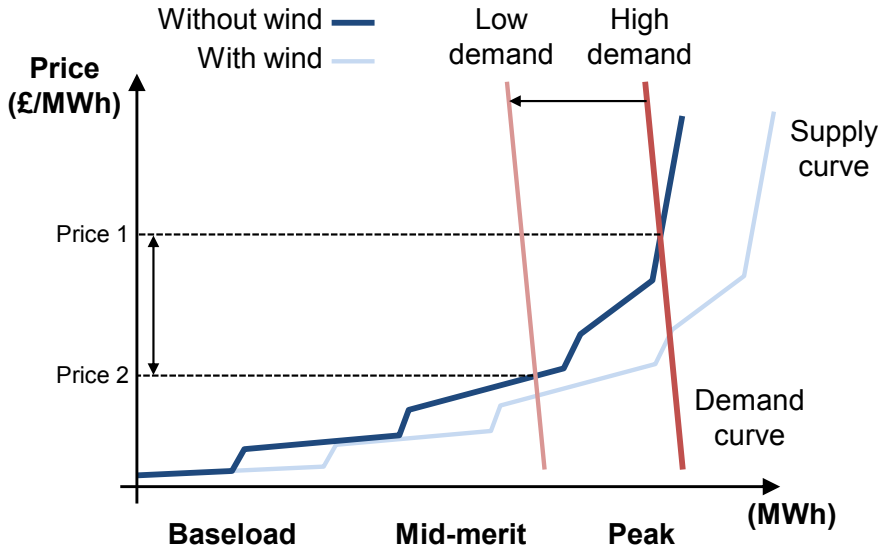

Figure 2.2: The effect of wind on net demand and short-run marginal costs.

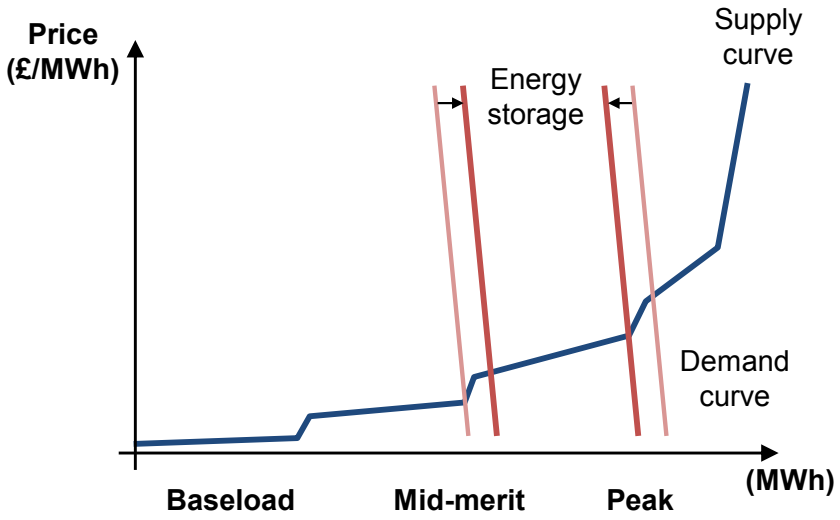

Figure 2.3: The effect of energy storage on net demand and short-run marginal costs.

Demand duration curves

Typical duration curves for demand and demand net wind are shown in Figure 2.4. Long-term demand is most commonly illustrated using a demand duration curve. It describes the demand profile over time sorted in order of decreasing demand. Demand durations curves in GB in recent times are characterised by a sharp peak and then a fairly smooth mid-section. The area under the demand duration curve gives the total energy requirement. With large amounts of wind, the duration curve changes significantly. Firstly, the area under the curve reduces as the demand for non-wind generation falls. Peak demand tends to change very little as it is not always certain that it will be windy during peak demand periods. The tail of the duration curve also becomes more pronounced (on the left), implying that the utilisation of peaking plant reduces. With large amounts of wind it is also likely that there may be periods where wind power output exceeds demand. This can lead to negative demand net periods where wind curtailment is very likely. Using power-to-gas to convert surplus electricity into hydrogen is one possible way to increase the flexibility of the power system but also utilise and absorb surplus wind [Qadrdan *et al.*, 2015].

Traditionally, the least flexible power plants had the lowest SRMC and highest capital costs (for example nuclear and coal) and the most flexible power plant had the highest SRMC and lowest capital costs (for example OCGT). This meant that power plants were dispatched in order of short-run marginal costs but also (roughly) in terms of flexibility. During periods of high demand the most flexible generating units with the lowest short-run costs could afford to come online for short periods of time. Baseload power plants (nuclear and coal) had higher loads factors which correlated with lower short-run marginal costs. Generation technology screening curves are a simplistic way of demonstrating this, see Figure 2.4. Screening curves

are commonly used to construct an optimal generation portfolio based on fixed costs C^{fixed} that include for both investment and fixed operational costs, variable costs C^{var}, and load factors. These costs measure the long-term average cost of capacity (£/MWh) and so are not suitable for short-term applications.

The impact of wind generation on prices is demonstrated in Figure 2.4. Here, wind generation displaces traditional peaking plant and mid-merit plant, reducing the marginal price of generation. The distribution of prices will change with large amounts of wind generation. Price duration curves can be constructed to analyse the potential volatility of prices as in Poyry [2009].

CO_2 duration curves

It is possible to create CO_2 duration curves by estimating the total CO_2 emissions produced by the generation portfolio for each time period and then sorting them in order of decreasing CO_2 emissions, see Figure 2.5. The aim of decarbonisation policies is therefore to minimise the area under the curve at least-cost while maintaining a reasonable level of system reliability. It is possible to visualise the impact of increasing low-carbon generation, such as wind or CCS, or more efficient power plants on the shape of the CO_2 duration curve. CO_2 durations curves are likely to have longer tails than demand duration curves since peak demand periods typically require large amount of CO_2 intensive plant, such as OCGT, to come online for a small number of hours, significantly increasing the CO_2 emissions. It would also be possible to have periods where the CO_2 duration curve is negative, for example, in a scenario with large amounts of sustainable bio-energy with CCS and other renewables.

2.2.3 Renewable energy policy

Green and Yatchew [2012] outline a number of support policies for renewables. Regulatory policies include including Feed-in tariffs (FiT), renewable portfolio standards, and tradable green certificates. These require electricity consumers to pay for renewable generation. Fiscal incentives can also be provided in the form of subsidies and/or tax reductions for renewables. Finally, public financing in the form of public investments or loans is possible as a support mechanism for renewable generation. In short, there are several possible support schemes and instruments for renewables with varying degrees of effectiveness. The proposed market framework for GB to incentivise decarbonisation in the electricity sector is now be introduced.

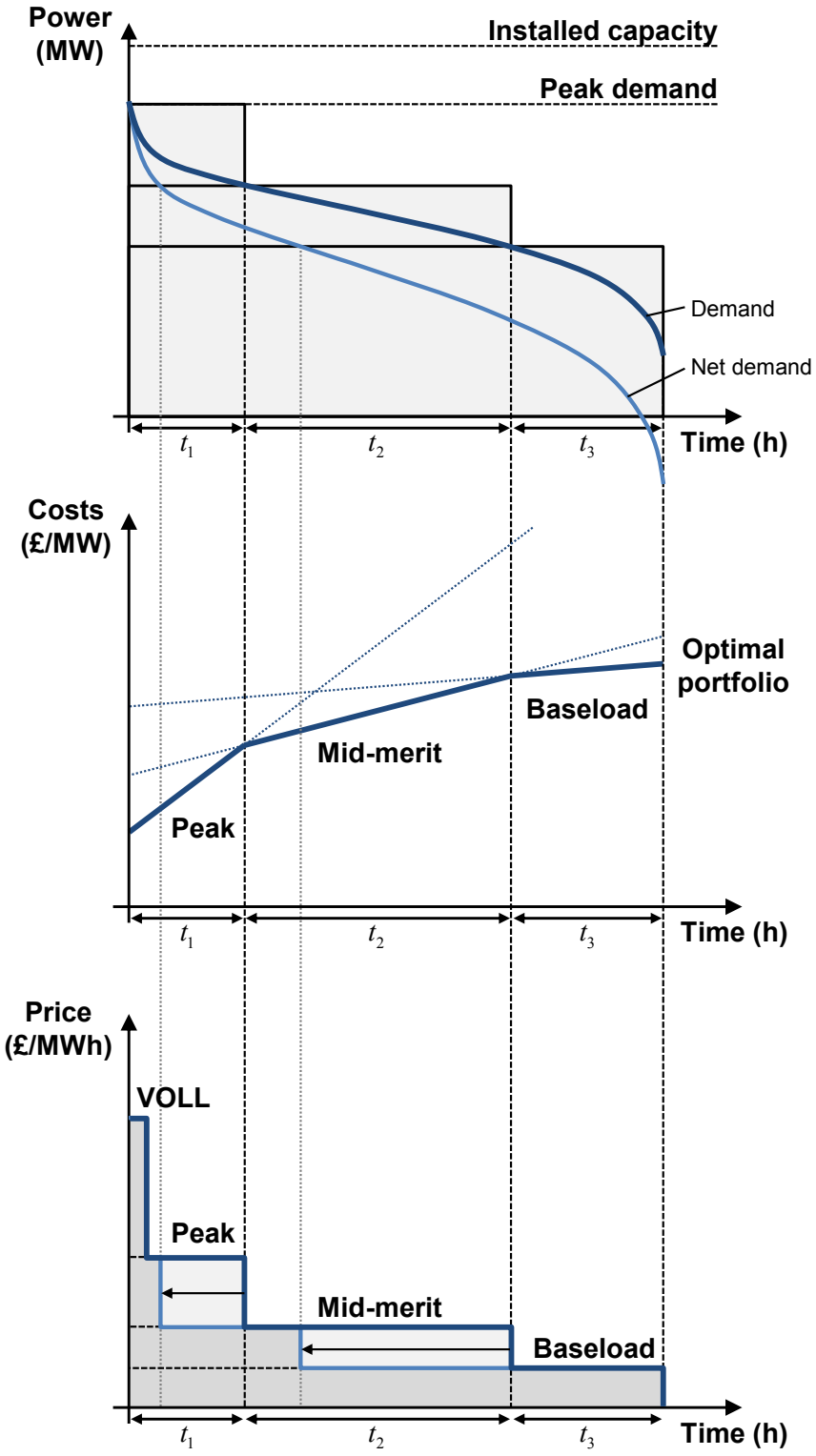

Figure 2.4: (top) The duration curves for demand and net demand, (middle) screening curves, and (bottom) short-run marginal cost curves for illustrative peaking, mid-merit and baseload power plant technologies.

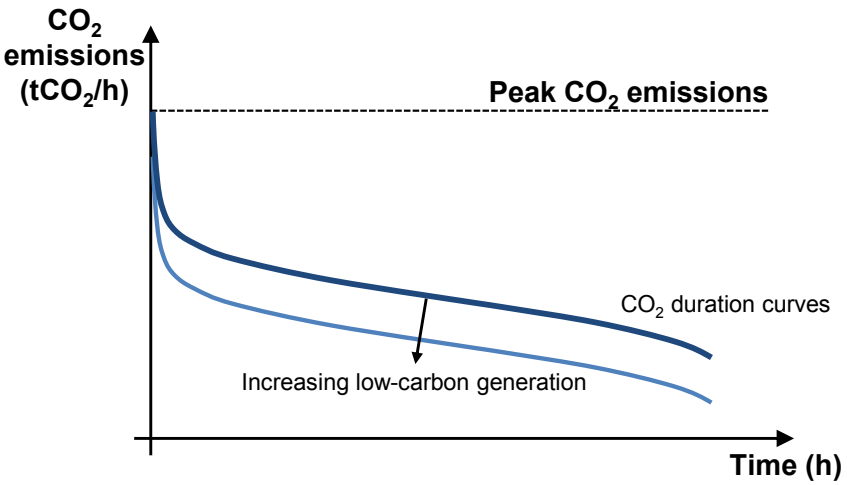

Figure 2.5: CO_2 duration curves.

Electricity Market Reform (EMR)

Electricity Market Reform (EMR) has been designed to incentivise investment in secure, low-carbon electricity, improve security-of-supply, and improve affordability for consumers. EMR introduces two new mechanisms to provide investment incentives: Contracts for Difference (CfD) and a Capacity Market [Energy Act, 2013]. A Carbon Price Floor (CPF) has been introduced and an Emissions Performance Standard (EPS), limits emissions of new generation capacity to 450 gCO_2/kWh [National Grid, 2014a]. The EPS is a requirement that effectively ensures no new coal-fired power stations are deployed without CCS.

CfDs are designed to support new investment in low-carbon generation technologies, such as renewables, nuclear, and CCS, and should provide greater and more cost-effective price stabilisation for new generation capacity. CfDs reduce exposure to the more volatile wholesale electricity prices by providing a variable top-up to meet a pre-arranged strike price. When wholesale electricity prices exceed the strike price generators are required to pay back the difference.

Green and Staffell [2013] assess the impact of proposed CfD contracts for new nuclear power plants across a range of different scenarios to understand what the market might deliver. A number of different weighted average cost of capital (WACC) values for new nuclear power plants are considered to represent different levels of government support. Investment in new nuclear capacity occurs with a lower WACC and lower wholesale electricity prices are reported. CfDs are therefore seen as the most effective policy to stimulate early investment in new nuclear capacity in GB [Green and Staffell, 2013].

A capacity market provides a regular payment to capacity (both demand- and supply-side), that are available during periods of peak demand. Electricity Capacity Regulations [2014] outlines legislation for the reliability standard to be used in the capacity market. The Department of

Energy and Climate Change (DECC) provide further details about the EMR delivery plan and renewables roadmap in DECC [2013c] and DECC [2013a].

2.2.4 Operating regimes

Power plants can be categorised by their operating regime into baseload, mid-merit and peaking plant. Mid-merit power plants will typically two-shift by either part-loading overnight or by shutting down. It is the short-run marginal costs of different power generation technologies that typically determine the operating regime.

Coal power plants in GB built from 1960 to 1980 were designed to provide power at full load and operate for 24 hours a day for most of the year [Parsons Brinkerhoff, 2014]. Recently however, during times where the price of coal is significantly higher than the price of natural gas, coal power plants two-shift by either shutting down or part loading overnight. The ability to cycle on and off and operate at a reduced power output (below 50%) may, however, require a number of modifications to adapt the power plant.

Maintenance is required to reduce the number and magnitude of cycling-related outages. Plant operators attempt to optimise the balance between the lost revenue associated with forced outages and the additional capital required to minimise forced outage rates.

2.2.5 Levelised cost of electricity generation

One simple way to compare the costs of generation for different technologies is to estimate the levelised cost of electricity (LCOE)[2]. The levelised costs for a particular generation technology represent the ratio of the total costs (both capital costs and operating costs over the plant lifetime) by the total amount of expected electricity generation [DECC, 2013d]. These values are discounted and presented in terms of their net present value (NPV). The LCOE only relates to the costs accruing to the owner and not the costs of system balancing etc. The costs and load factors of the generation assets are usually assumed to be constant over the plant lifetime.

DECC and Parsons Brinkerhoff have worked together to produce a Levelised Electricity Cost Model which details the LCOE of different non-renewable [Parsons Brinkerhoff, 2013a] and renewable [Parsons Brinkerhoff, 2013b] generation technologies. The most recent update by DECC [2013d] includes both renewable and non-renewable technologies. These recent studies provide cost estimates for relevant generation technologies in GB and also for some less mature technologies such as CCS.

---

2. The levelised cost of electricity generation is the discounted lifetime cost of ownership and use of a generation asset, converted into an equivalent unit of cost of generation in £/MWh [DECC, 2013d].

2.2.6 Risk metrics

There are a number of risk metrics that help inform security-of-supply calculations. This section will introduce some of the main risk metrics that are relevant for power system studies.

Loss of Load Probability (LOLP)

The Loss of Load Probability (LOLP) in time period t is the probability that the available generation capacity C_t^{A} will not be able to meet system demand D_t:

$$LOLP_t = p(C_t^{\mathrm{A}} < D_t) \cdot p(C_t^{\mathrm{A}} = C_t^{\mathrm{R}}) \tag{2.2}$$

where C_t^{R} is the remaining generation capacity at time t. Loss of load occurs when system demand exceeds the available generation capacity. Reliability criteria are used in generation capacity planning assessments. The LOLP of a system is used to characterise the generation adequacy and the ability to meet peak demand.

Loss of Load Expectation (LOLE)

The Loss of Load Expectation (LOLE) at time period t is the expected number of time periods over a given time horizon T that the available generation capacity will not meet system demand. The LOLE is usually expressed in hours per year.

$$LOLE_t = \sum_{t=1}^{T} LOLP_t \tag{2.3}$$

The LOLE forms the basis of reliability standards in most power systems. For example, the UK sets a reliability standard using an LOLE of 3 hours per year [Electricity Capacity Regulations, 2014]. The LOLE risk metric is commonly used in most generation reliability assessments. The LOLE and LOLP, however, are not able to indicate the frequency of duration of possible loss of load events or the severity of the shortfall.

Loss of Energy Expectation (LOEE)

The Loss of Energy Expectation (LOEE) is the number of MWh per year that are not supplied. Other equivalent metrics are the Expected Energy Unserved (EEU). These metrics however are not commonly used in power system reliability studies.

Loss of Wind Estimation (LOWE)

Ma [2012] developed an index to calculate the probability of wind curtailment over the period of a year. The Loss of Wind Estimation (LOWE) is an offline index that represents the estimated probability that wind is curtailed as a result of insufficient upwards/downwards ramping capability and periods where net demand is below the minimum load level of the system.

Additional metrics

Other metrics that will not be defined here are the Loss of Load Frequency (LOLF) and the Loss of Load Duration (LOLD) which are useful for understanding the frequency and duration of loss of load events.

2.3 Power system flexibility

2.3.1 Introduction

Power systems with large proportions of VRE, in particular wind, will have to manage additional variability and uncertainty over all operational timescales. It is therefore likely that in wind-based power systems with too much wind, additional operational reserve and flexibility services will be required to manage the short-term balancing challenge. These changes will have significant impacts to the operating regimes of thermal power plants, which currently contribute the most towards power system flexibility.

The term flexibility, however, is not well defined in the literature. In this work, it is assumed that flexibility is used in the context of the technical abilities and constraints of either individual units or the overall power system. The term flexibility is therefore defined as the technical ability of an individual unit or the power system to manage variability and uncertainty in generation and demand at reasonable cost. Generation flexibility refers to the flexibility provided by generation assets so either the flexibility of individual generating units or the generation portfolio. Power system flexibility, on the other hand, is used more broadly to refer to the overall flexibility of the power system, which may include demand-side management and interconnectors. NERC [2010] and IEA [2011] provide a very detailed review of power system flexibility.

Sources of flexibility

Operational flexibility is very valuable to power system operators, but is not very valuable for suppliers. It is therefore important to distinguish between the different sources of flexibility. The main sources of operational flexibility in power systems are:

- thermal units;
- energy storage;
- wind curtailment;
- interconnectors; and
- demand-side management.

Increasing the flexibility of power systems can be achieved in a number of ways. Firstly by increasing power plant up/down ramp rates and decreasing minimum stable generation limits, start-up/shut-down times and minimum up/down times. Large fluctuations in the level of demand and wind generation may increase the need for improved technical ramping capabilities and lower start-up and shut-down times/costs. Lowering start-up/shut-down costs of thermal power plants decreases the resistance to change states (on/off). Increasing the operational reserve will also allow the power system to meet any unexpected changes in net demand. Operational reserve is composed of both upwards and downwards reserve. The economic impacts, however, of providing increased levels of reserve and flexibility are not fully understood.

Costs of providing flexibility

The costs of flexibility options can be used to construct and map a flexibility supply 'curve' [Nickell, 2008]. The flexibility supply curve includes both demand-side and supply-side flexibility and orders resources in terms of least-cost. When flexibility is required, the least-cost resources are deployed in order by the system operator. In order to construct a representative flexibility supply curve for a given system detailed costs of each flexibility resource are required. In addition, the availability of each flexibility resource also has to be known. For example, flexible demand may not be available at the same time as energy storage or wind curtailment. A map illustrating the flexibility supply characteristics is shown in Figure 2.6.

Improved demand and VRE forecasting may increase power system flexibility by reducing the amount of reserves required to manage variability and uncertainty. A market design that updates VRE forecasts and improved forecasting techniques are relatively inexpensive ways to decrease flexibility costs [IEA, 2011]. Increase trading flexibility will allow market participants to balance variability across markets. Increased access to supply- or demand-side flexibility will decrease the reliance on high marginal cost fast-start or fast-response units. Aggregating VRE and net demand over adjacent markets can reduce net demand variability by spatially diversifying VRE. Increased integration by new transmission capacity can allow markets to reduce balancing costs. Traditional energy storage technologies such as pumped storage are

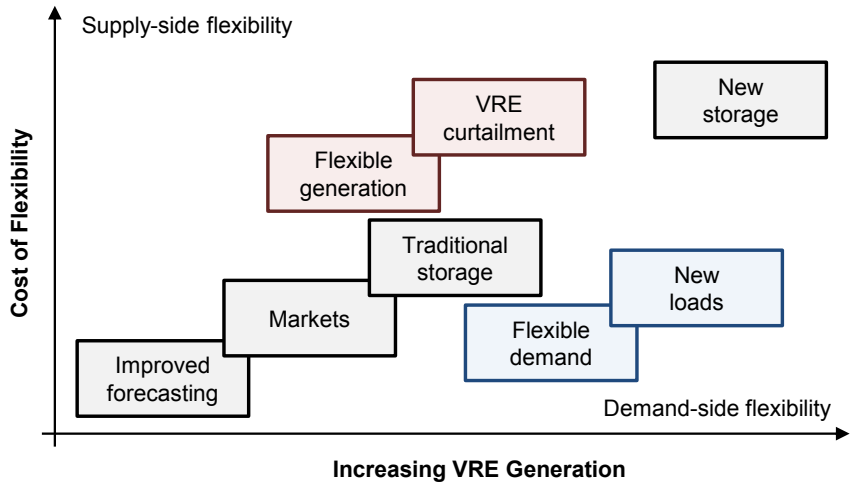

Figure 2.6: Illustrative flexibility supply 'curve'. The positions and costs of flexibility resources are for illustration purposes only. Adapted from [Nickell, 2008].

relatively mature and can be used to manage both demand and generation. Flexible generation includes modifying existing thermal power plants such as CCGTs and OCGTs to be more flexible, but also the addition of new flexible generation resources. VRE curtailment is also one possible way to increase the flexibility of the system by increasing the proportion of conventional generators providing balancing services. Flexible demand includes ways of increasing the proportion of responsive and price-sensitive demand. Curtailing demand for short-periods by time-shifting demand can provide flexibility. New loads could be deployed to accommodate surplus VRE generation. This could include power-to gas-technologies that produce hydrogen through electrolysis and space heating. Additional energy storage capacity could be added to the system using batteries, flywheels, compressed air energy storage (CAES), liquid air energy storage (LAES), and electric vehicles. Further work is needed, however, to accurately define the shape of the flexibility supply curve and the costs of each flexibility resource. In addition, this approach does not consider the availability of each flexibility resource.

Quantifying flexibility

IEA [2011] has developed a Flexibility Assessment (FAST) method to distinguish the sources of power system flexibility to manage and balance VRE. The technical flexibility of each flexibility resource is assessed over different timescales and summed to determine the technical flexible resourse for a given area. This takes into account both the technical and time limitations of each specific flexibility resource. Then the availability of the flexible resource is considered. The flexibility requirement is then estimated to determine the need for flexibility over different timescales. This gives the maximum expected magnitude and rate of change in the variability and uncertainty of demand and VRE fluctuations.

There are a large number of metrics that are used by power system operators to estimate the reliability and efficiency of power systems [Lannoye *et al.*, 2012]. Metrics such as the Loss of Load Probability (LOLP), Loss of Load Expectation (LOLE), and Loss of Energy Expectation (LOEE), are used to assess generation adequacy. However, there are currently only a few recently developed metrics to assess power system flexibility.

Lannoye *et al.* [2012] describe the Insufficient Ramping Resource Expectation (IRRE), which is similar to the LOLE, but estimates the expected number of time periods when a power system cannot meet the predicted/unpredicted net demand changes. The LOLE calculation uses a Capacity Outage Probability Table (COPT) and uses the sizes and forced outage rates of generators to generate a probability distribution of the unavailable capacity. The IRRE uses a distribution of the available flexible upwards and downwards resources for each time horizon. An Available Flexibility Distribution (AFD) is then used to calculated the probability where there will be insufficient resources to meet net demand changes.

Makarov *et al.* [2009]; Ulbig and Andersson [2012, 2014] use a geometric approach to represent flexibility. The flexibility trinity consists of the ramp rate ρ (MW/h), power P (MW), and energy E (MWh), see Figure 2.7. The ramp duration is then $\delta = P/\rho$. Power is generated and exported into the grid when $P > 0$ and power is taken from the grid when $P < 0$. The metric terms ρ, P, and E are very closely linked by integrating/differentiating with respect to time t. These metrics allow the available operational flexibility of a power system to be assessed.

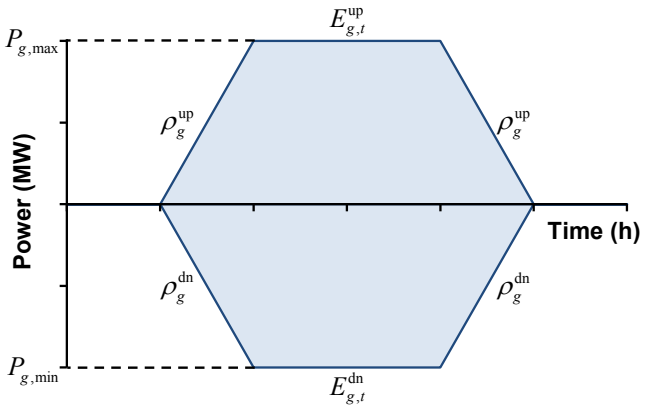

Figure 2.7: Flexibility metrics including the ramp rate ρ, power P, and energy E. Adapted from Ulbig and Andersson [2014].

Ma *et al.* [2011] also describe a flexibility metric to quantify the flexibility of a thermal generator. This flexibility metric is expressed mathematically as:

$$\mathrm{flex}_g = \frac{\frac{1}{2}(P_{g,\max} - P_{g,\min}) + \frac{1}{2}(\rho_g \cdot \Delta t)}{P_{g,\max}} \tag{2.4}$$

where $\frac{1}{2}\rho_g$ represents the average value of both the upwards and downwards ramp rates, ρ^{up}_g and

ρ_g^{dn}, during normal operation. For fast-start plant, it is assumed that $P_{g,\min} = 0$. This flexibility metric therefore allows generators to be characterised in terms of their flexibility within their operating range $P_g^{\max} - P_{g,\min}$.

Ma *et al.* [2011] also define a flexibility metric for the whole electricity system. It is described as the weighted sum of the flexibility indices flex_g. The whole system flexibility index is described as:

$$\text{FLEX}_G = \sum_{g=1}^{G} \left(\frac{P_{g,\max}}{\sum_{g=1}^{G} P_{g,\max}} \cdot \text{flex}_g \right) \tag{2.5}$$

This method allows for a simple calculation of power system flexibility and allows different generation portfolios to be compared. This index can also be extended to include other technologies such as energy storage, interconnection, or demand-side flexibility. However, the flexibility metrics described in Ma *et al.* [2011] are an average of the upwards and downwards ramping capabilities of units. This work extends the flexibility metrics in Ma *et al.* [2011] to include both upwards and downwards flexibility metrics. The new metrics for quantifying the upwards and downwards flexibility of a unit are as follows:

$$\text{flex}_g^{\text{up}} = \frac{\frac{1}{2}(P_{g,\max} - P_{g,\min}) + \frac{1}{2}(\rho_g^{\text{up}} \cdot \Delta t)}{P_{g,\max}} \tag{2.6}$$

$$\text{flex}_g^{\text{dn}} = \frac{\frac{1}{2}(P_{g,\max} - P_{g,\min}) + \frac{1}{2}(\rho_g^{\text{dn}} \cdot \Delta t)}{P_{g,\max}} \tag{2.7}$$

The whole system upwards and downwards flexibility indices are formulated as:

$$\text{FLEX}_G^{\text{up}} = \sum_{g=1}^{G} \left(\frac{P_{g,\max}}{\sum_{g=1}^{G} P_{g,\max}} \cdot \text{flex}_g^{\text{up}} \right) \tag{2.8}$$

$$\text{FLEX}_G^{\text{dn}} = \sum_{g=1}^{G} \left(\frac{P_{g,\max}}{\sum_{g=1}^{G} P_{g,\max}} \cdot \text{flex}_g^{\text{dn}} \right) \tag{2.9}$$

A flexibility envelope is one possible solution that may help facilitate the procurement and provision of flexibility and reserve in future markets [Poyry, 2014]. Nosair and Bouffard [2015] present a dispatch approach based on flexibility envelopes to describe the flexibility potential of individual generation assets. The technical characteristics of flexibility providers can be utilised to produce an envelope of possible delivery options [Poyry, 2014]. This envelope outlines the notice that is required before reserve can be provided, the maximum and minimum ramp rates, and the maximum and minimum delivery periods, see Figure 2.8. This solution may allow system operators to procure reserve and flexibility more cost effectively. A more detailed review of each of the sources of operational flexibility in power systems is now presented.

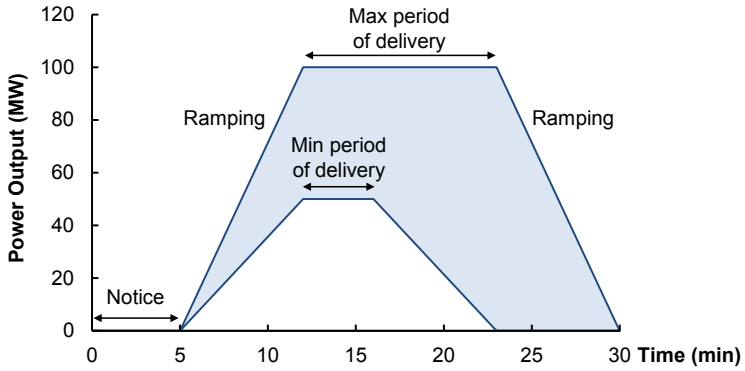

Figure 2.8: Flexibility envelope. Adapted from Poyry [2014].

2.3.2 Thermal power plants

Increased VRE capacity will create new operational flexibility challenges for power systems. Higher penetrations of VRE will increase the frequency of low net demand periods and increase ramping requirements and reserve levels. System operators will have to optimise the technical flexibility of the existing thermal power plant portfolio to meet generation flexibility requirements. Thermal units can provide operational flexibility by ramping up and down to meet net demand variations. Increased cycling capabilities and reduced cycling costs will make it easier for future thermal power plants to adjust output and provide operational flexibility. In traditional power systems, flexibility is typically provided by large-scale part-loaded synchronised thermal units and fast-start units. Thermal power plants also typically provide system inertia, frequency response, and reserve services. The flexible characteristics of thermal units are:

- ramp up/down rates;
- operating range $P_{g,\max} - P_{g,\min}$;
- start-up/shut-down times and costs; and
- minimum up/down times.

These flexibility characteristics will now be described in more detail.

Ramp up/down rates

Peaking plant, such as open cycle gas turbine (OCGT) power plants or fast-start units, are categorised by high ramping capabilities, fast start-up and shut-down times, and high marginal costs, and can respond very quickly to short-term variations in net demand. Mid-merit plants, such as combined cycle gas turbine (CCGT) power plants, can ramp up/down and perform cycling operations, but respond more slowly than peaking power plants [IEA, 2011]. Baseload power plants respond more slowly to net demand variations and are typically designed and/or financed to operate at their maximum power output continuously. Modern nuclear reactors,

however, have been demonstrated to provide significant amounts of operational flexibility and load following [NEA, 2011].

Operating range

The operating range of power plants is the difference between the maximum power output limit $P_{g,\max}$ and the minimum power output limit $P_{g,\min}$[3]. Thermal units may be required, at times, to reduce output to minimum power output limits, operating at reduced efficiency. Power plants must operate at or above their minimum stable generation limits to maintain combustion stability and design constraints. Power plants operators will seek to minimise the time spent at unprofitable loads so it may be more economical to shut-down, rather than spend time at minimum output. However, this may be constrained by a power plants minimum down time.

Minimum up/down times

Once a power plant has shut-down, it typically has to remain idle for a minimum number of hours. This is referred to as the minimum down time. The minimum down time of thermal power plants can be anything from hours to days, due to temperature related technical constraints and economic considerations. A power plant will also have to remain in operation for a minimum number of hours after start-up. This is referred to as the minimum up time. Developing power plants with lower minimum up/down times will allow power plants to change states more quickly and hence improve the operational flexibility.

Start-up times

Power plant operators require notice to start-up a power plant to the point of synchronisation. This is referred to as the notice to deviate from zero. The start-up time is then the time taken to increase load from synchronisation up to full load. A number of actions are required to prepare a power plant (gas or coal) for a start-up. These preparations include: adjusting the boiler drum water level, purging the heat recovery steam generators (HRSG) to remove explosive gases, lighting burners, increasing steam pressure levels, temperature matching, and increasing the turbine frequency to sychronisation [Parsons Brinkerhoff, 2014]. Indicative hot/warm/cold start-up times for various GB power plant technologies are shown in Table 2.1.

The most critical factor that limits the start-up times of power plants is thermal fatigue and temperature ramp rates.

---

3. The minimum power output limit is sometimes referred to as the minimum stable generation limit, which in typical steam units is caused fuel combustion stability and design constraints Wood and Wollenberg [1996].

	Power plant	Notice to deviate from zero (mins)	Synchronisation to full load (mins)
Hot start	Coal	80-90	50-100
	CCGT (existing)	15	40-80
	CCGT (modern)	15	25
	OCGT	2-5	15-30
Warm start	Coal	300	>85
	CCGT (existing)	15	>80
	OCGT	2-5	15-30
Cold start	Coal	360-420	80-250
	CCGT (existing)	15	190-240
	OCGT	2-5	15-30

Table 2.1: Indicative hot/warm/cold start-up times of coal and gas power plants from Parsons Brinkerhoff [2014].

Ambient temperature

The impact of climate change on ambient temperatures and therefore the efficiency of thermal power plants is of particular interest to the UK which relies heavily on the thermal generation technologies. Small changes to ambient air conditions such as temperature and air density can have significant implications on the operation and therefore the efficiency of thermodynamic cycles. In addition, the seasonal impacts of extreme temperature variations on efficiency, cost, and CO_2 emissions of the thermal fleet are not well understood.

Gas turbines are typically designed to operate with a narrow or constant volumetric flow of air. Any change in the ambient air temperature or density entering the compressor will affect the volumetric air flowrate and therefore possibly impact the heat output. In general for a CCGT, an increase in ambient air temperature will typically reduce the power output of the gas turbine. This is because the ambient air temperature compression ratio effects the overall power output and efficiency of the combined cycle [Ibrahim and Rahman, 2012]. The relationship between ambient temperature and overall efficiency should be further investigated and included in future power system models.

2.3.3 OCGT power plants

OCGTs use gas turbines to generate electricity and do not utilise the waste heat. Modern gas turbines use high-pressure air from a compressor which enters a combustion chamber. The high-pressure air mixes with natural gas and is ignited. The hot air then exits the combustion chamber and enters the first stage of the turbine. Inlet temperatures into the turbine are typically around 1400°C [Breeze, 2005].

OCGTs typically have very short start-up times and are able to provide frequency response and black start capability. OCGTs are based on either aeroderivative turbines with fast response times or large frame gas turbines.

2.3.4 CCGT power plants

CCGTs use gas turbines to generate electricity and utilise the waste heat by passing it through heat recovery steam generators (HRSG) to raise additional steam. This creates more steam which is then used to generate additional electricity in a steam turbine. The majority of CCGTs in the GB market were designed and built in the 1990s and 2000s. CCGTs typically have a high efficiency at part-load [IEAGHG, 2012].

There are a number of limiting factors that affect the flexibility of CCGTs. Traditional HRSGs with thick-walled high-pressure drums experience higher thermal stresses and temperature gradients which limit the potential load, start-up, and shut-down gradients [Balling, 2011]. Critical thick-walled components, such as the main steam pipework, the steam turbine, and valves, are limited by the material yield point [Parsons Brinkerhoff, 2014].

However, Benson-type boilers in CCGT power plants do not contain high-pressure steam drums and are therefore not limited by these constraints. Benson-type boilers use evaporator tubes for direct evaporation and therefore significantly reduce the stress induced fatigue in the high-pressure section. Developers are working on reducing the start-up times of thermal power plants to provide additional flexibility. Reducing start-up times of CCGT power plants can be achieved in a number of ways. High capacity de-superheaters can limit the maximum steam temperatures during cold/warm start-ups which minimises the temperature gradients and thermal stresses, and therefore decreasing start-up times [Balling, 2011].

2.3.5 Coal power plants

Coal power plants can be divided into three categories depending on the mode of combustion including pulverised fuel fired plants, fluidised bed plants, and stock fired plants. In pulverised fuel fired boilers, coal and/or biomass is first dryed, then pulverised/milled into a fine powder, and then blown into the combustion chamber. In fluidised bed boilers, coal and/or biomass is crushed and then burnt in a column combustion chamber where is it fluidised/agitated by flowing air. In stock fired boilers, coal is burnt in lumps within the combustion chamber [Zhang, 2013].

The thermodynamic steam cycles of coal power plants can be differentiated into subcritical, supercritical, and ultra-supercritical pulverised coal (USC-PC) power plants. These boiler designs operate at different steam pressures, with the evaporator part of subcritical boilers operating below the critical pressure of water 22.1 MPa abs, 374°C [Ghosh and Prelas, 2009; Zhang, 2013]. In supercritical and ultra-supercritical boilers, water boils and is converted into superheated steam above the critical pressure of water. Above the critical point, steam behaves as a single phase fluid, so once through boiler drums are used in supercritical cycles because of the homogeneous steam properties. Subcritical reheat steam power plants have steam conditions in the order of 16.5 MPa, 538°C. Large boiler drums in subcritical power plants have large

amounts of stored energy which can be extracted to provide primary frequency response and meet the UK Grid Code [Lawal *et al.*, 2010]. Supercritical power plants operate in the regions between 22.1 MPa and 28.9 MPa, below 600°C. In general, USC-PC power plants have steam parameters greater than 28.9 MPa, and above 600°C [Zhang, 2013].

In pulverised fuel fired boilers, primary air blows the fine pulverised coal out of the mills and transports it through burners in the combustion chamber, burning at approximately 1500-1800 K. The flue gas rises through the furnace, passing through a superheater and reheater which generates superheated steam. The flue gas carries out approximately 70-90% fly ash out of the top of the furnace during the coal combustion process and the residual bottom ash falls to the bottom of the furnace [Zhang, 2013].

The major pollutants that are emitted during the coal combustion process are then removed such as SO_2, NO_X, and particulate emissions. Electrostatic precipitators or bag filters will remove and capture most of the fly ash before being released. Flue gas desulphurisation (FGD) units reduce the majority of SO_2 emissions. However, for certain coal-fired units FGD equipment may be kept offline during plant start-up until minimum stable generation has been reached [Parsons Brinkerhoff, 2014]. This is to ensure that the FGD unit has stabilised before being ramped up to full load. Coal-fired units also typically require oil to be burnt during start-up to provide circulation in the boiler before coal is ignited. The delayed start-up of the FGD unit may prohibit the quick start-up of any amine-based CO_2 capture systems. This is because amine-based CO_2 capture systems require very low SO_2 levels.

2.3.6 CO_2 capture and storage (CCS)

It is generally regarded that CO_2 capture and storage (CCS) will be required to meet global CO_2 emissions targets. Typically, CCS involves four stages: capture, compression, transport, and storage. It is expected that CO_2 will be transported either by pipeline or ship to a suitable storage location. Typical storage locations include:

- depleted hydrocarbon fields
- saline formations

There are a number of different technological options used for CO_2 capture with different engineering fundamentals. Each of the different capture processes have different techno-economical characteristics. The main CO_2 capture technologies closest to commercial development are:

- post-combustion CO_2 capture (PCC);
- pre-combustion CO_2 capture; and
- oxy-fuel combustion.

Figure 2.9 shows an overview of each of the main capture processes.

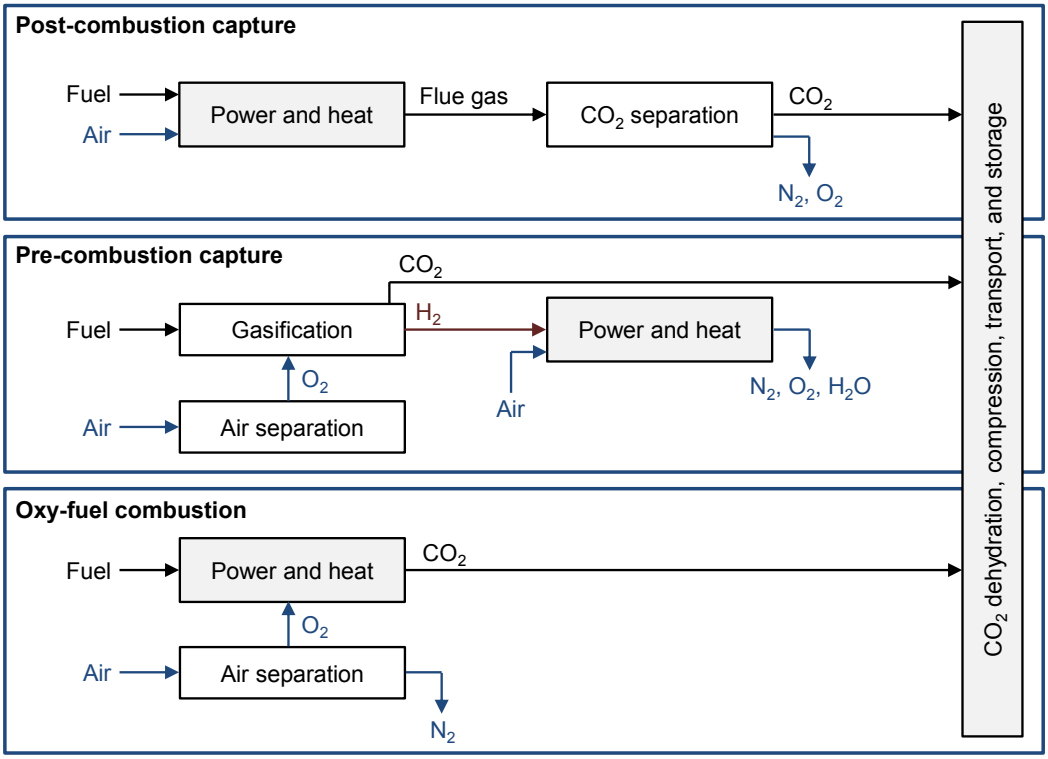

Figure 2.9: A simplified overview of CO_2 capture technologies that are closest to commercial deployment.

Oxy-fuel combustion plants use pure O_2 for the combustion of fuel. This produces a flue gas that consists of mainly H_2O and CO_2 which is easily separated. The very high combustion temperatures, because of the high O_2 environment, requires a proportion of the flue gas to be recirculated to manage internal temperatures.

Pre-combustion capture plants convert fuel (coal or natural gas) into a gaseous mixture of H_2 and CO_2. H_2 is then separated and burnt. This combustion process does not produce any CO_2. The separated CO_2 is then be compressed.

Post-combustion capture (PCC) plants separate CO_2 after the combustion process. PCC can be retrofitted to existing power plants with very little modification of the power cycle. Some additional power and steam are required for the chemical absorption/desorption process. Typically, an amine-based solvent is used to capture the CO_2 which is then separated from the solvent by heating it with steam.

Post-combustion CO_2 capture with amine scrubbing is used in this thesis as a representative capture technology because of its relative maturity and suitability for retrofit [IEAGHG, 2011]. Many amine-based solvents are currently being investigated by researchers and CCS companies. However, it is industry standard to use 30 wt% solution of monoethanolamine (MEA) as a benchmark for amine-based capture systems [Kohl and Riesenfeld, 1974]. However, MEA-

based capture systems are well known to require a significant amount of thermal energy to regenerate the solvent and separate the CO_2 [Lucquiaud and Gibbins, 2011].

Retrofitting CCS to existing power plants is one possible way of substantially reducing electricity sector CO_2 emissions. Power plants that are CO_2 capture ready (CCR) can be retrofitted with CCS with minimal efficiency reductions when compared to a new-build CCS power plant [IEAGHG, 2011]. However, there are a number of other retrofit options for CCR plants including:

- boiler power-matched retrofit;
- boiler heat and power-matched retrofit;
- gas turbine combined cycle power-matched retrofit; and
- gas turbine combined cycle heat-matched retrofit.

For further details about CCS retrofits see [IEAGHG, 2011]. This work assumes CCS power plants are an integrated retrofit where the net power output of the plant reduces due to the power consumption of the capture plant.

The electricity output penalty (EOP) of CCS plants is sometimes reported in different ways. For example, some studies report it as the fractional fall in the total electricity output of the power plant [IEAGHG, 2011]. Other studies report it as the percentage point drop in the thermal efficiency. The overall energy requirement of CCS is, however, generally independent of the base power plant thermal efficiency [IEAGHG, 2011]. Therefore, the EOP is defined here as is the loss of generator output incurred by steam extraction and the power consumption for ancillary and compression systems by the mass flow of CO_2 that is treated [IEAGHG, 2011]. The EOP (kWh_e/tCO_2) is described mathematically as:

$$\text{EOP} = \frac{\text{Loss of generator output + Compression \& ancillary power}}{\text{CO}_2\text{ mass flow}} \times 10^6/3600 \qquad (2.10)$$

where the loss in generator output and compression & ancillary power values are in MW and the CO_2 mass flow is in kg/s. The electricity output penalty (EOP) for an integrated PCC retrofit with MEA is around 300-400 kWh_e/tCO_2 [IEAGHG, 2011].

Flexible capture

IEAGHG [2012] have reviewed the operating flexibility of the current leading CCS power plant technologies. For an up-to-date review of operating flexibility, performance, and costs of CCGT, USC-PC, IGCC, and oxy-fuel combustion see IEAGHG [2012]. The electricity output penalty (EOP)[4] for an integrated PCC retrofit with MEA is around 300-400 kWh_e/tCO_2 [IEAGHG, 2011].

4. The electricity output penalty (EOP) is the loss of generator output incurred by steam extraction and the power consumption for ancillary and compression systems by the mass flow of CO_2 that is treated [IEAGHG, 2011].

A flexible PCC unit with amine scrubbing can rapidly redirect steam from the reboiler in the capture plant to the low pressure (LP) turbine in the base power plant to generate additional electricity [Lucquiaud *et al.*, 2009]. This flexible configuration requires sufficient LP turbine capacity to accommodate the additional steam flow and additional export capacity to the grid.

This work assumes an integrated retrofit where the net power output of the plant reduces due to the power consumption of the capture plant.

A flexible CCS unit with venting/bypass capabilities is able to vary the capture rate $Y_{g,t}^{\text{capt}}$ between:

$$Y_{g,\min}^{\text{capt}} \leq Y_{g,t}^{\text{capt}} \leq Y_{g,\max}^{\text{capt}} \tag{2.11}$$

where $Y_{g,\min}^{\text{capt}}$ is the minimum design capture rate and $Y_{g,\max}^{\text{capt}}$ is the maximum design capture rate. A CCS unit is considered inflexible if $Y_{g,t}^{\text{capt}}$ cannot be adjusted and remains constant at the design capture rate.

By redirectly steam from the reboiler, PCC units can temporarily increase the steam entering into the LP turbine, providing primary frequency response for up to 30 s without affecting the CO_2 capture rate [Haines and Davison, 2013]. Upwards spinning reserve can also be provided for longer periods of time but this may reduce the capture rate. This reduces the spinning reserve and response services that are needed from other sources. Solvent storage tanks could be installed to minimise exhaust gas venting during bypass, start-up and shut-down procedures.

CCS-equipped power plants with MEA-based PCC are able to operate the absorption, stripping, and compression units independently of each other for process optimisation. Solvent storage and regeneration systems could be added to enhance process flexibility and decrease operating costs [Arce *et al.*, 2012]. However, this would require adding capital intensive solvent storage tanks and oversizing the reboiler to accommodate the increased solvent during regeneration periods. Multiple absorbers/strippers could also be used to enhance the flexibility of PCC systems. An advanced solvent control system could also be implemented to optimise rich/lean solvent flow rates to achieve an optimal EOP.

However, for the purpose of this study, it is assumed that real-time flue gases must either be treated or vented and that no solvent storage is available. This implies that the absorption and stripping systems can be modelled using a single decision variable that indicates their operational status. This is important if a large number of CCS plants are to be modelled as this significantly simplifies the modelling complexity.

CCS-equipped power plants are expected to have potentially slightly faster ramp rates than the same power plant without CCS since the power consumption of the capture plant $P_{g,t}^{\text{capt}}$ can be adjusted in addition to ramping the base power plant. This increases the operating range of CCS power plants over non-CCS units because of lower minimum power output limits. However, this is not true for all power plant technologies. Domenichini *et al.* [2013] outline the operating

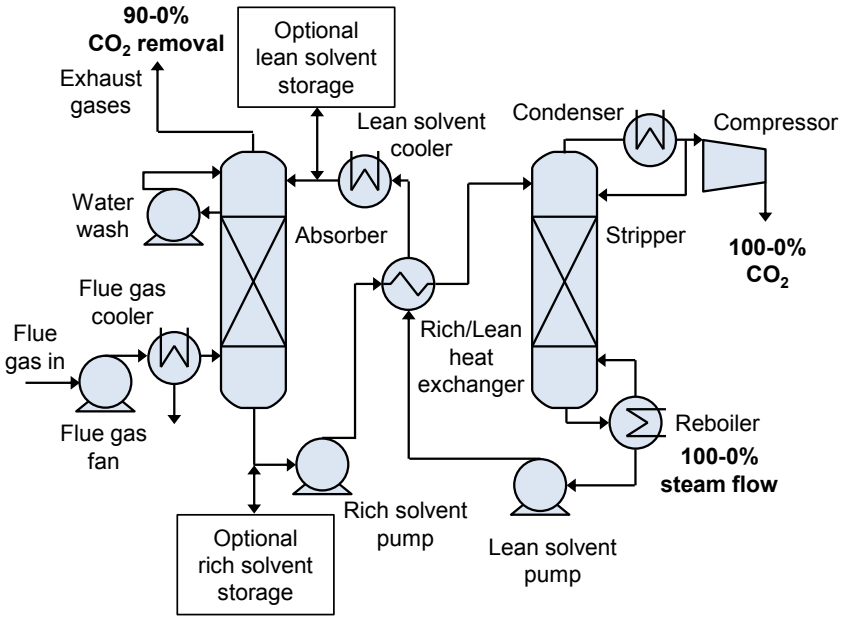

Figure 2.10: Simplified diagram of a configuration for a post-combustion CO_2 capture and compression system.

flexibility of different power plants with and without CCS.

Brouwer *et al.* [2013] assesses the operational flexibility of three power plant types including ultra-supercritical pulverised coal (USC-PC) with PCC, integrated gasification combined cycle (IGCC) with pre-combustion capture, and natural gas CCGT with PCC. Flexibility parameters were assumed for each of the power plant types and dynamic modelling showed that start-up times were relatively unaffected by the capture plants. However, PCC plants need to heat up the stripper to operating temperature and so depending on the volume of solvent and the availability of steam during start-up, this might taken longer.

Flexible compression

CCS power plants have to compress CO_2 and transport it for storage. However, one additional constraint imposed on CCS-equipped power plants is the part-load operation of CO_2 compressors, which are typically limited to a 70% turn down [Domenichini *et al.*, 2013]. It may be possible to avoid this constraint by recycling a proportion of the compressed CO_2, by installing multiple CO_2 compressors, or by using variable speed drive compressors. There is a severe energy penalty associated with recycling compressed CO_2 and it is capital intensive to employ multiple CO_2 compressor trains or use variable speed drive compressors. The flow of CO_2 may therefore be more like a step function during start-up and shut-down as additional compressors with a 70% turn down are brought online. However, for the purpose of this thesis,

it is assumed that any CO_2 captured can be accommodated by the CCS-chain including the compression, transportation, injection, and storage infrastructure. A quantitative assessment of flowrate constraints and boundary conditions of compressor trains, pipelines, and injection wells is considered beyond the scope of this study.

Flexible transportation and storage

It is likely that any CCS-equipped power plant will be part of a CCS network consisting of multiple CO_2 sources and sinks. There is currently very little information about the ability of future CO_2 transportation networks to manage variable and intermittent CO_2 flows [IEAGHG, 2012]. It is common engineering practice to first consider the boundary conditions and specifications of the storage and injection infrastructure and then calculate the required design characteristics for the rest of the CCS transportation and compression infrastructure network.

The typical specifications of the storage site that need considering include:

- minimum CO_2 flow requirements;
- O_2 concentration; and
- delivery pressure.

Iron and steel pipelines are susceptible to corrosion from increased levels of water and O_2. CO_2 can dissolve in water to produce carbonic acid and it is thought O_2 concentrations higher than 2 ppmv can increase the corrosion rate of iron in conventional steel pipelines [HSE, 2011]. It is therefore essential that impurities such as O_2 are removed during the capture process to safe levels.

CO_2 pipelines will be designed to handle a maximum pressure which will allow for a certain amount of short-term linepacking to increase flexibility. The value of linepacking flexibility comes from the ability to cover temporal imbalances and act as a short-term buffer. However, CO_2 is far less compressible than natural gas which may limit the value of linepacking. The inherent flexibility of a dense phase CO_2 pipeline system is limited by the compressibility. In CO_2 pipelines it may be more important to manage the velocity of the CO_2 as very little linepacking will be possible.

It may be important to add levels of strategic flexibility into the transportation system in order to manage variable and intermittent flows of CO_2. Buffer storage could be used to manage the requirements of both the electricity and storage systems, either when the pipeline is too full (by adding CO_2 to the buffer store) or when the pipeline is too empty (by extracting CO_2 from the buffer store). Saline formations offshore could be used to add strategic flexibility to the pipeline system. Buffer storage could be situated at the capture plant in the form of solvent storage or cylindrical tanks [IEAGHG, 2012]. Solvent operating conditions should be optimised to reduce the solvent degradation rate. Salt domes or storage at CO_2 shipping terminals could also be used

if available. Recompression and throttling may also be necessary to match the delivery pressure requirements which may evolve over time depending on the storage site.

The pipeline dimensions, CO_2 compression requirements, and delivery pressure will all depend on the storage arrangements. Long-term planning and policy flexibility includes pipeline oversizing to allow future tie-ins and allow storage sites to come online/offline. Typical storage locations include:

1. depleted hydrocarbon fields
    (a) open (hydrostatic pressure)
    (b) closed (rising pressure with time)
2. saline formations

Saline formations (aquifers) for CO_2 storage would ideally be an open aquifer but this will be unproven until injection starts and the pressure is monitored over the long-term. Initial injection tests are expected to assess the permeability of the formation, but will not be able to assess how the formation pressure will change over time. Very little data is currently available about saline formations and the potential permeability. On the other hand, there is far more information available about depleted hydrocarbon fields.

Enhanced Oil Recovery (EOR) and Enhanced Gas Recovery (EGR) are two possible methods of extracting additional hydrocarbons from depleted reservoirs by injecting and permanently storing a fraction of the CO_2. The additional revenue gained from EOR could provide the necessary funding for CO_2 transportation infrastructure in GB waters. However, the operating conditions at EOR storage sites are likely to be more controlled and constrained than saline formations. Depending on the EOR storage site, the delivery pressure may change with time and will vary significantly between open and closed reservoirs. Therefore careful consideration is needed when designing compression trains and boosters.

At the well inlet, CO_2 injection at 85 bar is typically required to avoid two-phase flow during injection. However, the integrity and temperature of the well will place strict limitations on the permitted injection rates and injection conditions [Veltin and Belfroid, 2013]. Throttling may be required to reduce the pressure of the CO_2 entering the reservoir. For depleted hydrocarbon fields, the reservoir pressure may be considerably lower than the critical point of CO_2.

The Joule-Thomson cooling during CO_2 injection and expansion into depleted hydrocarbon reservoirs with low pressures could affect the injectivity and permeability of the formation [Oldenburg, 2006]. It is also possible that the introduction of large amounts of very cold CO_2 could cause thermal or hydraulic fracturing around the reservoir. CO_2 hydrates may also form due to the interaction with water. Ice may also form at the manifold at the well head. This will require heaters to preheat the CO_2 entering the well.

CO_2 pipeline networks will have to transport the compressed CO_2 from either a single or a number of large CO_2 sources. CO_2 sources are typically divided in tiers depending on the

annual CO_2 produced per year [AMEC, 2008]. The sources that would be considered for a CCS cluster depend on load factor, location, CO_2 emissions and concentration, and any required investment to connect the source to the rest of the network. Another important consideration is the operating pattern of the CO_2 sources. The operating patterns and therefore the CO_2 flows of CCS-equipped power plants (biomass, gas, coal) and industry sources may be very different. The relative sizes of the CO_2 sources also needs careful consideration. For example, if a number of CO_2 sources share a common transportation pipeline, and one CO_2 source is much larger then any of the other sources, e.g. a large coal power plant, then the remaining smaller CO_2 sources may not be able to collectively maintain a minimum pipeline pressure if the pipeline has been designed to accommodate the larger CO_2 source operating at full-load. Planned outages at the storage and capture side could be synchronised so that they do not interfere and cause increasing down time of the network.

The CCSA [2013] have published a report which details a number of ways to achieve cost reductions for CCS networks. The development of CCS clusters, starting from a few key anchor projects, should allow for additional CO_2 sources and storage sites to connect over time. Therefore the early configuration of the CCS network should consider the likely future development. Operational switching between storage sites may be necessary to facilitate varying flows of CO_2 [CCSA, 2013]. DECC [2012c] have outlined a CCS storage strategy that includes some of the challenges with commercial-scale CO_2 storage. Some possible routes for transport and storage configurations are shown in ETI [2015]. It should be noted that these are only possible scenarios detailing different assumed deployment strategies.

More work is needed to understand the likely compression, transportation, injection, and storage constraints imposed on the CCS-equipped power plant.

2.3.7 Nuclear units

Nuclear power plants in France and Germany provide primary and secondary frequency response and load following duties. They have been designed to follow a varying load schedule throughout the day and also perform up to 2 large power changes per day [NEA, 2011]. Many modern reactors have ramp rates between 3-5% of their maximum rated capacity per minute.

The European Utilities Requirements cover a large range of conditions for light water reactors including Boiling Water Reactors (BWR) and Pressurised Water Reactors (PWR). PWRs and European Pressurised Reactors (EPR) are capable of changing the power level of the reactor by rapid control rod adjustments or by adjusting the concentration of boron in the primary coolant [NEA, 2011]. This means that PWRs have very fast ramp rates with nuclear plants in France and Germany commonly performing load following and frequency response services.

However, the reported maneuvering capability of modern EPRs is even greater. EPRs are capable of light and deep daily load following between 25% and 100% of rated capacity. Light

load following is defined as a cycle between 60% and 100% of rated capacity ramping at a maximum of 5% of rated capacity per minute. Deep load following is defined as a cycle between 25% and 60% of rated capacity ramping at a maximum of 2.5% of rated capacity per minute [NEA, 2011]. However, EPRs cannot perform these load following services at the end of their fuel cycles.

The economic losses associated with load following are almost all a result of operating at a reduced load factor, as fuel costs are so low. It is likely that during periods of high VRE output and therefore low net demand, baseload flexibility and minimum stable generation limits will be particularly important.

Advanced Gas-cooled Reactors (AGR), the most common nuclear reactor design in the UK, are the second generation of British gas cooled reactors. To date, AGRs have not been used in the UK to follow load changes. This is because AGRs suffer from potential Xenon poisoning, thermal stresses, reactor instability and control system limitations [Pouret and Nuttall, 2007]. In addition, the majority of AGRs in the UK are due to be decommissioned in the next few decades so it is unlikely they will provide flexibility services.

2.3.8 Energy storage

Electrical energy storage technologies are capable of providing both upwards and downwards operational flexibility. An electrical energy storage device s, where $s = 1,2,3,...,S$, can be categorised in terms of round-trip efficiency η_s^{rt} (%), ramping capability ρ_s (MW_e/h), power limits $P_{s,\min}$ and $P_{s,\max}$ (MW_e), and storage energy limits $E_{s,\max}$ (MWh_e). The amount of time that an energy storage device s can discharge at its maximum rate is known as the storage duration or discharge time (h):

$$\text{Duration} = \frac{E_{s,\max}}{P_{s,\max}} \tag{2.12}$$

IMechE [2014] provide a recent and detailed description of a wide range of developed and emerging energy storage technologies including the storage energy ranges, discharge times, and costs ($/kW and $/kWh). Energy storage units can be used for arbitrage, ancillary services, absorbing curtailed wind, defer generation/transmission infrastructure investments, and emergency applications.

The flexibility characteristics and response times of different energy storage technologies also varies. However, in comparison to the start-up times of thermal power plants (>1 hour), the response times of energy storage units ($\ll$1 hour) can be considered negligible. For example, pumped storage has a response time of less than 30 seconds and compressed air energy storage (CAES) can go from 0% to 100% in less than 10 minutes [ScottMadden, 2009].

2.3.9 Wind curtailment

In periods when wind generation is higher or when demand is lower than forecast, wind can be curtailed or gradually ramped down to reduce the rate at which thermal or energy storage units have to reduce output. Wind power can therefore be curtailed to provide downward flexibility, if it is incentivised.

Using power-to-gas technologies to convert surplus wind generation into hydrogen is one possible way to increase the flexibility of the power system but also utilise and absorb surplus wind [Qadrdan *et al.*, 2015]. This involves using hydrogen electrolysers and the injection of hydrogen into the gas network. This reduces natural gas volumes that need to be supplied from gas terminals and reduces wind curtailment.

2.3.10 Interconnectors

Interconnectors effectively aggregate the output of VRE across adjacent systems, smoothing the output over a broader geographical area and combining the variability of different VRE technologies. Interconnectors allow another system that is connected to provide balancing services and enhance system security, increasing the flexibility. However, recent work by Poyry [2011] showed that combining the outputs of wind and solar across Northern Europe did not average out, despite the large geographical area and interconnectivity.

2.3.11 Demand-side response

Demand-side response is traditionally provided by large and usually energy intensive customers who reduce their power consumption at short notice. There are now price-based mechanisms and incentives to provide demand-side responses. Many smaller demand-side systems can be aggregated through automatic control systems. Demand-side aggregators facilitate the electricity usage of small to medium size customers to provide balancing services. These commercial aggregation services use internal or external system signals, such as price, frequency, or forecast errors.

2.3.12 Summary

The main sources of operational flexibility in power systems were introduced and described. A qualitative assessment of the potential flexibility of post-combustion CO_2 capture, compression, and transportation was presented. Power system reserve and response requirements in systems with large amounts of wind are now be discussed.

2.4 Reserve requirements

2.4.1 Introduction

Reserve requirements are typically divided according to response time. Many system operators have different definitions and methods for quantifying reserve requirements. However, the various types of operating reserves can be broadly defined as either event-based reserves or non-event based reserves [NREL, 2012].

Contingency reserve is required to cover the loss of the largest credible contingency which can be provided by a combination of either spinning, standing, and interruptible loads [NREL, 2012]. Many systems operators use deterministic reserve criteria to ensure that there is sufficient reserve to cover the largest credible loss in generation. This is sometimes referred to as the N-1 reserve criterion. Setting reserve requirements to cover the loss of the largest generator $\max(P_{g,\max})$, however, ignores the stochastic nature of generator failures. A probabilistic reserve assessment considers individual generator failure histories and uses them to estimate the probable loss of usable capacity for each time period. One method for estimating the reserve requirements for generation outages uses a capacity outage probability table (COPT).

The National Grid [2011a] define basic reserve as the reserve for conventional generation outages and demand forecast error. Reserve for wind is defined as the additional reserve that is required to manage wind variability. Comprehensive definitions of operating reserve requirements for power systems with significant proportions of wind are provided in [Milligan *et al.*, 2010; Ela *et al.*, 2011].

Typically, traditional power systems schedule reserve requirements to cover the largest credible loss in generation and any short-term deviations and forecast errors in demand. Power systems with large amounts of wind will have to provide reserve to meet the combined forecast errors and short-term variations in demand and wind output.

2.4.2 Determination of reserve requirements

Upwards reserve R_t^{up} is typically provided by thermal generators operating below their maximum power output $P_{g,\max}$. When there is an unexpected increase in net demand, these thermal generators increase their outputs as required. Downwards reserve R_t^{dn} is typically provided by thermal generators operating above their minimum stable generation limit $P_{g,\min}$ and decrease power output when there is an unexpected decrease in net demand.

Upwards reserve R_t^{up} is therefore required to cover the largest credible loss in generation (plant outage), a short-term increase in demand, or a short-term decrease in wind generation. Downwards reserve R_t^{dn} is required to cover that largest credible loss in demand, a short-term decrease in demand, or a short-term increase in wind generation. Power systems can

utilise energy storage, interconnectors, demand-side management, and load shedding to provide additional reserve if required.

However, the ability of thermal power plant to provide reserve is a function of its ramp rate over a given time frame. This complicates the problem of meeting both ramping requirements and reserve requirements as they are both interrelated.

Estimating the required levels of reserve for wind power involves first understanding the potential wind variability and uncertainty at the corresponding operational timescale, then understanding the amount of flexible reserves that are required to cover the unexpected changes in wind output, usually to 3σ or 99.73% of events, see Figure 2.11. However, different electricity systems sometimes use a range standard deviations 2-5σ values [Holttinen *et al.*, 2008]. The National Grid [2014a] have proposed a reliability standard for security of supply of 3 hours per year, using the Loss of Load Expectation (LOLE) risk metric. This corresponds to a standard deviation of approximately 3.5σ.

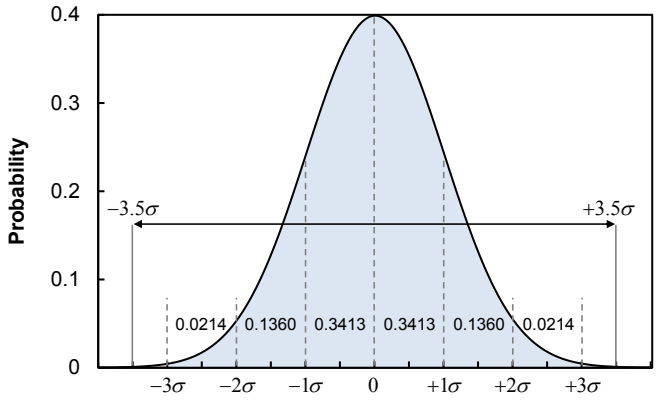

Figure 2.11: Probability density function of a normal distribution with confidence intervals.

The total uncertainty at any period of time faced by power systems is the sum of demand and wind forecast errors and the largest credible demand/generation outage. It is assumed that these three sources of power system uncertainty are uncorrelated. This implies that demand and wind forecast errors and generation outages are statistically independent of each other. Uncertainty in electricity demand forecasts can be approximated as a normally distributed function with zero-mean with a standard deviation of typically 1% of current demand [Gross and Galiana, 1987; Bunn, 2000; Silva, 2010]. Forecasting electricity demand is relatively accurate and so demand forecast errors are typically small. It is also possible to represent wind forecast errors as a normally distributed function with zero-mean [Silva, 2010; Ma, 2012]. The National Grid [2011a] currently assume that the wind forecast uncertainty is 10% root mean square of installed wind capacity, although this is likely to fall in the future with increased wind forecast accuracy. This allows the reserve requirements for demand and wind forecast uncertainty to be combined with credible plant outages.

Figure 2.12 shows an illustrative example of the demand-wind uncertainty. If demand is forecast to be 40000 MW and the standard deviation in demand uncertainty is 1% of current demand then σ_t^D = 400 MW. The net demand uncertainty can be found by an analytical method that combines that standard deviations of demand and wind.

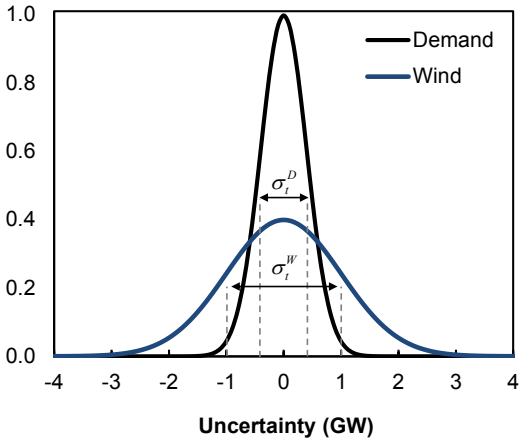

Figure 2.12: Probability density functions for demand and wind uncertainty approximated using normal distributions where σ_t^D = 400 MW σ_t^W = 1000 MW.

The upwards and downwards system reserve requirement are expressed mathematically as:

$$R_t^{\text{up}} = \mu_t^{\text{up}} + \sqrt{(3.5\sigma_t^D)^2 + (3.5\sigma_t^W)^2} \tag{2.13}$$

$$R_t^{\text{dn}} = \mu_t^{\text{dn}} + \sqrt{(3.5\sigma_t^D)^2 + (3.5\sigma_t^W)^2} \tag{2.14}$$

where μ_t^{up} is the reserve required for the largest credible loss in generation, μ_t^{dn} is the reserve required for the largest credible loss in demand, σ_t^D is the standard deviation in demand forecast uncertainty, and σ_t^W is the standard deviation in wind forecast uncertainty. It is assumed that reserve requirements must be set to cover any unexpected changes in demand-wind forecast uncertainty within 3.5 standard deviations or 99.95% of events.

In certain circumstances, for example when wind output is forecast to be very low or when large amounts of wind is forecast to be curtailed, $3.5\sigma_t^W$ is likely to be too much reserve. To account for this, if the standard deviation in the wind forecast error is greater than the expected wind output (wind forecast W_t^{f} less wind curtailment W_t^{curt}), then the uncertainty in the wind forecast is reduced. Considering this, the upwards reserve requirement becomes:

$$R_t^{\text{up}} = \mu_t^{\text{up}} + \sqrt{(3.5\sigma_t^D)^2 + \min\left(3.5\sigma_t^W, (W_t^{\text{f}} - W_t^{\text{curt}})\right)^2} \tag{2.15}$$

where W_t^{f} is the wind forecast and W_t^{curt} is the wind curtailment [Ma, 2012]. This approach does not take into account how market participants might balance wind uncertainty within their own

generation portfolios. The approaches to estimate the reserve requirements for wind are now be investigated.

2.4.3 Reserve for wind

Wind forecast error

There are a number of methods to forecast the wind power output including the persistence method and more advanced forecasting methods that use numerical weather prediction (NWP) models. NWP models either use a physical or statistical approach.

The physical approach to wind power forecasting gathers a large amount of meteorological resource measurements to derive the wind speed at hub-height. Then, the power output is estimated using wind speed, wind direction, temperature and other variables. The statistical approach translates meteorological measurements directly into estimated power outputs by comparing the large amount of historical meteorological predictions with realised power output. The uncertainty in wind power output is expressed as the standard deviation of wind power output forecast error.

Although the accuracy of different wind forecasting and NWP models is different and likely to increase in the future, the overall trend in wind forecast errors is similar. For example, the standard deviation of the wind forecast errors increases rapidly with just a 1-4 h time lag. The forecast errors then increase only slightly with increasing time lag and follow a logarithmic trend as seen in Figure 2.13.

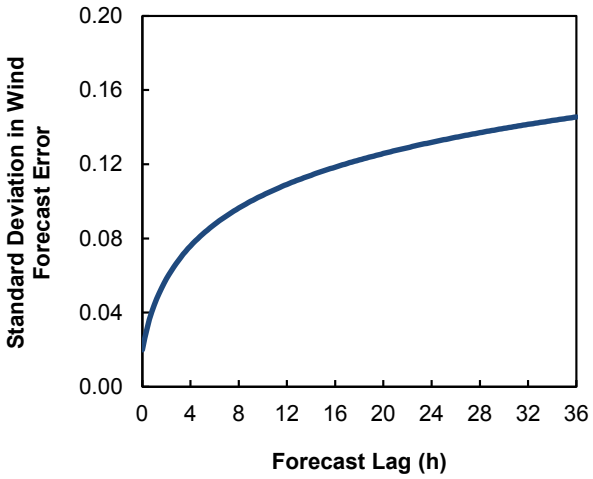

Figure 2.13: The capacity normalised standard deviation in wind power forecast error as a function of forecast time. Adapted from Ummels [2009].

There are also a number of methods to incorporate wind forecast error into unit commitment (UC) models. The wind power output forecast error, and therefore the amount of reserve

requirements for wind, can be estimated either as a function of installed wind capacity or as a function of wind power output.

Many studies estimate the standard deviation in wind forecast error normalised by the installed wind capacity. For example, in a study of the ERCOT electricity system in the USA, GE Energy [2008] found a linear relation between the standard deviation in wind forecast error and installed wind capacity. This implies that increasing the installed wind capacity increases the wind forecast error. Another study in the UK by Strbac *et al.* [2012] assumes that the forecasting error of wind 4-h ahead of real-time is 15% of installed wind capacity. It is then anticipated that the wind power output forecast error will fall to 10% after 2020 and then may possibly fall below 6% in the future.

Ummels [2009] estimated the capacity normalised wind forecast error for the Danish power system with 12 GW of installed wind capacity over a 0-36 h time horizon, see Figure 2.13. Statistical analysis demonstrated that 99% of the events are within $\pm 3.5\sigma$. Ummels [2009] also compared the mean absolute error, the variation between the forecasted and actual wind generation, with the day-ahead forecast error of the Danish system operator and found a very good agreement. This method takes into account for the increasing inaccuracy of wind forecasts with increasing time lag and is also easily implemented into unit commitment models.

However, wind speed forecast errors are typically normally distributed [Pinson *et al.*, 2007]. For an individual wind turbine or small group of turbines, wind speed errors are amplified by the non-linear shape of the power curve translating into more dispersed and non-normal capacity factor errors. Figure 2.14 shows a normally distributed wind speed forecast error with standard deviation σ^U being translated into a non-normal distribution function.

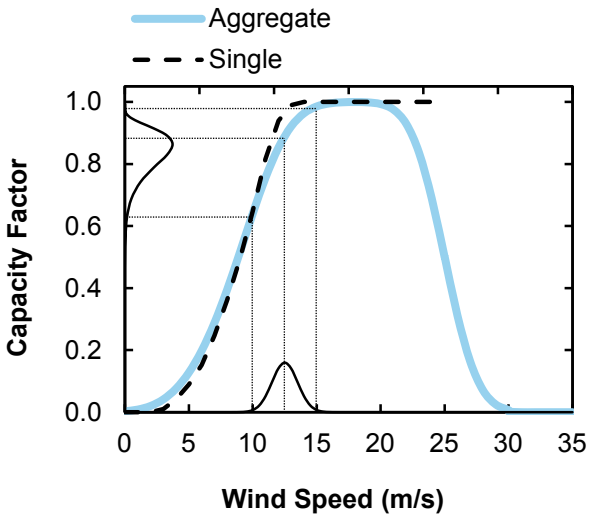

Figure 2.14: Illustrative wind speed forecast distributions with a standard deviation of 1.0 m/s and corresponding capacity factor forecast error distributions.

For a sufficiently large number of independent wind farms spread over a large geographical area (such as GB), wind power forecast errors can be modelled as normally distributed random variables with zero-mean and then fitted to a normal distribution function [Ma, 2012; Silva, 2010].

For a given wind speed and standard deviation in wind speed forecast error σ^U, it is possible to estimate the upwards and downwards forecast errors. Figure 2.15 shows the 90% confidence intervals for upwards and downwards forecast errors at different wind speeds and standard deviations in wind speed errors. The up and down forecast errors are not symmetric and increasing the standard deviation in wind speed forecast errors further skews the error distributions. This is explained further with an example.

If the wind speed forecast 4 hours ahead of real-time is 12.5 m/s and the wind speed forecast error is known to be 0.5 m/s then it is possible to estimate the possible variation in capacity factors that might occur if there is an unexpected change in wind speed. At 12.5 m/s any unexpected increase in wind speeds will result in a only a small increase in output because of the slight gradient of the power curve at this point. Thermal power plants would only be required to provide a small amount of downwards reserve to maintain power balance. However, at 12.5 m/s an unexpected decrease in wind speeds would result in a large decrease in power output from the wind farm because below this point the power curve gradient is very steep. Thermal power plants would be required to provide a large amount of upwards reserve to cover this sudden decrease in wind output.

Figure 2.15 shows how the standard deviation in wind speed forecast errors impact the upwards and downwards reserve requirements to cover an unexpected change in wind speeds. Increasing the standard deviation in wind speed forecast error from 0.5 m/s to 1.5 m/s skews the plots and increases the probability of an even larger unexpected increase in wind speed and so increases the distribution of capacity factors. At wind speeds where the power curve is flat, for example 18 m/s, any unexpected variation in wind speeds has very little impact on power output.

For an individual farm with a normally distributed wind speed forecast error, the wind power output forecast error and reserve requirements for wind are therefore non-linear. For a large geographical area with a large number of wind farms, however, it is possible to approximate the wind power output forecast error as a normally distributed function with zero mean [Silva, 2010; Ma, 2012]. Therefore this method is not explored in further detail.

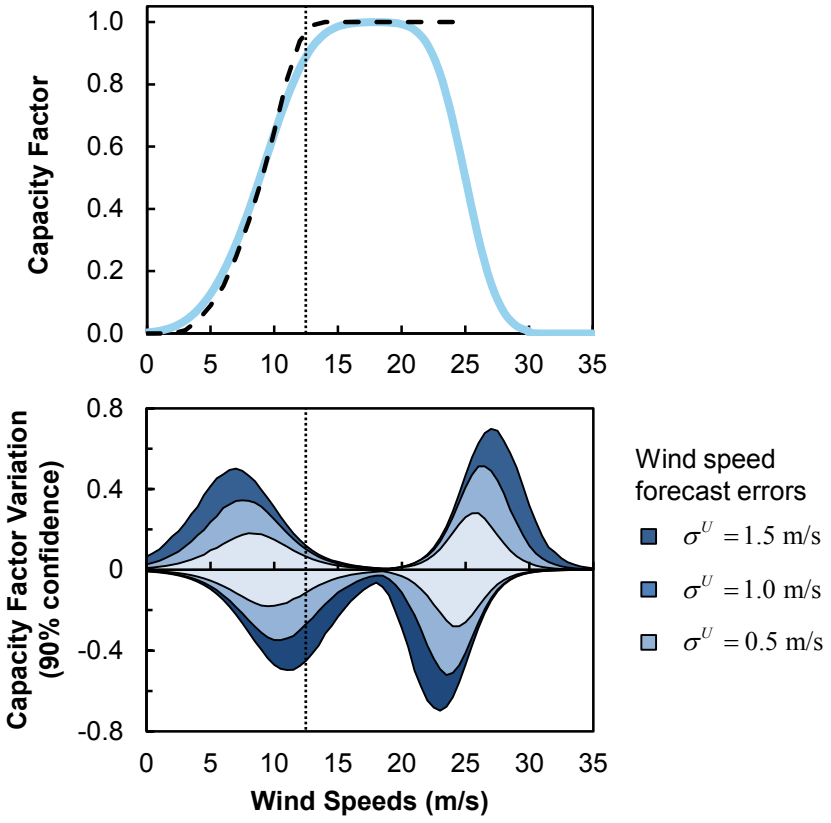

Figure 2.15: 90% confidence intervals for the capacity factor forecast error as a function of wind speed. Upwards reserve is required for a negative variation in the capacity factor after a wind speed forecast error. Downwards reserve is required for a positive variation in the capacity factor after a wind speed forecast error. Increasing the standard deviation σ in the wind speed forecast error increases the variation in capacity factors and skews the distribution because of the non-linear power curve.

Wind forecasting techniques

One way to simulate the wind power forecast error is to use a stochastic differential equation to model both the stochastic distribution of errors and the temporal correlation between forecasting periods.

Bibby *et al.* [2005]; Ma [2012] present a stochastic differential equation that is used to simulate the wind power forecast error. The wind power forecast error is then added to a known historical wind power output time-series to produce a wind power forecast time-series. These time-series are then used to understand the required flexibility to manage wind uncertainty over different timescales.

An autocorrelation function models the temporal correlation in the wind forecast errors between each forecasting period. That is, wind forecast errors with a short interval between time

lags will have a stronger correlation between them. The correlation between wind forecast errors as a function of the time lag k between them is known as the autocorrelation, which can be approximated as an exponentially decreasing function with increasing time lag [Doquet, 2007; Ma, 2012]. If k is the time lag, where $k = 1, 2, 3, ..., K$, the autocorrelation ψ_k of the wind forecast error is:

$$\psi_k = e^{-\theta k}, \theta > 0 \qquad \forall k \in K \tag{2.16}$$

It is assumed that the accuracy of the wind power forecasts into the future are known and the uncertainty in the wind power forecast error is assumed to be normally distributed with standard deviation σ_t^{W} that increases with increasing time lag, see Figure 2.13.

This method can also be applied to any time-series such as wind speed or demand. It is the wind speed forecast error that is normally distributed, and not the wind power forecast error[5], However, this work simulates the wind power forecast error and then adds it to the realised wind power output to produce the forecast wind power output.

For a stationary process with normal distribution and autocorrelation function $e^{-\theta k}$, it follows that the wind forecast error time-series X_t must be mean-reverting and ergodic. The stochastic differential equation can be expressed as:

$$dX_t = -\theta X_t dt + \sigma_t \sqrt{2\theta} dB_t \tag{2.17}$$

where σ_t is the standard deviation in the wind forecast error and B_t is a standard Brownian motion. From the solution to the stochastic differential equation above, the wind forecast error X_t is iteratively obtained and added to the realised wind power time-series.

$$X_t = X_{t-1} + dX_t \tag{2.18}$$

The forecast wind power time-series, after the addition of the wind power forecast error, must be strictly positive as negative wind power outputs cannot occur. An illustrative example of the simulated forecast W_t^{f} and realised W_t^{r} wind power output time-series are shown in Figure 2.16.

---

5. The simulated wind speed error, once applied to a non-linear power curve will produce a non-linear wind power output forecast error.

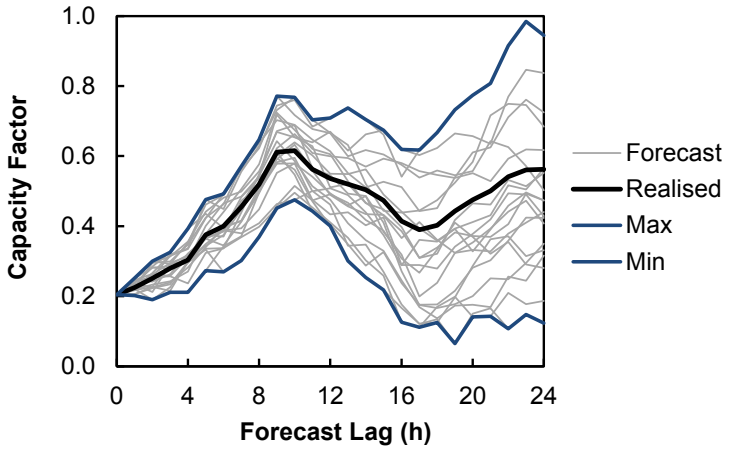

Figure 2.16: Simulated 24-h forecast and realised wind power output time-series. Wind forecast error is stochastic with a temporal correlation between forecasting periods.

2.5 Response requirements

2.5.1 Introduction

Traditional power systems provide response and reserve services to maintain any system imbalances. The National Grid [2015a] is the system operator in GB and provides definitions for the primary, secondary, and high frequency response. High frequency response must be deployed within 10 s to reduce system frequency after a positive frequency deviation. Primary frequency response must be deployed within 10 s of an event to increase system frequency after a negative frequency deviation and be sustained for an additional 20 s. Primary frequency response services limit the initial frequency deviation to -0.5 Hz after a normal infeed loss and -0.8 Hz after an infrequent infeed loss. Secondary frequency response takes over and must be deployed within 30 s of the initial contingency and be sustained for at least an additional 30 mins. A combination of spinning and standing reserve is typically utilised to restore system frequency back to pre-contingency levels. The typical frequency response and reserve services that are deployed to control and stabilise the system frequency within statutory limits after a infrequent generator outage are shown in Figure 2.17.

The increase in non-synchronous VRE capacity is expected to decrease the amount of system inertia [National Grid, 2013]. Many wind turbine designs are connected to the electricity system via power electronic converters which decouple the rotational mass of the wind turbine from the electricity system [National Grid, 2013]. However, certain wind turbine designs are potentially capable of providing a small amount of synthetic inertia or rapid frequency response, although they provide less inertia per MW of installed capacity compared with large-scale synchronised power plants [National Grid, 2013]. The activation of synthetic inertia or rapid frequency response from wind turbines can therefore contribute to primary frequency response requirements by releasing stored kinetic energy for a short period of time. However,

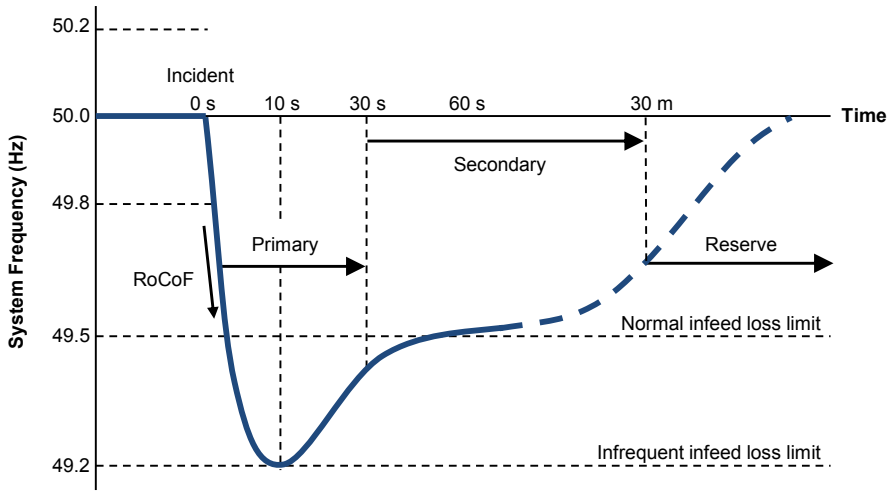

Figure 2.17: Typical frequency response and reserve services after a infrequent generator outage in the GB system. Adapted from National Grid [2013].

it is important that any emulated inertial response occurs during the first few seconds of a negative frequency deviation so that the frequency recovery is not delayed. The utilisation of fast demand-side or frequency energy storage response is not considered. Estimating the inertial and primary frequency response of different wind turbine technologies at different wind speeds is also considered beyond the scope of this work. See Muljadi *et al.* [2012] for an assessment of the potential inertial and frequency response contributions of various wind turbine technologies to restore system frequency and limit the initial Rate of Change of Frequency (RoCoF).

It is expected that certain power plants may be able to provide synchronous compensation and therefore contribute to system inertia during low power output operating conditions. For example, a CCGT unit with a clutch on the generator shaft can contribute to system inertia and provide reactive power to the grid without generating active power. The provision of inertia whilst operating in synchronous compensator mode could provide large amounts of system inertia to compensate for the large amounts of VRE [National Grid, 2013].

It has also been highlighted by National Grid [2013] that a weaker power system may result in the shift towards lower order harmonics. The system resonance will therefore peak at lower order harmonics, which is expected to cause an amplification of voltage distortion. Variable speed converter connected wind turbines generate harmonic oscillations at different frequencies. The harmonic order and resonant conditions will change depending on the number of turbines, shunt capacitors, and ambient grid conditions. The superposition of higher frequency harmonic oscillations to the original sinusoidal 50 Hz waveform will affect power quality and may cause additional impacts such as increased losses, voltage distortions, over-voltages, electromagnetic interference, and the malfunctioning of protection relays [National Grid, 2013].

2.5.2 Frequency response characteristics

The frequency response contribution of an individual power plant depends on the power output and the plant response characteristics. Experimental tests are typically performed on power plants to assess the frequency response characteristics at different loading levels. These results are used to create functions of the frequency response capability over the operating range $P_{g,\max} - P_{g,\min}$ of each power plant. An approximation of the typical power plant frequency response profiles in Erinmez *et al.* [1999] is described in detail in Silva [2010] and is shown graphically in Figure 2.18.

Upwards response is provided by a generating unit's primary and secondary frequency response capabilities. Downwards response is provided by a generating unit's high frequency response capability. The symbol f_g^{up} represents an approximation of the maximum upwards primary and secondary frequency response contribution of a generating unit and the symbol $-f_g^{\text{dn}}$ represents an approximation of the maximum downwards high frequency response contribution.

The maximum response contributions that can be provided by a generating unit is generally less than the amount the unit's power output has been reduced. This is the reason the gradient m_g^{up} in Figure 2.18 is less than 1.

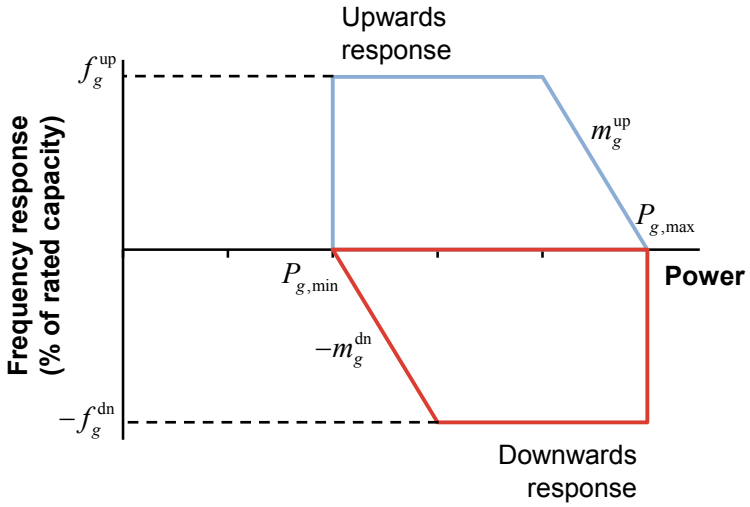

Figure 2.18: An approximation of the upwards and downwards frequency response contributions for typical generating units. Adapted from the UK Grid Code in National Grid [2015a] and Silva [2010].

The response characteristics for different power plant technologies, based on a number of frequency tests during emergency conditions, are detailed in Erinmez *et al.* [1999] and summarised in Table 2.2. It is assumed that the frequency response characteristics of future power plants are broadly the same as the GB units described in Erinmez *et al.* [1999]. The minimum primary, secondary, and high frequency response requirements after a 0.5 Hz frequency deviation from the nominal grid frequency for all GB generating units are described in National

Grid [2015a].

	Primary	Secondary	High
CCGT	0.11	0.13	0.13
Coal	0.12	0.13	0.14
Oil	0.15	0.15	0.13

Table 2.2: Average response contributions (% of rated capacity) for different GB power plant technologies based on a number of frequency tests during emergency conditions from Erinmez *et al.* [1999]

Post-combustion CCS-equipped power plants have been theoretically demonstrated to provide additional primary frequency response in the from of a rapid diversion of steam from the stripper to the steam turbines [Haines and Davison, 2013]. Supercritical steam power plants, in particular, store less energy in the form of steam than subcritical steam power plants with large steam drums. Exactly how the response capabilities change after the addition of CCS is an important question that requires further attention.

2.6 Inertia requirements

2.6.1 Introduction

As the proportion of wind generation increases in a power system, the amount of synchronised thermal generation will decrease. This is likely to deteriorate the support for frequency control as the rotational inertia in the rotating masses of synchronised thermal power plants determines the immediate frequency response of the power system.

When a large frequency event occurs, possibly because of a large change in generation or demand, the energy stored in the magnetic fields of synchronous units provides an immediate electrical response. This is followed by an inertial response that occurs over the first 1-2 s of the frequency deviation. Synchronous generators either absorb or inject kinetic energy to counteract the frequency deviation [Tielens and Hertem, 2012]. Immediately after a fall in system frequency, kinetic energy is extracted from synchronised power plants to limit the initial Rate of Change of Frequency (RoCoF). System inertia reduces the severity of frequency disturbances and reduces the RoCoF. Scheduling sufficient inertia is therefore critical to ensure the stability of the power system. The inertial response of thermal generators therefore dampens the frequency deviation. If the frequency exceeds certain set limits, automatic governor control is then activated.

2.6.2 System inertia

Large-scale synchronised power plants store kinetic energy proportional to its rotating mass and square to its angular velocity. When at part-load, synchronised power plants automatically adapt their power output after a negative frequency deviation according to their droop characteristics. The initial RoCoF is determined by the magnitude of the generation loss and the system inertia.

National Grid [2013] note that embedded generators have mains protection relays that are set to trip when the RoCoF exceeds 0.125 Hz/s. The reason for this RoCoF limit is to disconnect embedded generators during an islanding condition where the frequency in an isolated part of the network diverges from the frequency of the system. However, embedded generators may not be able to distinguish between islanding and a genuine frequency disturbance and are therefore in danger of tripping when the RoCoF exceeds 0.125 Hz/s. This will lead to a greater loss in generation and accelerate the fall in system frequency. It is therefore extremely important that sufficient inertia is provided to limit the initial RoCoF after a large generation outage.

Wind turbines do not typically contribute to total system inertia. Variable speed wind turbines with power electronic converters are decoupled from changes in system frequency. Updated control algorithms, however, could be implemented so that wind turbines provide an emulated inertial response [Muljadi *et al.*, 2012; Tielens and Hertem, 2012; Seyedi and Bollen, 2013; Zhang *et al.*, 2013; Licari *et al.*, 2013].

Wind turbines could provide high frequency response when the system frequency exceeds 50 Hz by reducing output at a given rate [Martinez de Alegria *et al.*, 2007]. During normal operating conditions when the system frequency is 50 Hz, wind turbines could decrease their power output, below their maximum achievable extraction level. If the system frequency suddenly dropped below 50 Hz, wind turbines could rapidly increase their power output back up to their maximum achievable extraction level. This would help to restore system frequency after a negative frequency event.

However, variable speed wind turbines can only provide a small amount of inertia compared with large conventional thermal power plants, see Section 3.4.3. The provision of synthetic inertia depends on the amount of kinetic energy stored in the rotating parts of a wind turbine which is a function of wind speed.

Before automatic governor control is activated, the extraction of stored kinetic energy over the inertial time frame determines the initial RoCoF after a frequency disturbance. The stability of a power system therefore depends on the overall response and the mean frequency of the system [Daly *et al.*, 2015]. For a synchronously isolated power system, such as GB, a single bus frequency model is thought to be an appropriate representation of the system-level frequency response characteristics [Daly *et al.*, 2015]. Details of this method to model system inertia using a simplified version of the swing equation is now be given.

2.6.3 Inertial constraint

After the loss of a large generating unit, the drop in active power ΔP causes the system frequency to drop. The active power imbalance after the loss a generator is the difference between the original electricity demand before the contingency D_0 and the generation available after the contingency $G_{\Delta P}$. It is anticipated that the largest loss in generation in GB will be 1800 MW in the near future with the connection of new larger 1800 MW units, offshore wind farms, and double circuit spurs [National Grid, 2011a]. It is therefore expected that $\Delta P = P_g^{\max} = 1800$ MW. In GB, it is a reasonable approximation to assume that the impact of load damping is zero. This is because disturbances that cause power flows to oscillate are usually damped by synchronous generators connected to the system [National Grid, 2013].

If the maximum RoCoF limit is known, the system inertia H_{s} can be estimated to ensure the RoCoF is within limits after a large generator outage. It is therefore possible to estimate the system inertia for each time period and curtail wind as necessary to ensure that the RoCoF never exceeds its maximum limit in the event of a large generator outage. The minimum amount of system inertia $H_{\mathrm{s}}^{\min}$ to limit the RoCoF and maximum frequency deviation can be modelled by a minimum number of synchronised power plants with known inertia constants.

The kinetic energy E_g stored in the rotating mass of each synchronised generating unit g is:

$$E_g = \frac{1}{2} J_g \omega^2 \tag{2.19}$$

where J_g (kg/m^2) is the moment of inertia of unit g and $\omega_g = 2\pi f_g$ (radians/s) is the electrical angular frequency where f_g (Hz) is the rotating frequency of the unit [Muljadi *et al.*, 2012].

The rotational inertia constant H_g (s) of each synchronised generating unit g is therefore:

$$H_g = \frac{E_g}{S_g} = \frac{J_g \omega_g^2}{2 S_g} \tag{2.20}$$

where S_g is the base rated power (MVA) of each unit. The inertia constant H_g for a typical power plant is between 2-10 s. This can be interpreted as the length of time that kinetic energy can be extracted at full power output. The per-unit system inertia constant H_s (p.u. s) is therefore:

$$H_{\mathrm{s}} = \sum_{g=1}^{G} \frac{H_g S_g}{S_s} \tag{2.21}$$

where S_s is the base rated power (MVA) of the system [Tielens and Hertem, 2012].

If the inertia weighted average of all the generator frequencies is f_c then the initial RoCoF (Hz/s) immediately after the imbalance and before the initiation of automatic governor control

($t_0 < t \ll t_{\text{gov}}$) is given by the equation:

$$\left.\frac{df_c}{dt}\right|_{t>t_0} = \frac{\Delta P f_0}{2H_s} \tag{2.22}$$

where f_0 is the frequency before the contingency and ΔP is the net active power imbalance (p.u. in system base) [Sharma *et al.*, 2011; Daly *et al.*, 2015].

In order to ensure system stability, the initial RoCoF must not exceed the maximum RoCoF:

$$\left.\frac{df_c}{dt}\right|_{t>t_0} < \left.\frac{df_c}{dt}\right|_{\max} \tag{2.23}$$

The constraint to ensure there is sufficient system inertia to maintain stability after a contingency event is therefore:

$$H_s \geq \frac{\Delta P f_0}{2\left.\frac{df_c}{dt}\right|_{\max}} \tag{2.24}$$

The next section provides a literature review of power system models and their applications before outlining the proposed model.

2.7 Literature review

2.7.1 Power system integration studies

Integration studies have been conducted for power systems that plan to deploy large amounts of VRE. These studies typically focus on the impact of VRE on power system operation, costs, and CO_2 emissions to assist with policy making. These research efforts all highlight the importance of increased flexibility in power systems to manage increased variability and uncertainty from VRE. Despite this, the flexibility and operating characteristics of thermal power plants are sometimes simplified and misrepresented.

A study by Poyry [2009] on the implications of intermittency used a bespoke mixed-integer linear programming (MILP) tool to simulate the outputs of individual units in the GB and Irish power systems. This least-cost dispatch model used scaled demand and wind data for 28 sites in GB over an 8 year period between 2000 to 2007. These 28 wind sites were chosen to be representative of the future onshore and offshore GB wind fleet. But with just 9 offshore and 19 onshore wind sites it is unlikely to provide an accurate representation of a geographically dispersed wind fleet. Several Monte Carlo simulations were used to assess the probability of certain events occurring, such as peak demand coinciding with low wind output. A number of insights are provided on the future operating patterns of thermal power plants.

Pfenninger and Keirstead [2015] compared scenarios with different combinations of generation technologies: renewables, nuclear and fossil fuels with and without CCS. High-resolution wind and solar resource data are derived from the NASA MERRA reanalysis. Overall system costs of electricity, CO_2 emissions and energy security are analysed. They employed ternary diagrams to represent the relative proportions of renewables, nuclear and fossil fuels. They reported that overall costs between scenarios remains similar, implying that the different assumed generation portfolios are feasible, both from a technical and economic standpoint. However, some portfolios with very high proportions of renewables require a significant amount of either interconnection, energy storage, or new resources such as tidal power. The model does not consider detailed constraints such as ramp rates, minimum up/down times or start-up times.

The Renewable Electricity Futures Study by NREL [2012] analyses the challenges of renewable energy resources and the technical issues related to the operation of the future US electricity system. A commercial security-constrained unit commitment and economic dispatch model with DC optimal power flow and unit operating constraints is used to assess the reliability and grid operability at hourly resolution in high renewable electricity futures. The frequency that load is not served is assessed and projected for different renewable scenarios to understand system adequacy and it specifically highlights the need to improve the flexibility of the thermal fleet.

More complex integration studies consider both electricity and heat networks. Liu *et al.* [2015] considers a integrated electricity and heat network and analyses the performance of the combined networks. Technologies such as combined heat and power (CHP), heat pumps, and electric boilers requires the development of new integrated electricity and heat models to understand the optimal dispatch of heat and electricity [Liu *et al.*, 2015]. Two methods were developed to investigate the performance of the integrated whole heat and electricity network including a decomposed method and an integrated method. The development of these models is important to understand the potential value of thermal energy storage, for example, in future energy systems. The inclusion of other energy vectors into these integrated heat and electricity models would allow for a more enhanced understanding of energy losses, costs, and CO_2 emissions.

The modelling tools used to assess future power systems are now introduced and discussed.

2.7.2 Power system models

There are a large number of modelling tools that are used to assess electricity system requirements covering a range of different time frames and temporal resolutions. An overview of some of these model types are presented.

Economic dispatch models

Generator production costs are minimised and the generation levels of each generator are combined to meet a known demand profile to find the least-cost dispatch schedule. Economic dispatch (ED) models use the incremental costs of generators and unit operational constraints to find optimal generation levels [Wood and Wollenberg, 1996]. Generally, transmission losses are not included in this constrained optimisation problem unless Optimal Power Flow (OPF) is included. OPF models are a sub-type of economic dispatch models which consider power system transmission constraints and losses.

Unit commitment models

The aim of unit commitment (UC) models, in general, is to minimise the production and start-up/shut-down costs of all generating units over an optimisation time horizon. Traditional unit commitment and economic dispatch (UCED) models look ahead and decide which generating units to commit and how much power and spinning reserve to dispatch. The UC problem determines the schedule of thermal power plants after considering the individual units operational characteristics. Certain unit commitment models focus on generation adequacy and reliability. Several metrics are typically used to categorise and assess power systems in terms of reliability, such as the Loss of Load Probability (LOLP), Loss of Load Expectation (LOLE), and Loss of Energy Expectation (LOEE). Extensive academic research has been done in the past to improve the optimality and accuracy of UC methods such as Sheble and Fahd [1994]; Baldick [1995].

More recent UC models have been used to study the impacts of variable renewables on power system operation and CO_2 emissions. Unit commitment models use an objective function most typically to minimise overall system costs including emissions costs, start-up and shut-down costs and ramping costs. Depending on the requirements of the model, objective functions can also be used to maximise profits. Vertically integrated utilities have traditionally used UC models to advise their dispatch strategies over the next 72 hours.

Newer and more recent stochastic UC models simulate variability and uncertainty in systems with large amounts of renewables. Probabilistic forecasting techniques can be used to simulate demand and wind uncertainty on a rolling window basis to clear day-ahead markets and assess intra-day balancing requirements [Ma *et al.*, 2011, 2012]. Sub-hourly UC models have also been used to analyse wind and energy storage systems [O'Dwyer and Flynn, 2014]. In short, there are an extensive number of unit commitment studies with wide ranging applications.

However, very few unit commitment models have been used explicitly to study the impacts on power plant operating patterns.

Capacity planning models

Capacity expansion and planning models include both the operational and investment costs of units and decide when new capacity should be built. Variations of traditional UC models that incorporate capacity expansion include unit construction and commitment (UCC) models that minimises the operational costs of existing units and investment costs of additional units. These UCC models attempt to optimise power system investment and can be used to maintain reliability targets and/or emission targets. They can be employed for both transmission and/or generation capacity planning, however the complexity of modelling both increases substantially [Palmintier, 2013].

2.8 Unit commitment

2.8.1 Background

There are a wide range of approaches when using unit commitment models in electricity system modelling. Typically, unit commitment models attempt to minimise the costs of supplying electricity and reserve services. However, wind power introduces new challenges that affects the unit commitment problem. The addition of CCS also adds a new layer of complexity to the unit commitment optimisation problem. Additional binary decision variables and operational constraints are required for CCS-equipped units.

In traditional power systems, with little or no VRE, power plants with the lowest variable operating costs are dispatched first to meet forecast demand. As demand increases, power plants with higher variable operating costs are then dispatched. Power plants with the highest variable operating costs are typically the most flexible. This meant that in traditional power systems priority lists were a suitable method for committing generators in terms of both cost and flexibility.

Priority lists typically arrange generators according to short-run marginal costs, with the lowest cost generators dispatched first. This pre-determined order is used to commit generators until net demand is met. However, priority lists can also be dynamically ranked in terms of full-load average costs, commitment utilisation [Sheble and Fahd, 1994], or even flexibility. Priority list methods are extremely fast but highly heuristic.

In contrast, exhaustive or complete enumeration methods compute all of the possible unit commitment combinations to find the optimal least-cost solution. Exhaustive methods are

therefore limited to smaller systems with fewer generators because of exponentially increasing dimensionality. The total combinations is calculated by:

$$\text{Total combinations} = (2^G - 1)^T \tag{2.25}$$

There are a large number of other methods for implementing unit commitment problems with various advantages and disadvantages. Detailed descriptions outlining a number of methods are available in Sheble and Fahd [1994] and Bhardwaj *et al.* [2012]. A number of recent unit commitment models and their applications are now critically reviewed.

2.8.2 Unit commitment and optimal investment

Rosso *et al.* [2011] investigates the potential demand-side flexibility and the impacts on the optimal generation mix. An extended unit commitment model is used to examine the operational and investment costs using the IEEE Reliability Test System (RTS-96). Results showed that increasing wind generation requires an increase in flexibility. The available demand side management (DSM) capacity that can provide flexibility is modelled as a fraction of demand in each time period. The committed DSM capacity adjusts the demand profile, a sine wave, by shifting the demand to another time period in the day.

Kirschen *et al.* [2011] also employ the IEEE RTS-96 system and determine the optimal amount of flexibility for a given generation portfolio and installed wind capacity. A unit commitment model is developed to consider both the short-term operational costs and the long-term investment costs. The problem is divided into seasons instead of using a complete time-series of the whole time period. This reduces the computational intensity and allows both the operational and investment costs to be calculated for each season. This assessment, however, only considers four weeks of data to represent a typical winter, spring, summer, and autumn week. This limited amount of data cannot capture the large number of weather events experienced over a typical year. It may therefore not be able to predict the optimal commitment and investment decisions of generators.

Palmintier [2013] uses both the IEEE RTS-96 and the Electric Reliability Council of Texas (ERCOT) systems to demonstrate how flexibility impacts both short-term operating decisions but also long-term planning decisions in future scenarios with large amounts of renewables.

Ma *et al.* [2011] uses an offline index to estimate the required flexibility of a generation portfolio and implements it using a unit construction and commitment (UCC) model. Also considering both the operational and construction costs and the RTS-96 system, this algorithm demonstrates the profits of flexibility using a flexibility metric to quantify flexibility. This work only considers conventional thermal units and wind and so no consideration is paid to energy storage or CCS.

In short, these models try to simulate optimal investment and capacity additions into the future as well as minimising operational costs in the short-term. However, very few models have implemented CCS into the unit commitment problem.

2.8.3 Unit commitment with CCS

Until recently, CCS had not been considered within unit commitment models. Alie [2005] presented a unit commitment formulation that includes CO_2 capture, transportation and storage costs and is implemented in GAMS[6]. The CO_2 capture rate is implemented as a decision variable. However, this analysis is limited to a case study of the IEEE RTS-96 system.

Cohen [2012]; Cohen and Webber [2012] developed a mixed-integer program, also in GAMS, to model several CO_2 capture configurations. A detailed model of a post-combustion capture plant with amines is developed to understand the value of flexible capture operation. A 500 MW coal-fired unit with 7 molal (7m) monoethanolamine (MEA) solvent captures 90% of the CO_2. Detailed costs are assumed for MEA solvent, caustic NaOH, water, waste and reclaimer costs. Additional configurations using solvent storage are also investigated. However, it is assumed that the ramp rate of the modelled power plant is 20 MW/min, which equates to 1200 MW/h, more than double the installed capacity. Ramp rates, in effect, do not constrain power plant operation and therefore have no impact on system operability. The potential operational flexibility of CCS is therefore not fully investigated.

Martens *et al.* [2012] developed a mixed-integer linear program for an USC-PC power plant with PCC. The capture plant can operate dynamically (start-up and shut-down). The start-up costs are a function of the downtime of the power plant. Hot/warm/cold start-ups are modelled with varying start-up times. However, the formulation is only applied to a simple 4 unit system.

Li *et al.* [2015] developed a low-carbon unit commitment model with CCS using a modified New England 39-bus system. A simple relationship describes the capture plant load as a function of the capture rate for CCS power plants. The upward spinning reserve contribution of CCS is modelled, but only under emergency conditions when additional spinning reserve is required to accommodate wind forecast deviations.

Lou *et al.* [2015] incorporated CCS into a unit commitment model to understand the potential spinning reserve provision. A conventional thermal power plant that is retrofitted with CCS, where steam is extracted from the IP/LP crossover, is assumed. Additional LP turbine capacity is assumed to accomodate the increased steam flow during lower capture rates. The reduced net power output is formulated into the unit commitment model and updated generator constraints are described. The CO_2 capture rate for each unit can be optimised to either export additional electricity or provide spinning reserve. A simplified linear relationship describes the power consumption of the CO_2 capture system as a function of the CO_2 capture rate.

---

6. General Algebraic Modeling System (GAMS) modeling language.

2.8.4 Unit commitment with energy storage

O'Dwyer and Flynn [2014] propose a unit commitment model in PLEXOS to examine power plant cycling operations with large amounts of energy storage and wind in Ireland. Energy storage is modelled to reduce operating costs and enhances power system flexibility by time-shifting energy, providing reserve and sub-hourly balancing. The inherent flexibility of energy storage units allows them to ramp much faster than conventional units and provide both reserve and response.

Black and Strbac [2005] used a MIP formulation and a priority list to commit units in a day-ahead market. A linear program was used to dispatch thermal units, wind, and energy storage. Fuel costs are minimised over a full year with committed generators providing power to meet net demand and spinning reserve requirements.

Black and Strbac [2007] implement an updated unit commitment model and present methodology to optimise the allocation of spinning and standing reserve. Wind power forecast uncertainty is estimated using the standard deviations of wind output changes at 1-h and 4-h lead times. In the model, spinning reserve is provided by synchronised thermal power plants such as CCGTs or coal power plants. Standing reserve is provided by energy storage and OCGTs. Standing reserve can only be provided by energy storage units when there is sufficient energy available in the storage volume. Energy storage is able to provide both upwards and downwards standing reserve in contrast to an OCGT power plant which can only provide upwards standing reserve. This allows energy storage to utilise surplus wind and reduce fuel costs. Most of the value of storage comes from accommodating the frequency and smaller imbalances by reducing the proportion of synchronised thermal units providing spinning reserve.

Wen *et al.* [2015] present an enhanced security constrained unit commitment formulation (ESCUC) to capture the fast response operation of utility-scale energy storage for corrective security. After a transmission line outage, utility-scale energy storage units either inject or extract power to restore branch flows so that lines are within power rating limits. This ESCUC model therefore determines the optimal unit commitment and economic dispatch but also the corrective actions that are required to redispatch generators after a contingency event.

2.8.5 Summary and proposed work

This chapter introduced and characterised different sources of generation flexibility and other sources of flexibility such as energy storage, CO_2 capture power plants, wind curtailment, interconnectors, and demand-side management. The reserve requirements needed to manage additional variability and uncertainty from wind are then evaluated and discussed. A review of the different types of power system models and a critical review of recent unit commitment models and their applications that are relevant to this thesis are presented. A number of gaps in the literature are presented and are addressed in later chapters.

Chapter 3 introduces a wind reanalysis dataset that is used to generate high-resolution wind data to study the impacts of wind variability.

Chapter 4 then analyses the potential variability of a portfolio of onshore and offshore wind capacity as a prerequisite for understanding power plant flexibility.

Chapter 5 presents a unit commitment and economic dispatch (UCED) model that includes flexible CO_2 capture power plants and energy storage units. Security constraints for reserve and power plant operating constraints, such as power output limits, ramp rates, minimum up/down times, and start-up times, are formulated to ensure the operational feasibility of dispatch schedules. Detailed reserve and flexibility constraints are also outlined for flexible and non-flexible CO_2 capture units. This method explicitly represents key reserve requirements and considers short-term operational flexibility at hourly time-scales. A heuristic scheduling method is used to improve computational requirements while maintaining high accuracy.

Chapter 6 then investigates the impacts of increasing amounts of wind capacity on the start-up and ramping requirements of thermal power plants, utilising the outputs of the UCED model. The operating regimes of thermal power plants in future power systems are then evaluated to understand the fundamental and structural changes that will impact future generation portfolios with large contributions from variable-output wind power.

Chapter 3

Wind modelling

3.1 Introduction

As the proportion of weather-variable renewables, such as wind, increases within an electricity system, the flexibility requirement of residual generation assets increases. Weather-variable wind generation capacity is characteristically variable as its availability is determined by the passage of large-scale weather systems. It is therefore essential to understand spatial and temporal variations in surface wind speeds in order to understand the impacts of wind power on the power system.

The UK offers a highly informative case study to assess the impacts of wind generation on the power system, since it positioned at the boundary between two convective cells that, at mid-latitudes, causes the UK to experience a wide range of possible weather events, high average wind speeds, and therefore significant wind variability. In addition, the UK has a diverse generation portfolio and significant amounts of baseload capacity (can provide very limited flexibility), limited existing energy storage and hydro capacity, and high renewable targets, most of which will be met by wind capacity. The relatively small size of the UK with limited interconnectivity, generating large amounts of geographically concentrated wind output will offer highly indicative insights to other electricity systems. With aging generation infrastructure and small proportions of energy storage, the flexibility challenge in GB is thought to be more severe than other systems. It is therefore critical that the potential variability and uncertainty in the wind resource is characterised and understood.

The geographical and temporal characteristics of the wind resource are presented in Section 3.2 and examined in order to understand potential wind variability over different timescales. A high-resolution wind speed reanalysis dataset of UK wind sites from Hawkins [2012] is then introduced and described in Section 3.3. A detailed description of the wind speed reanalysis dataset and the Weather Research and Forecasting (WRF) modelling system is provided. Section 3.4 then extends work done by Hawkins [2012] to simulate wind power outputs at existing and proposed wind locations in the future, representing the expected spatial distribution of onshore and offshore wind capacity. This approach takes into account short-term wind speed fluctuations experienced by a group of wind turbines spread across a spatial area, non-linear

electrical losses, wake losses, and the technical availabilities of typical onshore and offshore wind farms. The simulated power outputs at operational onshore and offshore wind farms are then compared with observed historical wind production data in Section 3.6 to validate the methodological approach. This work is then used in later chapters to assess the impacts of wind variability and increasing levels of wind generation on the operating characteristics of the power generation portfolio.

The aim of this chapter is therefore to:

- understand the characteristics of the UK wind resource;
- introduce the wind speed reanalysis dataset of the UK from Hawkins [2012];
- transform wind speeds into power outputs; and
- validate simulated wind power outputs and analyse key sensitivities.

3.2 The wind resource

It is important to accurately simulate the variability in surface wind speeds because of the cubic relationship with the power output from a wind turbine. Understanding the possible sources of variability in the wind resource and the impacts on wind power output is therefore essential. In addition, in order to estimate the mean wind speed at hub-height, a surface roughness length must be assumed for each grid square. This means understanding the underlying forces in the turbulent boundary layer and wind speed profiles close to the surface. This section therefore presents an overview of the meteorological mechanisms that drive the wind resource and define its variability.

The wind resource is primarily driven by differential surface heating and can be characterised in terms of its spatial and temporal variability. As the Earth rotates on its axis, warm air rises, circulates, and sinks towards the surface in cooler regions. Coriolis forces influence the large-scale motion of air which gives rise to a global circulation pattern [Burton *et al.*, 2011]. The varying topography and physical features of land masses and oceans disturbs the circulation of air at smaller regional scales, creating spatial variability between geographical areas. This is illustrated in Figure 3.1 which shows the relatively high average wind speeds experienced in the UK and highlights the terrain effects, spatial distribution, and variability of wind speeds across the UK.

The UK is positioned at the boundary between two convection cells where cold and warm air mix and create a pressure gradient. The varying position of this boundary, or polar front, the jet stream, and the location of Rossby waves[1] causes significant temporal variations in the weather across the British Isles and other regions at mid-latitudes. These weather variations

1. Atmospheric Rossby waves are a major influence on the weather and are associated with pressure systems and the positioning of the jet stream.

occur predominantly because of mid-latitude cyclones when cold air is pulled south and warm air is pulled north around an area of low pressure at the surface [Holton and Hakim, 2013]. These effects cause the availability of the wind resource to vary over different timescales and so understanding these temporal variations is important for wind-based power system studies. The spatial and temporal variations in surface wind speeds are now be discussed in more detail.

3.2.1 Short-term temporal wind variability

Synoptic variations

Synoptic variations vary over time scales from days to weeks and occur because of the passing of high and low pressure systems and weather fronts [Holton and Hakim, 2013]. Synoptic scale processes occur on a horizontal length scale in the order of 1000 km. The temporal frequency[2] of synoptic variations, such as depressions, peaks at approximately 96 hours, see Figure 3.2.

Mesoscale and diurnal variations

Mesoscale variations vary over time scales from hours to days and diurnal variations occur because of surface heating and temperature variations. Mesoscale processes occur on a horizontal length scale between several kilometers to several hundred kilometers. The temporal frequency of diurnal variations peaks at 24 hours. Local thermal effects and intense heating in the day cause the large-scale convection of air in the atmosphere, which reduces in the night. At coastal boundaries, the differential heating between the land and sea also causes diurnal variations in surface wind speeds. The reversal in wind direction each day at coastal boundaries creates a 12-hour diurnal peak.

Microscale and turbulent variations

Microscale variations vary over time scales from seconds to minutes. Wind speeds can be decomposed into a slower moving mean components and turbulent components, referred to as Reynold's averaging or Reynold's decomposition. The spectral gap between synoptic and turbulent processes, can be observed in wind speed spectrums, see Figure 3.2 [Van der Hoven, 1957; Stull, 1988]. This means that low frequency synoptic scale processes can be treated differently and therefore separated from higher frequency turbulent variations. The large spectral peak at turbulent frequencies illustrates the high kinetic energy available from turbulent processes [Burton *et al.*, 2011]. It is therefore common practice to model synoptic processes independently from turbulent variations.

Turbulence is caused by complex and dynamic interactions and friction with the surface; and thermal effects which result in the vertical movement of air masses. The overall level of

2. The temporal frequency is the number of occurrences of a repeating event per unit time.

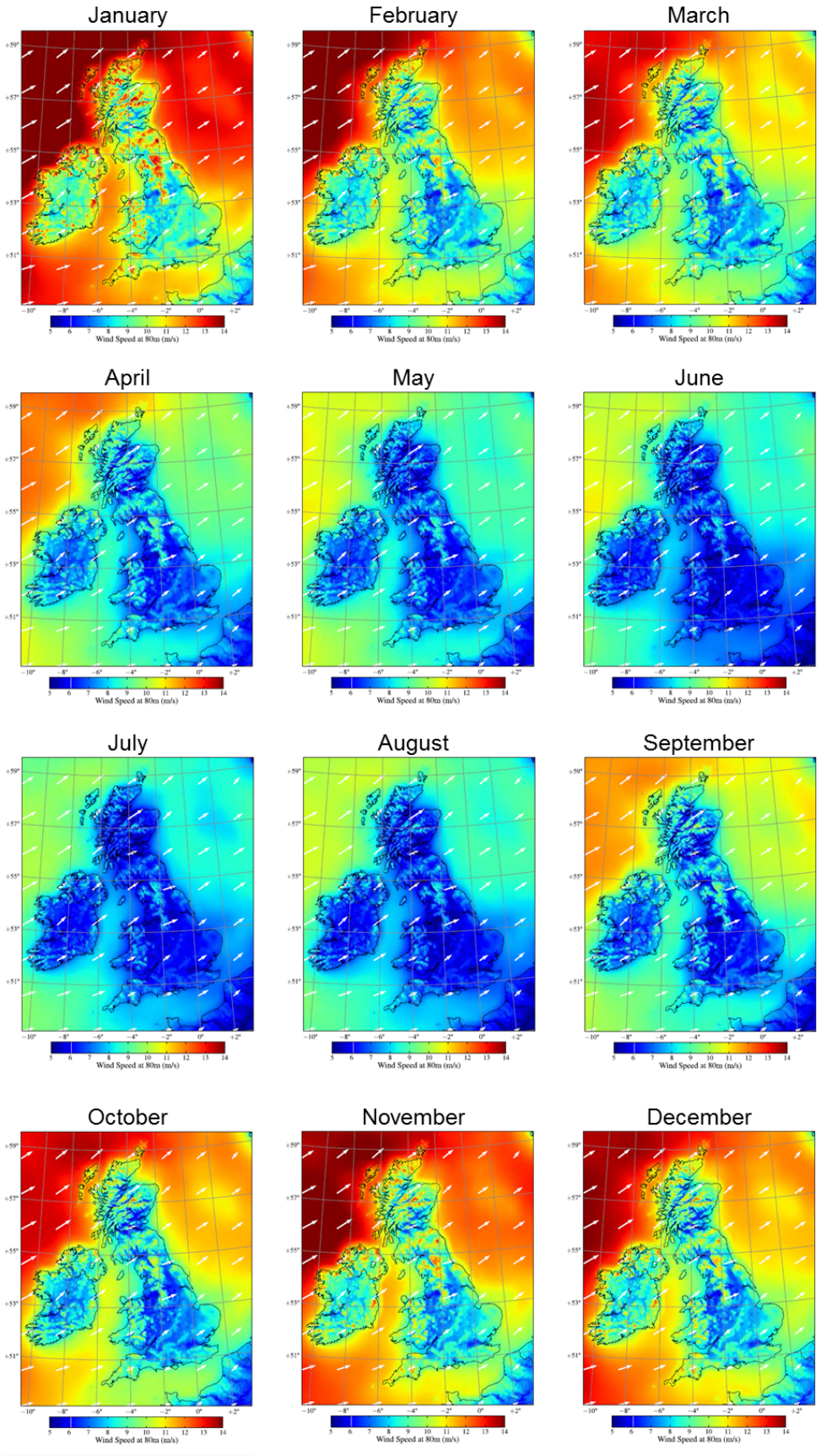

Figure 3.1: Average wind speeds and direction in the UK at 80 m above ground level between January 2000 and December 2010 by month. Adapted from [Hawkins, 2012].

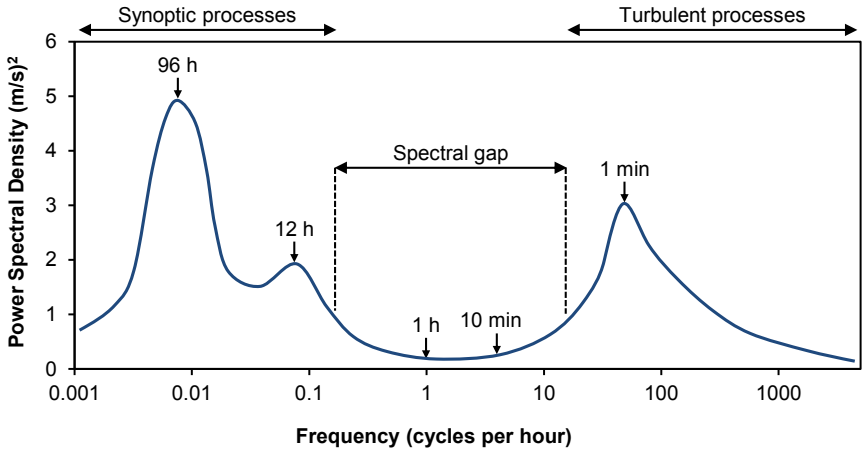

Figure 3.2: Schematic representation of the observed wind spectrum and spectral gap of surface wind speeds based on work from Van der Hoven [1957], adapted from [Martin-Martinez *et al.*, 2012].

turbulence experienced at a wind location, assuming a normal distribution, is known as the turbulence intensity I:

$$I = \frac{\sigma^U}{\overline{U}} \tag{3.1}$$

where σ^U is the standard deviation in the horizontal wind speed (m/s) and $\overline{U}$ is the mean wind speed (m/s) over a time period. The turbulence intensity varies according to the roughness length of the local terrain and height above ground level, and is sensitive to the sampling rate and time period used. As the height above ground level increases and the interactions with surface variations reduce in strength, the turbulence intensity decreases. The turbulence intensity over a geographical area will influence the spread of wind speeds across that location. Whilst turbulent effects have important impacts on the design and performance of wind turbines, three-dimensional turbulent fluctuations and stochastic loads also impact other factors such as the reliability and availability of wind turbines. Wind shear and atmospheric conditions can also significantly impact wind variability and therefore the performance of wind turbines.

Wind shear forces in the planetary boundary layer close to the surface vary over space, time, and height. However, at the surface, in the turbulent boundary layer, the wind speed is zero. Wind speeds increase with height above ground level, but are dependent on the atmospheric conditions and turbulence. The theoretically derived semi-empirical logarithmic wind speed profile in neutral atmospheric stratification conditions is:

$$U(z) = \frac{u_*}{\kappa} \ln\left(\frac{z}{z_0}\right) \tag{3.2}$$

where $U(z)$ is the wind speed (m/s) at height z above ground level (m), u_* is the friction velocity (m/s), κ is von Karman's constant derived from observations of around 0.4, and z_0

is the surface roughness length (m). Here, turbulence is an instability that is generated by the wind shear. Both mean wind speeds and turbulent components are zero at the surface. Neutral atmospheric conditions exist when there is thermal equilibrium between the parcel of air and the surrounding environment and the temperature lapse rate equals the dry adiabatic lapse rate. Monin-Obukhov stability corrections are required for non-neutral stability conditions. The surface roughness length z_0 is the height above the displacement plane where the mean wind speed tends to zero due to surface roughness. Surface roughness lengths can vary according to season (vegetation and crop cycles) and wind direction. However, time- and space-averaged parameters are not able to fully represent the inter-annual, seasonal, and short-term temporal wind speed variations.

3.2.2 Long-term temporal wind variability

There exists very limited historical data to carefully analyse long-term wind speed variations. Consistent and reliable wind speed data is not typically available before 1990 and so alternative datasets have to be used to investigate historic wind speed trends [Atkinson *et al.*, 2009], such as the North Atlantic Oscillation index. There is also limited understanding about the characteristics and trends of future wind patterns. For example, the effects of global wind power extraction and the saturation and geophysical limits of global wind capacity are not fully understood [Adams and Keith, 2013]. In addition, the long-term effects of anthropogenic climate change on surface wind speed profiles requires further research. However, there is an understanding that in current long-term atmospheric predictions that climate change will affect, to some extent, the characteristics of future wind patterns. Therefore, long-term wind speed variations are considered beyond the scope of this work. However, these effects will become increasingly important over the coming decades.

3.2.3 Wind variability at peak electricity demand

It is particularly important to understand the potential contribution of wind generation to peak electricity demand for a variety of operational and system planning reasons. The wind-demand relationship during high and extreme peak demand periods is an area of significant uncertainty. At times of peak electricity demand, a common simplification is to approximate wind speeds as being statistically independent to demand. However, in the UK it has been shown that wind availability typically falls at times of peak demand [Ofgem, 2012, 2014a], but given the limited quantity of historical data during peak demand periods, the trend is not likely to be statistically significant [Ofgem, 2014a]. Therefore, in electricity capacity assessments, it is generally assumed that there is no correlation between wind output and electricity demand to ensure that available capacity is not overestimated [National Grid, 2014a; Ofgem, 2014a]. This is because it is entirely possible for the wind generation across an entire electricity system, such as Great Britain, to be near-zero during peak demand periods. On other occasions it is

also possible that the wind generation at a certain point in time for the same electricity system to be very high at peak demand.

National Grid [2014b] project likely peak demand for the winter ahead using an appropriate temperature variable, sunset time, day of week, and the underlying demand profile [Ofgem, 2014a]. There are several metrics used to assess the wind's contribution to peak electricity demand including capacity value and effective load carrying capability. However, there exists limited historical wind generation and electricity demand data and so close attention must be paid when deriving results about the capacity value of wind.

3.3 Wind speed reanalysis dataset

3.3.1 Introduction

In order to make an assessment regarding the fundamental changes that will occur to electricity systems with the addition of large amounts of wind generation capacity, high-resolution wind speed data is required to capture the spatial and temporal variability.

This work assumes that the use of a high-resolution wind resource model, such as the WRF modelling system in Hawkins [2012], allows for an appropriate method to assess wind generation profiles in the UK. This work uses wind speeds and site information from Hawkins [2012], and then generates wind power outputs using an aggregate power curve approach. This is then used to study the impacts on thermal power plant operating regimes at hourly resolution.

Surface-based wind speed observations from meteorological stations have typically been used in the past for power system studies. More recently, however, modern wind reanalyses have been used to generate wind data. Wind reanalyses are based on advanced numerical weather prediction models and assimilate meteorological observations from an extensive array of sources. Compared to surface wind speed observations, wind reanalyses are able to represent local topography and land-use data and are therefore able to capture complex wind conditions. Furthermore, measurements from meteorological stations may suffer from defects caused by changing equipment and recording practices, which may generate significant biases over long observational periods. Wind renanalyses are also able to generate wind speeds at multiple vertical levels closer to the surface, simulating different atmospheric stability conditions and boundary layer profiles. In contrast, surface-based wind observations require scaling up data points logarithmically and do not account for varying surface wind speed profiles. Wind reanalyses are also capable of covering a region at sufficient temporal- and spatial-resolution over a long period of time.

A number of recent studies also use wind reanalyses to produce wind speed data. For example, Kiss *et al.* [2009] use wind speed estimates provided by the European Centre for Medium-Range Weather Forecasts ERA-40 and compare them with the observed power output from 2

Enercon E-40 wind turbines in Hungary. Calibration was required to match the ERA-40 reanalysis data with the observed power outputs. Kubrik *et al.* [2012] use global NASA reanalysis data and compare it with the metered power outputs from wind farms in Northern Ireland, UK. Ofgem [2012] use NASA's Modern Era Retrospective-analysis for Research and Applications (MERRA) reanalysis dataset to examine wind power output at peak electricity demand. Staffell and Green [2014] also use NASA's MERRA reanalysis dataset which is processed using the Goddard Earth Observing System (GEOS-5) to highlight the performance losses of wind farms with age.

Cannon *et al.* [2015] also use NASA's MERRA reanalysis over a period of 33 years to study the frequency of short-term extreme weather events. A fixed, non-evolving distribution of wind farms is used to examine aggregated hourly wind power outputs for GB. MERRA data is compared with 328 Met Office Integrated Data Archive System (MIDAS) observations between 1980-2011. NASA's MERRA renalysis dataset, however, generates wind speeds in a 1/2 degree latitude and 2/3 degree longitude grid. This represents a grid that is 55 $\times$ 44 km. In addition, wind speeds are only available at 2 m, 10 m, and 50 m heights above ground level meaning additional extrapolation to hub-height is required.

Given the complex geography of certain areas of the British Isles, and the influence of local topography on wind variability, it is important to use wind reanalysis data at high spatial resolution. The study in Hawkins [2012] uses the Weather Research and Forecasting (WRF) modelling system to produce a wind reanalysis dataset at 3 km spatial resolution. Even a spatial resolution of 3 km will not be able to accurately capture complex terrain, such as parts of Scotland, for example, where are a significant proportion of UK wind capacity is likely to be installed.

The extensive wind speed reanalysis dataset developed by Hawkins [2012] at the Institute for Energy Systems, School of Engineering, University of Edinburgh, UK, includes wind speed and directionality data at hub-height at existing/proposed wind locations in the UK, and integrates both static data (land-use and terrain elevation) and dynamic data (temperature, pressure, and other meteorological data). During the model configuration in Hawkins [2012], 28 vertical levels were used to predict the wind speed profile close to the ground and interpolated to provide an accurate logarithmic wind speed profile at 3 vertical levels (10 m, 80 m, and 100 m).

High vertical resolution and a low vertical interpolation distance are important to reduce interpolation errors when verifying wind speeds against observations and transforming wind speeds at hub-height into wind power outputs. Surface layer wind profiles for different atmospheric stability classes are also characterised and surface roughness lengths are used for individual grid squares and are used to accurately calculate surface layer wind speed profiles. Terrain evaluation data at 500 m resolution is used to simulate the topography of each grid square at high-resolution.

The primary advantage of this dataset is that it incorporates the complex relationship between wind patterns, temperature, and other meteorological variables at high-resolution, and includes a large quantity of wind resource data that can be matched with historic electricity demand over the same time period. The wind speed reanalysis dataset contains information on:

- hourly wind speeds (m/s) at the 3 vertical levels (10 m, 80 m, and 100 m), and wind directionality measurements (degrees) for 337 onshore wind sites and 49 offshore wind sites between January 2000 and December 2010;
- locational information including latitudes, longitudes, and distribution network operator;
- operational status such as in operation, under construction, in consent, in planning, or in scoping, and the development round for offshore sites as of June 2012;
- capacity information such as number of wind turbines, turbine rated capacity, turbine manufacturer, and total site capacity; and
- wind site I.D. and timestamp.

In total the reanalysis dataset has 148.9 million data points = 96432 h $\times$ 386 locations $\times$ 4 (3 vertical levels + 1 directionality). Figure 3.3 shows two wind roses illustrating the simulated capacity factor distributions by direction for two wind farms, one onshore and one offshore wind farm. Although hourly wind directionality data is available in the WRF reanalysis dataset for each wind farm, it is not used extensively in this thesis.

Wind farm information comes from the UK Wind Energy Database [Renewable UK, 2015] where a comprehensive list of all the operational and other wind sites that are under construction, consented, in planning, or in scoping is provided. A complete list of all the wind sites and their respective longitudes and latitudes used in this thesis is shown in Appendix A.

The remainder of this section highlights key features of the WRF modelling system used by Hawkins [2012] to compile the wind speed reanalysis dataset and the important assumptions and features that influence the simulated wind speeds that are used later to generate hourly wind power outputs. A complete description of the wind speed reanalysis dataset, modelling approach, configuration, and comprehensive validation/verification can be found in [Hawkins, 2012].

3.3.2 Weather Research and Forecasting (WRF) model

The WRF model is a numerical weather prediction and atmospheric simulation system [NCAR, 2008]. It was initiated as a collaborative partnership between a number of institutions including the National Center for Atmospheric Research (NCAR) and the National Oceanic and Atmospheric Administration (NOAA) [NCAR, 2008; Hawkins, 2012]. It is a next-generation, fully-compressible, non-hydrostatic mesoscale model and data assimilation system that utilises a pressure based terrain-following coordinate system [NCAR, 2008; Hawkins *et al.*, 2011]. The WRF is composed of the WRF Pre-processing System (WPS), which provides the software

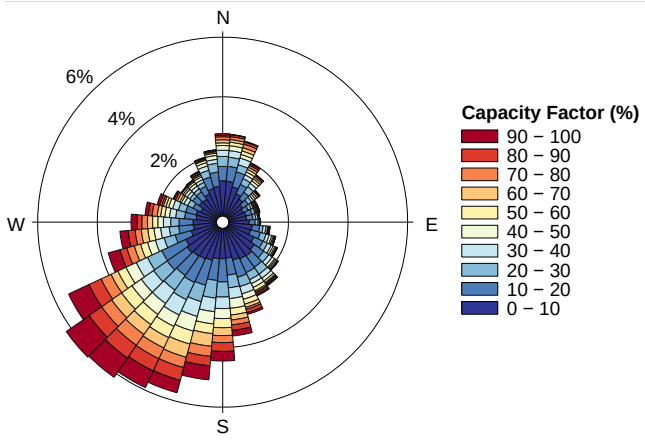

(a) Whitelee onshore wind farm.

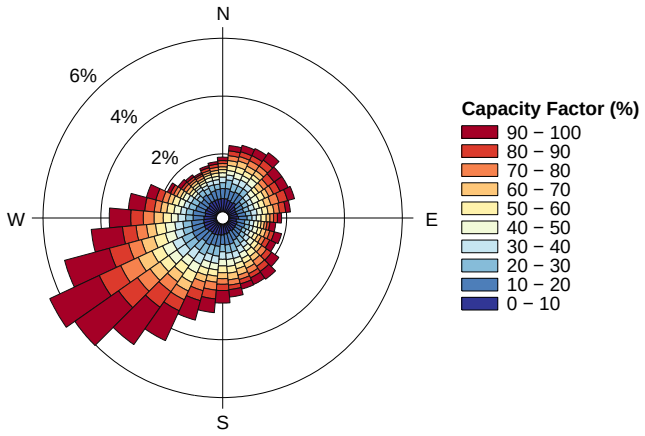

(b) London Array offshore wind farm.

Figure 3.3: Simulated capacity factors by wind direction for Whitelee onshore wind farm and the London Array offshore wind farm.

architecture and infrastructure that accommodates the dynamic solvers and physics packages, and the Advanced Research WRF (ARW) solver, see Figure 3.4 [Klemp *et al.*, 2008; NCAR, 2014].

The Non-hydrostatic Mesoscale Model (NMM) is an additional dynamic solver that can be supported. An explicit time-split integration scheme separates time-steps for different meteorological temporal analysis. It is used extensively in academic studies and is regularly combined with other atmospheric models such as the Wind Atlas Analysis and Application Program (WAsP) for wind energy assessment studies. A further detailed description of the WRF model can be found in [NCAR, 2008; Klemp *et al.*, 2008; NCAR, 2014].

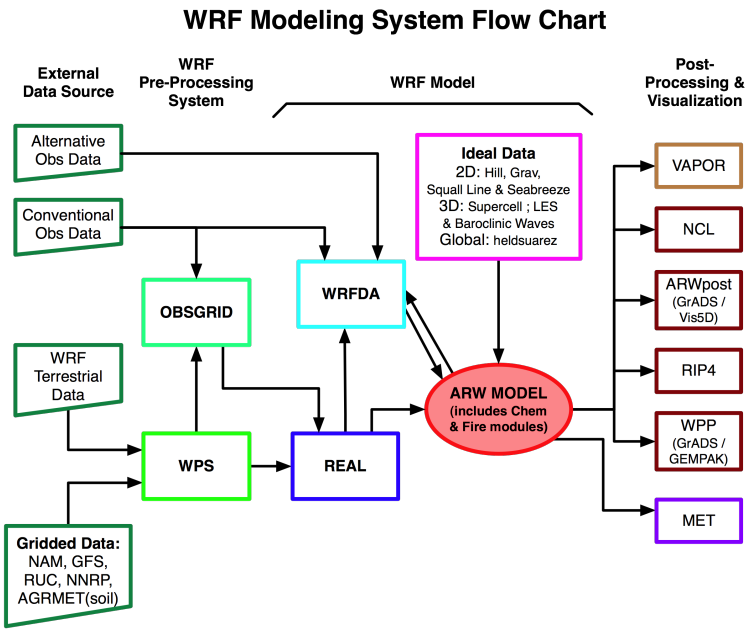

Figure 3.4: Weather Research and Forecasting (WRF) modelling system flow chart [NCAR, 2014].

3.3.3 WRF model configuration

The WRF modelling system integrates both static data (land-use and terrain elevation) and dynamic data (temperature, pressure, and other meteorological data). The modelling system employs US Geological Survey (USGS) land-use data by default which categorises areas in terms of designated parameters such as surface roughness and leaf-area index [NCAR, 2008]. These parameters can be used to determine evapotranspiration rates and the movement of water. Hawkins [2012] uses Shuttle Radar Topography Mission (SRTM) terrain evaluation data at 500 m resolution to simulate the topography of the UK at high-resolution. The High-End Computing Terascale Resource (HECToR) computing platform was used by Hawkins [2012] to process the outputs of the WRF model.

Horizontal resolution

For high-resolution simulations, Hawkins [2012] used three nested domains of increasing horizontal resolution. The model domains were performed at 27 km, 9 km, and 3 km resolution. An integration time-step of 15 s was used in the inner domain at 3 km spatial resolution, with the final output at 1-hour temporal resolution. 331 west-east and 391 south-north cells were used.

Vertical resolution

28 vertical levels were used to complement the high 3 km horizontal resolution. The vertical spacing between levels close the the surface was increased to reduce interpolation errors.

Time resolution

Hawkins [2012] also performed an investigation into the accuracy of the WRF output at 10-minute and 1-hour intervals, concluding that very little information is added to the higher resolution 10-minute time-series, compared to the 1-hour time-series, whilst the data storage requirement increases dramatically. The WRF solver computes Reynold's averaged equations and so it is not possible to simulate higher frequency short-term variations such as turbulent fluctuations, so a 10-minute WRF output is not necessary. Hawkins [2012] therefore concludes that it is therefore reasonable to assume that a WRF output at 1-hour intervals is sufficiently accurate to capture meteorological activity.

3.3.4 WRF model calibration

An extremely large number of in-situ meteorological observations were used by Hawkins [2012] to calibrate the WRF model outputs during the configuration phase. A summary of the observational data used is shown in Table 3.1.

Observation class	Observation type	Data source	Number	Time length
In-situ	MET Office stations	UK MET Office	200	11 years
		MET Eireann	22	11 years
	Wind farm masts	Scottish Power Renewables	3	2 years
		Community Wind Scotland	3	2 years
	Buoys	UK MET Office	4	11 years
		Irish Marine Institute	5	4 years
	Light ships	UK MET Office	4	11 years
	Oil platforms	Shell UK	3	1 month
Remote sensing	Radar profilers	UK MET Office	6	10 years
	QuickSCAT satellite	Ifremer	-	9 years
	ASCAT satellite	Ifremer	0	2 years

Table 3.1: Summary of meteorological observations used to calibrate the wind speed outputs of the WRF model during the configuration phase. Adapted from Hawkins [2012].

The output of the WRF modelling system is a high-resolution and spatially and temporally coherent wind speed reanalysis dataset that captures a large number of historic weather episodes and variations in the UK between 2000 and 2010. This work explicitly differentiates onshore and offshore wind generation, because of the different bid prices that will determine curtailment in future energy scenarios. A detailed description of the methodological process to transform wind speeds into wind power outputs for power system studies is now provided in the next section.

3.4 Transformation to power outputs

3.4.1 Introduction

This section will discuss the engineering fundamentals of wind turbines that are relevant for wind-based power system studies and the dynamic effects that affect the power output of wind farms. Then, the methodology used to transform WRF wind speed reanalysis data into power outputs is presented and discussed. A flowchart of the methodological framework used to transform wind speeds into power outputs is shown in Figure 3.5.

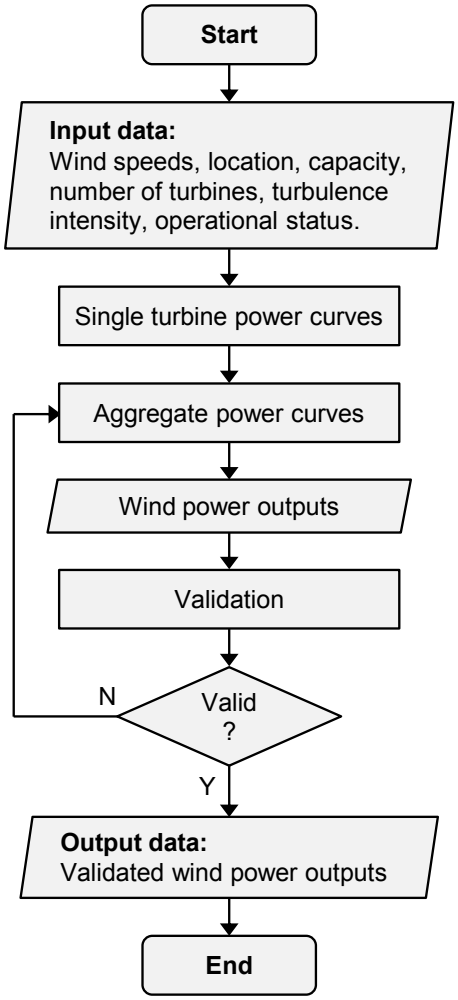

Figure 3.5: Flowchart of wind power output time-series' for each wind capacity scenario.

3.4.2 Data cleaning

First, the WRF wind speed reanalysis data, produced by Hawkins [2012], is cleaned to remove any blank data points. The dataset contains .csv files each representing a wind site in the UK. Each wind site has an associated I.D. and an associated file name (i.e. 100001.csv ...) containing hourly wind speed data displayed as 4 column vectors with wind speeds (m/s) at 10 m, 80 m, and 100 m and wind directionality (degrees), for the years 2000-2010. Of the 386 sites, 337 are onshore and 49 are offshore. A full list of the wind sites and the corresponding longitudes and latitudes can be found in Appendix A. The dataset contains an index containing the operational status of each of the wind projects. The sites are either already in operation, under construction, in consent, in planning, or in scoping [Renewable UK, 2015]. However, since the compilation of the WRF wind reanalysis dataset in 2012, the status of many wind sites may have advanced or changed. For example, wind sites that were under construction are now likely to be operational. For validation purposes, only wind projects operational during or before 2010 are studied as wind speed data is only available up until this time, so changes to the operational status after 2012 does not matter. The exact timing that a wind farm becomes operational is also of little importance in this study. What is of greater importance is where wind farms are located, especially offshore turbines, and therefore close attention is paid to the expected spatial distribution of wind projects in the later part of this chapter.

It was found that there were 36 missing rows of data from each of the 386 .csv files. Timestamp data showed that the missing data was lost or corrupted over two time periods, 17 hours between 31/05/2005 07:00 - 01/06/2005 00:00 and 19 hours 01/05/2005 05:00 - 02/06/2005 00:00. Wind speed and directionality data was missing from all 386 wind sites for the same two time periods. There was little meteorological activity at this time so a linear interpolation was used to complete the missing data points for the two periods, see Figure 3.6.

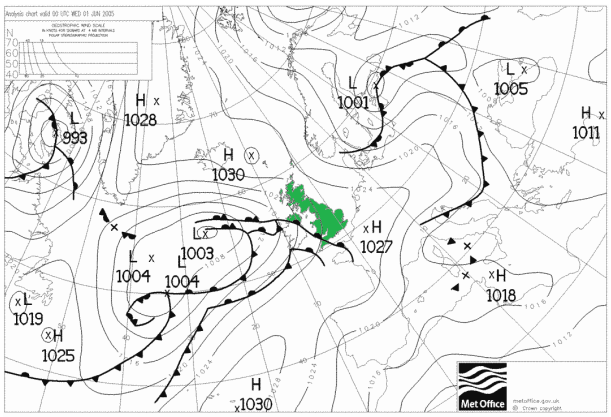

Figure 3.6: Surface pressure chart of NW Europe on 01/06/2005, archived at Wetterzentrale [2015].

An algorithm in MATLAB was then created to read each of the 386 cleaned files and extract the required time-series' with the complete hourly wind speed and directionality data at hub-

height (80 m onshore, 100 m offshore). This allows the use of wind speed time-series' to estimate the power output of each wind farm. However, estimating the power output of a wind farm requires knowledge of the engineering fundamentals of wind turbines and their power conversion characteristics. This is addressed and discussed in the following sections.

3.4.3 Modern wind turbine characteristics

Modern wind turbines convert kinetic energy from surface wind speeds into mechanical work. There are a number of common wind turbine design concepts with different power output functions. Fixed rotational speed induction generator wind turbines are directly coupled to the electricity grid and stall regulated. Variable speed pitch controlled wind turbines use multi-stage gearboxes and variable rotor resistance for power output control. Variable speed wind turbines with doubly-fed induction generators (DFIG) use multi-stage gearboxes and power conversion equipment connected to the rotor windings to achieve power output control. Direct-drive wind turbines use multi-pole synchronous gearless generators and power converters to achieve power output control and reduce mechanical failures.

It is important to understand the mechanical and electrical principles of modern horizontal axis wind turbines before modelling their characteristics. Therefore a short description of the fundamental engineering principles of wind turbines and power conversion is provided here.

The kinetic energy available in the air depends on the swept area A of the blades, the mass of air, and the velocity of the column of incident air. The power in the air at time t is therefore:

$$P_t^{\text{air}} = \frac{1}{2}\rho A U_t^3 \tag{3.3}$$

where ρ is the density of air (kg/m^3), A is the rotor swept area (m^2), and U_t is the incident wind speed (m/s) at time t, see Figure 3.7. The proportion of power that can be transferred from the air to the wind turbine rotor is reduced by the power coefficient C_P. This gives the power output P_t (MW) of an individual wind turbine by the equation:

$$P_t = C_P \frac{1}{2}\rho A U_t^3 \tag{3.4}$$

The power coefficient C_P of a modern horizontal axis wind turbine describes the fraction of the total power available in the column of incident wind that can be converted into mechanical work [Burton *et al.*, 2011]. The upper limit of the power coefficient is known as the Betz limit with a maximum theoretical value of:

$$C_{P,\max} = 0.593 \tag{3.5}$$

The power coefficient of individual turbines varies according to the tip speed ratio. Optimising

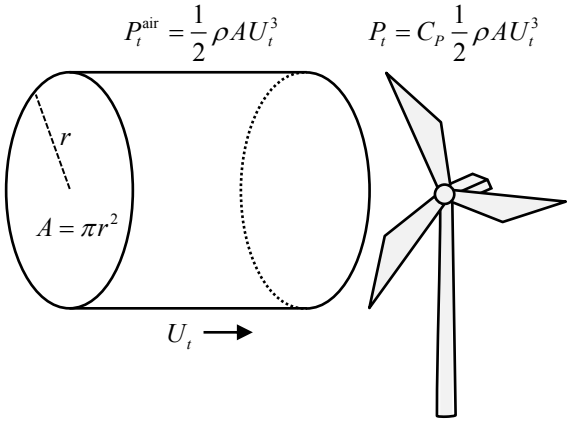

Figure 3.7: Kinetic energy available in the wind.

the power coefficient requires operating wind turbines at variable speed and therefore maximising the achievable power coefficient over the design range of wind speeds. The normalised power output or capacity factor of a wind turbine or farm can be described as:

$$CF_t = \frac{P_t}{P_{\max}} \tag{3.6}$$

where CF_t is the capacity factor, and $P_{\max}$ is the rated power output of the wind turbine or farm (MW).

Wind turbine power curves describe the relationship between the incident wind speed U_t and the power output P_t of a wind turbine over a range of wind speeds. Some key factors of wind turbine design including factors that affect the shape of wind turbine power curves are now outlined and discussed.

Pitch control

Stall regulated wind turbines utilise passive, or sometimes active, stall control to limit power output above the rated wind speed U^{rated}, reducing the lift coefficient and increasing the drag coefficient. However, most modern wind turbines are pitch regulated and maintain power output above the rated wind speed U^{rated} by reducing the blade angle of attack and lift coefficient [Burton *et al.*, 2011]. Pitch regulated wind turbines achieve active pitch control and even have the capability to control active power output as a response to changing grid frequency [Cardinal and Miller, 2006; Muljadi *et al.*, 2012]. Controlling the pitch allows the wind turbine to react rapidly to localised gusts.

Variable speed operation

Fixed speed wind turbines with induction generators are directly coupled to the electricity system whereas variable speed wind turbines decouple the relationship between the rotational speed of the wind turbine and generator from electricity system frequency. The power output of fixed speed wind turbines varies with turbulent fluctuations in wind output, increasing the short-term variability and decreasing power quality. Fixed speed wind turbines with induction generators require reactive power during start-up, which is provided by the network.

Variable speed wind turbines maintain peak aerodynamic efficiency or power coefficient $C_{P,\max}$ below the rated wind speed U^{rated}, and therefore maximise the energy captured. Variable speed turbines also control torque and therefore reduce mechanical loads and reduce noise in low wind speeds with noise reduction algorithms. It is also theoretically possible for these turbines to control both active and reactive power and therefore power factor [Thiringer and Petersson, 2005]. Variable speed wind turbines with full power conversion synchronise using frequency converters. There are a number of turbines designs that achieve variable speed operation including broad range variable speed or full power conversion turbines; and narrow range variable speed turbines with doubly-fed induction generators (DFIG) [Burton *et al.*, 2011]. Broad range full power conversion turbines use two fully rated frequency converters through an AC-DC-AC connection.

Braking

Mechanical braking systems and blade pitch control algorithms are generally used in modern wind turbines to regulate power output and avoid runaway conditions [Muljadi *et al.*, 2012].

Inertial and frequency response

Wind turbines provide very little inertia per unit of capacity compared with large conventional thermal power plants that are online and synchronised with grid frequency. The large rotating mass in the turbine shafts of large thermal power plants provides the system with inertia, which lowers the rate of change in system frequency after a disturbance [National Grid, 2013]. Wind generation displaces large conventional power plants and may therefore reduce system inertia and possibly risk increasing the maximum rate of change in frequency after a negative frequency deviation. There are few power systems with grid codes that require generators to provide an inertial response after a frequency deviation.

However, where fixed speed wind turbines cannot control inertial response, pitch regulated, variable speed wind turbines are able to adjust active power output and provide a controlled inertial and frequency response for up to 10 s. This can contribute to frequency stabilisation and fast transient frequency support after a large frequency drop [Muljadi *et al.*, 2012]. Wu and Infield [2012] demonstrated a probabilistic approach to assess the frequency support and

inertial response from a wind farm with time-varying probabilistic wind speeds, aggregating the contributions of individual turbines operating under different conditions. It is shown that wind farms are capable of providing an emulated inertial response, although the amount of kinetic energy available for extraction depends on wind speed. Wind turbines have to decelerate and reduce power output to release the stored kinetic energy, which is necessary to avoid stall conditions. This may therefore increase the system frequency recovery time.

3.5 Power curves

3.5.1 Single wind turbine power curves

Various wind turbine design concepts have different power curves. Variable speed wind turbines are the most predominately used wind turbine technology at present. The following work will describe the wind-to-power conversion characteristics of variable speed wind turbines.

The power output P_t of a variable speed, pitch regulated wind turbine over a range of wind speeds can be expressed mathematically as:

$$P_t = \begin{cases} 0 & \text{for } U_t < U^{\text{cut-in}} \\ f^{\text{rated}} & \text{for } U^{\text{cut-in}} \leq U_t < U^{\text{rated}} \\ 1 & \text{for } U^{\text{rated}} \leq U_t < U^{\text{cut-out}} \\ 0 & \text{for } U_t \geq U^{\text{cut-out}} \end{cases} \tag{3.7}$$

where f^{rated} is a function that describes the power output of a wind turbine between the cut-in wind speed $U^{\text{cut-in}}$ and below the rated wind speed U^{rated}. It is possible to represent f^{rated} as a continuous function with a high-order polynomial (for example a 6th order polynomial).

When wind speeds at hub-height are below the cut-in wind speed $U^{\text{cut-in}}$ there is zero power output. Above the cut-in wind speed $U^{\text{cut-in}}$ and below the rated wind speed U^{rated}, the power output increases proportionally to the cube of the incident wind speed, see Equation 3.4. Between the rated wind speed U^{rated} and the cut-out wind speed $U^{\text{cut-out}}$ the normalised power output is 1, see Equation 3.7. When wind speeds exceed the cut-out wind speed $U^{\text{cut-out}}$ the power output is 0. The power curves for a range of onshore and offshore wind turbines are shown in Figure 3.8.

However, when attempting to determine power output of a wind farm, it is not possible to simply use a power curve for a single wind turbine then extrapolate the power output by multiplying a single turbine power curve by the number of wind turbines. Instead, when considering the power output from a group of wind turbines spread across a spatial area, there are a number of complex and dynamic effects that influence the aggregate power output. These influences and their impact on the aggregate power curve of a wind farm will now be discussed.

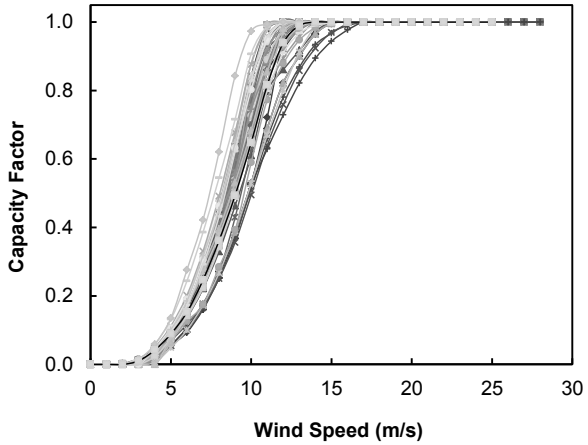

Areva M5000
AWE 52-750
AWE 52-900
AWE 54-900
Doosan WinDS3000
Enercon E33/330
Enercon E44/900
Enercon E48/800
Enercon E53/800
Enercon E70/2300
Enercon E82/2000
Enercon E70/E4
Enercon E126/7500
Enercon E82/2300
Enercon E101/3000
Enercon E82/3000
GE Energy 1.5sl
GE Energy 2.5xl 100
GE Energy 2.5xl 103
Hyundai AV928
Mitsubishi MWT-100-2.4
Mitsubishi MWT-102-2.4
Mitsubishi MWT-95
Mitsubishi MWT-92
Nordex N90/2500 HS
Nordex N90/2500 LS
Nordex N90/2300
Nordex N90/2500 HS Offshore
Nordex N90/2500 LS Offshore
Nordex S82
Nordex N100/2500
Nordex N80/2500
Siemens SWT-2.3-82 VS
Siemens SWT-2.3-93
Siemens SWT-2.3-101
VestasV80/2000
Vestas V80/2000 Offshore
Vestas V80/2000 Grids.
Vestas V90/1800
Vestas V90/1800 Grids.
Vestas V90/2000
Vestas V90/2000 Grids.
Vestas V112/3000 Offshore
Vestas V112/3000
Vestas V100/1800
Vestas V100/1800 Grids.
Samsung 25s

Figure 3.8: Wind turbine power curves for a number of onshore and offshore wind turbines from Carrillo *et al.* [2013].

3.5.2 Aggregate wind farm power curves

There are many approaches that have been taken to modify a power curve to take into account for the losses that occur at real wind farms. The most simple is to utilise an individual manufacturers' wind turbine power curve and scale up by the number of wind turbines. However, this approach ignores losses throughout the wind array and then applies a loss factor to reduce and calibrate ideal power outputs so that they correlate with observed measurements and long-term historic averages.

A site-by-site analytical approach that accounts for wind array losses using computational fluid dynamics (CFD) models can also be used to determine the aggregate power output as a function of wind speed and direction. However, this approach is extremely complex and computationally expensive and is not possible without detailed information about turbine layout and physical site features. Whilst this approach offers the most realistic and accurate method to predict losses, modelling operational and future wind farms individually is not feasible for power system studies considering the large number of wind sites.

Multi-turbine aggregate power curves, on the other hand, offer an appropriate representation of the power output of a wind farm as a function of wind speed that takes over a spatial area. They provide a more accurate representation of the power output from a wind farm whilst avoiding the computational cost of performing CFD simulations on a site-by-site basis. The approach was proposed first by Norgaard and Holttinen [2004] and used extensively in many wind-based power system studies such as Poyry [2009]; Ofgem [2012]; Staffell and Green [2014].

Ummels [2009] uses a normal distribution function to represent the wind speed deviations to produce location-dependent power curves based on local standard wind speed deviations and the physical dimensions of the park. Wake losses are ignored and therefore annual energy yields are expected to be different. Hayes *et al.* [2010] for example, uses field measurements to create and validate an aggregate-measured power curve for two wind arrays in the UK and Italy.

An important feature of multi-turbine aggregate power curves is that they account for turbulence intensity and the spread of wind speeds experienced across a wind site. This offers a more appropriate method to convert wind speeds into power outputs. Within this study, UK sites are characterised and represented to account for turbulence, without having to perform high-level CFD simulations of individual wind arrays. The process of creating a multi-turbine aggregate power curve to represent the power output of a typical UK wind farm is now presented.

Consider an array of wind turbines distributed across an area. Some wind turbines might experience slightly higher or lower than average speeds depending on the variation in wind speeds across the site. The larger the spatial area, the larger the standard deviation in wind speeds. This can be modelled using a wind speed probability distribution function. For example, when the site average wind speed is just below the cut-in wind speed $U^{\text{cut-in}}$, it is expected that some wind turbines will be producing a small amount of power.

Wind farms are typically designed to minimise wake losses in the prevailing wind direction, so, as average wind speeds across a wind site increase, the first row of turbines facing the prevailing wind will extract kinetic energy at the rotor disk first, causing a reduction in wind speed downstream of the first row and an increase in the turbulent fluctuations in the short-term mean wind speed. The loss in wind power output throughout the site caused by this effect is called the wake loss. Additionally, at higher average wind speeds just below the cut-out speed $U^{\text{cut-out}}$, turbulent gusts might activate the storm control mechanism causing individual turbines to shut down. This will cause the aggregate power output of the wind site to drop before the short-term average wind speed reaches the cut-out speed $U^{\text{cut-out}}$. Electrical losses within the wind farm will also compound together and reduce the net electrical power output.

The available power output $P_{f,t}$ of wind farm f at time t within a geographical area is the summation of the individual power outputs $P_{i,t}$ from each turbine i, where $i = 1,2,3,...,I$ and is represented by the equation:

$$P_{f,t} = \sum_{i=1}^{I} P_{i,t} \tag{3.8}$$

There are a number of influences that impact the power output of a wind farm that must be considered before attempting to estimate the aggregate power output of a group of wind turbines. A non-exhaustive list of the influences include:

- short-term wind variations
  - turbulence intensity
  - wind shear profile
- storm control strategies
- wake losses
- technical availability
  - component and turbine reliability
  - planned, preventive, and predictive maintenance
  - access for maintenance
  - turbine aging
  - de-rating
- electrical losses
  - resistive losses in cables, converters, transformers and other electrical equipment
- mechanical and control system losses
  - mechanical sub-optimal performance and misaligned components
  - sub-optimal control systems
- environmental
  - icing, insects, and dirty blades

The main influences that affect wind array losses and the aggregate power output of a wind farm are now discussed in more detail.

Short-term wind variations

Turbulent short-term wind speed variations and changes in wind direction can affect the power output of a group of wind turbines. For example, atmospheric stability conditions and the turbulence intensity of a wind site are reported to impact the shape of aggregate power curves [Harman, 2012]. The turbine thrust coefficient determines the momentum extracted from the wind. When wind speeds are low, the thrust coefficient is high, implying that a large amount of momentum is extracted, reducing wind speeds downstream. Quarton and Ainslie [1989] proposed an empirical formula to describe the additional turbulence I_+ produced by the rotor downstream of a wind turbine:

$$I_+ = 4.8 C_T^{0.7} I_0^{0.68} (x/x_n)^{-0.57} \tag{3.9}$$

where C_T is the thrust coefficient of the wind turbine, I_0 is the ambient turbulence intensity at that location, x is the distance downstream of the turbine (m), and x_n is the length of the near wake region [Burton *et al.*, 2011].

It is important to consider the additional turbulence created by wind turbines within a wind farm, as this will compound with ambient turbulent fluctuations. Hassan [1992] proposed an improved empirical formula to describe the added turbulence intensity, although analysis by Chamorro and Porte-Agel [2009] demonstrates that in the far wake region the added turbulence shows good agreement with the results reported in Quarton and Ainslie [1989].

The aggregate power output at wind speeds just below the rated wind speed U^{rated} decreases with increasing turbulence intensity, which can be around 2% of total power output with a turbulence intensity between 14-20% [Harman, 2012]. A number of technical studies including Kaiser *et al.* [2007]; Tindal *et al.* [2008]; Rareshide *et al.* [2009]; Antoniou and Pedersen [2009]; Kooijman [2012] have shown how turbulence intensity and wind shear both affect wind turbine power curves. For example, Rareshide *et al.* [2009] illustrate a diurnal relationship between turbulence intensity and wind shear, with a diurnal peak in turbulence intensity during the day.

Storm control strategies

Manufacturers have different storm control strategies that determine the wind speeds for turbine shut-down and restart. Very high wind speeds occur extremely infrequently and so simulating the exact storm control strategy is not essential. However, the cut-out speed $U^{\text{cut-out}}$ for most modern wind turbines is generally around 25 m/s for onshore turbines and is estimated to be between 25-30 m/s for offshore wind turbines.

Pitch-regulated wind turbines can adjust the blade angle to regulate power output. When wind speeds exceed the cut-out speed $U^{\text{cut-out}}$, the blade angle can be adjusted so that blades are

fully pitched towards the incident wind to stop generating electricity. In extreme cases, this may occur quite rapidly, with all wind turbines throughout a geographical area cutting-out at similar times, resulting in a sudden drop in generation. Work reported by National Grid [2013] is being undertaken to ensure that the sudden and widespread loss of wind power output is minimised under these extreme circumstances, possibly by a coordinated gradual ramp-down in wind power output before a widespread and rapid cut-out occurs.

Wake losses

Wind farms operating at mean wind speeds below the rated wind speed U^{rated} may experience large wake losses [Burton *et al.*, 2011]. The increased turbulence and the steep gradient of the power curve just below the rated wind speed U^{rated} means that a small reduction in wind speeds can potentially result in a large reduction in power output for a wind turbine downstream. Deep within a wind farm, this becomes more complex. The superposition of multiple upstream wind turbine wakes can dramatically reduce wind speeds and increase turbulent variations. Therefore wake losses disproportionately affect the aggregate power output of a wind array at wind speeds where the power curve is steepest. The spacing and positioning of wind turbines within an array with respect to the prevailing wind direction will also impact wake losses. Regularly ordered turbines within an array may suffer large wake losses in certain narrow directions when the wakes of downstream turbines compound directly down a row. Figure 3.9 illustrates one example of how this can occur in offshore wind farms. An accurate assessment of wake losses throughout a wind array as a function of wind speed requires high-level CFD simulations.

Figure 3.9: Wake effect at Horns Rev 1 offshore wind farm. Photograph by Christian Steiness.

Wakes in offshore arrays are assumed to exist for longer and more extended periods of time

due to the lower turbulence intensities experienced offshore. However, very little data about offshore wake effects is available. Where data is available, it is for offshore wind sites close to the coastal boundary where atmospheric stability conditions are different from farms further offshore. In short, the wake losses of offshore arrays are not fully understood.

A study by Barthelmie and Jensen [2010] examines the wake losses of an offshore wind array under different stability conditions, wind speeds, and directions. It shows the spatial variability of wake losses and therefore power output throughout the 165.6 MW offshore wind array. Wake losses are least under unstable stability conditions at wind speeds between 5-6 m/s and highest for stable stability conditions between 9-10 m/s. The study also highlighted the immense difficulty of obtaining confidential and sensitive offshore wind data, with the results presented in a way that hides the overall wind farm efficiency.

Estimates vary but wake losses at hub-height for a number of onshore and offshore wind farms of different sizes and spacing have been reported to be between 5-15% by a number of sources [Barthelmie *et al.*, 2004; Sorensen *et al.*, 2006, 2008; Johnson *et al.*, 2009; Phillips *et al.*, 2010; Ali *et al.*, 2012; Schallenberg-Rodriguez, 2013].

In the absence of detailed information about the impacts of wind direction on the power output of all the proposed locations in the wind reanalysis dataset, it is assumed that the wind array efficiency[3] is the same across all wind directions. Although wind directionality data is available in the wind reanalysis dataset, it is beyond the scope of this work to estimate wake losses as a function of wind direction for each wind site. This would require detailed CFD simulations and information about the positioning and layout of individual turbines, local topography etc. Therefore it is reasonable to assume an isotropic wind direction probability distribution throughout the array and constant wake losses as a function of wind direction.

Estimating the wake losses as a function of wind speed for a typical onshore and offshore wind farm is, however, very difficult. A study by Sorensen *et al.* [2006, 2008] evaluated the Horns Rev offshore wind array and examined the wake losses as a function of wind speed. The average wake losses of Horns Rev as measured in all directions were reported to be 20-25% between 5-10 m/s reducing to 0% at 15 m/s, using the N.O. Jensen Park model and a wake decay constant of 0.04. The wake losses as a function of wind speed were demonstrated to be very sensitive to wind direction, although all of the observations showed a similar trend as a function of wind speed.

Hayes *et al.* [2010] describes an aggregate power curve and the per-unit array losses based on measured values for two onshore wind farms. Here, a single turbine power curve is transformed using per-unit adjustments to account for wake losses. Hawkins [2012] also uses per-unit adjustments to account for wake losses. Aggregate power curves were adjusted by ± 1.3 m/s

3. The wind array efficiency or the relative power output is the average power output of the wind array (per turbine for a known wind speed) divided by the power output of a individual wind turbine without wake losses.

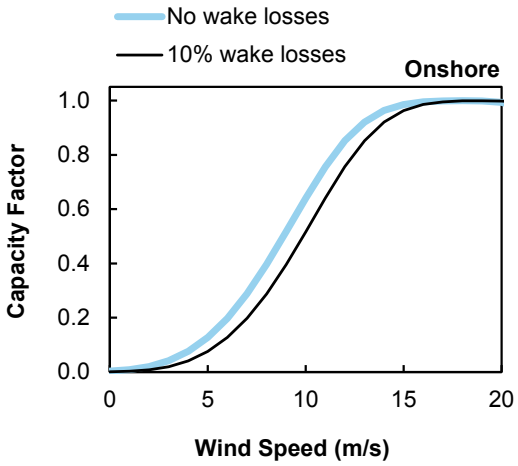

Figure 3.10: Illustrative onshore aggregate power curve with 10% wake losses as a function of wind speed.

between cut-in and rated wind speeds to study the sensitivity of wake losses. It was also found that increasing or decreasing wind speeds by 1.3 m/s changed the averaged capacity factors by $\pm 10\%$. Given that the thrust coefficient of a wind turbine is relatively constant between 4-10 m/s, the wake induced wind speed reductions between 4-10 m/s should also be equal. These adjustments give similar results that are consistent with observations for offshore wind farms reported in Sorensen *et al.* [2006, 2008]. It is therefore reasonable to assume that other wind arrays will experience similar wake induced losses as a function of wind speed.

This work assumes that typical wind farms will experience wake array losses that will reduce the annual energy yield by 10%. Aggregate power curves are adjusted between cut-in and rated wind speeds to reduce the annual energy yield. Figure 3.10 shows an aggregate power curve of a wind farm that has been adjusted to account for average wake losses, with a 10% reduction in energy yield over the period of one year. This approach does not change the gradient of the power curve and is therefore not expected to have an impact on simulated wind variability. Validation of the rate of change in wind power output is demonstrated in Section 3.6.3.

Technical availability

The technical availability of a wind farm depends on many factors including the frequency and duration of electrical-mechanical problems; component-material failures; corrective, planned, preventive, and predictive maintenance schedules; and extreme weather conditions. The time-weighted technical availability defines the number of hours per year that a wind turbine or farm is available, for example 98% availability = $0.98 \times 8760.0 = 8584.8$ h. The energy-weighted availability uses both the actual energy generated and the expected energy generated, which takes into account the importance of availability during high wind periods. For the remainder of this work, it is assumed that the technical availability is time-weighted, however Conroy

et al. [2011] argue that there are reasons to use energy-weighted availabilities so long as the wind farm developers have monitoring equipment to measure wind speed and SCADA data[4].

One approach to measure the technical availability of wind turbines is the Mean Time To Failure ($MTTF$), or $1/\lambda$ where λ is the failure rate, and the Mean Time To Repair ($MTTR$), or $1/\mu$ where μ is the repair rate. This is a metric which measures the reliability of wind turbines. The Mean Time Between Failures ($MTBF$) = $MTTF$ + $MTTR$ + time delay. A time delay to repair may occur because of logistic, supply, and administrative delays. A simple representation of the time-based technical availability A_t is:

$$A_t = \frac{MTTF}{MTBF} < 1 - \frac{\lambda}{\mu} \tag{3.10}$$

The inherent availability A_i as seen by maintenance personnel is:

$$A_i = \frac{MTTF}{MTTF + MTTR} = 1 - \frac{\lambda}{\mu} \tag{3.11}$$

which excludes planned, preventative, and predictive maintenance, and time delays. The Mean Time Between corrective, planned, preventive, and predictive Maintenance $MTBM$, and the Mean Active Maintenance Time $MAMT$ define the achieved availability A_a as:

$$A_a = \frac{MTBM}{MTBM + MAMT} \tag{3.12}$$

which includes corrective, planned, preventive, and predictive maintenance, but excludes time delays. Including all forms of corrective, planned, preventive, and predictive maintenance and time delays, the technical availability A_t becomes:

$$A_t = \frac{MTBM}{MTBM + MDT} \tag{3.13}$$

where MDT is the Mean Down Time. These expressions of availability do not include the periods when the electricity system is unavailable.

Typical values for onshore wind farm technical availability are around 98% [Greenacre *et al.*, 2010; Greenacre, 2012; Harman, 2012; Kaldellis and Zafirakis, 2013] in the UK and Europe. The Crown Estate have leased areas for commercial offshore wind development in rounds. These are Round 1, Round 2, Round 3, and Scottish Territorial Waters (STW). Early offshore Round 1 fleet technical availability has been reported to be 80.3% [Feng *et al.*, 2010], considerably lower than the observed technical availability of onshore turbines in the UK.

The technical availability is also likely to fall with increasing distance from maintenance centres [Carbon Trust, 2008], which is likely to be more severe for offshore farms, where access

4. SCADA (supervisory control and data acquisition) enables users to monitor and control remote operations and wind turbines in real-time

for maintenance is more difficult, increasing the time delay to repair. In addition, the limited maintenance experience, harsher offshore environment, and reduced access for maintenance, are all reasons the technical availability of offshore wind farms is less than onshore. However, it is likely in the future that improved component-material reliability, remote condition monitoring, and advanced predictive and preventative maintenance strategies might help increase technical availability.

Most power system studies, however, assume a constant technical availability throughout the year [Poyry, 2009; Ofgem, 2012; Staffell and Green, 2014], although it is likely that the failure rate and therefore technical availability will show some variability with the season. However, Hawkins [2012] demonstrated that the impact of seasonal variations in technical availability for wind farms is small and has little impact on capacity factors, so the use of a constant technical availability appears to be a reasonable approach.

Kaldellis and Zafirakis [2013] demonstrates an approach to calculate the technical availability as a function of wind speed, which takes into account the relationship between higher wind speeds and an increased failure rate. However, the technical availability as a function of wind speed is likely to be highly site specific and vary between turbine manufacturer, weather conditions, and maintenance strategies. There is a limited amount of data regarding the variation and seasonality of the technical availabilities for onshore and offshore UK wind farms. Estimating the technical availability or the failure rate of wind turbines as a function of wind speed is therefore both unnecessary and beyond the scope of this work.

For flexibility studies, it is the variability and uncertainty of wind output that is important. Since the technical availability will not adjust the shape of the power curve, the exact value is not important. Technical availabilities should therefore be selected so that simulated capacity factors match long-term published data. Another important requirement for scenario analysis is to be internally consistent. Therefore a fixed technical availability for onshore and offshore wind will be selected after a sensitivity analysis and comparison with observed historical wind data.

Electrical losses

Electrical losses through the site will be compounded at the point of connection. Resistive losses in on-site transmission cables, power electronics, converters, transformers, and other electrical equipment typically incur losses of approximately 2% of annual energy production [Manwell *et al.*, 2009]. Wan *et al.* [2010] measured the electrical losses as a function of the gross power output at the point of connection for a typical onshore wind farm. The electrical losses are proportional to the square of the current, plus any fixed losses (for example transformer no-load losses). Colmenar-Santos *et al.* [2014] also describe methodology to calculate the electrical losses as a function of wind speed and report the annual energy losses for wind sites with different Weibull parameters. For an onshore wind farm with typical mean wind

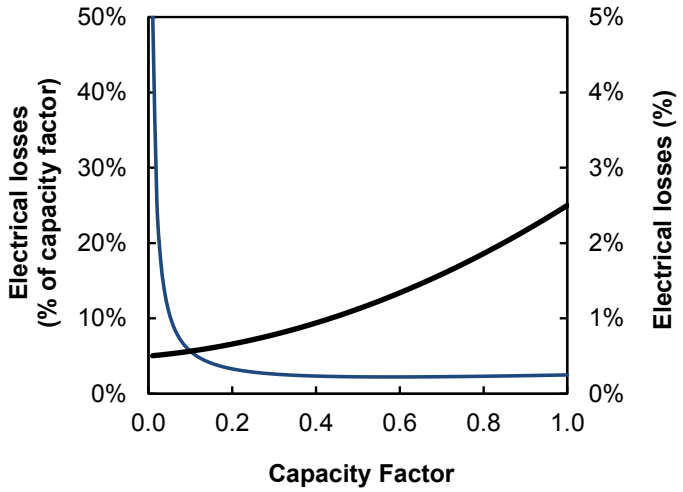

Figure 3.11: Electrical losses in a typical wind farm. Adapted from Wan *et al.* [2010]; Colmenar-Santos *et al.* [2014].

speeds this corresponds to approximately a 2% reduction in annual energy production, similar to values reported by Manwell *et al.* [2009]. It is expected that most wind farms will display similar on-site electrical loss characteristics as the electrical equipment and length of transmission cables connecting turbines and on-site transformers to the point of connection[5] are typically very similar [Wan *et al.*, 2010; Green *et al.*, 2007]. The typical electrical losses for a wind farm as a function of the capacity factor or gross power output is shown in Figure 3.11.

This work assumes that the electrical losses of typical wind farms will be in the order of 2% of the annual energy yield [Manwell *et al.*, 2009; Wan *et al.*, 2010; Colmenar-Santos *et al.*, 2014]. A second-order polynomial is used to represent the electrical losses, which are proportional to the square of the current plus a fixed term to represent ancillary equipment losses as in [Manwell *et al.*, 2009; Wan *et al.*, 2010]. Subtracting the electrical losses from the gross capacity factor at time t of each wind farm gives the net capacity factor.

Mechanical and control system losses

Mechanical losses can occur because of sub-optimal performance and misalignment of components. For example, sub-optimal control systems that adjust blade pitch or yaw inclination angle may also result in losses. A decrease in the power output with yaw inclination angle error has been reported by Harman [2012] that may impact the shape of multi-turbine power curves. Yaw misalignment correction and optimisation can improve yaw errors and performance losses.

5. The point of connection is where the wind farm power collection system connects with the distribution network. The point of common coupling, however, is the nearest point to which other customers connect to the network.

Turbine aging

It is reported by Staffell and Green [2014] that turbine aging decreases the technical availability, losing about 1.6% output per year, which is consistent for different generations of wind turbines and turbine designs. An efficiency loss of this order is typical of any rotating mechanical device. However, for the purpose of this study, the performance of wind farms is assumed not to degrade with time to allow intercomparisons to be made between scenarios. It is recognised that in reality wind turbines will suffer from performance losses related to aging and the impact of this could be considered in further work.

Environmental

A number of environmental effects can impact the shape of the power curve of individual wind turbines or farms such as icing, insects, and dirty blades. These effects are seasonal and highly site specific so are not considered in this study.

3.5.3 Constructing aggregate power curves

A representative power curve for both onshore and offshore wind turbines was selected after analysing a large number of manufacturers' power curves for turbines listed in the Renewable UK [2015] Wind Energy Database, see Figure 3.8. Following the methodology in Norgaard and Holttinen [2004]; Poyry [2009]; Staffell and Green [2014], the power curves for individual onshore and offshore wind turbines are convoluted with normal distribution functions to produce aggregate power curves. The standard deviations of the normal distributions are estimated using turbulence intensities derived from roughness factors and wind propagation times based on mean wind speeds and the assumption that a typical wind farm will occupy 0.1 km^2/MW installed capacity [Staffell and Green, 2014].

The function that describes a single wind turbine power curve denoted as $f(U_t)$, discussed in Section 3.5.1 is expressed as:

$$f(U_t) = \begin{cases} 0 & \text{for } U_t < U^{\text{cut-in}} \\ f^{\text{rated}} & \text{for } U^{\text{cut-in}} \leq U_t < U^{\text{rated}} \\ 1 & \text{for } U^{\text{rated}} \leq U_t < U^{\text{cut-out}} \\ 0 & \text{for } U_t \geq U^{\text{cut-out}} \end{cases} \tag{3.14}$$

The function to describe the wind speed probability distribution function denoted as $g(U_t)$, is expressed as:

$$g(U_t) = \frac{1}{\sigma^U \sqrt{2\pi}} \exp^{\frac{1}{2}\left(\frac{U_t - \mu^U}{\sigma^U}\right)} \tag{3.15}$$

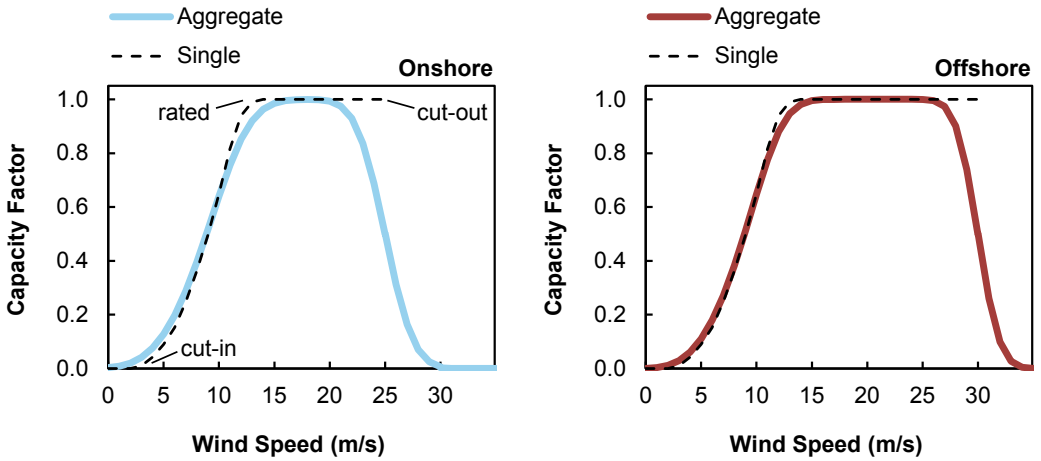

Figure 3.12: Onshore and offshore single turbine power curves are convoluted with wind speed probability distribution functions to create multi-turbine aggregate power curves.

where $g(U_t)$ represents the variation in wind speeds experienced across a spatial area, μ^U is the wind speed offset (m/s) and σ^U is the standard deviation in wind speeds (m/s) at hub-height. A numerical convolution method, described in El-Hajj and Kabalan [2004], is used in this work to convolute the two functions to produce the aggregate power curves:

$$f * g(U_t) = f(U_t) * g(U_t) \tag{3.16}$$

The aggregate power curves, after taking into account for short-term variations in wind speeds of typical onshore and offshore wind farms, are illustrated in Figure 3.12.

The multi-turbine aggregate power curves, representing the instantaneous power output of a group of wind turbines over a spatial area, then need to be adjusted to account for wake losses, technical availability, and electrical losses, see Section 3.5.2. First, the aggregate power curves are calibrated to reduce the annual energy yield by 10%, in-line with reported wake loss observations in Barthelmie *et al.* [2004]; Sorensen *et al.* [2006, 2008]; Johnson *et al.* [2009]; Phillips *et al.* [2010]; Ali *et al.* [2012]; Schallenberg-Rodriguez [2013], as shown in Figure 3.10.

Multiplying the hourly wind speed time-series for each wind site in the wind reanalysis dataset by the aggregate power curves gives the capacity factor for each onshore and offshore wind site.

Given that not all wind turbines will be operational all of the time, the capacity factor time-series' are then corrected to account for the technical availability of typical onshore and offshore wind farms, as described in Section 3.5.2, so that they correlate with long-term observed wind output. Average values for technical availability are assumed to be 98% for onshore and 90% offshore wind farms, respectively [Greenacre *et al.*, 2010; Greenacre, 2012; Harman,

2012; Kaldellis and Zafirakis, 2013; Feng *et al.*, 2010]. In this work, the impact of technical availability is assumed to be equivalent to a constant wind array loss. Array losses reduce the capacity factor or power output and not the time period that turbines are available. This is a reasonable assumption because it has been demonstrated previously that seasonal variations in technical availability has little impact on capacity factors [Hawkins, 2012], see Section 3.5.2.

Finally, the electrical losses of each wind site are then estimated using the capacity factor time-series'. The electrical losses are non-linear and are a function of the gross power output or the capacity factor and correspond to approximately a 2% reduction in annual energy production [Manwell *et al.*, 2009; Wan *et al.*, 2010; Colmenar-Santos *et al.*, 2014], see Section 3.5.2. Sensitivities to these assumptions are analysed in later chapters.

In summary, the steps used in this work to estimate the power output of onshore and offshore wind farms using simulated wind speed reanalysis data is as follows:

- identify and select representative onshore and offshore wind turbine power curves;
- identify typical dimensions, wind speed propagation times, and turbulence intensities of onshore and offshore wind sites to formulate wind speed probability density functions that represent the spread of wind speeds across typical wind farms;
- convolute single turbine power curves with wind speed probability density functions to create aggregate power curves that account for the short-term fluctuations in wind speeds experienced at real wind farms and storm control strategies;
- account for wake induced losses;
- multiply hourly wind speed time-series' of each wind farm by the aggregate power curve functions to produce hourly capacity factor time-series' for each wind farm;
- adjust available power outputs by accounting for onshore and offshore technical availability; and
- subtract the non-linear electrical losses as a function of the capacity factor for each wind farm.

The methodology to construct aggregate power curves, that take into account for the size and turbulence intensities experienced at typical UK wind farms and the non-linear electrical losses that compound and reduce the net power output, has been outlined and discussed. A linear correction factor for technical availability reduces the ideal capacity factors so they agree with long term published values. The following section validates the aggregate power curve approach and further demonstrates the accuracy of the WRF wind speed reanalysis data for estimating the power outputs of onshore and offshore operation wind farms in GB.

3.6 Validation

3.6.1 Introduction

There is limited available data on the power outputs of operational wind sites in the UK. This is because detailed information about the operation of wind farms is considered commercially sensitive and is therefore not released to the public. However, some large-scale transmission connected wind farms are metered in real-time and appear in data provided by Elexon [2015] in the form of Balancing Mechanism (BM) reports at half-hourly time periods. In addition, there is the Renewable Obligation Certificate (ROC) register which provides coverage of the number of ROCs issued to each eligible renewable generator each month, and therefore provides a good indicator of the monthly capacity factor of that generator [Ofgem, 2014b].

Extensive validation of the wind reanalysis dataset has been previously conducted by Hawkins [2012] using BM reports, ROC Register, and capital grants reports to validate the simulated power outputs of onshore and offshore wind farms at hourly and monthly timescales. In addition, aggregate power curves have been extensively used and validated in other power system studies such as Norgaard and Holttinen [2004]; Poyry [2009]; Ofgem [2012]; Staffell and Green [2014]. This section validates the proposed aggregate power curve approach by employing the methodology described in Section 3.5.3.

3.6.2 Previous validation

Hawkins [2012] acquired hourly BM unit production data for seven onshore operational wind farms from Elexon [2015], monthly ROC submissions for 107 distributed and transmission connected wind farms from Ofgem [2014b], and monthly capital grants reports for four offshore operational wind farms. The observed data was then compared with simulated data covering the same time period at the same temporal frequency. Logistic functions were used to represent aggregate power curves and then used to convert the simulated wind speeds into power outputs, with almost all of the results showing very good temporal agreement with observed production data. Hourly BM unit data for seven onshore transmission connected wind farms when averaged showed a very high correlation with simulated outputs. Before accounting for technical availability, a slight bias existed in the trend between observed and simulated capacity factors for hourly BM unit data. After accounting for the technical availability of a typical onshore wind site, the bias-corrected wind power outputs showed a very strong correlation with observed data. The simulated results also showed a very close fit with observed monthly capacity factors using ROC submissions, for 107 distributed and transmission connected onshore and offshore wind sites, and capital grants reports, for four offshore wind sites.

In short, Hawkins [2012] used numerous sources of operational wind farm data, both onshore and offshore, to validate the wind speed reanalysis dataset using simulated hourly and monthly

power output time-series' of existing wind farms. Simulated wind speed data for existing wind locations, when transformed into power outputs using the aggregate power curves in Hawkins [2012], show a strong fit with published data for onshore and offshore operational wind sites in the UK. It was therefore demonstrated that aggregate power curves can be successfully applied to produce accurate and unbiased wind power output time-series' for onshore and offshore wind sites in the UK across a range of weather conditions using WRF wind speed reanalysis data.

3.6.3 Validating the aggregate power curve approach

This section validates the aggregate power curve approach by comparing observed and simulated wind output data on a short- and long-term basis, illustrating that aggregate power curves are able to accurately simulate hourly and seasonal capacity factors. Then, the frequency and magnitude of wind ramp events is compared with observed data. This is to demonstrate that the aggregate power curves produce capacity factors that agree well with observed wind output variability at operational wind sites.

BM unit data

To assess the performance and accuracy of the proposed aggregate power curves at hourly resolution, observed power outputs from four operational wind farms in the UK, see Table 3.2, are used and compared with simulated capacity factors before and after wake and electrical losses and technical availability has been accounted for. These were selected as a representative sample because observed BM unit data for the four wind sites from Elexon [2015] were available at half-hourly resolution. The available data was then temporally matched so that it coincided with the hourly temporal resolution of the wind reanalysis data. As there was no available data for offshore wind sites between 2000 and 2010, no direct comparison could be made between simulated and observed data at hourly resolution.

Name	Capacity (MW)
Whitelee Phase 1	322
Hadyard Hill	117
Millennium	50
Kilbraur	47
	536

Table 3.2: Onshore wind farms with available production data from Elexon [2015].

Figure 3.13a shows the observed power outputs as a function of the simulated wind speed for each of the four wind sites. There is a high degree of scatter because there are a number of factors, other than just wind speed, that affect the power output, as discussed in Section 3.5.2.

Figure 3.13b shows the capacity weighted-average observed power outputs for each hour of the four wind farms as a function of the simulated wind speed. The results show that aggregating the power outputs of just a small number of wind farms drastically reduces the degree of scatter.

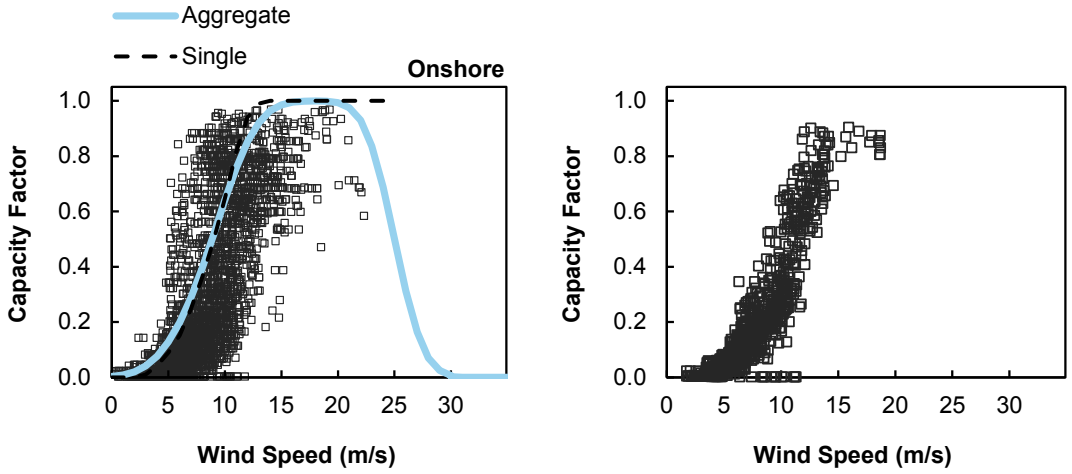

(a) Individual wind farms **(b)** Capacity weighted-average

Figure 3.13: Observed capacity factors from Elexon [2015] for onshore wind sites listed in Table 3.2 plotted as a function of the simulated wind speed.

Figure 3.14 shows the distribution of simulated wind speeds for the weighted-average output of the four wind farms. The results show that the distribution of wind speeds follow a Weibull distribution with a mean wind speed σ^U = 7.47 m/s, and shape factor k = 2.2. This illustrates that the majority of the time wind speeds are between cut-in and rated wind speeds where the power curve is steepest and wake losses are most severe.

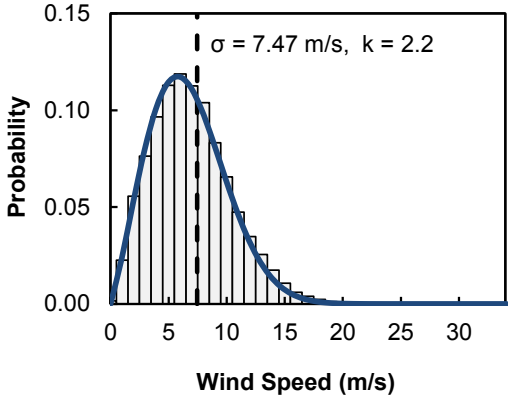

(a) Weibull distribution

Figure 3.14: Observed onshore hourly capacity factors from Elexon [2015] for four individual onshore wind sites listed in Table 3.2 as a function of the simulated wind speed.

Figure 3.15 shows the comparison between observed and simulated capacity factors before losses for each of the four wind farms and the weighted-average capacity factors including losses. The large degree of scatter illustrates how other factors influence the power output of a wind farm and not just wind speed. The fit between observed capacity factors and simulated capacity factors before losses is 0.834, indicating that the simulated capacity factors are slightly overestimated. This is as expected since these ideal capacity factors have not yet been corrected for losses.

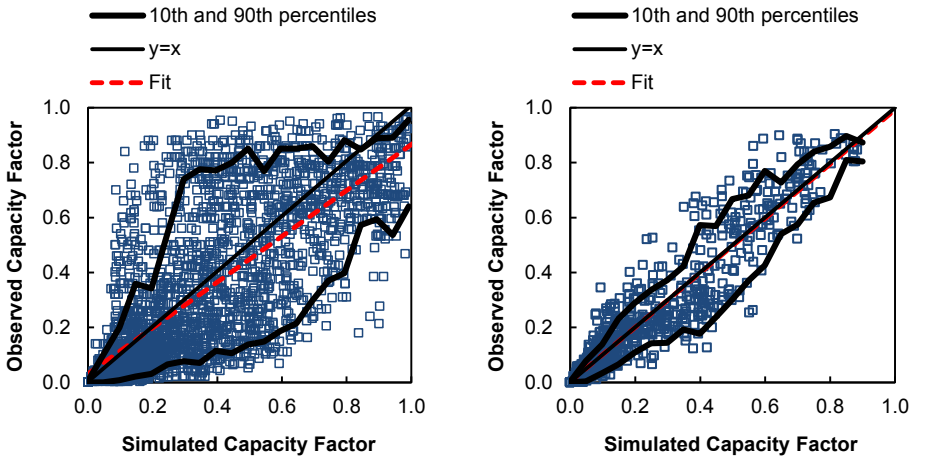

(a) Individual wind farms

(b) Capacity weighted-average (including losses)

Figure 3.15: Observed and simulated onshore hourly capacity factors from Elexon [2015] for four individual onshore wind sites listed in Table 3.2.

The capacity weighted-average capacity factors, derived from the WRF wind speed reanalysis dataset, including wake losses, technical availability, and electrical losses described in Section 3.5.3 show a close fit with the observed capacity factors as expected. A technical availability of 98% is assumed and gives good results.

The fit between the weighted-average observed capacity factors and simulated capacity factors is 0.989. This close match demonstrates the accuracy of the aggregate power curve to successfully simulate capacity factors for onshore wind farms at hourly temporal frequency. Figure 3.15 also shows that after including losses, the simulated capacity factors are unbiased across a range of different wind speeds and conditions.

To illustrate this further, Figure 3.16 shows a capacity weighted-average time-series of the observed capacity factors for the four wind farms in January 2010 and the simulated capacity factors before and after losses are included. The time-series of the weighted-average capacity factors including losses closely matches the observed capacity factor time-series at hourly temporal frequency for a highly active meteorological period in winter.

On an annual energy basis, if we combine the terms discussed in Section 3.5.3 for wake losses,

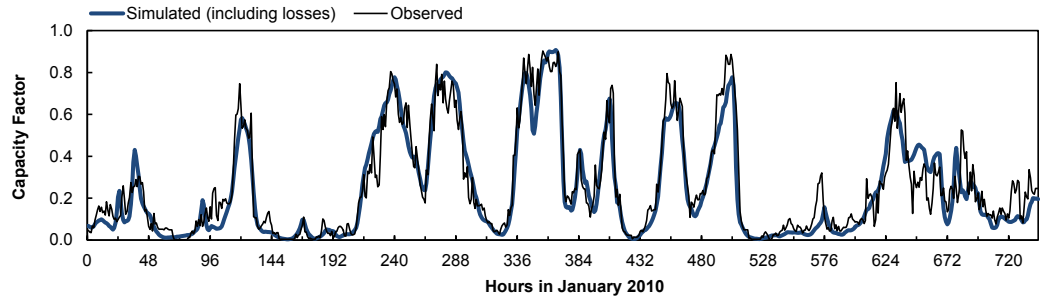

Figure 3.16: A capacity weighted-average time-series of the simulated capacity factors for four onshore wind sites listed in Table 3.2 and observed production data from Elexon [2015] for January 2010.

technical availability, and electrical losses, we would expect the onshore capacity factors to reduce by $0.90 \cdot 0.98 \cdot 0.98 = 0.864$, respectively. As reported above, the fit between observed and simulated capacity factors is 0.834 for the 4 wind farms listed in Table 3.2. The remaining difference is likely attributable to other site-specific effects such as mechanical or control system losses, turbine aging, or environmental effects. Although non-linear functions are used to account for wake and electrical losses, on an annual energy basis we would expect the wake and electrical losses in a typical wind farm to amount to 10% and 2%, respectively, in-line with reported values discussed in Section 3.5.2.

Analysis by Staffell and Green [2014], using a similar reanalysis dataset, shows that by applying a linear correction factor to take into account for technical availability, wake losses, and electrical-mechanical losses, corrected capacity factors agree well with both short- and long-term observed values and are also unbiased across a range a wind speeds and conditions. This suggests that this approach to account for losses provides a realistic method to estimate capacity factors.

Overall this analysis shows that the onshore aggregate power curve used to convert UK reanalysis wind speed data into power outputs at hourly temporal resolution is an appropriate and accurate conversion method.

Applying the array losses, outlined in Section 3.5.3, to the aggregate power curve produces simulated capacity factors that closely match observed capacity factors derived from operational BM unit data across a range of different wind conditions. Aggregating multiple wind farms reduces the scatter. Whilst there is no available observed data at hourly temporal resolution to compare with the simulated power outputs of the offshore aggregate power curve, it is reasonable to assume that the simulated outputs would also be accurate.

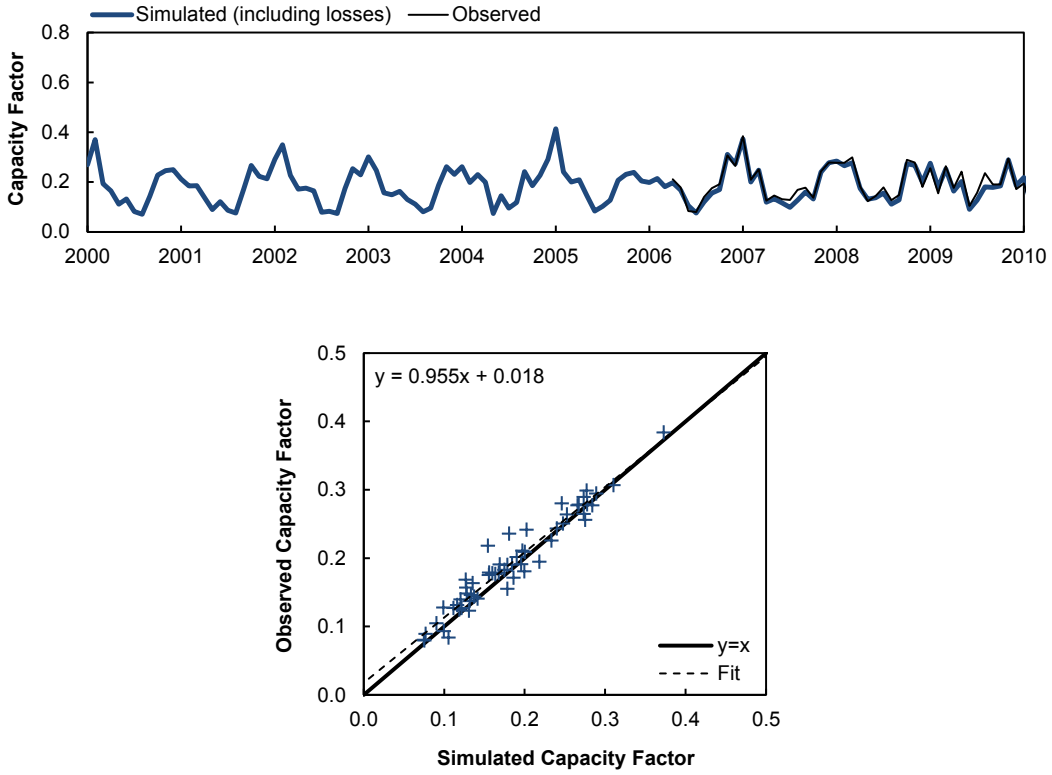

Figure 3.17: Plots of simulated monthly capacity factors for Artfield Fell Windfarm compared to the observed Renewable Obligation Certificate (ROC) submissions [Ofgem, 2014b].

ROC submissions

The ROC register Ofgem [2014b] provides a good source of monthly production data for onshore and offshore wind farms in the UK. The monthly capacity factors for individual wind farms can be derived from the number of ROC certificates earned. Data is available between 2006 and 2010. During this time, onshore wind was eligible for 1 ROC per MWh of renewable electricity generated and offshore 2 ROCs per MWh. Figure 3.17 shows the simulated and observed monthly capacity factors between 2006 and 2010 for an individual onshore wind farm in the UK. Simulated capacity factors including losses are derived from the WRF wind reanalysis data and observed monthly capacity factors are taken from monthly ROC data from Ofgem [2014b]. The match for this wind farm is very good indicating that the aggregate power curve approach proposed in this thesis is able to accurately simulate long-term capacity factors even at individual sites. However, this is not the case for all wind sites. A spatial resolution of 3 km will not be able to accurately capture the complex terrain of every wind farm and so some systematic differences should be expected. However, these site-specific individual differences will disappear when simulating the aggregate output of all operational wind farms.

Figure 3.18 shows the the simulated monthly capacity factors including losses for operational

onshore wind sites between 2000 to 2010 and observed monthly capacity factors derived from ROC submissions after April 2006. There is a strong agreement between simulated capacity factors and ROC submissions for onshore operational wind farms. Almost all of the observed monthly capacity factors are within $\pm 1\sigma$ standard deviation of the mean simulated capacity factor. The distribution of simulated capacity factors agree very well with observed monthly capacity factors, demonstrating that the methodology to convert WRF reanalysis wind speed data into long-term capacity factors is accurate for the operational onshore wind fleet. This illustrates that the aggregate power curves and assumed array losses are appropriate and unbiased.

However, early reliability issues associated with the initial phase of offshore turbine deployment in GB waters, as reported in Feng *et al.* [2010], causes low observed capacity factors between 2006 and 2008 in Figure 3.18. It is therefore expected that simulated capacity factors overestimate initially because of the low technical availability. After 2008, there is a much closer fit between observed and simulated capacity factors when offshore reliability is likely to have improved.

It should also be noted that there were a small number of discrepancies found in the Ofgem ROC register. A small proportion of the observed capacity factors were very low, <5% suggesting excessive downtime or an error in the reported turbine capacity. It is also likely that there may be date discrepancies when reporting the number of ROC submissions to Ofgem or the time individual turbines or clusters of turbines started operation within a wind farm. Although there is a reasonably high correlation and a very close long-term average between observed and simulated monthly capacity factors for offshore operational wind sites, the use of low temporal resolution ROC submission data hides the non-linearity and steep gradients of the assumed power curves. Understanding the variability in wind output is more important for flexibility and power plant operating regimes.

Aggregate ELEXON wind data

Elexon [2015] publish generation data by fuel type every half-hour. This includes aggregated data for GB transmission connected wind farms. Since the data is aggregated, it is not possible to match and compare the outputs from individual operational wind sites in the WRF reanalysis dataset over the same time period. This data will instead be used to assess the validate the variability of the simulated wind portfolio.

For this analysis, the most important factor is therefore the rate of change in wind output or the gradient. This is frequently referred to as a wind ramp. A wind ramp event is characterised by the gradient of the wind power output W_t or capacity factor CF_t over a given time period Δt:

$$\Delta W_t = W_{t+\Delta t} - W_t \tag{3.17}$$

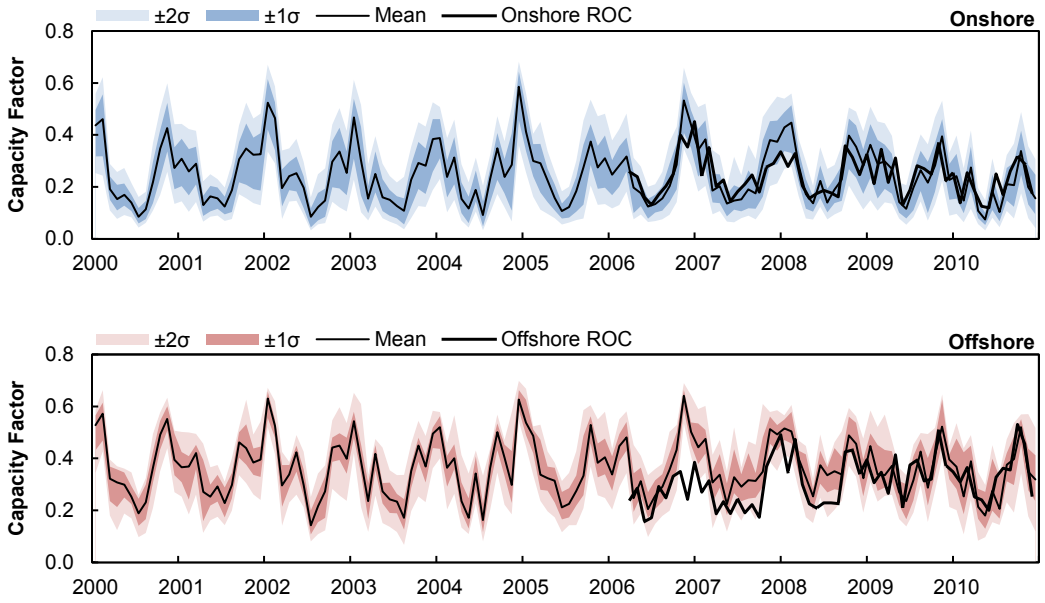

Figure 3.18: Distribution of simulated monthly capacity factors for onshore/offshore wind sites compared to the observed Renewable Obligation Certificate (ROC) submissions [Ofgem, 2014b]. Darker shaded regions within $\pm 1\sigma$ standard deviation (15.9 - 84.1th percentiles) and lighter shaded regions within $\pm 2\sigma$ standard deviations (2.3 - 97.7th percentiles) of the mean.

$$\Delta CF_t = CF_{t+\Delta t} - CF_t \tag{3.18}$$

A 1-h time window is the shortest value of Δt that is possible using the WRF reanalysis dataset as the simulations used Reynold's averaged equations and do not resolve sub-hourly turbulent fluctuations.

Figure 3.19 shows the frequency distributions for 1-h wind ramps for Elexon [2015] aggregated wind output data and simulated data using operational wind sites in 2010 on a linear and $\log_{10}$ scale. It shows the shape of the frequency distributions for observed wind power output fluctuations in 2010. The frequency and magnitude of wind ramp events for ELEXON aggregated wind output data in 2010 from Elexon [2015] closely matches that of the simulated wind ramps derived from WRF wind speed reanalysis data. Wind ramps are characterised by a concentrated peak of smaller and more frequent ramp events. However, it is the most extreme wind ramp events at the tails that will require the highest flexibility requirements. It is therefore important to ensure the simulated wind power data correctly models extreme events of wind variability. The logarithmic plot illustrates that the simulated WRF wind data matches both upwards and downwards ramp events with close accuracy.

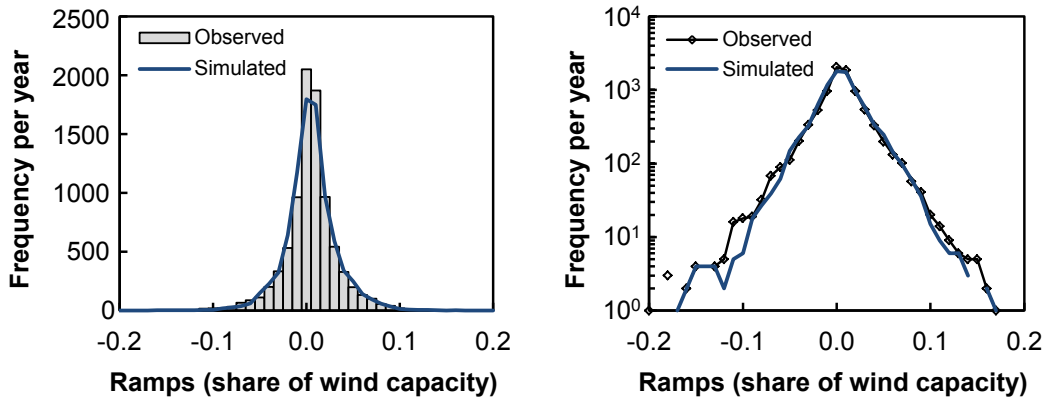

Figure 3.19: Frequency distributions for simulated 1-h wind ramp events using operational wind sites in WRF wind reanalysis dataset and observed wind ramp events using aggregated Elexon [2015] data.

3.6.4 Summary

This section introduced a WRF wind speed reanalysis dataset and an approach that uses aggregate wind farm power curves to simulate wind capacity factors for onshore and offshore wind farms. The aggregate power curves developed in this thesis account for the non-linear electrical losses and wake losses that occur in wind farms. The simulated hourly wind capacity factors for operational wind sites are compared with published BM unit and ROC data, demonstrating that the aggregate power curve approach can produce credible production profiles for onshore and offshore wind in GB.

The next chapter will introduce and characterise wind scenarios of increasing wind capacity to represent the expected spatial distribution of wind farms in the future. The scenarios are then analysed to understand the expected generation and variability of the future wind portfolio.

Chapter 4

Wind analysis

4.1 Introduction

Chapter 3 introduced and described a historic wind reanalysis dataset for the UK at hourly resolution between 2000 and 2010 for 386 wind sites. Building on this reanalysis dataset, an aggregate power curve approach was validated against existing operational wind farm production data. Aggregate power curves were demonstrated to accurately capture the temporal variability for wind sites and long-term published data was shown to match well with simulated capacity factors. Considered alongside previous validation by Hawkins [2012], it is clear that the high resolution wind reanalysis dataset and proposed wind model can provide detailed information about wind variability in GB.

A key assumption of this work is that the historic wind resource dataset between 2000 and 2010 is expected to be representative of future wind patterns, as it contains a very large number of historic weather events at high-resolution. The underlying methodology is to use historic weather as a basis for understanding future wind output and variability. Combining historic wind data at plausible locations for a range of future wind deployment scenarios allows for a detailed assessment of expected future wind variability. The exact location of individual wind farms is not essential for modelling wind variability. However, wind farms should be spatially distributed in a way that closely approximates the distribution of expected future wind capacity. It is therefore important to ensure this work uses realistic wind capacity projections to provide a good representation of future wind deployment. Using available information about the existing locations and proposed locations of wind farms from Renewable UK [2015], it is possible to model plausible scenarios of the expected spatial distribution of wind capacity.

Another important underlying principle of this work is the use of consistent historical wind and demand data to ensure that, for example, electricity demand (driven to a high degree by both wind speeds and temperature) is correctly matched with wind speeds on a consistent temporal basis. This is very important and crucial for an accurate analysis of demand-wind variability in the context of wind-based power systems. The resulting wind output time-series' can be matched temporally with electricity demand to make detailed assessments about the UK electricity system in scenarios with high levels of installed wind capacity. This maintains the

complex relationship between electricity demand and weather patterns.

The dataset contains an extremely large record of historic weather events including both violent and calm periods. Although 11 years of historic wind data will not allow for climatology assessments or to understand the impacts of climate change, the dataset is of sufficient length to show large interannual variability.

The next section will identify and characterise future UK wind capacity projections that are used in the remainder of this work from the literature and then develop internally consistent wind deployment scenarios. These scenarios are a snapshot of the plausible onshore and offshore wind fleet in the future and are intended to illustrate a feasible pathway of wind capacity deployment in GB. For example, the growth of the onshore and offshore wind fleet and the changing spatial distribution of wind capacity can be investigated. The remaining part of this chapter will then investigate the power output and variability of each of the scenarios to understand the characteristics of the future wind fleet.

4.2 Wind scenario characterisation and development

4.2.1 Wind site locations

The WRF reanalysis dataset contains the detailed locational and wind capacity information on each of the individual 337 onshore and 49 offshore wind projects that are greater than 10 MW in size. The operational status of each wind site is listed and reported either as operational, under construction, consented, in planning, or in scoping, at the time the reanalysis dataset was compiled in 2012 [Hawkins, 2012]. This was updated using more recent information found in the Renewable UK Wind Energy Database [Renewable UK, 2015]. Since the compilation of the wind reanalysis dataset, more detailed estimates and projections for offshore wind have been published in Crown Estate [2014] and project timelines in Renewable UK [2014]. Scenarios are then constructed using the most up-to-date information about existing operational wind farms and the future pipeline and timing of future wind projects.

The simulated long-term capacity factors for each of the wind sites along with the locations and operational/planned installed capacities are shown in Figure 4.1. A detailed list of all of the wind sites and locations is available in Appendix A.

The wind reanalysis dataset also classifies each wind farm by region or distribution network. This would allow future network studies using this dataset to assess the impacts of wind on individual distribution networks within the GB electricity system. Table 4.1 shows a list of each onshore wind region, broadly representing each of the distribution network operator boundaries in GB.

Onshore wind sites are typically situated in high wind regions that have good access to the transmission or distribution systems. The exact location, however, of each individual wind farm

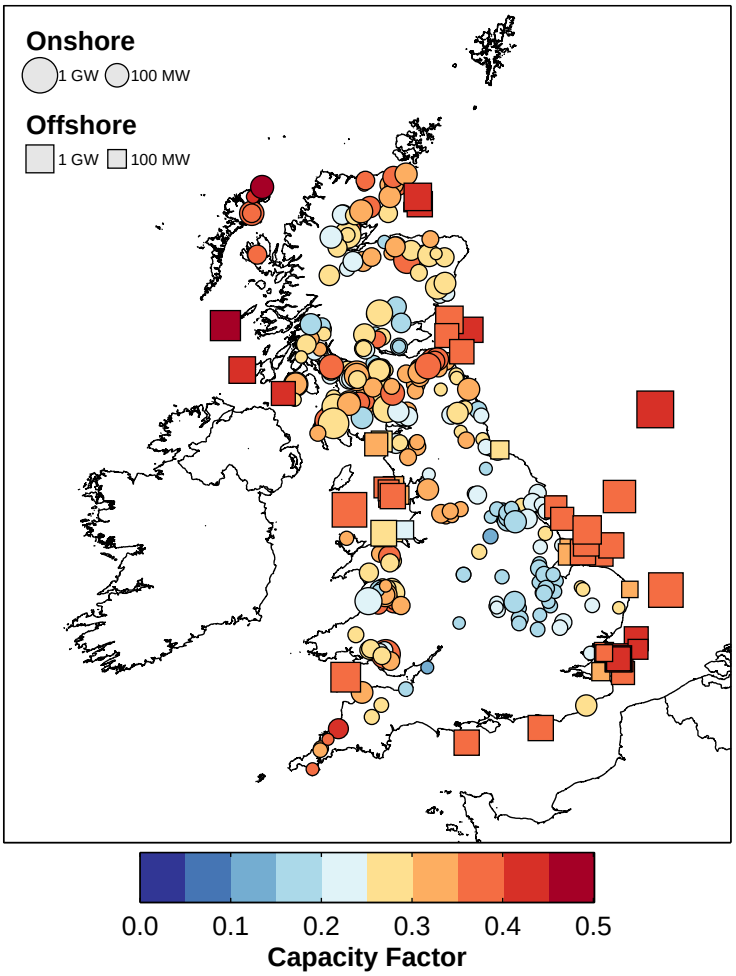

Figure 4.1: Long-term capacity factors between 2000 and 2010 and the locations of onshore and offshore wind sites in the wind reanalysis dataset.

is not critical for understanding the impacts of wind variability. What is important is that wind farms are spatially distributed in a way that closely resembles the distribution of future wind capacity. By analysing the locations of wind farms that are operational as of 2015 and wind farms that are either consented, in planning, or in scoping, it is then possible to understand the potential geographic distribution of future wind capacity.

Given it is not possible to predict the exact size of each wind farm, the installed capacity of each region, or the timing of new wind farm installations into the future, this approach is therefore only intended to be used to analyse the relative distribution of wind capacity in each of the scenarios. This is to represent the evolving geographic distribution of wind capacity into the future and the incremental development of offshore wind capacity, moving from shallow water sites in close proximity to the coast to deeper water sites. It is therefore reasonable to assume that the wind farm locations in the wind reanalysis dataset are appropriate and will provide a good representation of future wind deployment.

4.2.2 Wind regions

The simulated capacity factor $CF_{f,t}$ of each wind farm f at time t, derived from WRF reanalysis data, and the operational/planned capacity of each farm is used to calculate the weighted-average capacity factors $CF_{r,t}$ for each region r, where $r = 1, 2, 3, ..., R$. The weighted-average capacity factor CF_t for GB is then calculated by the equation:

$$CF_t = \frac{\sum_{r=1}^{R} w_r \cdot CF_{r,t}}{\sum_{r=1}^{R} w_r} \tag{4.1}$$

where w_r are the capacity weights for each region. Weights for each region are used to model the relative distribution of wind capacity between wind regions. A map showing the locations of the wind regions is shown in Figure 4.2 and Table 4.1 shows a list of each of the distribution network operator boundaries.

4.2.3 Wind development scenarios

This section analyses a number of key government, industry, and consultancy projections for onshore and offshore wind capacity to develop a range of plausible wind capacity deployment projections into the future.

The UK Renewable Energy Roadmap DECC [2011] and its updates DECC [2012a, 2013a] contain projections of the installed onshore and offshore wind capacity that is expected to be deployed in the future. These projections are consistent with one approach to allow the UK meet its binding target to provide 15% of its total energy consumption from renewables by

	Onshore		Offshore
EA	East Anglia	CRO	Cromarty
EE	East England	ECH	English Channel
EM	East Midlands	FRT	Forth
NEE	North East England	HU	Humber
NES	North East Scotland	IRS	Irish Sea
NI	Northern Ireland	LUN	Lundy
NWA	North Wales	MAL	Malin
NWE	North West England	TD	Tyne and Dogger
NWS	North West Scotland	TH	Thames
SE	South England		
SEE	South East England		
SS	South Scotland		
SWA	South Wales		
SWE	South West England		
WM	West Midlands		

Table 4.1: Onshore and offshore regions used to split up the UK according to distribution network operator boundaries.

2020 [EU, 2009; DECC, 2013a]. By June 2012 the UK had 5.4 GW of installed onshore wind capacity with a further 1.3 GW under construction, 4.8 GW awaiting construction, 3.0 GW being considered, and 3.4 GW in the pipeline [DECC, 2013a]. In 2015, the UK had 8.5 GW of installed onshore wind capacity and 5.1 GW of offshore wind capacity [Renewable UK, 2015].

By 2020, it is estimated there will be between 10-13 GW (central projection) and 10-19 GW (industry projection) of installed onshore wind capacity, and between 11-18 GW (central projection) and 10-26 GW (industry projection) of installed offshore wind capacity [DECC, 2013a].

The Crown Estate [2014] have leased areas of the seabed for offshore wind development. They are categorised into rounds for commercial development. Round 1 started in 2000 and as of 2015 consisted of 13 operational offshore wind farms with a capacity of 1.2 GW. Round 2 started in 2003 and has a total projected capacity of 8.5 GW. Up to 33 GW has been identified for Round 3 sites and almost 3 GW has been awarded leasing agreements in Scottish Territorial Waters.

The National Grid [2013, 2014a] provide more recent Gone Green scenarios that show onshore wind capacity increasing to 7.9 GW in 2015, 13.6 GW in 2020, 18.1 GW in 2025, and 19.2 GW in 2030, and for offshore to increase to 5.0 GW in 2015, 12.6 GW in 2020, 26.6 GW in 2025, and 31.9 GW in 2030. Poyry [2009] also provide onshore and offshore wind capacity projections up to 2030 and are consistent with estimates in DECC [2011, 2012a, 2013a]. In 2020 they project there will be 32.5 GW of wind capacity, with 14.1 GW of onshore and 18.4 GW of offshore wind capacity. In 2030 this increases to 43.0 GW of wind capacity, with 15.6 GW of onshore and 27.4 GW of offshore wind capacity.

A range of wind generation capacity projections are developed to represent the potential growth and spatial distribution of GB wind capacity, illustrating a feasible pathway of wind deployment

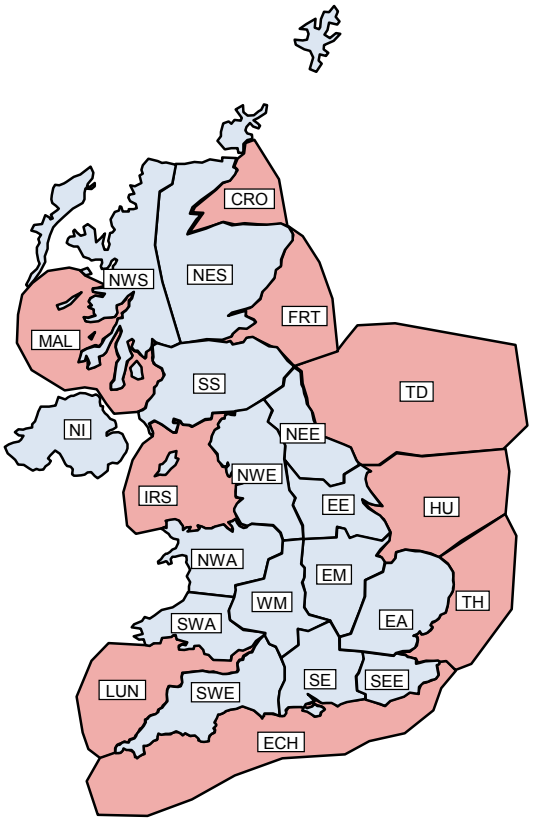

Figure 4.2: The locations of onshore and offshore wind regions according to distribution network operator boundaries, see Table 4.1.

that is consistent with a number of key and reputable government, industry, and consultancy expectations. In particular, the data used to formulate the onshore and offshore wind capacity projections is consistent with 2020 and 2030 targets and is amalgamated from Poyry [2009]; National Grid [2013, 2014a]; DECC [2011, 2012a, 2013a]; Renewable UK [2014, 2015]; RAENG [2014].

Each scenario represents a geographic distribution of wind capacity which is thought to be feasible and may be achieved at some point in the future. The development and characterisation of the wind capacity scenarios is internally consistent and illustrates the progression of wind installations between 10 GW and 45 GW in GB without conforming to a timeframe. The scenarios start with 10 GW of wind capacity, and add 5 GW with each increment. Each scenario has a progressive increase in the proportion of offshore wind capacity. This is to represent the expected development of offshore wind rounds into the future.

As it is quite difficult to accurately forecast and predict the build rate of new onshore and offshore wind capacity, it is quite sensible to use multiple parallel pathways to represent the upper and lower bounds of expected wind deployment at various points in time in the future.

Scenario	Wind capacity (GW)					
	Total	Onshore	Offshore			
			R1	R2	R3	STW
a	10.0	7.0	1.1	1.9	0.0	0.0
b	15.0	9.8	1.2	4.1	0.0	0.0
c	20.0	12.0	1.2	6.8	0.0	0.0
d	25.0	13.8	1.2	7.2	2.3	0.6
e	30.0	15.0	1.2	7.2	5.3	1.3
f	35.0	15.8	1.2	7.2	8.7	2.2
g	40.0	16.4	1.2	7.2	12.2	3.0
h	45.0	16.7	1.2	7.2	16.0	4.0

Table 4.2: Wind deployment scenarios ranging from 10 GW wind capacity increasing to 45 GW, see Figure 4.4. Offshore wind capacity is divided into commercial rounds: Round 1, Round 2, Round 3 and Scottish Territorial Waters.

However, this work assumes only one potential pathway for wind capacity deployment to reduce the total number of scenarios. It is more important in this work to accurately represent the spatial distribution of wind capacity, not the timeframe at which capacity comes online. It is also possible to differentiate between wind capacity throughout GB in areas such as England, Wales, and Scotland. A summary of the wind capacity development projections can be seen in Figure 4.3. Table 4.2 shows the proportions of offshore wind capacity in each of the scenarios and the growth of Round 3 wind sites. The regional distribution of wind capacity is shown graphically in Figure 4.4.

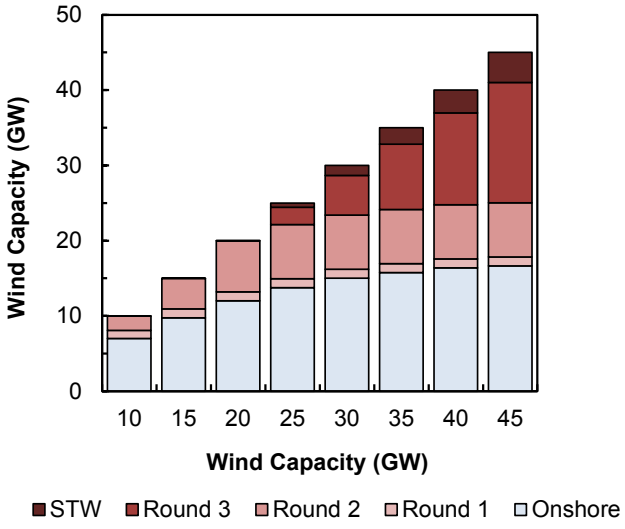

Figure 4.3: Wind deployment scenarios ranging from 10 GW wind capacity increasing to 45 GW, see Figure 4.4. Offshore wind capacity is divided into commercial rounds: Round 1, Round 2, Round 3 and Scottish Territorial Waters.

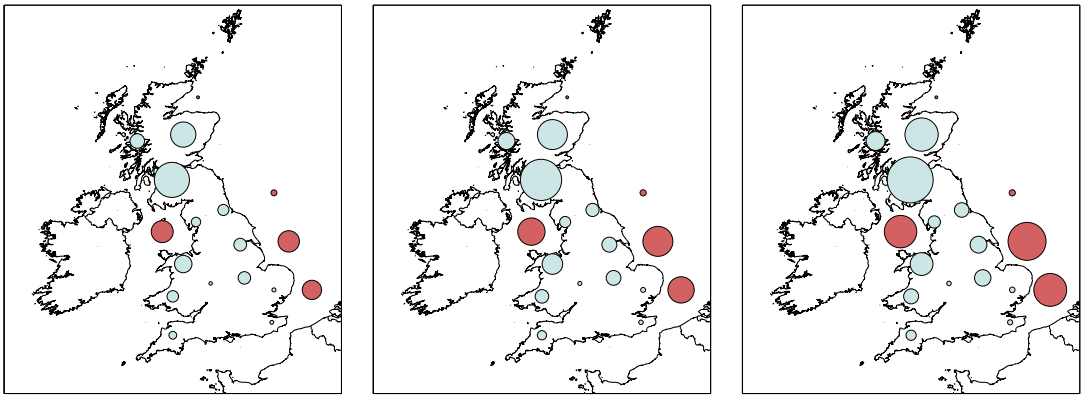

(a) 10 GW **(b)** 15 GW **(c)** 20 GW

(d) 25 GW **(e)** 30 GW **(f)** 35 GW

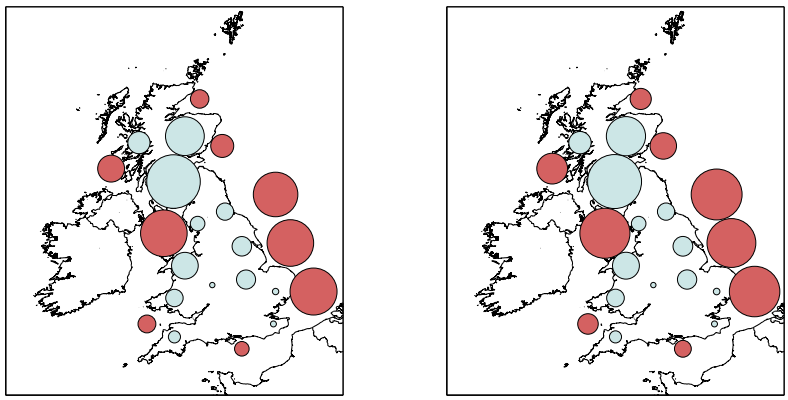

(g) 40 GW **(h)** 45 GW

Figure 4.4: Wind deployment scenarios by region showing onshore and offshore wind capacity. The radius of each region is proportional to the logarithm of its installed capacity.

4.3 Wind analysis

The capacity factors of individual wind regions and the aggregate outputs of the deployment scenarios are examined to understand the relative probability of high/low wind periods and the average wind output between regions and scenarios. The effects of aggregation are also analysed to understand the variability of the future wind fleet.

4.3.1 Capacity factors

Annual variation

Figure 4.5 shows the inter-annual variations in capacity factors between 2000 and 2010 for the onshore and offshore wind fleet. 2008 experienced the highest annual capacity factors of 33.4% for onshore and 40.5% for offshore. 2010 experienced the lowest annual capacity factors at 24.3% for onshore and 32.7% for offshore. There is a significant difference between annual capacity factors. The standard deviation in the onshore annual capacity factors is 2.4% and for offshore 2.0%. The onshore wind fleet is therefore slightly more sensitive to annual variations in wind speeds. This illustrates the importance of using wind datasets that capture long-term effects.

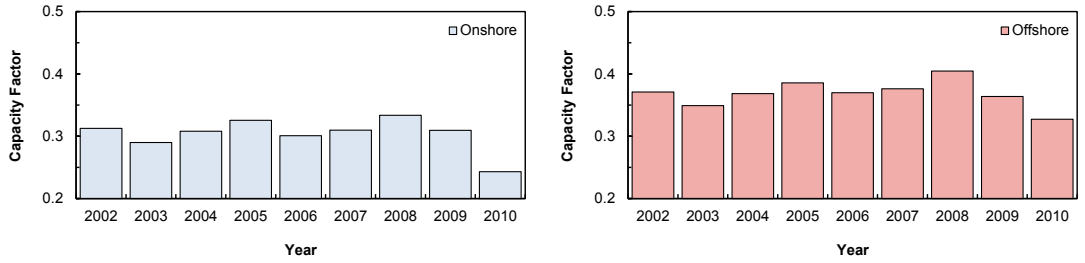

(a) Onshore by year **(b)** Offshore by year

Figure 4.5: Capacity factors by year for the onshore and offshore wind fleets with 30 GW capacity.

Seasonal variation

Figure 4.6 shows the variation in monthly capacity factors. Offshore capacity factors follow the same pattern as onshore capacity factors, falling most in summer months. January experiences the highest average monthly capacity factor at 49.2% for onshore and 50.6% for offshore. The standard deviation in monthly average capacity factors is relatively large, illustrating the large seasonal variation. The standard deviation for onshore monthly capacity factors is 10.0% and offshore 7.6%. July experienced the lowest onshore monthly average capacity factor at 17.2% whereas June experienced the lowest offshore monthly average capacity factor at 26.0%.

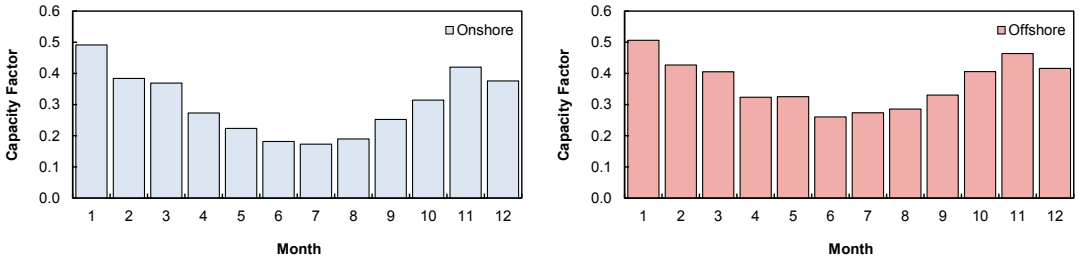

(a) Onshore by month **(b)** Offshore by month

Figure 4.6: Capacity factors by month for the onshore and offshore wind fleets with 30 GW capacity.

Figure 4.7 shows the number of hours per year by month where capacity factors fall below 10% for the onshore and offshore wind fleets. For the onshore wind fleet, capacity factors fall below 10% for an average of 290 hours in June. There is a strong seasonal relationship with low wind events occurring in summer months.

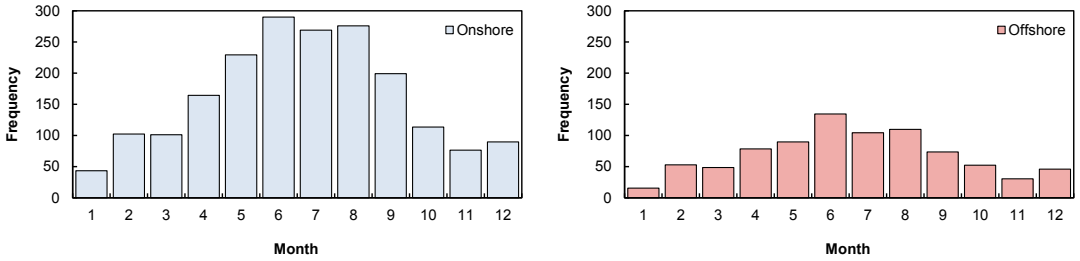

(a) Onshore by month **(b)** Offshore by month

Figure 4.7: Number of hours per year by month where capacity factors are below 10% for the onshore and offshore wind fleet with 30 GW capacity.

Figure 4.8 shows the frequency distributions for capacity factors by season where Spring={Feb, Mar, Apr}; Summer={May, Jun, Jul}; Autumn={Aug, Sep, Oct}; Winter={Nov, Dec, Jan}. There is an astounding difference in the seasonality in the onshore/offshore capacity factor distributions. In Summer, onshore capacity factors are lower than 20% for 66.3% of the time. Whereas offshore capacity factors in summer months are lower than 20% for 30.4% of the time.

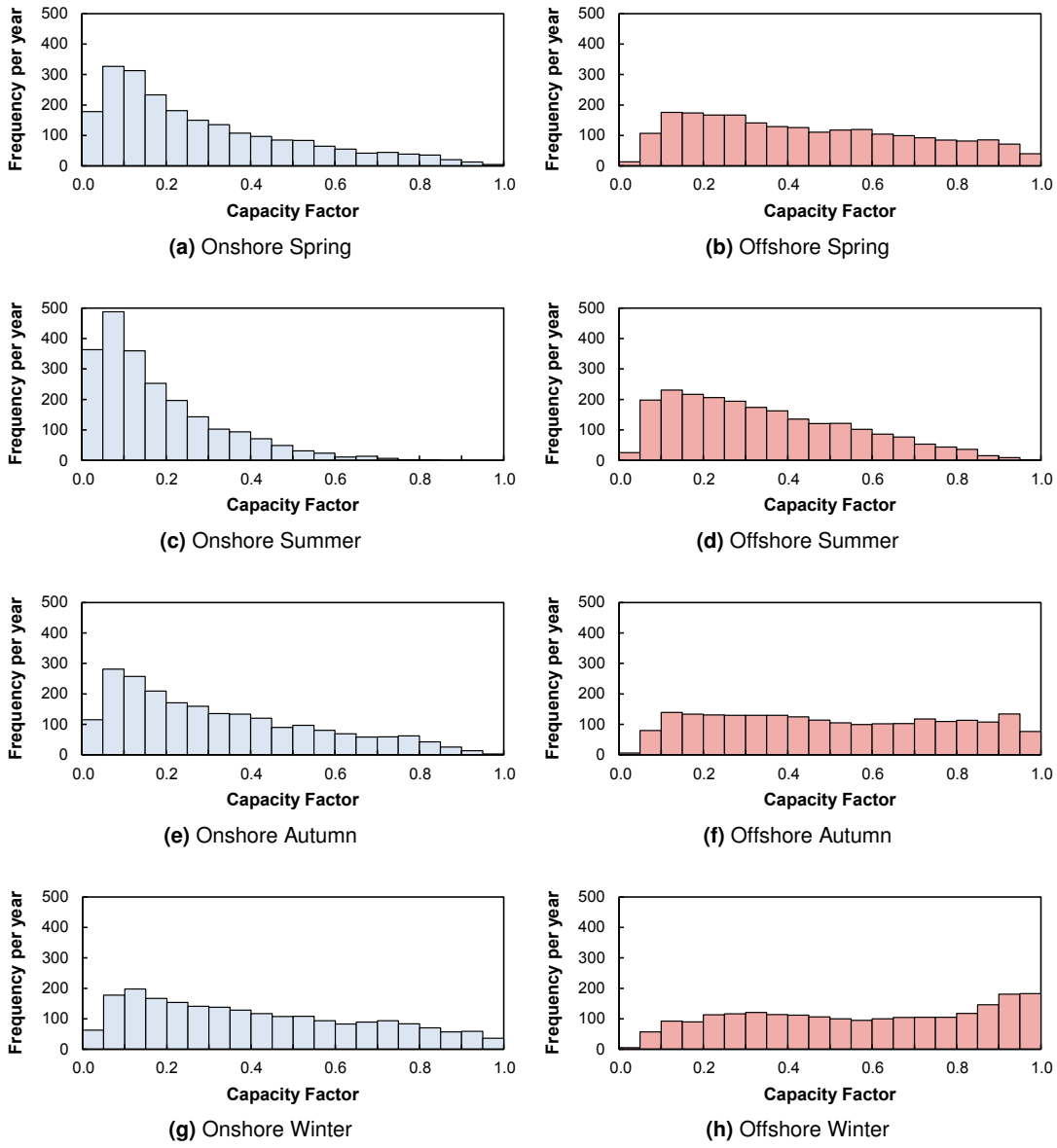

(a) Onshore Spring

(b) Offshore Spring

(c) Onshore Summer

(d) Offshore Summer

(e) Onshore Autumn

(f) Offshore Autumn

(g) Onshore Winter

(h) Offshore Winter

Figure 4.8: Distribution of capacity factors by season for the onshore and offshore wind fleet with 30 GW capacity.

Hourly variation

Figure 4.9 shows the average capacity factors by hour of day for summer and winter. There is a pronounced diurnal pattern that is strongest for the onshore fleet in summer. For onshore wind farms, capacity factors are lowest at 05:00 which then rise until approximately 13:00. The diurnal pattern is weakest in winter months as solar insolation is lower.

The wind reanalysis dataset and the WRF modelling system both capture these diurnal variations in capacity factors [Hawkins, 2012]. Sinden [2007] has also reported a strong diurnal effect using 10 m MET office data for onshore wind sites. The effect is strongest for onshore wind sites and offshore wind sites that are situated close to the coastal boundary.

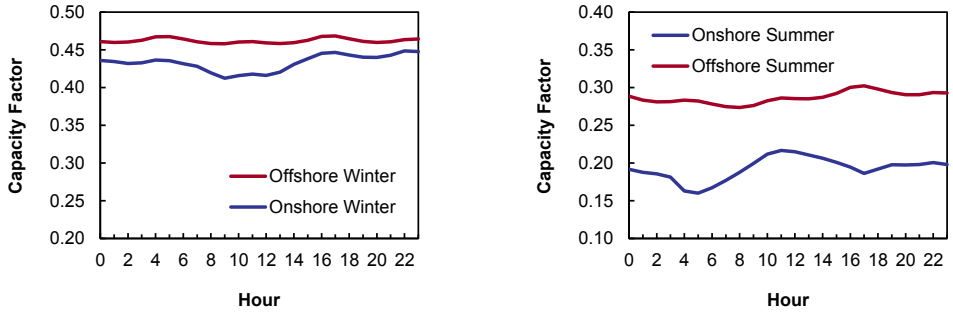

(a) Winter **(b)** Summer

Figure 4.9: Capacity factors by hour in day for summer and winter for onshore and offshore wind fleet with 30 GW capacity.

Figure 4.10 shows the temporal distributions of capacity factors for the onshore and offshore wind portfolios in the year 2010. The remaining temporal distributions for each year between 2000 to 2010 are shown in Appendix B. Both plots for the onshore and offshore portfolios show similar low output periods in dark blue. There is a sustained period around October where offshore capacity factor are consistently high. The main points to illustrate in these figures are the differences between the onshore and offshore wind resource and the degree of variability throughout the year.

Figure 4.11a shows the capacity factors between 2000 - 2010 for individual wind regions and the aggregate 30 GW scenario. Here, capacity factors are used (before technical availabilities are included) to highlight the theoretical output that could be extracted under ideal historical wind conditions. This provides an upper limit of the wind resource. The technical availability is not included at this step only to illustrate the differences between the onshore and offshore wind resource and the differences between geographic wind regions. Later work includes technical availabilities. See Chapter 3 for a detailed description of the assumptions used to account for wind array losses.

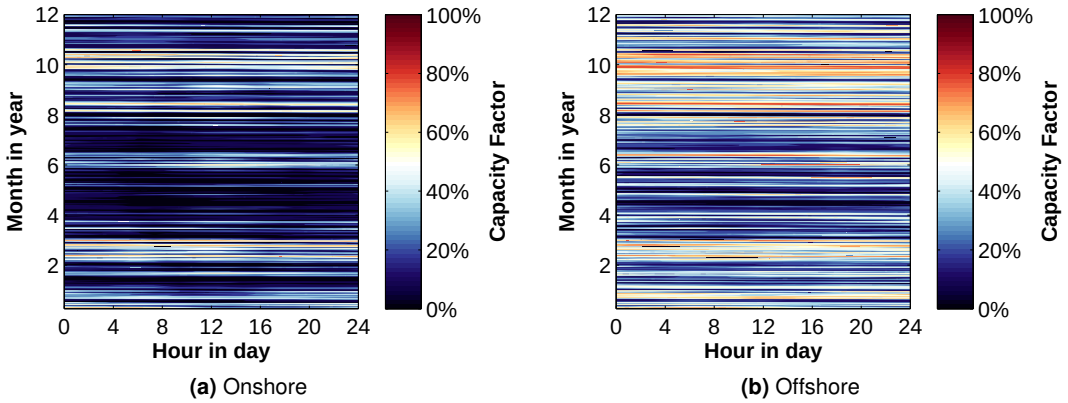

Figure 4.10: Temporal distributions for onshore and offshore capacity factors in 2010.

Regional variation

The thick black line in Figure 4.11a shows the duration curve for the aggregate onshore/offshore wind output from scenario e with 30 GW of wind capacity. Individual wind regions are described in Table 4.1. The aggregate output from the geographically diverse 30 GW wind portfolio, including both onshore and offshore wind capacity, reduces the probability of very low wind output. Offshore wind regions experience higher average wind speeds and so the offshore wind region duration curves are typically concave in shape. Onshore wind regions experience lower wind speeds on average and so onshore wind region duration curves are typically convex. There is also a large variation in the spread of the capacity factor duration curves between regions which is caused by the large variance in wind conditions at different geographic locations across and around GB.

The 30 GW wind portfolio is below 10% output for 9.3% of the time and above 90% output for only 2.4% of the time. This compares to the East Anglia onshore wind region which is below 10% output for 37.7% of the time and only above 90% output for 2.2% of the time. The effect of geographic aggregation is very clear. It is far less likely for the whole of the GB wind portfolio to experience its output drop below 10% when compared to an individual region.

The frequency distributions of capacity factors for each of the individual wind regions are shown in Figure 4.11b. There is a large variation between the frequency distributions of individual wind regions. Overall, offshore wind regions have a flatter distribution with a more even spread of capacity factors. Onshore wind regions have a concentration of capacity factors below 20%. The aggregate wind portfolio combines the characteristics of the onshore and offshore wind regions.

The average capacity factors including losses and technical availabilities for onshore wind regions between 2000 and 2010 is 28.3%. The capacity factors for each of the offshore commercial development rounds accounting for losses described in Chapter 3 are 35.6%, 40.8%,

43.1%, and 45.6% at Round 1, Round 2, Round 3, and in Scottish Territorial Waters, respectively.

4.3.2 Temporal variability

Ramp events for individual wind farms are most severe when wind speed changes occur at the point on the power curve where the gradient is steepest. For a geographically diverse wind fleet, short-term mesoscale variation, diurnal variations, and both microscale and turbulent variations are smoothed out as a result of geographic aggregation. It is only large-scale weather systems that occur for a period of hours to days that drive wind variability. To investigate this further, the variability of the onshore and offshore wind fleets are now analysed at different timescales.

Annual variation

Figure 4.12 shows the annual variation in the distributions of onshore and offshore 1-h wind ramps. The distribution of wind ramps can be approximated as a normal distribution with zero mean. 68.26% of wind ramp events occur within the dark shaded areas or ± 1 standard deviation. 95.44% or $\pm 2\sigma$ of wind ramp events occur within the medium shaded areas and 99.74% or $\pm 3\sigma$ of wind ramp events occur within the light shaded areas. The same shading rules apply for Figure 4.13.

The variation in the annual distribution of onshore wind ramps is approximately the same. In other words, from year to year the magnitude of wind ramps does not change significantly. The spread of onshore wind ramps are greater than the spread of offshore wind ramps. This is most likely because onshore wind sites are situated more closely and are more correlated. This is shown in more detail in Figure 4.19.

Seasonal variation

Figure 4.13 shows the monthly variation in the distributions of onshore and offshore 1-h wind ramps. Onshore wind ramps are significantly less extreme in summer months where 99.74% of all onshore wind ramp events are less than $\pm$ 900 MW/h. In comparison, this increases to nearly $\pm$ 1500 MW/h in winter months implying that seasonal flexibility requirements may be required for wind variability. There is a slight seasonal variation in offshore wind ramps by month however this effect may be smoothed by the geographical spread of offshore wind sites.

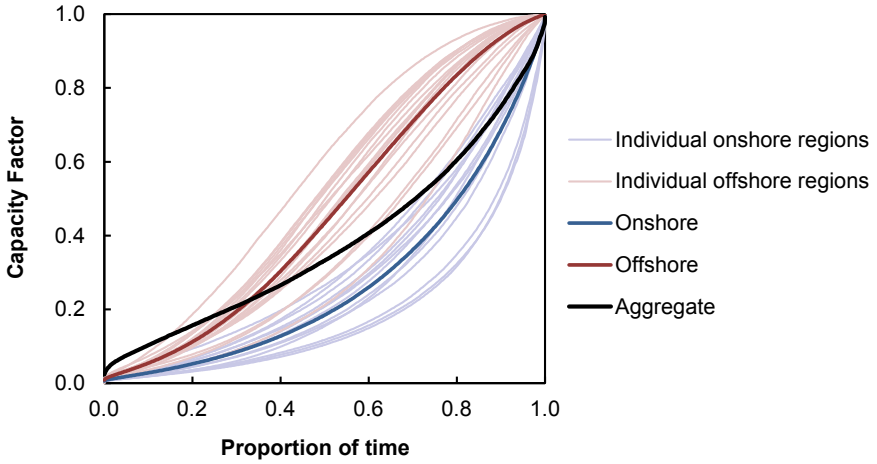

(a) Capacity factor duration curves.

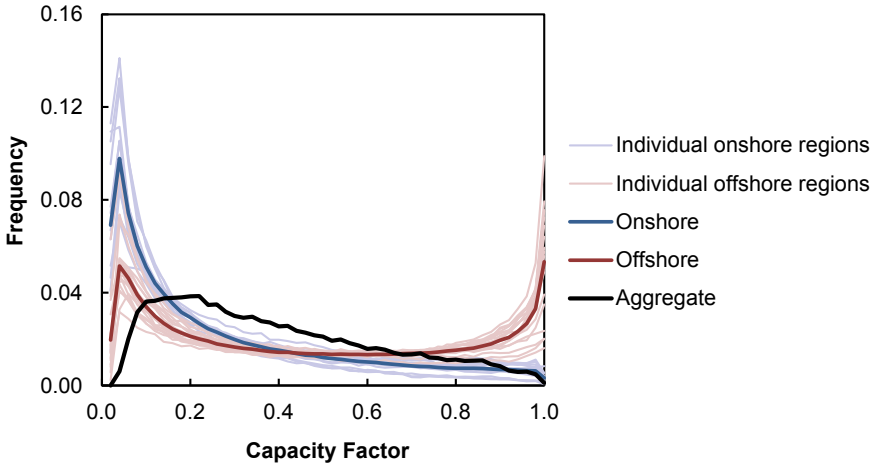

(b) Frequency distributions for capacity factors.

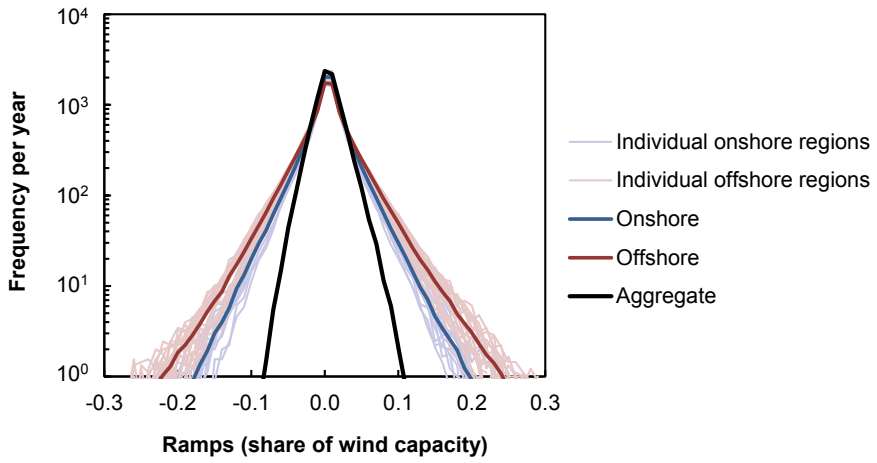

(c) Frequency distributions for 1-h wind ramp events.

Figure 4.11: Capacity factors and wind ramp events for individual onshore/offshore wind regions and the aggregate wind portfolio with 30 GW capacity.

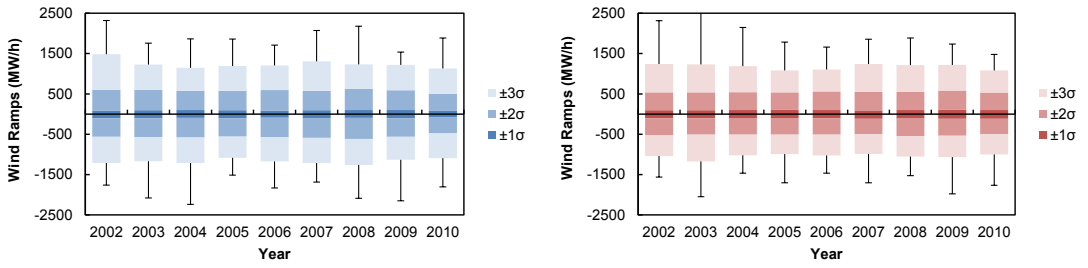

(a) Onshore **(b)** Offshore

Figure 4.12: Variation in 1-h wind ramps by year for onshore and offshore wind fleet with 30 GW capacity.

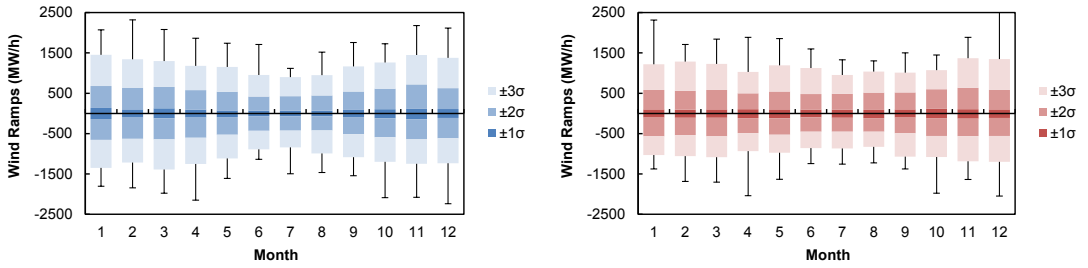

(a) Onshore **(b)** Offshore

Figure 4.13: Variation in 1-h wind ramps by month for onshore and offshore wind fleet with 30 GW capacity.

Hourly variation

The temporal distributions for 1-h wind ramp events are shown in Figure 4.14 for the onshore and offshore wind portfolios in 2010. The temporal distributions for each year between 2000 to 2010 are shown in Appendix B. The most striking observation in Figure 4.14 are the diurnal variations in onshore wind ramp events occurring in the mornings and evenings. The diurnal variability in land-sea temperatures creates thermally induced winds at the coastal boundary. An increase in wind speeds occurs in the morning until noon followed by a decrease in wind speeds in the afternoon. This creates upwards onshore wind ramps in the morning and downwards ramps in the afternoon. This observation is consistent with observations in Huber *et al.* [2014] which analysed onshore wind ramp events in Ireland, Germany, and Italy. Sinden [2007] also analysed the wind speeds profiles in the UK and found a similar diurnal pattern. However, this effect does not occur offshore. As the distance from the coast to offshore wind sites increases, the effect reduces. This is why there is no observable diurnal pattern.

Figure 4.11c shows the 1-h wind ramp events for each of the individual onshore and offshore wind regions and the aggregate ramp events for the 30 GW wind scenario. Offshore wind regions experience significantly larger and more extreme ramp events than onshore wind regions. This is partly because of the complex onshore topography that reduces the correlation between

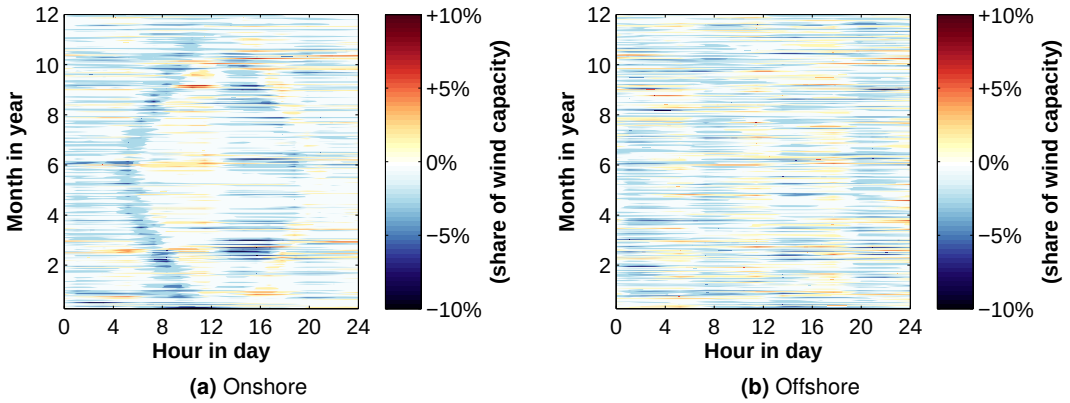

Figure 4.14: Temporal distributions for onshore and offshore 1-h wind ramp events in 2010.

onshore wind sites and partly because there are fewer offshore wind farms in each region. In other words, offshore wind regions contain fewer wind farms which experience similar conditions so the ramp events are more extreme.

The frequency distributions in Figure 4.11c have zero-mean and are broadly symmetric. When the outputs of all the regions are aggregated the frequency distribution becomes much tighter with the number of wind ramp events greater than ± 0.1 falling significantly. This is very important for flexibility considerations in systems with large penetrations of wind. The relative change of ramp events is reduced with greater geographic smoothing.

Extreme wind ramp events

The largest and most severe upwards and downwards wind ramp events occur when the outputs from multiple wind regions are highly correlated. Figure 4.15 shows the largest upwards and downwards 1-h ramp events during the time period between 2000 and 2010. The large changes in output occur when a large number of wind regions all change in output over a short time window. The result is a very large ramp event that occurs across the whole of GB.

The duration of wind ramp events is also important for understanding wind variability. So far only 1-h wind ramp events have been considered. In order to compare wind ramp events on the same scale, each wind ramp event is divided by the time window Δt:

$$\frac{\Delta W_t}{\Delta t} = \frac{W_{t+\Delta t} - W_t}{\Delta t} \tag{4.2}$$

Figure 4.16 shows the frequency distributions for wind ramp events by time window. This allows longer and more sustained wind ramp events over longer time-scales to be compared with ramp events that occur for shorter durations. For the aggregate portfolio, the effect of increasing the time window from 1-h up to 24-h narrows the frequency distributions and

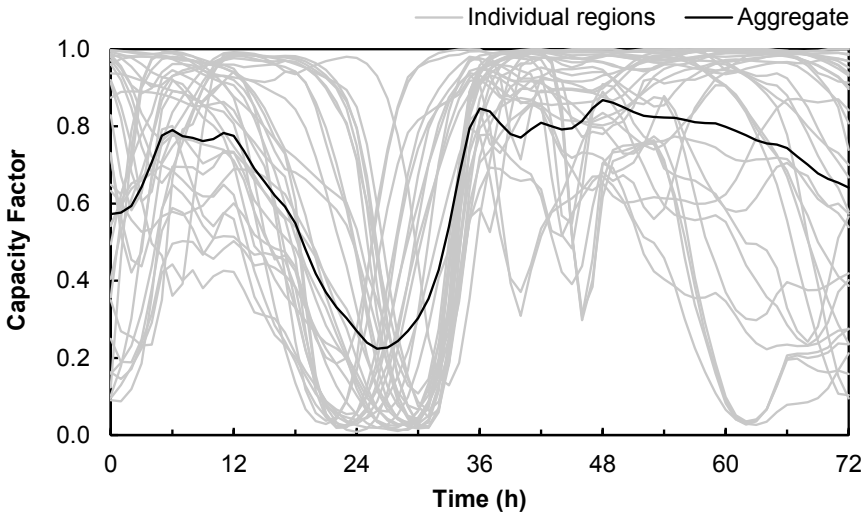

(a) Largest upward 1-h wind ramp event starting at 24/01/2002 00:00.

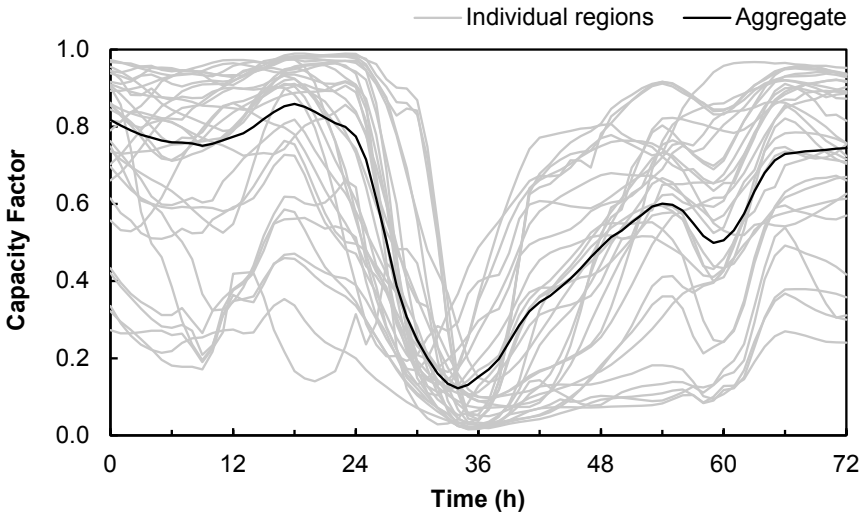

(b) Largest downward 1-h wind ramp event starting at 05/11/2003 00:00.

Figure 4.15: Largest upwards and downwards 1-h wind ramp events showing individual onshore/offshore wind regions and the aggregate wind portfolio with 30 GW capacity.

reduces the probability of ramp events greater that ±0.05 h. There is also very little difference between the frequency distributions for ramp events over 1-h, 2-h, and 4-h time-scales between ±0.05 h. This is primarily because wind ramp events are driven by the passage of large-scale synoptic weather systems over GB which typically persist for a number of hours to days. These mid-latitude and slow moving weather systems are well understood and are relatively predictable. Aggregate wind ramp events therefore occur over a longer period of time and at a reduced gradient as compared to individual farms or regions.

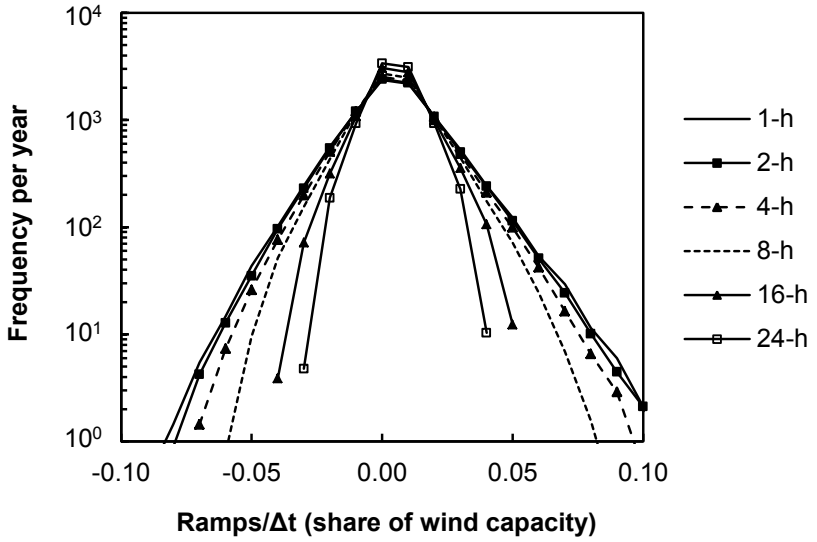

Figure 4.16: Frequency distributions for 1-h, 2-h, 4-h, 8-h, 16-h, and 24-h wind ramp events by time window Δt.

Limiting extreme wind ramp events

The blade pitch of wind turbines can be adjusted to limit the rate of change in wind power output. This control strategy could be utilised by both wind farm operators and system operators to ensure the power system has sufficient ramping capability to meet rapid changes in wind output. Figure 4.17 shows the ramp duration curve for onshore and offshore wind in the aggregate 30 GW wind portfolio between 2000 and 2010.

Limiting the upwards wind ramp rate to a maximum rate of change of 5% of rated capacity per hour (for the 30 GW scenario this corresponds to 1500 MW/h) results in an average energy loss of 40 GWh per year or 0.04% of total wind generation. It is possible to curtail an extreme upwards wind ramp with only limited losses in wind output.

Downwards wind ramps that exceed 5% of rated capacity per hour are less frequent but still occur 0.8% of the time or an average of 66 h per year. An extreme drop in wind output would require a rapid increase in power output from another generation asset.

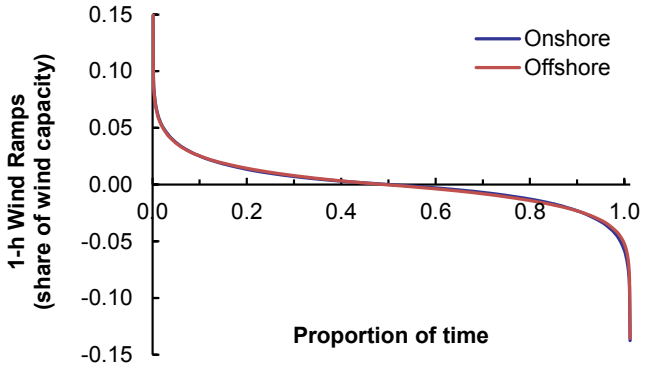

Figure 4.17: Duration curve of all 1-h wind ramps between 2000 and 2010 for the aggregate wind portfolio with 30 GW capacity.

4.3.3 Spatial variability

Wind sites in different geographical locations will not experience the same wind speed conditions. A wind portfolio that is geographically diverse will typically experience less wind output variability. Reducing wind variability and smoothing wind power output can be achieved with a geographically dispersed wind portfolio. This section examines the spatial wind variability from onshore and offshore wind sites to understand geographic smoothing and wind variability.

Previous work by Sinden [2007] first highlighted the wind power output correlation between pairs of onshore UK wind sites. The hourly power outputs of 66 onshore wind sites between 1970 and 2003 were used to calculate the correlation between each wind site pair. The correlation was found to fall exponentially with increasing distance between pairs of wind sites. In other words, wind sites that are situated further away from each other have a lower correlation between their hourly capacity factors. This work used discrete points from weather recording sites 10 m above ground level then extrapolated to hub-height.

Hawkins [2012], however, computed the correlation of a continuous field of wind speed data over the British Isles using outputs from the WRF modelling system. The hourly wind speeds from each 3 km grid square across the British Isles were compared against a reference point. The results showed that complex terrain influenced the correlation and that the fall in correlation with distance was steeper in the east-west direction. The highest rate of change in correlation was in the south-east direction, with wind site pairs aligning in this direction having the lowest correlations. The results agreed well with work by Sinden [2007], although Hawkins [2012] used wind speed data and not derived wind power outputs.

To further investigate this, wind sites from the wind speed reanalysis dataset are grouped as either onshore or offshore wind sites. Then, the hourly capacity factors for 337 onshore wind sites and 49 offshore wind sites between 2000 and 2010 are used to calculate the correlation between pairs of wind sites.

The latitudes and longitudes of each onshore and offshore wind site is used to calculate the

Euclidean distance between each wind site pair. This assumes the distance between wind sites is small and neglects the curvature of the Earth. The correlation between the instantaneous capacity factor of each wind site pair is calculated and plotted against the distance. Figure 4.18 shows the correlation coefficient of each onshore/offshore wind site pair as a function of distance. The instantaneous capacity factors of neighbouring wind sites with short distances are very well correlated. This is true for both onshore and offshore wind sites. However, The correlation between pairs of onshore wind sites falls more rapidly with increasing distance because of the more complex onshore terrain. There are a large number of correlated onshore wind pairs that are situated between 200 - 400 km apart shown in red in Figure 4.18. These results agree well with both Sinden [2007] and Hawkins [2012], indicating that the simulated capacity factors correctly capture spatial wind variability.

Extreme wind ramp events occur when a large proportion of wind farms change in output at a similar time. The correlation in the change in wind power output between wind sites is therefore more important for flexibility studies. To investigate this, 1-h wind ramp events are calculated using Equation 3.18 and the correlations between wind sites are computed. Figure 4.19 shows the correlations in the 1-h wind ramp events between pairs of onshore and offshore wind sites. The correlation coefficients fall very rapidly with increasing distance and fall to near-zero when wind sites are greater than 800 km apart. The correlation improves slightly with increasing time step. This is because the large-scale weather systems that drive wind speeds across the British Isles occur over a time-scale of several hours to days.

This is a positive result for power system operation and flexibility as it demonstrates how correlated operational/proposed wind sites are over time-scales similar to the start-up times of thermal power plants. It also shows that it is only wind sites that are close to each other that experience similar wind ramp events and that wind sites far away from each other have low correlations.

The capacity factor time-series for the 30 GW wind scenario $CF_t^{30\,\mathrm{GW}}$ is used to compute the correlations between the wind portfolio and each of the wind sites, see Figure 4.20. This gives an indication of how each wind site is correlated with the wind portfolio. The wind sites with the highest correlations with the wind portfolio are shown in red, and wind sites with a low correlation shown in blue. Wind locations on the periphery have the lowest correlations with the portfolio. These are known as asymmetric wind sites. It would be interesting to perform the same analysis but after cataloging and classifying each type of weather system. This would likely help improve wind forecasting and provide an improved method for estimating the reserve requirements for wind.

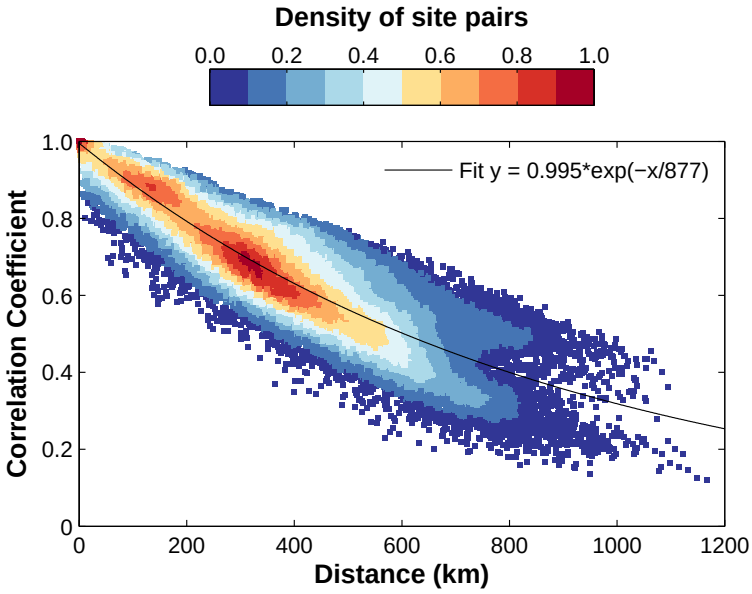

(a) Onshore wind sites

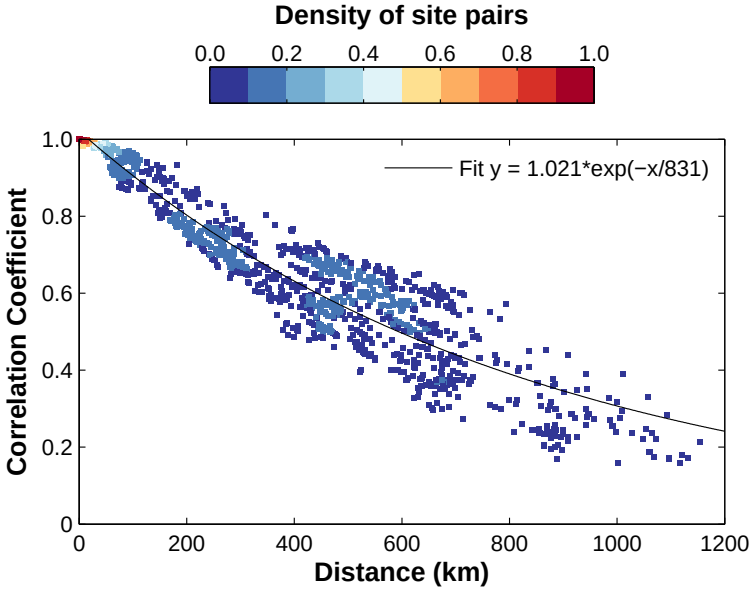

(b) Offshore wind sites

Figure 4.18: Correlation coefficients of capacity factors for onshore/offshore wind site pairs with distance.

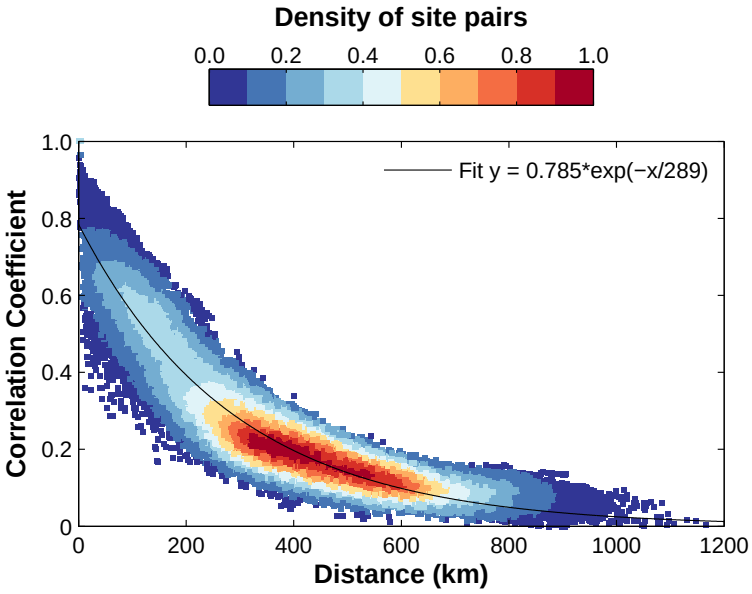

(a) Onshore wind sites

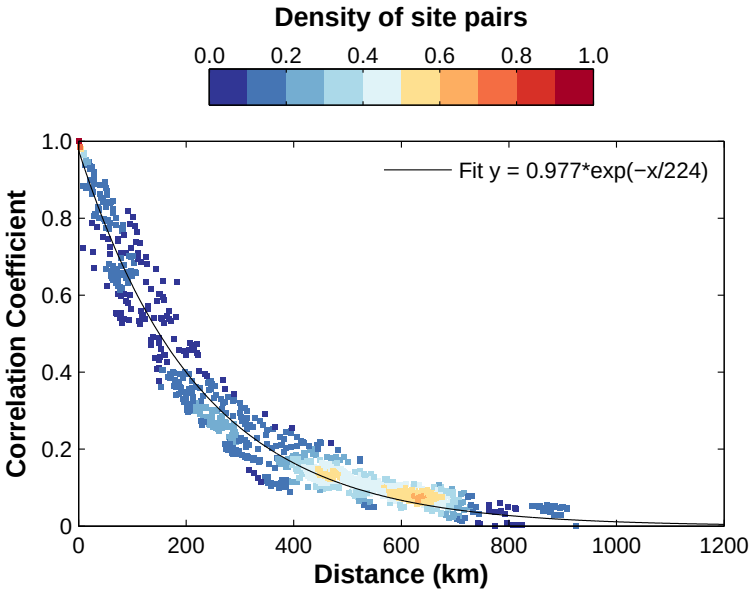

(b) Offshore wind sites

Figure 4.19: Correlation coefficients of 1-h wind ramp events for onshore/offshore wind site pairs with distance.

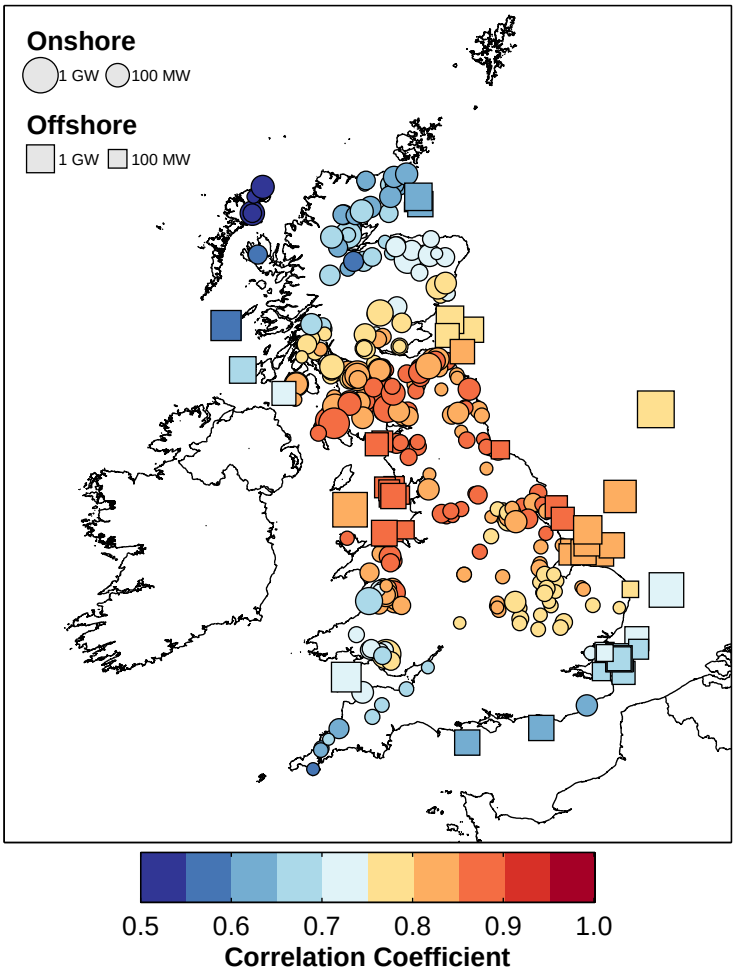

Figure 4.20: Map of correlation coefficients between wind sites and aggregate GB wind portfolio. It shows how the power output of each wind site is correlated with aggregate GB wind output.

4.3.4 Sensitivity analysis

Chapter 3 highlighted some of the factors and sensitivities that impact the output from wind farms. One important factor that affects wind farm output is the technical availability. The technical availability of a wind farm in any given region, whether onshore or offshore, depends on a number of factors that include the frequency and duration of faults such as electrical-mechanical problems; component-material failures and other considerations such as corrective, planned, preventive, and predictive maintenance schedules and extreme weather conditions. Typical values for onshore wind farm technical availability are around 98%. Onshore wind farm technical availability is typically higher than offshore wind where access for maintenance is more difficult and further away from maintenance centres, increasing the duration of outages. Technical availabilities may also be sensitive to season, with wind speed conditions in winter being more extreme with fewer calm periods where maintenance can be conducted. This is likely to disproportionately affect the technical availabilities of offshore wind farms.

To explore the sensitivity of capacity factors to technical availability, the average capacity factors of offshore wind regions are estimated assuming a constant technical availability of 100%, 90%, and 80% throughout the year, see Figure 4.21. The average capacity factors for offshore wind regions are 46.7% with a technical availability of 100%, 42.0% with 90%, and 37.4% with a technical availability of 80%. This shows that average capacity factors are very sensitive to technical availability. However, the main purpose of this exercise is to highlight the impact of seasonal differences in technical availability.

Taking the central 90% value for offshore technical availability, the impact of seasonal changes in technical availability is then investigated for offshore wind regions. Here, each month is divided into seasons where Spring={Feb, Mar, Apr}; Summer={May, Jun, Jul}; Autumn={Aug, Sep, Oct}; Winter={Nov, Dec, Jan}. Then a technical availability is applied to each season where Spring 90%, Summer 95%, Autumn 90%, Winter 85%. The average capacity factor assuming a constant technical availability of 90% is 42.0%. When seasonal technical availabilities are assumed, the average capacity factor of offshore wind regions falls to 41.7%. This very small decrease occurs because offshore wind sites typically have higher outputs during winter months. The impact of seasonal variations in technical availability is also very small when compared to absolute changes in the technical availability (i.e. changing from 90% to 80%).

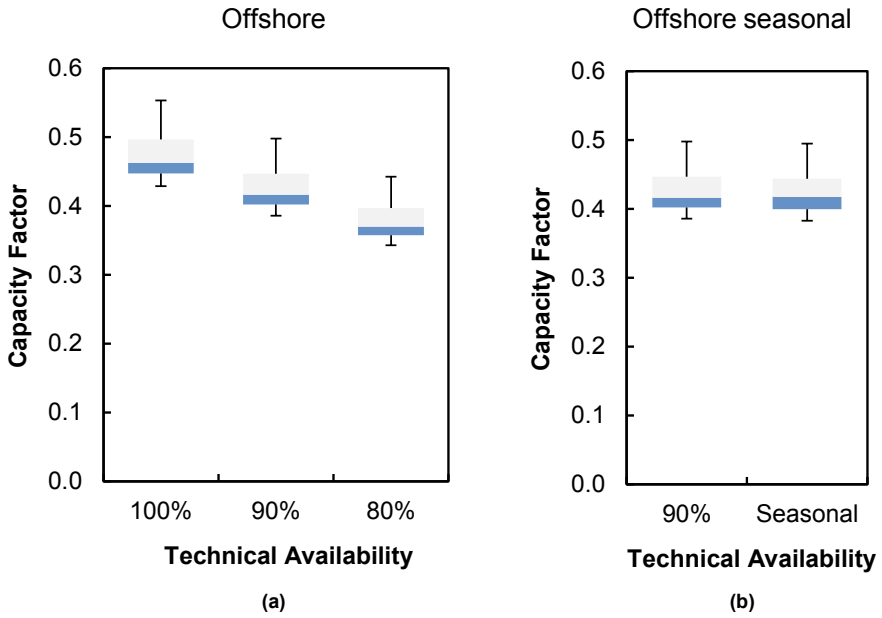

Figure 4.21: a) Average capacity factors for offshore wind regions and sensitivity analysis of technical availabilities that are constant throughout year. b) Average capacity factors for offshore wind regions with a constant technical availability of 90% and seasonal technical availability (Spring 90%, Summer 95%, Autumn 90%, Winter 85%). Box plot shows 25%, 50%, and 75% percentiles in regional capacity factors and whiskers show the minimum and maximum ranges.

4.3.5 Summary

This section examined the spatial wind variability of existing/proposed wind sites in GB between 2000 and 2010 and estimated the long-term correlation coefficients between wind site pairs. The correlation in capacity factors of wind site pairs falls exponentially with increasing distance and falls faster for pairs of onshore wind sites.

What is important for flexibility studies, however, is not the correlation in capacity factors but the correlation in the change in capacity factors or wind ramp events between wind sites as this will determine the maximum rate of change in wind output. This section calculated the correlation coefficients for wind ramp events over different time-scales between onshore/offshore wind site pairs. The correlation drops very rapidly with increasing distance.

A sensitivity analysis of technical availability on onshore and offshore wind capacity factors highlighted the sensitivity of technical availability values on annual capacity factors. The main purpose of this exercise was to highlight how average capacity factors drop significantly with decreasing technical availability and how relatively insensitive capacity factors are to seasonal changes in technical availability.

The next section introduces historical electricity demand data which is temporally matched with wind output data to assess net demand variability.

4.4 Electricity demand and wind output variability

The previous section analysed wind variability and wind ramp events over various time-scales. Wind variability, however, should be considered in context with electricity demand variability as it is net demand variability and uncertainty that will drive flexibility and reserve requirements in future wind-based power systems. This section considers both wind and electricity demand variability by examining temporally-consistent time-series' of demand and wind data. This section introduces historic electricity demand and outlines the methodology to produce temporally-matched weather-corrected demand data. Demand net wind ramp events are then assessed to understand the potential variability.

4.4.1 Electricity demand

Data sources

The extent to which wind power will impact power system operation will depend on its relation to electricity demand. In order to explore the impacts of various wind events on power system operation, it may be necessary to use many years worth of demand and wind input data in parallel. It is therefore important to use temporally consistent time-series' of electricity demand and wind generation to uphold the complex non-linear relationship between demand and weather patterns. However, electricity demand evolves over time with changing economic and winter weather conditions. Therefore it is necessary to normalise electricity demand to correct for varying winter demand peaks. This normalisation process allows different years of demand-wind data to be compared with the same generation portfolio whilst maintaining the underlying weather and demand patterns and interdependencies.

One approach would be to use a number of typical daily demand profiles to represent a year of demand data. Green *et al.* [2014] use a k-means clustering algorithm to simulate clustered electricity demand data for GB and report vast increases in simulation times when running a dispatch model. It would then be possible to run a large number of simulations and perform a rigorous sensitivity analysis on critical input parameters [Green *et al.*, 2014]. However, the purpose of this study is to examine the impacts of variability on operating regimes. This requires using complete time-series' of demand-wind data to capture the range of possible weather events.

National Grid [2013] publish historic Average Cold Spell (ACS) Winter Peak (WP) demand data in their Winter Outlook reports for each winter period. The realised ACSWP demand is published after each winter period and is the peak demand level under normal winter weather conditions, or the peak demand which would have been observed for that winter's underlying demand profile given historically typical winter weather conditions. ACS peak demand is also forecast by the National Grid for each approaching winter period and compared with the expected de-rated generation availability at the time of ACS peak demand forecast plus 750

MW of interconnector imports [National Grid, 2014b]. Given an amount of reserve, this allows the LOLE to be calculated for that winter period.

Weather-corrected demand

Using the realised ACS Winter Peak demand D_t^{ACS} from National Grid [2013] between 2001 and 2011 allows peak electricity demand D_t^{peak} for each winter period t to be normalised and rescaled around 60 GW. The normalised weather-corrected peak demand D_t' for each winter period is found by:

$$D_t' = \frac{60 \cdot D_t^{\mathrm{peak}}}{D_t^{\mathrm{ACS}}} \tag{4.3}$$

where values for ACS Winter Peak demand D_t^{ACS} and normalised peak demand D_t' are shown in Figure 4.22a. The normalised weather-corrected peak demand D_t' values for each winter period are used to rescale hourly electricity demand data from National Grid [2015b].

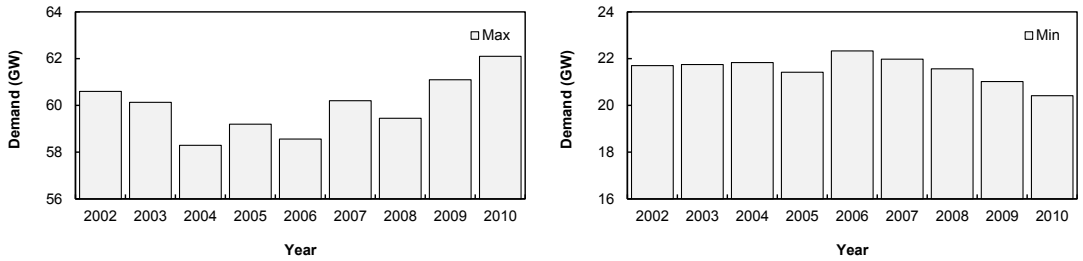

(a) Maximum demand **(b)** Minimum demand

Figure 4.22: Weather-corrected electricity demand by year.

This methodology allows historic electricity demand to be temporally-matched with wind data whilst preserving both short- and long-term underlying changes in demand. This process also maintains the interdependencies and complex relationships between electricity demand and weather conditions and normalises absolute peak demand levels caused by evolving economic activity and extreme winter weather conditions. This approach of using linear scale factors to adjust demand data does not reflect the underlying demand patterns that may evolve into the future because of energy efficiency measures, consumer behaviour, economic conditions, or changing heat/transport demands.

The weather-corrected electricity demand time-series is then reduced in temporal frequency to match the hourly WRF wind speed reanalysis hourly time-series'. For each hourly demand data point, the average of the two half-hourly demand data points is used. An alternative approach is to take the higher of the two half-hourly demand data points, which is sometimes necessary for generation adequacy and reliability capacity assessments. The result gives temporally consistent demand and wind generation data, derived from WRF wind speed reanalysis data. Using multiple years of historic demand and wind input data allows for a temporally explicit

intercomparison of power system operation to be made for numerous demand-wind events and wind deployment scenarios. The process of using historic weather-corrected demand data that is then normalised follows the approach in Eager [2011].

Annual and monthly variation

Figure 4.23a shows the annual electricity demand in TWh between 2002 and 2010. The standard deviation in annual demand is 4.5 TWh. Figure 4.23b shows the average demand in TWh for each month. Although 11 years worth of wind renalysis data is available between 2000 and 2010 from Hawkins [2012], the years 2000 and 2001 are discarded because reliable demand data for GB could not be found. This means that only 9 years worth of consistent demand and wind data is available between January 2002 and December 2010. It is therefore not possible to draw solid conclusions about the availability of wind during peak demand periods. In addition, the impacts of medium- to long-term climate change are considered beyond the scope of this work as it is not understood how the relationship between electricity demand and meteorological weather patterns will change in the future. An alternative approach is to scale historic demand data on an energy basis. For example, Staffell and Green [2016] increased historic electricity demand data by the ratio of 350 TWh to the weather-corrected annual energy demand for each year.

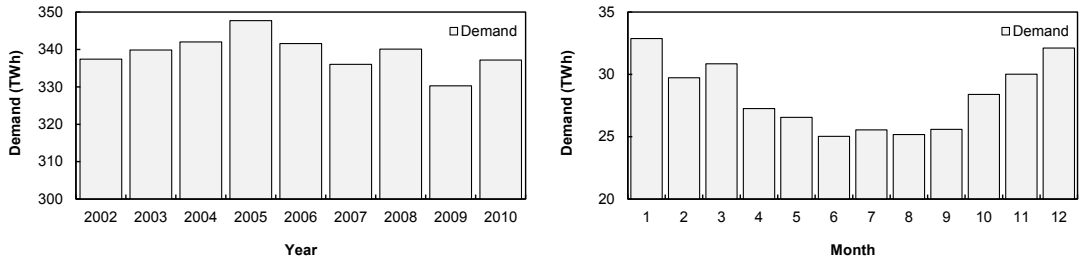

(a) Average demand by year **(b)** Average demand by month

Figure 4.23: Normalised electricity demand by year and month.

Hourly variation

Figure 4.24 shows the temporal distributions of electricity demand and demand net 30 GW of wind capacity using 2010 data. The temporal distributions illustrate the net demand profile by day and month as a share of peak demand. Peak demand occurs in winter months at around 17:00 - 18:00 on week days. Increasing amounts of wind capacity significantly impacts net demand patterns. Large volumes of wind generation can reduce net demand for up to several days.

Demand variability has been met traditionally by thermal power plants performing dedicated ramps. The next section examines historic electricity demand variability by analysing demand

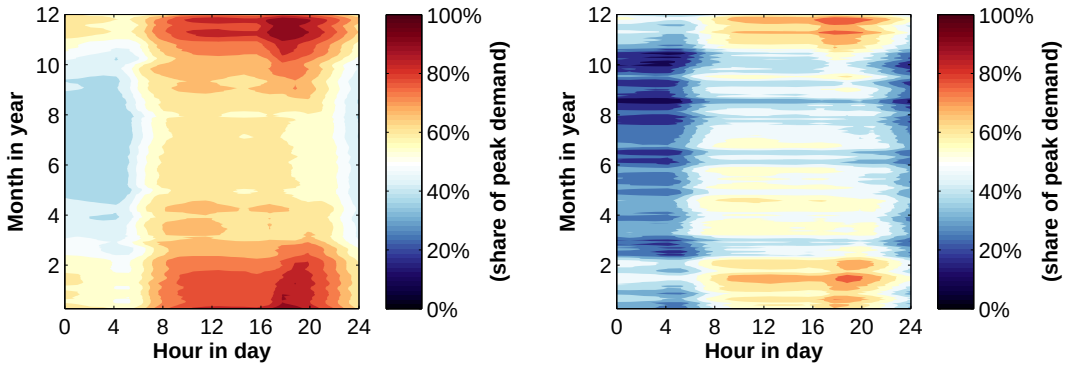

(a) Demand **(b)** Demand net 30 GW wind

Figure 4.24: Temporal distributions of demand and demand net wind as a share of peak demand using demand-weather data for 2010.

ramp events and puts it in context with expected future wind variability. This will allows assessments to be made about existing and additional flexibility requirements.

4.4.2 Net demand variability

Demand net wind

Net demand is calculated by subtracting hourly wind generation from electricity demand. This is the net demand that needs to be supplied by generation assets. For wind capacities of 15 GW, 30 GW and 45 GW, the demand net wind duration curves are shown in Figure 4.25 for 2010 with a peak load of 62.1 GW. The area under the curves gives the total energy that needs to be supplied by generating units.

Annual and monthly variation

In order to understand the potential flexibility and reserve requirements in power systems with large amounts of wind generation, it is important to consider the variability in net demand over various time frames. This will allow a basis for understanding the potential flexibility requirements and the additional flexibility required to manage wind variability. A demand ramp event is the gradient of the electricity demand D_t over a given time period Δt and is expressed as a fraction of the maximum demand $D_{\max}$ over the time period:

$$\frac{\Delta D_t}{D_{\max}} = \frac{D_{t+\Delta t} - D_t}{D_{\max}} \tag{4.4}$$

where 1-h is the minimum Δt. Figure 4.27 shows the temporal distributions for demand ramp events before wind is considered over 1-h and 4-h time-scales. Similarly, a net demand ramp

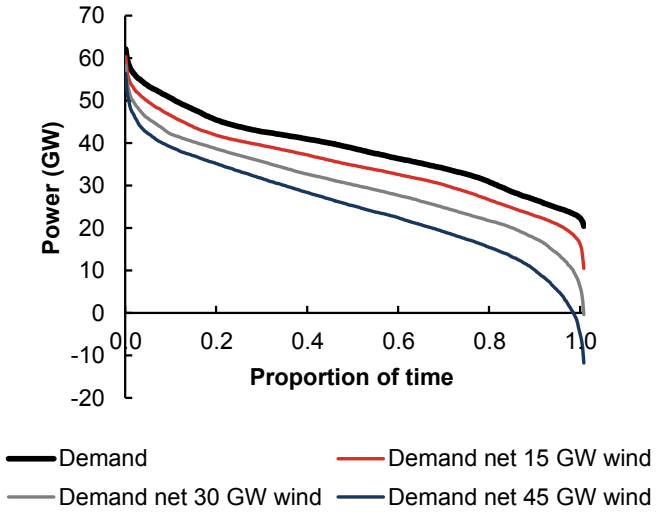

Figure 4.25: Net demand duration curves with 15 GW, 30 GW, and 45 GW of wind (2010 demand-wind year).

event, which considers both demand and wind variability where net demand $D_t^{\text{net}} = D_t - W_t$, is expressed as:

$$\frac{\Delta D_t^{\text{net}}}{D_{\max}} = \frac{D_{t+\Delta t}^{\text{net}} - D_t^{\text{net}}}{D_{\max}} \tag{4.5}$$

Figure 4.26a shows the inter-annual variation in 1-h demand ramp events. 68.26% of demand ramp events occur within the dark shaded areas or ± 1 standard deviation. 95.44% or $\pm 2\sigma$ of demand ramp events occur within the medium shaded areas and 99.74% or $\pm 3\sigma$ of demand ramp events occur within the light shaded areas. There is little inter-annual variation in demand ramp events. The maximum upwards 1-h ramp events are approximately 9000 MW/h and all occur in the morning between 06:00 and 08:00. The largest downwards ramp events are approximately 6000 MW/h. This is the variability in demand that traditional power systems have to manage.

Figure 4.26b shows the monthly variability in 1-h demand ramp events. There is an interesting seasonal pattern. The largest maximum upwards and downwards ramp events occur in winter months. July and August witness the smallest maximum upwards and downwards ramp events.

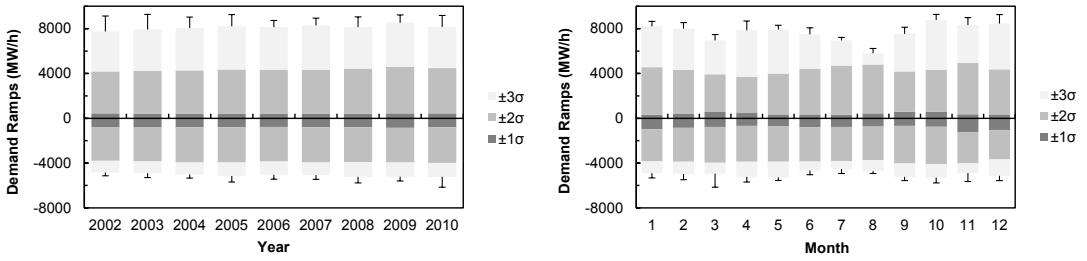

(a) Demand ramps by year

(b) Demand ramps by month

Figure 4.26: Variation in 1-h demand ramps by year and month. Box plots show demand ramps within $\pm 3\sigma$ and whiskers show maximum and minimum 1-h demand ramps.

Hourly variation

Figure 4.27 shows the temporal distributions of demand variability expressed as a proportion of peak demand over 1-h and 4-h timescales. These ramp events are dominated by the underlying and predictable changes in electricity demand, such as the morning pick-up.

The upwards ramping requirement is dominated by the morning pick-up, occurring between 06:00 - 10:00. The largest 1-h demand ramp is around 9200 MW/h or 14.9% of peak demand per hour which is far greater than any observed wind ramps on the same time-scale. It should be noted that daylight savings time causes the demand ramp events to shift 1 hour between the end of March and October.

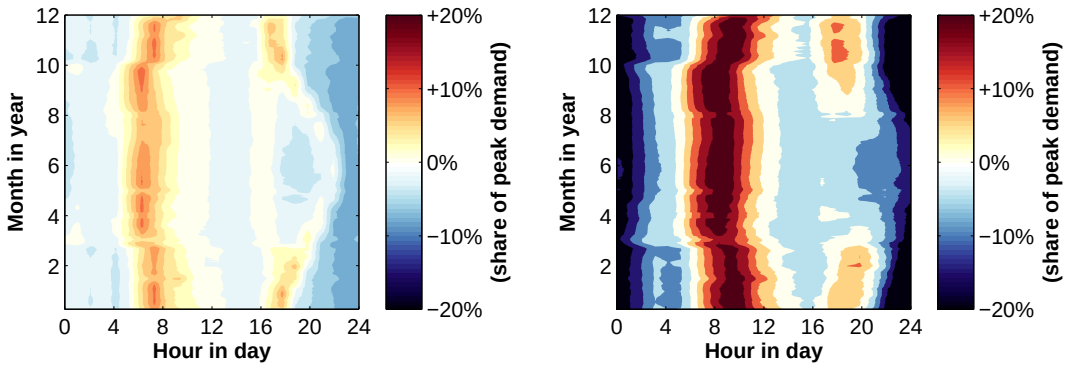

(a) 1-h ramp events

(b) 4-h ramp events

Figure 4.27: Temporal distributions of 1-h and 4-h demand ramp events in 2010 as a share of peak demand.

The duration curves of 1-h demand ramps with 45 GW of wind capacity is shown in Figure 4.28. The duration curve contains all of the net demand ramps between 2002 and 2010 (78888 hours). It contains all of the hourly changes in net demand ordered from largest to smallest. A positive value indicates that an increase in net demand occurs in the next hour and similarly a negative value indicates a decrease in net demand is required.

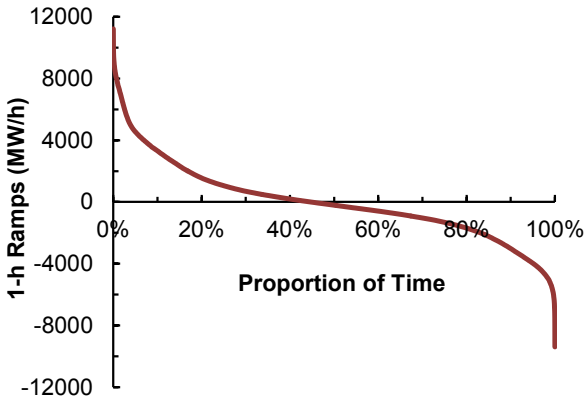

Figure 4.28: Ramp duration curve of demand net 45 GW wind capacity between 2002 and 2010.

Extreme demand ramp events

Figure 4.29 shows a close up of the 'tails' of the demand ramps in Figure 4.28. This figure shows in more detail how net demand variability changes with increasing wind capacity. The maximum hourly increase in net demand increases from 9264 MW/h with no wind to 11213 MW/h with 45 GW of wind capacity. The maximum hourly decrease in net demand increases from -6146 MW/h with no wind to -9388 MW/h with 45 GW of wind capacity.

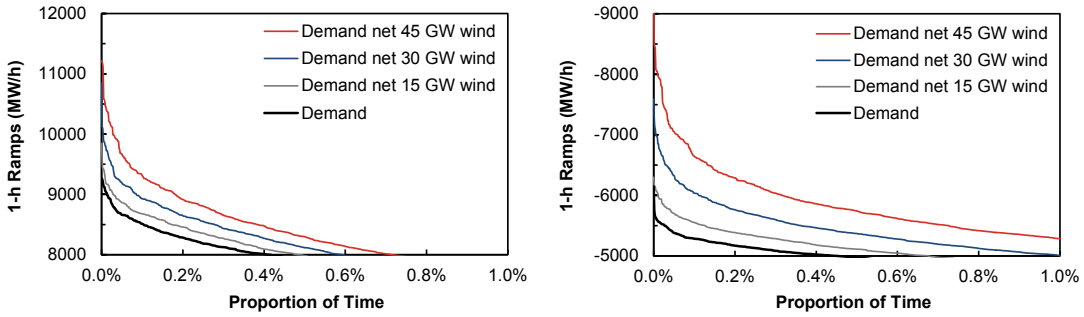

(a) Extreme upwards demand ramps

(b) Extreme downwards demand ramps

Figure 4.29: Extreme upwards/downwards 1-h demand ramps between 2002 and 2010.

After analysing the largest 100 morning pick-ups between 2002 and 2010, all of them occur during weekdays between Monday to Friday between 06:00 and 08:00 local time. 23% of them occur on Mondays, 21% on Tuesdays, 20% on Wednesdays and Thursdays, and 16% on Fridays. The largest 20 of these demand ramps are shown in Figure 4.30. Some of the demand ramps have been shifted by 1 hour to account for daylight savings time. The largest 20 morning pick-ups all follow the same profile. That is, between 04:00 and 06:00 there is a sharp increase in the ramping requirement which later falls at 08:00. This predictable pattern allows system operators to schedule power plants to come online in time for the morning pickup.

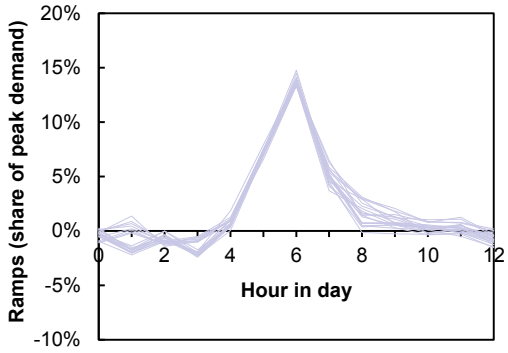

Figure 4.30: The largest 20 morning pick-up demand ramp events in 2010.

4.5 Summary

This chapter presented methodology to construct wind deployment scenarios that are used in later chapters to assess the impacts of wind variability. Wind site locations were selected from the Renewable UK Wind Energy Database and used to characterise and construct plausible wind deployment scenarios that meet future renewable targets.

Average capacity factors were then analysed between 2002 and 2010 and the inter-annual variations in wind output are demonstrated. The seasonal and hourly variations in wind output was also assessed to better understand the potential flexibility requirements for wind. The temporal variability was then assessed at different timescales by analysing wind ramp events. Extreme upwards and downwards wind ramp events were examined to understand the maximum rates of change in wind output.

The spatial variability in wind output was also assessed by plotting the correlation coefficients between pairs of onshore and offshore wind sites. The results show that the correlation between two wind sites falls with increasing distance. This is important for wind sites that are situated in the centre of GB which are highly correlated with the output of the aggregate wind portfolio. The sensitivity of capacity factors to seasonal technical availability assumptions was assessed for the onshore and offshore wind fleet.

Historic electricity demand was obtained and normalised using Average Cold Spell (ACS) Winter Peak demand data to obtain a weather-corrected demand time-series that was temporally-matched with the wind output time-series. This preserves both short- and long-term underlying changes in demand. The variability in demand was then assessed to understand net demand variability and extreme net demand ramp events.

Chapter 5

Unit commitment formulation

5.1 Introduction

Previous chapters outlined the sources of flexibility available in power systems and introduced the unit commitment problem. Chapter 4 modelled wind output variability for a range of future GB wind portfolios to understand the flexibility challenge. It is clear from this that thermal power plants will be increasingly required to provide flexibility services to manage the uncertainty and variability from additional wind generation. This may potentially involve more frequent start-ups/shut-downs for certain units and may require increased ramping capabilities and reserve contributions. This may significantly impact the operating regimes of thermal power plants, which are an important consideration for minimising fuel costs and maximising the operational flexibility of power systems. Part-load cycling operations and frequent load changes, caused by increasingly variable wind output, increases efficiency losses and CO_2 emissions. Also, the part-load technical limitations of thermal power plants will constrain their ability to provide flexibility during low net demand periods. It is therefore very important to consider CO_2 costs, start-up/shut-down costs, part-load efficiency losses, curtailment costs and the costs associated with providing additional reserve in unit commitment models.

5.1.1 Outline

This chapter presents a new framework for the unit commitment and economic dispatch (UCED) problem that considers a portfolio of energy storage units, flexible CO_2 capture equipped thermal power plants and conventional thermal units to minimise the operating costs (fuel, CO_2, and variable O&M costs) for future power systems with large proportions of wind. Security constraints for reserve are used with thermal power plant technical operating constraints (power output limits, minimum up/down times, ramp rates, start-up times) to model power system operation. Time-dependent start-up cost functions model hot/warm/cold start-ups and amine-based CCS-equipped units are assumed to capture a proportion of the CO_2 emissions during start-up and shut-down. New decision variables are introduced into the unit commitment problem for CO_2 capture plants and additional parameters are included for solvent costs, solvent degradation, and transport and storage costs. A detailed formulation of the operating and

system constraints is outlined and upwards and downwards reserve requirements are explicitly represented. Internally and temporally consistent demand-wind input data is used for GB for a range of future wind capacity scenarios. This is to capture the daily, weekly, and seasonal changes in demand-wind characteristics.

The model has both a unit commitment (UC) stage and an economic dispatch (ED) stage to account for changing demand-wind forecasts at the time when units are committed and at delivery time.

The UCED model balances the requirement for low computational time (several hours to run an 8760 h simulation) and the need to consider all of the key system and unit operating constraints such as ramp rates, minimum and maximum power output limits, start-up times, and minimum up/down times.

This UCED model is used for a range of simulations to assess the impacts of wind generation capacity on the operating regimes of thermal power plants and the interactions between CCS units and other generation assets. The relationship between CO_2 emissions and power plant output is further developed to help improve CO_2 emissions analysis for intense cycling/ramping operations.

5.2 Model formulation

5.2.1 Introduction

In order to study the operating regimes of thermal power plants in future wind-based power systems, a UCED model is developed for the following reasons:

- unit commitment models are a sophisticated and mature method for evaluating power system operation and the individual operating profiles and generation outputs of thermal power plants can be simulated for each time period;
- technical operational constraints of individual generating units are accounted for such as ramp up/down rates, minimum up/down times, minimum and maximum power output limits, and reserve contributions;
- piece-wise linear approximations can be used to represent the non-linear fuel consumption of thermal power plants, capturing detailed dispatch profiles; and
- key reserve and flexibility requirements can be represented.

For this work, a forward dynamic programming (DP) technique is used which can examine more than one predecessor, overcoming the traditional drawbacks of dynamic programming [Sheble and Fahd, 1994]. The unit commitment model is implemented in MATLAB and all simulations are conducted on an Intel Core i5-2540M 2.60 GHz processor.

Forward DP methods have been used extensively in unit commitment problems [Sheble and Fahd, 1994]. Foreward DP techniques start at an initial time period $t = 0$ and then work chronologically to find the least-cost solution, see Figure 5.1. DP techniques search the state space of feasible generators to find an optimal solution. They also allow for non-linear fuel consumption characteristics and time-dependent start-up costs to be modelled with high accuracy.

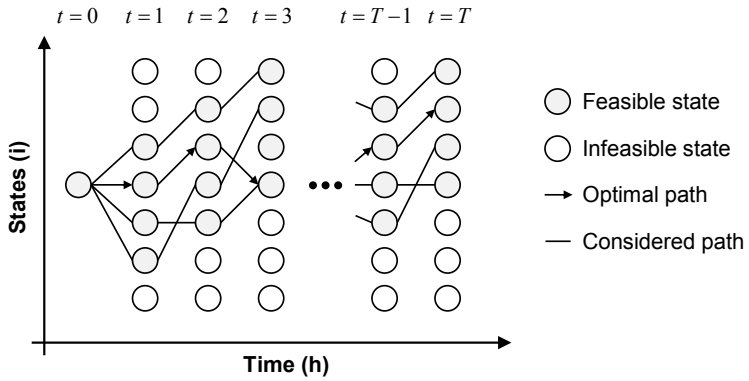

Figure 5.1: Transition paths for unit commitment schedule with dynamic programming.

The feasible states that satisfy net demand and both upwards and downwards reserve requirements are first identified. Generation states that are infeasible are not computed which vastly reduces the number of possible combinations of generators for each time period. The least-cost transition path between states is then found. Clustering of identical units or near-identical units can also vastly increase the speed of computation.

A dynamically ranked priority list method is used to categorise generators in terms of operating costs and flexibility [Ma, 2012]. Sets of flexible generators with similar or identical cost characteristics and technical operating parameters are dispatched in order of priority. The optimisation algorithm would otherwise spend a large amount of time comparing the outputs for generators with very similar flexibility and cost characteristics and yet the solution output would still be the almost identical. Flexible units are therefore dispatched according to the dynamically ranked priority list unless any of the operating constraints are violated such as the minimum down time. This heuristic constraint significantly reduces the computational time and enables the analysis of large thermal generation portfolios over multiple years.

5.2.2 Methodology

A brief overview of the structure of the UCED optimisation problem to evaluate power plant operating regimes is shown in Figure 5.2.

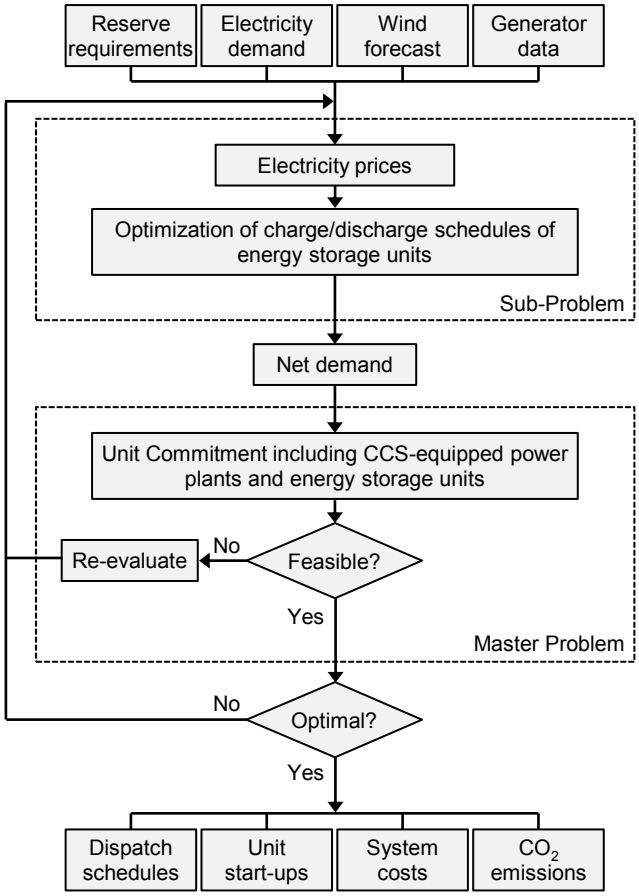

Figure 5.2: Structure of the unit commitment and economic dispatch (UCED) optimisation problem.

Input data

The unit commitment model requires input data in order to simulate the least-cost operating regimes and generation levels of the thermal generation portfolio. The sensitivity of the results to variations in input variables is investigated. This input data accounts for the following considerations:

- individual unit technical operating parameters such as minimum and maximum power output limits (MW_e), ramp up/down rates (MW_e/h), minimum up/down times (h), start-up times (h), and initial statuses (h);
- incremental heat rates are represented using piece-wise linear approximations (MW_{th}/MW_e);
- CO_2 emission intensities for different fuel types (tCO_2/MWh_{th}) [DECC, 2013b];
- generator costs include fuel costs (£/MWh_{th}), CO_2 costs (£/tCO_2), variable O&M costs (£/MWh_e), ramping costs (£/MW_e), start-up costs (£), shut-down costs (£);
- time-dependent start-up costs require values for the fuel input to minimum stable generation (MWh_{th}), fixed start-up costs (£), and thermal cooling constants (h) to represent

hot/warm/cold start-ups; and

- temporally-matched electricity demand data (MW_e) and onshore/offshore wind generation data (MW_e).

Additional input data is also required for CCS-equipped power plants which includes:

- technical operating parameters for each of the CO_2 capture plants including the minimum and maximum CO_2 capture rate limits (%), power consumption required to capture 1 tonne of CO_2 (MWh_e/tCO_2), and ramp up/down rates (%/h);
- bypass/venting capability (-);
- solvent degradation rates (kg/tCO_2);
- cost data includes additional variable O&M costs for the capture plants (£/tCO_2), solvent make-up costs (£/kg), and transport and storage costs (£/tCO_2); and
- CO_2 capture rates during start-up and shut-down (%).

Unit commitment and economic dispatch

At the unit commitment stage, the charge/discharge profiles of energy storage units are simulated using a Monte Carlo based optimisation technique and thermal units with/without CCS are committed to meet *forecast* net demand and system reserve requirements.

At delivery time, energy storage units and thermal power plants are re-dispatched to meet *realised* net demand and provide system reserve requirements. This two-stage UCED optimisation step is similar to the market arrangements in GB as discussed in Section 2.2.

Two methods are used in this work to analyse power plant operating regimes and system operation. The first is to use a stochastic differential equation to simulate wind imbalances which is then added to the realised wind time-series to produce a forecast wind time-series. This is then used to simulate energy storage operation and commit thermal units to meet *forecast* net demand and reserve requirements 4-h ahead of real-time. This is because it is current practice for the system operator of GB, the National Grid, to make commitment decisions 4-h ahead of real time [National Grid, 2011a]. At the economic dispatch stage at delivery time, energy storage and thermal units are re-dispatched to meet *realised* net demand and the change in plant dispatch can be studied. This is to understand the impacts of wind imbalances on the operational flexibility of the generation portfolio. However, the main limitation of this stochastic approach are the large computational requirements and solution times.

The second method uses the realised wind time-series at the UC stage (with prefect foresight) and commits energy storage and thermal units to provide reserve requirements to 3.5σ of demand-wind uncertainty. This ensures that the committed units can supply net demand and meet system requirements 99.95% of the time. This method, if repeated, will give an identical solution and so it is possible to understand how small changes in ramp rates, for example, affect the unit commitment schedule and total system costs.

The unit commitment model schedules reserve requirements to meet forecast demand and wind uncertainty to 3.5σ. Stochastic wind forecast errors are simulated and used at the unit commitment stage to make commitment decisions. Realised wind is then used at the economic dispatch stage (delivery time) to re-dispatch units to meet realised net demand. This process can also be performed with perfect foresight i.e. realised wind is used at both the unit commitment and economic dispatch stages. Reserve is still scheduled to meet 3.5σ in demand and wind uncertainty. Using wind and demand profiles with perfect foresight removes the need to perform multiple stochastic simulations while still allowing reserve to be scheduled to meet demand and wind uncertainty to 3.5σ.

Output data

The unit commitment and economic dispatch algorithm uses the input data and makes decisions on which individual generators to commit for each time period by incurring start-up/shut-down costs and adjusting the generation levels to meet net demand at least-cost. Dynamic reserve requirements reflect the level of wind that is forecast. A number of outputs are then produced by the model which can then be evaluated. The outputs of the unit commitment model include:

- power output (MW_e), fuel input (MW_{th}), CO_2 emissions (tCO_2), and operating costs of thermal power plants (£);
- reserve contributions of individual generators (MW_e);
- start-up and shut-down events and the time spent online/offline before each start-up/shut-down event (h) which can be used to evaluate the split between hot/warm/cold start-ups and the time spent offline;
- wind curtailment (MW_e); and
- charging/discharging power (MW_e) and energy stored (MWh) for individual energy storage units.

Metrics for assessment

The outputs of the UCED model are used to evaluate the total system cost, CO_2 emissions and operating regimes of power plants. The fuel costs, CO_2 costs, and operating costs for each power plant in each time period allows the total costs to be calculated. It is then possible to understand the influence of certain key technical operating parameters on the operating regimes of the generation portfolio. For example the value of a lower minimum stable generation limit or the value of faster ramp rates can be evaluated in each of the scenarios. Some of the possible ways to assess thermal power plant operating regimes include:

- load factor;
- total GW ramped;
- number, frequency and duration of large upwards/downwards ramps;

- time spent ramping;
- time spent at part-load;
- time spent at max/min power output limits;
- time spent online/offline; and
- number of hot/warm/cold start-ups.

5.2.3 Model limitations

The model includes many detailed constraints that take into account the operating and system constraints of power systems with large amounts of wind, CCS and energy storage. However, there are a number of model limitations that should be outlined.

- The UCED is performed at system level and the operational security and physical constraints of the transmission network are not modelled. This analysis therefore assumes a single-bus transmission network. This is to enable focus and isolate the impacts of wind generation capacity on power plant operating regimes and dispatch schedules. Although, it is acknowledged that transmission constraints are important in power system models and have important effects on price and the dispatch of electricity in real power systems.
- This analysis assumes post-combustion CO_2 capture technology with amine scrubbing. However, there are a number of other CO_2 capture technologies and configurations such as oxyfuel and pre-combustion CO_2 capture, that should be explored in future work.
- The work only includes time-series for onshore and offshore wind. It is likely that future power systems will have contributions from a number of renewable sources such as solar PV. Therefore future studies should consider the output, variability and uncertainty from a confluence of VRE technologies.
- The UCED does not take into account how real GB market participants would manage uncertainty within their own generation portfolios. Market participants are likely to adjust their contractual electricity traded positions to balance wind variability.

5.2.4 Decision variables

Tables 5.1 and 5.2 provide a description of the symbols used to represent system variables and parameters, respectively. Tables 5.3 and 5.4 describe the variables and parameters used to represent thermal generators, respectively. All set elements and parameters are lowercase. All sets and variables are uppercase.

A binary decision variable is required to represent the operational state of each base generator unit:

$$u_{g,t} = \begin{cases} 0 = \text{off} \\ 1 = \text{on} \end{cases} \tag{5.1}$$

for all thermal units g and time periods t.

For example, when a power plant is online $u_{g,t} = 1$. For CCS-equipped power plants, an additional binary decision variable is required to represent the operational state of the post-combustion CO_2 capture equipment:

$$u_{g,t}^{\text{capt}} = \begin{cases} 0 = \text{off} \\ 1 = \text{on} \end{cases} \tag{5.2}$$

where $u_{g,t}^{\text{capt}}$ represents the status of the CO_2 capture facility with no interim solvent storage. The superscript 'capt' refers to the CO_2 capture and compression system. Inflexible generators that cannot adjust power output are considered offline from the unit commitment model. Continuous decision variables are required to indicate the power output of each generator g at each time period t.

5.2.5 Start-up and shut-down events

A base power plant start-up or shut-down event occurs when:

$$u_{g,t} - u_{g,t-1} > 0 \tag{5.3}$$

$$u_{g,t} - u_{g,t-1} < 0 \tag{5.4}$$

For a thermal power plant with CO_2 capture facilities, it is essential to also model the start-up and shut-down events of the CO_2 capture systems. CO_2 capture plant start-up or shut-down event occurs when:

$$u_{g,t}^{\text{capt}} - u_{g,t-1}^{\text{capt}} > 0 \tag{5.5}$$

$$u_{g,t}^{\text{capt}} - u_{g,t-1}^{\text{capt}} < 0 \tag{5.6}$$

5.2.6 Objective function

The objective of traditional unit commitment formulations is to minimise the system cost of meeting demand. The objective function of the unit commitment model developed in this work is to minimise the variable operating costs, start-up/shut-down costs, and curtailment costs of thermal power plants as follows:

$$C^{\text{total}} = \min \sum_{t=1}^{T} \left(\sum_{g=1}^{G} \left(C_{g,t} + C_{g,t}^{\text{start}} + C_{g,t}^{\text{shut}} \right) + C_{t}^{\text{curt}} \right) \tag{5.7}$$

where C^{total} are the total system costs (£), $C_{g,t}$ are the variable operating costs (£), $C_{g,t}^{\text{start}}$ are the start-up costs (£), $C_{g,t}^{\text{shut}}$ are the shut-down costs (£), and C_{t}^{curt} is the cost of curtailment (£) for all generator units g and time periods t.

System variables		
D_t	Electricity demand at time t	(MW_e)
W_t	Wind power output at time t	(MW_e)
W_t^{on}	Onshore wind power output at time t	(MW_e)
W_t^{of}	Offshore wind power output at time t	(MW_e)
W_t^{curt}	Total wind power curtailed at time t	(MW_e)
$W_t^{on,curt}$	Offshore wind power curtailed at time t	(MW_e)
$W_t^{of,curt}$	Offshore wind power curtailed at time t	(MW_e)
R_t^{up}	Upwards reserve requirement at time t	(MW_e)
R_t^{dn}	Downwards reserve requirement at time t	(MW_e)
$R_t^{SR,up}$	Upwards spinning reserve requirement at time t	(MW_e)
$R_t^{SR,dn}$	Downwards reserve requirement at time t	(MW_e)
$R_t^{StR,up}$	Upwards standing reserve requirement at time t	(MW_e)
$R_t^{StR,dn}$	Downwards standing reserve requirement at time t	(MW_e)
C^{total}	Total system costs	(£)
C_t^{curt}	Cost of wind curtailment at time t	(£)
E^{total}	Total system CO_2 emissions	(tCO_2)
$D_{t,min}$	Minimum load level at time t	(MW_e)

Table 5.1: System variables.

System parameters		
c^{CO_2}	Cost of CO_2	(£/tCO_2)
$c^{on,curt}$	Cost of onshore wind curtailment	(£/MWh_e)
$c^{of,curt}$	Cost of offshore wind curtailment	(£/MWh_e)

Table 5.2: System parameters.

Generator variables		
$u_{g,t}$	Unit g base power plant binary decision variable at time t	(-)
$P_{g,t}$	Unit g power output at time t	(MW_e)
$F_{g,t}$	Unit g fuel consumption at time t	(MW_{th})
$F_{g,t}^{\text{start}}$	Unit g start-up fuel consumption at time t	(MW_{th})
$F_{g,t}^{\text{shut}}$	Unit g shut-down fuel consumption at time t	(MW_{th})
$E_{g,t}$	Unit g variable operating emissions at time t	(tCO_2)
$E_{g,t}^{\text{start}}$	Unit g start-up emissions at time t	(tCO_2)
$E_{g,t}^{\text{shut}}$	Unit g shut-down emissions at time t	(tCO_2)
$C_{g,t}$	Unit g variable operating cost at time t	(£)
$C_{g,t}^{\text{start}}$	Unit g start-up cost at time t	(£)
$C_{g,t}^{\text{shut}}$	Unit g shut-down cost at time t	(£)
$C_{g,t}^{\text{fuel}}$	Unit g fuel cost at time t	(£)
$C_{g,t}^{\text{O\&M}}$	Unit g variable operating and maintenance cost at time t	(£)
$C_{g,t}^{\text{ramp}}$	Unit g ramping cost at time t	(£)
$C_{g,t}^{\text{O\&M,capt}}$	Unit g additional CO_2 variable operating and maintenance cost at time t	(£)
$C_{g,t}^{\text{solv}}$	Unit g solvent cost at time t	(£)
$C_{g,t}^{\text{trans}}$	Unit g CO_2 transport and storage cost at time t	(£)
$C_{g,t}^{\text{CO}_2}$	Unit g CO_2 cost at time t	(£)
$Y_{g,t}^{\text{capt}}$	Unit g CO_2 capture rate at time t	(-)
$X_{g,t}$	Unit g time period online(+)/offline(-) at time t	(h)
SU_g	Unit g start-up time	(h)
$R_{g,t}^{\text{SR,up}}$	Unit g upwards spinning reserve contribution at time t	(MW_e)
$R_{g,t}^{\text{SR,dn}}$	Unit g downwards spinning reserve contribution at time t	(MW_e)
$R_{g,t}^{\text{StR,up}}$	Unit g upwards standing reserve contribution at time t	(MW_e)
$R_{g,t}^{\text{StR,dn}}$	Unit g downwards standing reserve contribution at time t	(MW_e)

Table 5.3: Generator variables.

Generator parameters		
$P_{g,\min}$	Unit g minimum power output of base power plant	(MW_e)
$P_{g,\max}$	Unit g maximum power output of base power plant	(MW_e)
$P_{g,\min}^{\text{capt}}$	Unit g minimum power output of CO_2 capture plant	(MW_e)
$P_{g,\max}^{\text{capt}}$	Unit g maximum power output of CO_2 capture plant	(MW_e)
$F_{g,\min}$	Unit g minimum fuel consumption	(MW_{th})
$F_{g,\max}$	Unit g maximum fuel consumption	(MW_{th})
$Y_{g,\min}^{\text{capt}}$	Unit g minimum CO_2 capture rate	(-)
$Y_{g,\max}^{\text{capt}}$	Unit g maximum CO_2 capture rate	(-)
$c_{g,t}^{\text{fuel}}$	Unit g cost of fuel at time t	(£/MWh_{th})
$c_g^{\text{O\&M}}$	Unit g cost of variable operation and maintenance for base power plant	(£/MWh_e)
$c_g^{\text{ramp,up}}$	Unit g upwards ramping cost	(£/MW_e)
$c_g^{\text{ramp,dn}}$	Unit g downwards ramping cost	(£/MW_e)
ρ_g^{up}	Unit g ramp up rate	(MW_e/h)
ρ_g^{dn}	Unit g ramp down rate	(MW_e/h)
h_g^{a}	Unit g quadratic fuel consumption parameter	(MW_{th})
h_g^{b}	Unit g quadratic fuel consumption parameter	(MW_{th}/MW_e)
h_g^{c}	Unit g quadratic fuel consumption parameter	(MW_{th}/MW_e^2)
$\alpha_{g,k}$	Unit g fuel consumption at zero load for linear segment k	(MW_{th})
$\beta_{g,k}$	Unit g heat rate for linear segment k	(MW_{th}/MW_e)
$\alpha_{g,k}^{\text{tan}}$	Unit g fuel consumption at zero load for tangent k	(MW_{th})
$\beta_{g,k}^{\text{tan}}$	Unit g heat rate for tangent k	(MW_{th}/MW_e)
$UT_{g,\min}$	Unit g minimum up time	(h)
$DT_{g,\min}$	Unit g minimum down time	(h)
SD_g	Unit g shut-down time	(h)
$F_g^{\text{start,cold}}$	Unit g fuel consumption during cold start-up	(MWh_{th})
F_g^{shut}	Unit g fuel consumption during shut-down	(MWh_{th})
$c_g^{\text{start,fixed}}$	Unit g fixed start-up cost	(£)
$c_g^{\text{shut,fixed}}$	Unit g fixed shut-down cost	(£)
τ_g^{c}	Unit g thermal cooling constant	(h)
$e_g^{CO_2}$	Unit g fuel-specific emission factor	(tCO_2/MWh_{th})

Table 5.4: Generator parameters.

It is assumed that energy storage units only have costs associated with storing energy since operating costs and the start-up/shut-down costs of energy storage units are assumed to be zero as in Zhao *et al.* [1998]. The operation of energy storage units depends on the availability of stored energy and so is formulated separately from thermal units. It is also assumed that the start-up times for energy storage units is negligible. The unit commitment objective function in Equation 5.7 therefore only considers conventional and CCS-equipped units. Another objective function models the optimal charge/discharge profiles of energy storage units in Equation 5.60.

The total cost of operating, starting-up, and shutting-down thermal units with and without CCS (including the fuel, CO_2, and variable operating and maintenance costs) is represented by the first three terms in Equation 5.7.

The fourth term is required to represent the costs associated with curtailment. During extreme periods of low demand and high wind output, sufficient synchronised thermal power plants are required to provide reserve. As a result, surplus generation is curtailed to maintain reserve requirements. The curtailment cost is in effect an opportunity cost that is included for a number of reasons. Under the current market arrangement in GB, wind farm operators are paid a generation curtailment price to reduce output or turn off when the system operator dictates. This directly compensates wind farm operators for lost energy or subsidy payments. A curtailment cost also ensures the numerical feasibility of the model at very low net demand periods.

CO_2 costs are accounted for and included in the variable operating costs, start-up costs, and shut-down costs for each time period. The total CO_2 emissions E^{total} over the optimisation time period are therefore:

$$E^{\text{total}} = \sum_{t=1}^{T} \sum_{g=1}^{G} E_{g,t} + E_{g,t}^{\text{start}} + E_{g,t}^{\text{shut}} \tag{5.8}$$

where $E_{g,t}$ are the CO_2 emissions during normal operation, $E_{g,t}^{\text{start}}$ are the CO_2 emissions emitted during start-up, and $E_{g,t}^{\text{shut}}$ are the CO_2 emissions emitted during shut-down.

The total system costs C^{total} (£), as in the unit commitment minimisation problem in Equation 5.7, are composed of variable operating, start-up and shut-down costs. The variable operating, start-up, and shut-down costs can each be broken down into fuel, CO_2, and variable operating and maintenance costs. This allows generation portfolios with different characteristics to be compared in terms of total fuel or CO_2 costs, for example. This can be useful when assessing the implications of increasing wind capacity on system costs.

5.3 Variable operating costs

The variable operating costs $C_{g,t}$ (£) for thermal power plants includes the fuel costs $C_{g,t}^{\text{fuel}}$, CO_2 costs $C_{g,t}^{\text{CO}_2}$, variable operating and maintenance (O&M) costs $C_{g,t}^{\text{O\&M}}$, ramping costs C_{g}^{ramp}, and the costs associated with CO_2 capture, compression and transportation, and the O&M and solvent costs for the CO_2 capture plant:

$$C_{g,t} = \overbrace{C_{g,t}^{\text{fuel}} + C_{g,t}^{\text{O\&M}} + C_{g,t}^{\text{ramp}}}^{\text{base power plant}} + \overbrace{C_{g,t}^{\text{O\&M,capt}} + C_{g,t}^{\text{solv}} + C_{g,t}^{\text{trans}}}^{\text{CO}_2\text{ capture plant}} + C_{g,t}^{\text{CO}_2} \tag{5.9}$$

For thermal power plants without CO_2 capture facilities, all of the CO_2 capture plant variables in Equation 5.9 are zero. The fuel consumption and CO_2 emissions during normal operation and start-up/shut-down are considered separately. The fuel consumption during start-up and shut-down and CO_2 emissions are described later.

Each of the cost components in Equation 5.9 is now described in more detail.

5.3.1 Fuel costs

The fuel costs are assumed to be linearly proportional to the instantaneous fuel consumption $F_{g,t}$ of the base power plant:

$$C_{g,t}^{\text{fuel}} = F_{g,t} c_{g,t}^{\text{fuel}} \tag{5.10}$$

where $F_{g,t} \geq 0$ and $c_{g,t}^{\text{fuel}}$ is the cost of fuel (£/MWh_{th}). It is assumed that the instantaneous fuel consumption $F_{g,t}$ of a thermal unit as a function of the instantaneous power output can be approximated as a convex quadratic function:

$$F_{g,t} = h_g^{\text{a}} + h_g^{\text{b}} P_{g,t} + h_g^{\text{c}} (P_{g,t})^2 \tag{5.11}$$

where h_g^{a}, h_g^{b}, and h_g^{c} are quadratic fuel cost coefficients that describe the fuel consumption of each generator g. Convex quadratic approximations do not consider any discontinuities or non-convexities such as valve-point effects or prohibited operation zones. Power plants with prohibited operation zones have discontinuous input-output characteristics and so require stochastic or genetic algorithms.

Part-load efficiency

An increased need for short-term flexibility in high VRE power systems will require more thermal units to operate at part-load. This will lead to an undesirable increase in part-load efficiency losses, and lower average load factors. It is therefore essential that unit commitment models analysing high VRE systems consider part-load efficiency losses.

The part-load efficiency curves and a number of other technical and cost parameters of typical GB thermal units (CCGT and coal) were obtained after extensive communications with a large UK energy company involved in both GB generation and transmission. Kehlhofer *et al.* [1999] also reports typical part-load efficiency curves for CCGT units. These sources are used to create representative functions that define the fuel consumption characteristics of typical designs and generation technologies. The functions in Figure 5.3 are used to create a set of functions in the form of Equation 5.11 to represent the typical fuel consumption characteristics of different generation technologies.

The part-load efficiency curves in Figure 5.3 are based on empirical data for existing CCGT and coal units in GB with the exception of CCGT 1 which represents the anticipated part-load efficiency of a new single-shaft H-class configuration with 1 gas turbine and 1 steam turbine (1+1) that achieves very high baseload efficiencies.

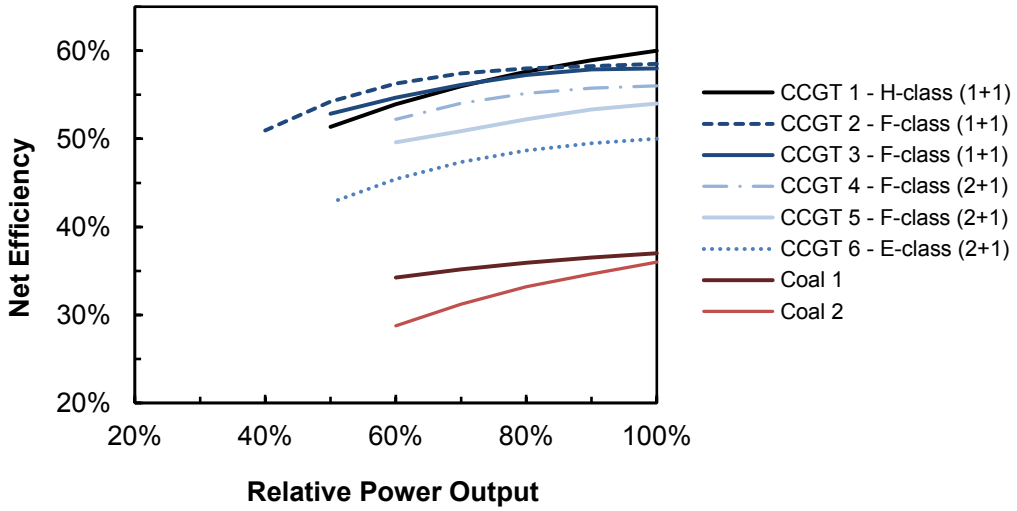

Figure 5.3: Empirical part-load efficiency curves for a number of CCGT and coal units. 1+1 refers to 1 gas turbine and 1 steam turbine. 2+1 refers to 2 gas turbines and 1 steam turbine.

The part-load efficiency curve for unit CCGT 2 is based on an empirical F-class single-shaft design (1+1) that achieves high baseload and part-load efficiencies. CCGT 3 is also an F-class single-shaft unit (1+1) but achieves mid-range baseload and part-load efficiencies. CCGT 4 is an F-class design with 2 gas turbines and 1 steam turbine (2+1) with mid-range baseload and part-load efficiencies. CCGT 5 represents an early F-class design (2+1) with lower baseload

and part-load efficiencies. CCGT 6 is an E-class (2+1) configuration that achieves reasonable baseload and part-load efficiencies compared to other E-class units.

The part-load efficiency curve for unit Coal 1 is an empirical subcritical coal plant that achieves high baseload and part-load efficiencies. Coal 2 is an empirical subcritical coal unit that achieves lower baseload and part-load efficiencies.

The real-time efficiency $\eta_{g,t}$ ($\mathrm{MW_e}/\mathrm{MW_{th}}$) of the base power plant is ratio of the net power output (electrical) to the fuel power input (thermal):

$$\eta_{g,t} = \frac{P_{g,t}}{F_{g,t}} \tag{5.12}$$

Unit-specific fuel cost functions are computed using a piece-wise linear approximation. These are now described in more detail.

Piece-wise linear approximation

A piece-wise linear approximation using several linear segments is used to represent the non-linear fuel consumption with high accuracy, see Figure 5.4. Each linear segment k of the piece-wise approximation has a gradient of $\beta_{g,k}$ ($\mathrm{MW_{th}}/\mathrm{MW_e}$), which represents the incremental heat rate. The intercept $\alpha_{g,1}$ ($\mathrm{MW_{th}}$) represents the extrapolated hypothetical fuel consumption at zero load. For K linear segments, where $k = 1,2,3,...,K$, the power output of generator g is:

$$P_{g,t} = \sum_{k=1}^{K} P_{g,t,k} \tag{5.13}$$

The gradients increase from minimum power output $P_{g,\min} = P_{g,t,1}$ to the maximum power output $P_{g,\max} = P_{g,t,K}$. The power output in the first segment is therefore between $P_{g,1}$ and $P_{g,2}$, with elbow points dividing the generation range into the desired number of segments. The number of segments and positioning of the elbow points is optimised using an iterative method to fit the quadratic function with high accuracy for each generator.

The quadratic fuel consumption function using a piece-wise linear approximation with segments is therefore:

$$F_{g,t} = \alpha_{g,k} + P_{g,t,k} \cdot \beta_{g,k} \tag{5.14}$$

However, this piece-wise linear approximation is always greater than or equal to the quadratic fuel consumption approximation. This is sometimes referred to as the upper piece-wise linear approximation [Sumbera, 2012]. Another approach that uses tangents gives the lower piece-wise linear approximation, see Figure 5.4.

The quadratic fuel consumption function using a piece-wise linear approximation with tangents

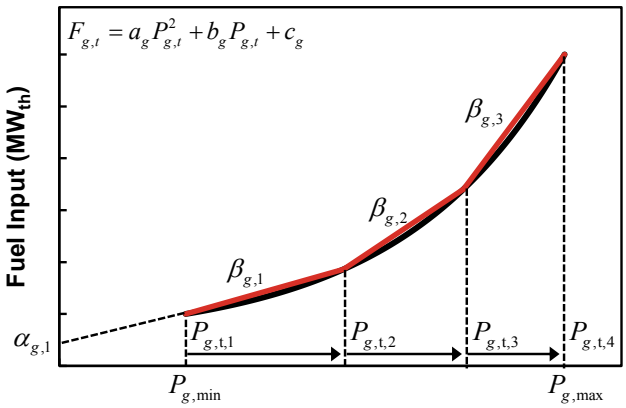

(a) Approximation using segments.

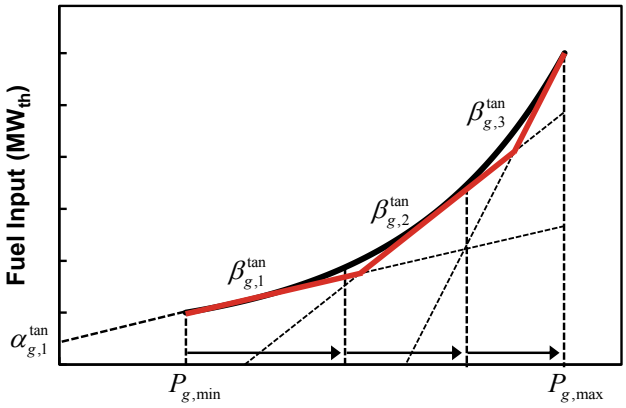

(b) Approximation using tangents.

Figure 5.4: Piece-wise linear approximations of the non-linear fuel consumption characteristics of thermal generators.

is therefore:

$$F_{g,t} = \alpha^{\tan}_{g,k} + P_{g,t,k} \cdot \beta^{\tan}_{g,k} \tag{5.15}$$

where the gradient of each tangent is $\beta^{\tan}_{g,k}$ ($\mathrm{MW_{th}/MW_e}$) and intercept $\alpha^{\tan}_{g,k}$ ($\mathrm{MW_{th}}$).

In this work, a piece-wise linear function with three linear segments is used to approximate the fuel consumption function as this approach gives a more conservative and accurate approximation of the quadratic fuel consumption function. It should be noted that the quadratic fuel consumption curves in Figure 5.4 have been exaggerated for illustration purposes. It is important to maintain the convexity of the problem to ensure that all generators are dispatched in order of their marginal costs.

5.3.2 Variable operating and maintenance (O&M) costs

During normal operation power plants incur slight damage that requires scheduled maintenance. Power plants also require chemicals and other non-fuel consumables. Typical variable O&M costs for different thermal power plants are taken from a number of sources [Kumar *et al.*, 2012; Parsons Brinkerhoff, 2013a]. Fixed O&M costs are not considered as these do not affect short-term dispatch decisions. The variable O&M costs are assumed to be linearly proportional to the instantaneous power output $P_{g,t}$ of the base power plant:

$$C_{g,t}^{\mathrm{O\&M}} = P_{g,t} c_g^{\mathrm{O\&M}} \tag{5.16}$$

where $P_{g,t} \geq 0$ and $c_g^{\mathrm{O\&M}}$ is the cost of variable O&M (£/MWh$_\mathrm{e}$). Additional variable O&M costs are required for the CO_2 capture plant, which are described later.

5.3.3 Ramping costs

Power plants that are designed for baseload operation can be damaged if they undergo frequent cycling operations and load changes [Kumar *et al.*, 2012]. Certain units may have well known damage mechanisms and so certain operational strategies can be employed to reduce the rate of damage. However, there are many damage mechanisms that can occur as a result of increased cycling and rapid variations in load. For example, there are costs associated with component replacements, forced outages, and de-ratings. There are also many hidden costs and consequences, such as increased failures during start-up, which are difficult to quantify accurately. However, it is important to represent the increased costs as a result of ramping in the UCED model.

Kumar *et al.* [2012] publish lower bound cycling costs for a number of power generation technologies. They categorise power plant cycling into load follow cycling and on/off cycling. Cycling here is referred to as changing the power output between minimum output and maximum output. Load following cycling is further categorised into significant and shallow load following. Shallow load following is any MW change in output that is between 15-20% of $P_{g,\max}$.

Whilst the exact relationship between increased cycling operations and increased damage (and therefore costs) is not known, not accounting for the impacts of ramping could lead to a significant over/under estimation in cycling costs [Kumar *et al.*, 2012]. Using incorrect ramping costs in the UCED model may cause dispatch errors.

These wear-and-tear elements can be captured using ramping costs which are proportional to the change in base power plant output. The ramping costs $C_{g,t}^{\mathrm{ramp}}$ for each generator g during normal operation consists of the absolute value of the change in power output and the upwards

and downwards ramping cost elements:

$$C_{g,t}^{\text{ramp}} = \begin{cases} \left(P_{g,t} - P_{g,t-1}\right) c_g^{\text{ramp,up}} & \text{for } P_{g,t} - P_{g,t-1} > 0 \\ -\left(P_{g,t} - P_{g,t-1}\right) c_g^{\text{ramp,dn}} & \text{for } P_{g,t} - P_{g,t-1} < 0 \end{cases} \tag{5.17}$$

where $c_g^{\text{ramp,up}}$ and $c_g^{\text{ramp,dn}}$ are the upwards and downwards costs of ramping (£/MW$_\text{e}$), respectively. It should be noted that the ramping costs $C_{g,t}^{\text{ramp}}$ do not include the additional costs incurred from frequent start-ups/shut-downs. These are considered separately.

5.3.4 CO_2 costs

The CO_2 emissions produced by each generator g at time t are assumed to be linearly proportional to the instantaneous fuel consumption. The CO_2 emissions that are emitted to the atmosphere depend on the CO_2 capture rate $Y_{g,t}^{\text{capt}}$ as follows:

$$E_{g,t} = F_{g,t} e_g^{\text{CO}_2} (1 - Y_{g,t}^{\text{capt}}) \tag{5.18}$$

where $e_g^{\text{CO}_2}$ is the fuel-specific emission factor of the base power plant (tCO$_2$/MWh$_\text{th}$), and $F_{g,t}$ is the instantaneous fuel consumption (MW$_\text{th}$). The fuel-specific emission factors $e_g^{\text{CO}_2}$ (tCO$_2$/MWh$_\text{th}$) for each generator are taken from DECC [2014a, 2013b, 2012b].

The CO_2 cost $C_{g,t}^{\text{CO}_2}$ that must be paid by each generator g during normal operation is therefore:

$$C_{g,t}^{\text{CO}_2} = E_{g,t} c^{\text{CO}_2} \tag{5.19}$$

where c^{CO_2} is the cost of CO_2 (£/tCO$_2$). The CO_2 emissions that are captured and treated by the CO_2 capture plant are therefore:

$$E_{g,t}^{\text{capt}} = F_{g,t} e_g^{\text{CO}_2} Y_{g,t}^{\text{capt}} \tag{5.20}$$

For thermal units without CO_2 capture and compression systems, the CO_2 capture rate $Y_{g,t} = 0$.

There are additional costs associated with capturing, compressing and transporting the CO_2 that is captured. Section 5.9 describes the CO_2 capture process and the implementation of flexible and non-flexible CO_2 capture in the model formulation.

5.4 Wind curtailment

Wind curtailment is necessary for a number of reasons: firstly to ensure must-run plants remain operational and that net demand remains above a minimal load level; secondly to ensure there is sufficient upwards/downwards reserve; and thirdly to ensure committed generators can meet positive/negative net demand variations. In real power systems wind is also curtailed to meet transmission constraints and voltage requirements.

A minimum load level ensures there is sufficient system inertia to limit the initial Rate of Change of Frequency (RoCoF) after a large imbalance in generation/demand. Wind curtailment can also occur when net demand increases/decreases too fast and committed thermal power plants have insufficient ramping capability. The concept of a minimum load level is now outlined.

5.4.1 Minimum load

A minimum amount of system load is required to ensure must-run plants remain operational, to ensure there is sufficient system inertia to limit the initial RoCoF after a large change in demand/generation, and to ensure power plants can provide sufficient downwards reserve during low net demand periods. This is modelled as a minimum load level which considers both the minimum stable generation limits of must-run units and system inertia requirements that are enforced to ensure that, if a contingency event happened, the initial RoCoF would remain within limits. Ensuring the initial RoCoF remains below a certain value (Hz/s) is critical in preventing embedded generators from cutting-out, causing the frequency to drop further [National Grid, 2013].

The total wind output W_t is the sum of the onshore and offshore wind power outputs:

$$W_t = W_t^{\text{on}} + W_t^{\text{of}} \tag{5.21}$$

Net demand is electricity demand subtracted by the total wind output:

$$D_t^{\text{net}} = D_t - W_t = D_t - (W_t^{\text{on}} + W_t^{\text{of}}) \tag{5.22}$$

If net demand D_t^{net} is greater or equal to the minimum load level $D_{t,\min}$ then no curtailment is necessary. If net demand D_t^{net} is less than the minimum load level $D_{t,\min}$ then wind is curtailed. The amount of wind to be curtailed is equal to the difference between $D_{t,\min}$ and D_t^{net}:

$$W_t^{\text{curt}} = \begin{cases} 0 & \text{if } D_t^{\text{net}} \geq D_{t,\min} \\ D_{t,\min} - D_t^{\text{net}} & \text{if } D_t^{\text{net}} < D_{t,\min} \end{cases} \tag{5.23}$$

A minimum load level is required to ensure the system has sufficient system inertia to limit the RoCoF after a large demand/generation outage. It is also required to ensure that must-run units are capable of operating at their minimum power output limits and do not have to shut-down.

Figure 5.5 shows a simple example of a system with a minimum load level of 15 GW. Onshore and offshore wind is curtailed to ensure net demand stays above the minimum load level. The wind generation that is curtailed is then shown graphically 'above' electricity demand as this represents a surplus of electricity.

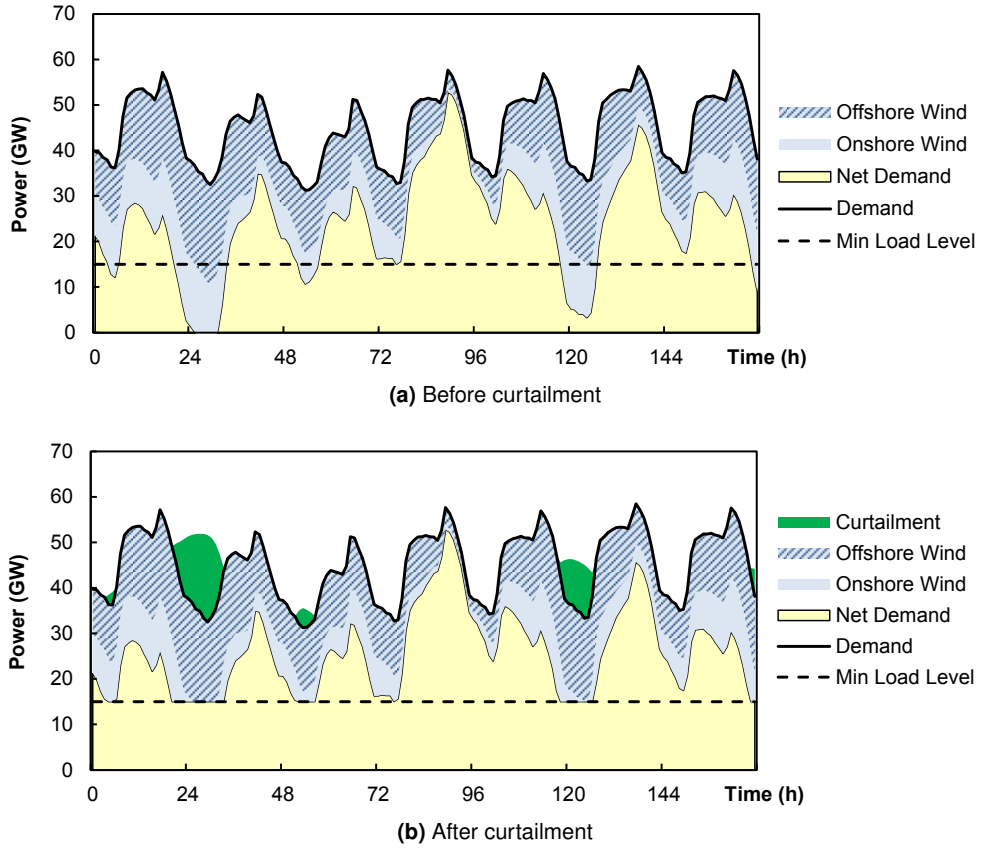

Figure 5.5: Wind curtailment, net demand and minimum load level.

5.4.2 Wind curtailment

Onshore and offshore wind is curtailed according to the assumed generation constraint price, which is paid to reduce generation. The National Grid [2013] outline the expected bid price to reduce generation for different generation technologies, with onshore wind at $c^{\text{on,curt}}$ = -£50/MWh$_e$ and offshore wind at $c^{\text{of,curt}}$ = -£100/MWh$_e$. This implies that onshore wind is to be curtailed before offshore wind as it is cheaper for the system operator to pay onshore wind farm operators to reduce output.

The total amount of curtailed wind W_t^{curt} is the sum of the curtailed wind output of the onshore

and offshore wind fleets:

$$W_t^{\text{curt}} = W_t^{\text{on,curt}} + W_t^{\text{of,curt}} \tag{5.24}$$

where $W_t^{\text{on,curt}}$ and $W_t^{\text{of,curt}}$ is the amount of onshore and offshore wind that is curtailed at time t, respectively.

Wind curtailment is bounded with upper and lower limits:

$$0 \leq W_t^{\text{on,curt}} \leq W_t^{\text{on}} \tag{5.25}$$

$$0 \leq W_t^{\text{of,curt}} \leq W_t^{\text{of}} \tag{5.26}$$

Onshore wind is curtailed before offshore wind since the expected bid price to reduce generation is less for onshore wind [National Grid, 2013]. If the amount of wind generation to be curtailed is greater than the level of onshore wind then offshore wind is also curtailed. The cost of wind curtailment is the summation of the costs paid to onshore and offshore wind operators:

$$C_t^{\text{curt}} = c^{\text{on,curt}} W_t^{\text{on,curt}} + c^{\text{of,curt}} W_t^{\text{of,curt}} \tag{5.27}$$

5.5 Electricity prices

5.5.1 Introduction

Least-cost electricity system dispatch models typically use input demand and generator data to minimise the overall system costs. This cost minimisation approach has been used to model the operation of CO_2 capture units [Ludig *et al.*, 2010]. The price-based profit maximisation of individual CO_2 capture units has been previously studied in Cohen [2012].

In this work, however, the UCED model schedules thermal units to meet net demand and reserve requirements to minimise total system costs but models the operation of energy storage and flexible CO_2 capture units using a price-based profit maximisation approach. This requires the simulation of electricity prices for each time step.

In this work, the electricity price is forecast at the unit commitment stage and used to optimise the operation of energy storage units and flexible CO_2 capture units. At delivery time, realised net demand is used to re-dispatch energy storage and flexible capture units using the realised electricity price.

Figure 5.6 shows the historic electricity prices between 2005 and 2010 taken from APX [2015].

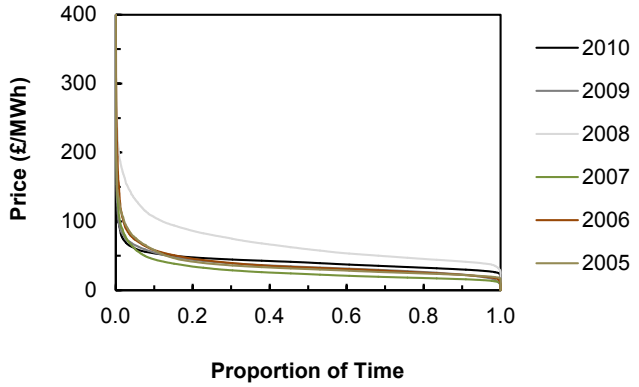

(a) Price duration curves – 100% of year

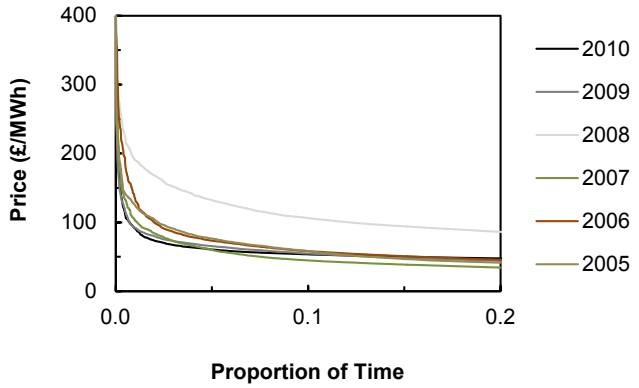

(b) Price duration curves – 20% of year

Figure 5.6: Historic price duration curves between 2005 and 2010 from APX [2015].

5.5.2 Background

Cohen [2012] presented a simple method to adjust historic electricity prices to account for increased fuel and CO_2 prices expected in the future and changes in the merit-order of power plants. The method preserves historic electricity price volatility but is unlikely to be suitable for power systems with large proportions of wind.

Green and Vasilakos [2010] used a supply function approach to model system electricity prices in the GB market with large amounts of wind power. Electricity wholesale prices were found to be significantly affected by the amount of wind generation. An industry supply function was used to represent the marginal costs of generators and modelled the strategic price offers of six symmetric energy companies. Start-up costs or minimum output levels were not considered.

Staffell and Green [2016] used a simple merit-order stack approach to simulate electricity prices and compare the results with a fully optimised dispatch model of the GB market. They found that start-up costs and minimum power output limits introduce differences between the two approaches. A modified merit-order stack approach that factors in start-up costs was found to replicate the results of the fully optimised dispatch model with reasonable accuracy.

Eager [2011] also modelled the electricity price for the GB market and demonstrated how an additional mark-up function was required to scale the marginal cost supply curve to account for the value of capacity or scarcity at very low capacity margins. This additional price mark-up adjusts the supply curve as demand approaches peak installed capacity.

Grunewald [2012] used an exponential uplift function to represent the behavior of electricity prices at low capacity margins. In addition, a linear function was employed to represent the infra-marginal rents gained by power plants bidding at the next most expensive plants SRMC.

Baringa [2015] found significant differences in the behaviour of electricity prices with different market and policy input assumption scenarios. They found that negative prices only occur for an average of 2 hours per year over the period 2020 to 2035 in their 'Market' scenario and an average of 68 hours per year in their 'Policy' scenario. The results highlighted the potential frequency of negative prices. The work showed that negative prices are likely to occur when the volume of available generation (that is willing to bid a negative price) exceeds demand. In addition, they found that there is some historical evidence from the Balancing Mechanism that certain low-carbon generation technologies offer negative prices, possibly to avoid shut-down and start-up costs, especially closer to real-time. For example, a combined heat a power (CHP) plant may bid at a price lower than its SRMC because it must generate heat (and therefore electricity). This suggests empirical evidence of a price mark-down that may become increasingly influential with increasing wind capacity.

5.5.3 Simulating electricity prices

This work proposes a simple electricity pricing model to produce an electricity price time-series that is then used to inform the operation of price-sensitive energy storage units and flexible CO_2 capture plants. It is thought to provide a reasonable approximation of the behaviour of price-responsive energy storage units and flexible CO_2 capture units since they are both likely to be incentivised by electricity price signals.

The electricity price is composed of:

1. system marginal price (SMP) – price required for the marginal 'price-setting' generator to cover its costs
   (a) operating costs
   (b) start-up and shut-downs costs
2. price mark-up – represents the bidding strategies and value of capacity for power plants in a competitive market
3. price mark-down – represents price behaviour when large proportions of negative bidding generation capacity suppresses prices.

The electricity price is estimated for each time step and used to inform the operation of energy storage units and flexible CO_2 power plants at the unit commitment and economic dispatch

stages. All generating units participate in the electricity market to produce the electricity price time-series.

Within the scope of this work, this simple electricity pricing model is intended to produce electricity prices that trend with demand to reflect the marginal costs of generators but also replicate periods of scarcity and surplus generation. This first-order approximation of the GB market is used to inform the operating profiles of price-responsive energy storage units and flexible CO_2 capture plants that respond to price-signals and adjust output to maximise profit.

System marginal prices

The system marginal price (SMP) is calculated in two steps. First, the marginal cost (£/MWh) of the last generator to be dispatched[1] is calculated for each time period. The marginal cost can be thought of as the cost of meeting 1 MWh of additional demand. The marginal cost considers the operating costs, which include fuel costs, CO_2 costs, and variable O&M costs (and additional CO_2 capture related costs for CCS-equipped units), and the power output at time t.

Second, an additional cost component is added to the marginal cost to account for start-up/shut-down costs. The time-averaged start-up and shut-down costs for each unit are used to ensure that for each day d (24 hour time period) each unit is able to cover both its operating and start-up/shut-down costs. The SMP is therefore the marginal cost of the last generator to be dispatched plus the time-averaged start-up and shut-down costs.

The SMP considers the marginal efficiency and the increased fuel consumption and associated CO_2 costs of the power plant when operating at part-load. It is thought that this first-order pricing model provides a reasonable approximation of electricity prices in liberalised electricity markets, such as GB.

The SMP is the price that the marginal generator requires in the market to cover its operating and start-up/shut-down costs at time t. All generators that participate in the market receive this price. This simplification of the GB market produces electricity prices that trend with net demand. This first-order system marginal pricing model, however, does not reproduce the volatile electricity prices that occur in real markets that result from complex market dynamics such as market power or asymmetric supply functions.

---

1. The last generator to be dispatched is sometimes referred to as the marginal ‘price-setting’ generator.

Price mark-up

This work uses an approach based on work done by Green and Vasilakos [2007, 2010]; Eager [2011]; Grunewald [2012]. A system-wide supply function is modelled using the short-run marginal cost of the last generator to be dispatched plus a price mark-up that increases as the system approaches peak demand. This is also intended to reflect the supply function that would result for a system with symmetric firms submitting strategic price offers [Green and Vasilakos, 2010].

The additional price mark-up is modelled as a hyperbolic function and an exponential function as they have been demonstrated to produce credible results for the GB market [Eager, 2011]. The hyperbolic price mark-up function is given by the equation:

$$w_t^{\text{hyp}} = \frac{k \cdot D_t^{\text{net}}}{P^{\max} - D_t^{\text{net}}} \tag{5.28}$$

where w_t^{hyp} is the hyperbolic price mark-up, k is a scale factor, D_t^{net} is the net demand provided by thermal units, and $P^{\max} = \sum_{g=1}^{G} P_{g,\max}$ is the total available capacity from all generators. A k-value of 5 provides results that agree well with Eager [2011].

Eager [2011] showed that a hyperbolic function agrees well with observed GB electricity prices during times when the system is 'healthy' and the capacity margin is between 20-50%. However, the hyperbolic function does not replicate the extreme price rises when the capacity margin is small. Eager [2011] and Grunewald [2012] use exponential price mark-up functions to represent the price uplift during times of scarcity. The exponential price mark-up function is given by the equation:

$$w_t^{\text{exp}} = a^{\text{up}} \times e^{-b^{\text{up}}\left((P^{\max} - D_t^{\text{net}})/P^{\max}\right)} \tag{5.29}$$

where the values for a^{up} and b^{up} are calibrated so that when the capacity margin is zero, the price mark-up w_t^{exp} is equal to the value of lost load (VOLL). National Grid [2013] assume the VOLL is equal to £4000/MWh which is approximately the GDP per unit of electricity consumed. An a^{up}-value of 4000 gives a price mark-up of £4000/MWh when the capacity margin is zero and a b^{up}-value of 20 gives results that agree well with Eager [2011] and Grunewald [2012].

The price mark-up function that considers the maximum values from Equations 5.30 and 5.29 is:

$$w_t^{\text{up}} = \max\left(w_t^{\text{hyp}}, w_t^{\text{exp}}\right) \tag{5.30}$$

The price mark-up or scarcity rent ensures that all power plants remain economically viable. The price mark-up methodology is based on analysis of historical prices from APX [2015]. The bidding behaviour of peaking units could change in future markets and the implementation of

a capacity market in GB may reduce or limit the extent of very large price spikes [Baringa, 2015].

Price mark-down

During periods when wind output exceeds electricity demand the electricity price is likely to become negative [Baringa, 2015]. This is because certain low-carbon generation technologies are paid support payments to generate electricity. The Renewable Obligation (RO) and Contracts for Difference (CfD) mechanisms provide support payments for onshore and offshore wind projects. This gives onshore and offshore wind an incentive to offer negative prices into the market.

In addition, wind farm operators are paid a generation constraint price to reduce or curtail generation by the system operator. For onshore and offshore wind, this value represents the lost subsidy payments that onshore/offshore wind farms would require as compensation.

Baringa [2015] analysed the potential frequency of negative prices in the GB market and provided insights on the implications of negative pricing. Two core scenarios were examined including a market scenario and a policy scenario, each with different levels of renewable deployment. They report that the amount of negative price hours is highly related to the proportion of low-carbon generation receiving support payments. The results showed that negative prices may occur when the volume of available generation that is willing to bid negative prices exceeds demand.

An exponential function is used to represent the price mark-down w_t^{dn}. As the amount of available wind approaches the level of electricity demand, the price mark-down becomes increasingly negative. The electricity prices are capped from falling below -£100/MWh as this is the price at which all offshore wind operators would be willing to self-curtail.

The price mark-down is formulated as:

$$w_t^{\mathrm{dn}} = a^{\mathrm{dn}} \times e^{b^{\mathrm{dn}}\left((W_t - D_t)/D_t\right)} \tag{5.31}$$

where the values for a^{dn} and b^{dn} are calibrated so that the price mark-down w_t^{dn} is equal to -1 ROC when the amount of available wind generation W_t is equal to demand D_t. A b^{dn}-value of 10 adjusts the shape of the price mark-down function so that negative prices only occur as frequently as reported in Baringa [2015].

Since there is very limited historical observations of negative prices in liberalised markets, and zero observations in the GB market until present, it is not possible to model with high accuracy the behaviour of electricity prices during periods of high renewable output and low net demand. It is therefore thought that this simple approach to modelling a price mark-down

will need modification in the future. However, for the purposes of this study it is thought to be a reasonable approach.

Electricity prices

The electricity price π_t is calculated as the system marginal price SMP_t plus the mark-up function w_t^{up} plus the mark-down function w_t^{dn}:

$$\pi_t = SMP_t + w_t^{\text{up}} + w_t^{\text{dn}} \tag{5.32}$$

This simplistic first-order pricing model is intended to produce an electricity price time-series that trends with net demand that reflects the marginal costs of generators, the time-weighted start-up/shut-down costs, a price component to represent the value of capacity during periods of scarcity, and a price component that represents the negative bidding behaviour of certain generation capacity, such as wind power.

5.5.4 Profit maximisation

This work assumes competitive (price-taking) behaviour. Energy storage units and CO_2 capture units optimise their individual strategies to maximise profit. The optimal strategy of each CO_2 capture unit depends on whether more profit can be gained by reducing the CO_2 capture rate. However, it should be noted that this approach does not consider the operation of other CO_2 capture units and the resulting flows of CO_2 into the transport and storage network. The operation of individual CO_2 capture units is likely to be constrained by the physical limitations of the CO_2 network. Future work should therefore consider the optimal strategy of the entire CO_2 network after considering the technical constraints of both individual capture units and the entire CO_2 network.

It was found that a linear formulation is suitable to model the optimal CO_2 capture rates of CCS-equipped units. This linear formulation finds the optimal capture strategy subject to technical operating constraints and after considering operating costs such as fuel costs, CO_2 costs, variable O&M costs, solvent costs, solvent degradation, and transport costs.

However, the optimal strategy of energy storage units depends the availability of energy in the store and so a linear formulation is not suitable. A Monte Carlo based optimisation approach is proposed to find the optimal charge/discharge strategy and storage levels for individual energy storage units. This price-based profit maximisation approach assumes that each unit is owned by a single operator. Full portfolio profit maximisation considers the expected strategies of competitors and uses this to inform the optimal strategy of the portfolio. However, modelling competitor strategies is considered beyond the scope of this work.

5.6 System constraints

The UCED model has a number of equality and inequality constraints to ensure, for example, that generation equals demand at all times and reserve requirements are maintained.

Demand balance constraint

The demand balance constraint maintains the balance between generation and demand.

$$\sum_{g=1}^{G} \left(u_{g,t} P_{g,t} - u_{g,t}^{\text{capt}} P_{g,t}^{\text{capt}} \right) + \sum_{s=1}^{S} P_{s,t}^{\text{d}} + W_t = D_t + \sum_{s=1}^{S} P_{s,t}^{\text{c}} + W_t^{\text{curt}} \tag{5.33}$$

where $P_{g,t}$ and $P_{g,t}^{\text{capt}}$ are the instantaneous power outputs of the base and CO_2 capture units, $P_{s,t}^{\text{d}}$ is the discharging power output and $P_{s,t}^{\text{c}}$ is the charging power input of energy storage units, W_t is the onshore and offshore wind generation, W_t^{curt} is the curtailed output, and D_t is the electricity demand.

System reserve constraint

The system operator must provide sufficient reserve to meet any unexpected changes in generation or demand. The sum of the maximum power outputs $P_{g,\max}$ from all online generators must be greater than or equal to net demand plus the upwards reserve requirement R_t^{up} at time t. The sum of the minimum power outputs $P_{g,\min}$ must also be less than or equal to net demand and the downwards reserve requirement R_t^{dn} at time t.

$$\sum_{g=1}^{G} \left(u_{g,t} P_{g,\max} - u_{g,t}^{\text{capt}} P_{g,\min}^{\text{capt}} \right) + \sum_{s=1}^{S} P_{s,t}^{\text{d}} + W_t \geq D_t + \sum_{s=1}^{S} P_{s,t}^{\text{c}} + W_t^{\text{curt}} + R_t^{\text{up}} \tag{5.34}$$

$$\sum_{g=1}^{G} \left(u_{g,t} P_{g,\min} - u_{g,t}^{\text{capt}} P_{g,\max}^{\text{capt}} \right) + \sum_{s=1}^{S} P_{s,t}^{\text{d}} + W_t \leq D_t + \sum_{s=1}^{S} P_{s,t}^{\text{c}} + W_t^{\text{curt}} - R_t^{\text{dn}} \tag{5.35}$$

As detailed in Section 2.4, the system-wide upwards and downwards reserve requirements assume that the demand and wind forecast uncertainties can be approximated as normal distributions with zero mean. This allows the demand and wind forecast uncertainties to be analytically combined.

Downwards reserve is required to meet the largest credible loss in demand μ_t^{dn}, and the combined demand-wind forecast uncertainties:

$$R_t^{\text{dn}} = \mu_t^{\text{dn}} + \sqrt{(3.5\sigma_t^D)^2 + (3.5\sigma_t^W)^2} \tag{5.36}$$

The upwards reserve, as previously discussed in Section 2.4, is required to meet the largest

credible loss in generation μ_t^{up}, and the combined demand-wind forecast uncertainties:

$$R_t^{\text{up}} = \mu_t^{\text{up}} + \sqrt{(3.5\sigma_t^D)^2 + \min\left(3.5\sigma_t^W, (W_t^{\text{f}} - W_t^{\text{curt}})\right)^2} \tag{5.37}$$

where W_t^{f} is the forecast wind power output, W_t^{curt} is the wind that is scheduled to be curtailed at time t, σ_t^D is the standard deviation in demand forecast uncertainty, and σ_t^W is the standard deviation in wind forecast uncertainty.

Silva [2010] demonstrated an approach to split the spinning and standing reserve requirements using a parameter λ after considering the fully- and part-loaded costs of spinning and standing plant. The system upwards reserve requirement R_t^{up} can be met through a combination of both synchronous spinning reserve $R_t^{\text{SR,up}}$ and non-synchronous standing reserve $R_t^{\text{StR,up}}$ [Wood and Wollenberg, 1996].

Spinning reserve is typically provided by large-scale synchronised power plants which provide more frequent and smaller imbalances. Standing reserve is typically provided by fast-start power plants, such as an open cycle gas turbine (OCGT) or interruptible loads, which provide less frequent but much larger imbalances.

Utilising power plants on stand-by to provide standing reserve decreases the amount of part-loaded power plants providing spinning reserve. This is an effective way to minimise part-load efficiency losses and reduce system costs and CO_2 emissions.

The allocation or split between spinning and standing reserve is formulated as:

$$R_t^{\text{SR,up}} = \lambda R_t^{\text{up}} \tag{5.38}$$

$$R_t^{\text{StR,up}} = (1-\lambda) R_t^{\text{up}} \tag{5.39}$$

Increasing λ increases the amount of synchronised thermal units that are required to provide spinning reserve and decreases the reserve contributions required from standing plant.

The upwards and downwards reserve requirements are therefore a combination of spinning and standing reserve:

$$R_t^{\text{up}} = R_t^{\text{SR,up}} + R_t^{\text{StR,up}} \tag{5.40}$$

$$R_t^{\text{dn}} = R_t^{\text{SR,dn}} + R_t^{\text{StR,dn}} \tag{5.41}$$

Both power plants and energy storage units that are between minimum and maximum power output limits can provide upwards or downwards spinning reserve.

The system-wide upwards spinning reserve requirement $R_t^{\text{SR,up}}$ must be less then or equal to the upwards spinning reserve contributions from synchronised thermal power plants $R_{g,t}^{\text{SR,up}}$ and

energy storage units $R_{s,t}^{\mathrm{SR,up}}$:

$$R_t^{\mathrm{SR,up}} = \underbrace{\overbrace{\sum_{g=1}^{G} u_{g,t} R_{g,t}^{\mathrm{SR,up}}}^{\text{thermal units}} + \overbrace{\sum_{s=1}^{S} R_{s,t}^{\mathrm{SR,up}}}^{\text{storage units}}}_{\text{upwards flexibility}} \tag{5.42}$$

Similarly, the system-wide downwards spinning reserve requirement $R_t^{\mathrm{SR,dn}}$ must be less then or equal to the downwards spinning reserve contributions from synchronised thermal power plants $R_{g,t}^{\mathrm{SR,dn}}$ and energy storage units $R_{s,t}^{\mathrm{SR,dn}}$:

$$R_t^{\mathrm{SR,dn}} = \underbrace{\sum_{g=1}^{G} u_{g,t} R_{g,t}^{\mathrm{SR,dn}} + \sum_{s=1}^{S} R_{s,t}^{\mathrm{SR,dn}}}_{\text{downwards flexibility}} \tag{5.43}$$

The amount of system-wide upwards and downwards reserve defines the ability of the system to provide upwards and downwards flexibility. The summation of individual upwards spinning reserve contributions from units gives the upwards spinning reserve time-series $R_t^{\mathrm{SR,up}}$, which represents the technical ability of the system to respond to positive net demand variations and provide upwards flexibility. This is the same for the the downwards spinning reserve time-series $R_t^{\mathrm{SR,dn}}$.

It is assumed that energy storage units can rapidly change between charging/discharging modes and have negligible start-up times. In addition, it is assumed that the time taken to adjust the charge/discharge rates of energy storage units is negligible compared to the time step in each period. Energy storage units are therefore not limited by ramp rates. The reserve contributions from energy storage units are described in Section 5.8.

Standing reserve can be provided by fast-start power plants and energy storage units. Fast start-up thermal units, such as OCGT, are assumed to start-up from zero with negligible start-up times.

$$R_t^{\mathrm{StR,up}} = \sum_{g=1}^{G} R_{g,t}^{\mathrm{StR,up}} \tag{5.44}$$

Minimum load constraint

A minimum load constraint can be set to ensure there is a sufficient amount of synchronised thermal units to ensure must-run units are not forced to shut-down; to ensure there is a minimum number of synchronised thermal units providing system inertia to limit the initial RoCoF after a large change in demand/generation; and to ensure there is sufficient downwards reserve.

$$\sum_{g=1}^{G} \left(u_{g,t} P_{g,t} - u_{g,t}^{\text{capt}} P_{g,t}^{\text{capt}} \right) \geq D_{t,\min} \tag{5.45}$$

5.7 Operational constraints

The technical operational constraints of conventional thermal power plants are now outlined. The operational constraints for CCS-equipped power plants are introduced later in Section 5.9.

Power plants that are controllable and are operating above their minimum power output $P_{g,\min}$ are in an 'up' state. Power plants that are below their minimum power output $P_{g,\min}$, either because they are following their defined start-up/shut-down trajectories or they are shut-down, are in a 'down' state. This is shown graphically in Figure 5.7 which shows the operational states and start-up/shut-down profiles for typical power plant.

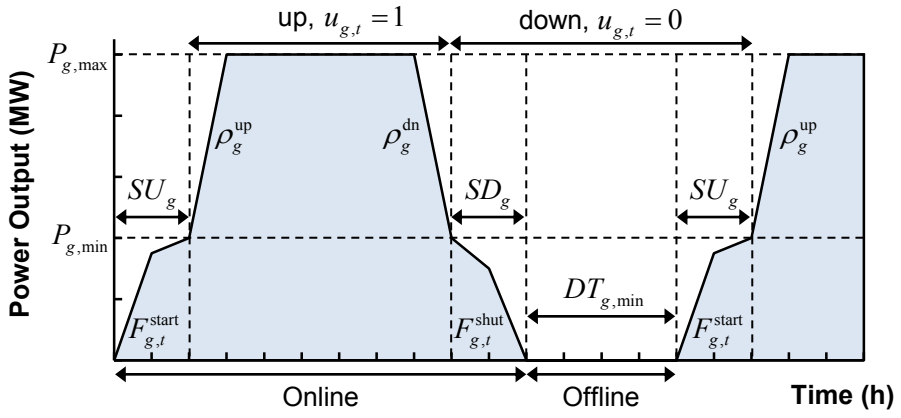

Figure 5.7: Illustrative dispatch pattern for a conventional power plant including the start-up time SU_g, shut-down time SD_g, fuel consumption during start-up $F_{g,t}^{\text{start}}$, fuel consumption during shut-down $F_{g,t}^{\text{shut}}$, upwards ramp rate ρ_g^{up}, downwards ramp rate ρ_g^{dn}, minimum down time $DT_{g,\min}$, and operational status $u_{g,t}$.

Power output constraints

The power output $P_{g,t}$ of a conventional power plant must be between its minimum power output $P_{g,\min}$ and maximum power output $P_{g,\max}$.

$$u_{g,t}P_{g,\min} \leq P_{g,t} \leq u_{g,t}P_{g,\max} \tag{5.46}$$

$$u_{g,t}P_{g,\min} \geq 0 \tag{5.47}$$

Ramping constraints

The increased magnitude of hourly net demand changes is likely to increase the ramping requirements of the generation portfolio. This may mean that thermal units are increasingly forced to change power output at their maximum up/down ramp rates.

The power output of each generator $P_{g,t}$ must be less than or equal to the previous time periods power output $P_{g,t-1}$ plus the generator ramp up rate ρ_g^{up} ($\mathrm{MW_e/h}$) at time t. The power output of each generator $P_{g,t}$ must also be greater than or equal to the previous time periods power output $P_{g,t-1}$ less the generator ramp down rate ρ_g^{dn} ($\mathrm{MW_e/h}$) at time t.

$$P_{g,t} \leq P_{g,t-1} + u_{g,t}\rho_g^{\mathrm{up}} \tag{5.48}$$

$$P_{g,t} \geq P_{g,t-1} - u_{g,t}\rho_g^{\mathrm{dn}} \tag{5.49}$$

These constraints are imposed when the power plant is in an up state and ready to adjust power output. However, these ramp rate constraints may be violated during start-up and shut-down events. It is possible to modify these ramp rate constraints to account for the rapid power output variations during start-up and shut-down if necessary:

$$P_{g,t} \leq P_{g,t-1} + u_{g,t}\rho_g^{\mathrm{up}} + \max\{P_{g,\min}, \rho_g^{\mathrm{up}}\}(u_{g,t} - u_{g,t-1}) \tag{5.50}$$

$$P_{g,t} \geq P_{g,t-1} - u_{g,t}\rho_g^{\mathrm{dn}} + \max\{P_{g,\min}, \rho_g^{\mathrm{dn}}\}(u_{g,t-1} - u_{g,t}) \tag{5.51}$$

The up and down ramp rates are expressed as a ratio of the maximum power output:

$$\rho_g^{\mathrm{up}} = \alpha_g^{\mathrm{up}} P_{g,\max} \tag{5.52}$$

$$\rho_g^{\mathrm{dn}} = \alpha_g^{\mathrm{dn}} P_{g,\max} \tag{5.53}$$

where α_g^{up} and α_g^{dn} are the maximum upwards and downwards ramping ratios of the base power plant, respectively.

Reserve constraints

The ability of a thermal power plant to provide reserve is a function of its ramp rate over the associated time frame. For a conventional thermal power plant, the upwards spinning reserve contribution $R_{g,t}^{\mathrm{SR,up}}$ provided by unit g is limited by either the difference between the maximum power output limit $P_{g,\max}$ and the power output $P_{g,t}$ at time t or the ramp up rate ρ_g^{up} over the time available for ramping Δt.

The downwards spinning reserve $R_{g,t}^{\mathrm{SR,dn}}$ provided by unit g is limited by either the difference between the power output $P_{g,t}$ and the minimum power output limit $P_{g,\min}$ at time t or the ramp down rate ρ_g^{dn} over the time available for ramping Δt.

$$R_{g,t}^{\mathrm{SR,up}} \leq \min\{(u_{g,t}P_{g,\max} - P_{g,t}), u_{g,t}\rho_{g,t}^{\mathrm{up}}\Delta t\} \tag{5.54}$$

$$R_{g,t}^{\mathrm{SR,dn}} \leq \min\{(P_{g,t} - u_{g,t}P_{g,\min}), u_{g,t}\rho_{g,t}^{\mathrm{dn}}\Delta t\} \tag{5.55}$$

Minimum up/down constraints

The physical characteristics of certain power plants mean that it may not always be possible to immediately shut-down a generator once it has just started-up. In addition, it may not always be possible to immediately start-up a generator once it has just shut-down.

The minimum down time $DT_{g,\min}$ (h) is equal to the shut-down time duration SD_g (h), plus the start-up time duration SU_g (h), plus the minimum technical time the unit must stay offline. The minimum up/down time constraints are:

$$(X_{g,t-1} - UT_{g,\min}) \cdot (u_{g,t-1} - u_{g,t}) \geq 0 \tag{5.56}$$

$$(-X_{g,t-1} - DT_{g,\min}) \cdot (u_{g,t} - u_{g,t-1}) \geq 0 \tag{5.57}$$

where $X_{g,t}$ is the time period (h) generator g has been online(+)/offline(-), and $UT_{g,\min}$ is the minimum up time. Power plants must remain online/offline for a minimum number of hours. The variable $X_{g,t}$ counts the number of hours each unit has been online/offline.

Initial operating hours

The number of hours that each generator has been online/offline $X_{g,t}$ needs to be defined for t = 0. This is then the initial status of each unit at the start of the time period.

5.8 Energy storage

Additional variability and uncertainty may increase the short-term balancing requirement and therefore increase the value of alternative sources of flexibility, such as energy storage. Increasing amounts of energy storage capacity could therefore be integrated into the existing electricity system to help manage the increasing proportions of VRE [IMechE, 2014]. Increasing amounts of VRE generation with near-zero marginal costs, such as wind, can suppress wholesale electricity prices and therefore possibly create additional electricity price differentials for energy storage arbitrage. Energy storage units can also readily utilise surplus generation and provide flexibility and reserve services to help accommodate the integration of new VRE capacity.

A large number of studies have investigated the economic impacts and potential role of energy storage [Strbac *et al.*, 2012; Grunewald, 2012]. Under current market arrangements, however, many studies report that the capital costs of existing energy storage technologies are prohibitively high to justify investment.

The traditional applications of energy storage include load shaping, peak shaving and reserve provision. Energy storage units will charge during time periods when prices are low and discharge during periods where prices are high. This is typically a daily charge/discharge cycle which is used to displace conventional peaking plant in the merit order. Energy storage units can also provide upwards reserve by discharging when there is a negative imbalance or provide downward reserve by charging when there is a positive net demand imbalance.

With increasing VRE capacity is likely that reserve and flexibility requirements of power systems will also increase. Given that energy storage can provide reserve and flexibility services, utilise low-carbon generation and displace more CO_2 intensive peaking plant, the potential role of energy storage in future power systems needs to be assessed.

5.8.1 Introduction

This section presents a Monte Carlo based energy storage optimisation model that simulates the outputs of a portfolio of energy storage units at the unit commitment stage using forecast net demand and at the economic dispatch stage using realised net demand data. This is to better understand the role of energy storage, the economic value, and provision of flexibility in future power systems. This work aims to explore the dynamic interactions that may occur between wind, conventional power plants, and CCS-equipped power plants. It is also important to understand how a portfolio of energy storage devices is likely to operate and interact with other generation assets.

Pumped hydro-electric storage makes up almost all of the grid-scale electrical energy storage in GB [Energy Research Partnership, 2011]. Table 5.5 shows a summary of key parameters for the existing and proposed pumped hydro-electric energy storage facilities in GB. The main assumptions of the energy storage model are now presented.

	Name	Output (GW)	Volume (GWh)	Duration (h)	Location	Year
Existing	Ffestiniog	0.36	1.3	3.6	Wales	1963
	Cruachan	0.40	10.0	25.0	Scotland	1966
	Foyers	0.30	6.3	21.0	Scotland	1974
	Dinorwig	1.80	9.1	5.1	Wales	1983
	Total	2.86	26.7			
Proposed	Sloy	0.06	0.36	6.0	Scotland	-
	Coire Glas	0.3-0.6	30.0	50-100	Scotland	-
	Balmacaan	0.3-0.6	30.0	50-100	Scotland	-
	Total	0.66-1.26	60.36			

Table 5.5: Existing and proposed pumped hydro-electric energy storage facilities in GB.

5.8.2 Model assumptions

When modelling energy storage units a number of assumptions are made in order to include energy storage in the optimisation process. A generic energy storage unit is defined with the following assumptions:

1. The start-up and shut-down times of energy storage units are negligible compared to the time step in each period. Whilst this depends on the storage technology, it is generally accepted that energy storage devices have very quick start-up and shut-down times.
2. The time taken to adjust the charging and discharging rates of energy storage units within power limits is negligible compared to the time step in each period. Energy storage units can rapidly adjust the charging and discharging rates.
3. The charging and discharging efficiencies and rate of leakage for energy storage units are assumed to be constant parameters that do not vary over time.
4. The charging power input and discharging power output are constant for each time period.
5. Energy storage units only have operating and storage costs. The operating costs for energy storage units is typically near-zero and the storage costs are dependent on the system electricity price at the time the energy is purchased.

Energy storage units are energy limited devices and so are formulated differently from thermal power plants in the model. This is because the operation of energy storage units and the charge/discharging profiles depend on the availability of energy in the store. The mathematical formulation of the Monte Carlo based energy storage optimisation model is now presented.

5.8.3 Model formulation

In order to understand the impact of electricity prices on the operation of energy storage, a Monte Carlo based optimisation algorithm is utilised in MATLAB to simulate the outputs of multiple large-scale, grid connected electrical energy storage devices. The Monte Carlo based energy storage optimisation model presented in this work is adapted from a generic energy storage model in Barbour *et al.* [2012] and Barbour [2013], see Figure 5.8. In Barbour *et al.* [2012] the model is applied to simulate the optimal charge/discharge schedule for pumped hydro-electric storage, hydrogen storage, and battery storage with Sodium Sulphur (NaS).

The optimal charge/discharge strategy for each energy storage unit is found over the optimisation time horizon. Energy storage technologies are characterised in terms of charging and discharging efficiencies, power output limits, and energy storage limits. It operates both at the unit commitment stage using forecast net demand and at the economic dispatch stage at delivery time using realised net demand.

The algorithm finds the upper boundary of the revenue available as a result of time-shifting energy. The optimal solution is therefore the maximum revenue available for a given energy storage device modelled with different storage capacities, charge/discharge power rates, and round-trip efficiencies. The Monte Carlo based optimisation algorithm converges on an optimal solution after a sufficient number of iterations.

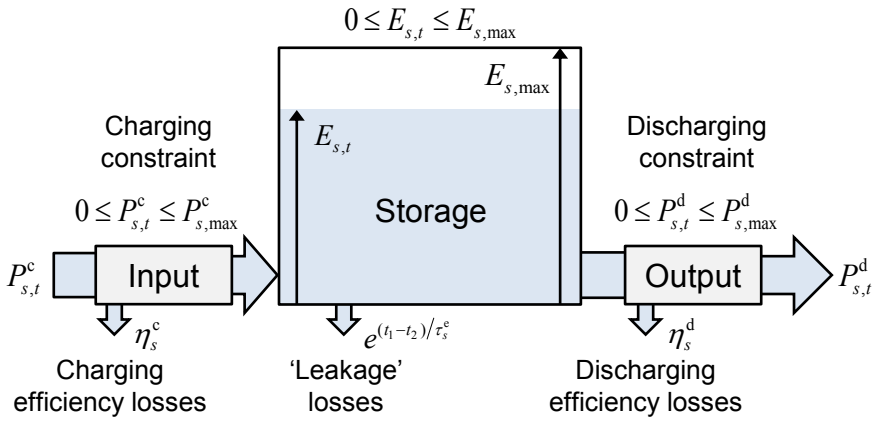

Figure 5.8: Generic energy storage conversion characteristics.

A typical energy storage device consists of an energy conversion unit. Some energy storage technologies have energy conversion systems for both charging and discharging modes of operation. Energy storage units consume energy and increase net electricity demand when electricity prices are low. Conversely, energy storage units discharge energy and decrease net electricity demand when electricity prices are high. Any energy storage device will incur efficiency losses during both charging and discharging. The charging efficiency η^{c}_{s} and discharging efficiency η^{d}_{s} for energy storage unit s, where $s = 1,2,3,...,S$, give the round trip-efficiency η^{rt}_{s}.

However, energy storage units may experience a rate of leakage from the storage volume over time.

The rate of leakage is represented in the model using the parameter τ_s^{e}. If an energy storage unit experiences no leakage, then $\tau_s^{\mathrm{e}} = \infty$. The time-dependent 'self-discharge' efficiency (% loss per hour) between two time periods t_1 and t_2, where $\Delta t = t_1 - t_2$, is given by the equation:

$$\eta_s^{\mathrm{leak}}(\Delta t) = e^{(t_1 - t_2)/\tau_s^{\mathrm{e}}} \tag{5.58}$$

The time-dependent round-trip efficiency between two time periods is the product of the losses for charging, discharging, and leakage:

$$\eta_s^{\mathrm{rt}}(\Delta t) = \eta_s^{\mathrm{c}} \cdot \eta_s^{\mathrm{d}} \cdot e^{(t_1 - t_2)/\tau_s^{\mathrm{e}}} \tag{5.59}$$

Figure 5.9 shows how the parameter τ_s^{e} impacts the overall round-trip efficiency. As the time Δt increases, the round-trip efficiency $\eta_s^{\mathrm{rt}}(\Delta t)$ decreases exponentially depending on the parameter τ_s^{e}.

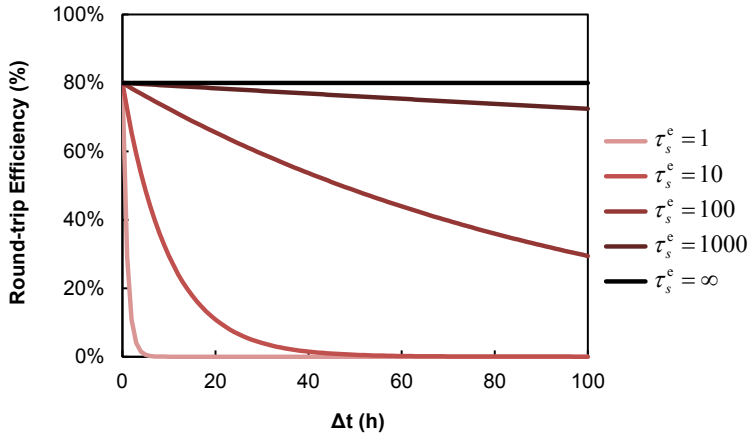

Figure 5.9: Round-trip efficiency with different rates of leakage.

It should be noted that transmission and distribution network constraints are not modelled. This analysis therefore assumes that the GB network is a single bus system, which represents a worst case scenario for energy storage. This is because transmission and distribution network constraints are likely to contribute towards congestion between areas and therefore make energy storage more economical.

A simple example explains the difference between charging and discharging. If the charge/discharge efficiencies of energy storage unit S_1 are $\eta_1^{\mathrm{c}} = \eta_1^{\mathrm{d}} = \sqrt{0.8}$, since $\eta_1^{\mathrm{rt}} = \eta_1^{\mathrm{c}} \cdot \eta_1^{\mathrm{d}} = 0.8$, then if unit S_1 charges at 1800 MW for 1 h only 1610 MWh of energy is stored ($1800 \times \sqrt{0.8}$). If unit S_1 discharges at 1800 MW for 1 h then 2012 MWh is extracted from the store ($1800 \div \sqrt{0.8}$).

Energy storage variables		
Π_s	Unit s profit	(£)
$P^{\mathrm{c}}_{s,t}$	Unit s charging power input at time t	($\mathrm{MW_e}$)
$P^{\mathrm{d}}_{s,t}$	Unit s discharging power output at time t	($\mathrm{MW_e}$)
$E_{s,t}$	Unit s energy stored at time t	($\mathrm{MWh_e}$)
η^{rt}_s	Unit s round-trip efficiency at time t	(-)

Table 5.6: Energy storage variables.

5.8.4 Objective function

The energy storage optimisation algorithm exploits differentials in the simulated electricity price and maximises the profit Π_s between time periods $\Delta t = t_1 - t_2$ for each energy storage device s as a result of time-shifting energy. The objective function of each individual energy storage unit is:

$$\Pi_s = \max \sum_{t=1}^{T} \left(P^{\mathrm{d}}_{s,t} - P^{\mathrm{c}}_{s,t} \right) \cdot \pi_t \tag{5.60}$$

where π_t is the simulated price of electricity at time t. The price of electricity π_t is the same for both charging and discharging.

For an energy storage device to make a profit, the ratio between the average electricity price must exceed the inverse of the round-trip efficiency $1/\eta^{\mathrm{rt}}_s(\Delta t)$. This implies that if the round-trip efficiency is 0.80, then the minimum price differential must be at least 1.25 for an energy storage unit to make a profit.

An iterative search procedure finds the feasible charging/discharging schedules for each unit and optimal charge/discharge strategy, subject to energy storage device constraints. A number of constraints are required to simulate the operational characteristics of individual energy storage units and the energy available in each store, which are now discussed in more detail.

Energy storage parameters		
$P^{\mathrm{c}}_{s,\max}$	Unit s maximum power input	($\mathrm{MW_e}$)
$P^{\mathrm{d}}_{s,\max}$	Unit s maximum power output	($\mathrm{MW_e}$)
$E_{s,\max}$	Unit s maximum energy stored	($\mathrm{MWh_e}$)
η^{c}_s	Unit s charging efficiency	(-)
η^{d}_s	Unit s discharging efficiency	(-)
τ^{e}_s	Unit s rate of leakage	(-)

Table 5.7: Energy storage parameters.

5.8.5 Operational constraints

Charging constraint

The power input $P^{c}_{s,t}$ of each storage unit must be between zero and its maximum charging input value $P^{c}_{s,\max}$:

$$0 \leq P^{c}_{s,t} \leq P^{c}_{s,\max} \tag{5.61}$$

Discharging constraint

The power output $P^{d}_{s,t}$ of each storage unit must be between zero and its maximum discharging output value $P^{d}_{s,\max}$:

$$0 \leq P^{d}_{s,t} \leq P^{d}_{s,\max} \tag{5.62}$$

Storage constraint

The stored energy $E_{s,t}$ of each storage unit must be between zero and its maximum storage capacity $E_{s,\max}$:

$$0 \leq E_{s,t} \leq E_{s,\max} \tag{5.63}$$

Reserve constraints

When energy storage units are charging, the loaded capacity of the unit can be considered as an interruptible load which is capable of providing upwards spinning reserve or primary frequency response. When energy storage units are discharging power, the power output of the unit could be rapidly decreased to provide downwards spinning reserve or high frequency response. The amount of upwards and downwards spinning reserve of energy storage units is formulated as:

$$R^{SR,up}_{s,t} \leq P^{c}_{s,t} \tag{5.64}$$

$$R^{SR,dn}_{s,t} \leq P^{d}_{s,t} \tag{5.65}$$

Energy storage units could also rapidly increase output by discharging to provide upwards spinning reserve but this depends on the availability of energy in the store. Also, energy storage units could rapidly increase the charging rate and input power to the store but this depends on there being space available in the store. The amount of non-spinning or standing reserve contributions of energy storage units depends on the availability of energy in the store.

$$R^{StR,up}_{s,t} \leq P^{c}_{s,\max} - P^{c}_{s,t} \tag{5.66}$$

$$R^{StR,dn}_{s,t} \leq P^{d}_{s,\max} - P^{d}_{s,t} \tag{5.67}$$

5.9 CO_2 capture

5.9.1 Introduction

CO_2 capture and storage (CCS) facilities are likely to be installed on fossil fuelled power plants in the future to reduce electricity sector CO_2 emissions. It is therefore important that researchers and system operators understand the potential operating regimes and flexibility requirements of future CCS-equipped power plants. This is to inform the design characteristics and improve the performance of CCS infrastructure in coping with potentially large amounts of wind variability and uncertainty.

5.9.2 Operating characteristics

This work models both inflexible CO_2 capture and flexible CO_2 capture plants with the capability to bypass the CO_2 capture plant and vent CO_2 to the atmosphere if it is economical. The unit commitment formulation developed in this work assumes a proportion of thermal power plants are retrofitted with integrated post-combustion capture (PCC). This requires adapting a number of operating constraints to account for CO_2 capture plants. PCC plants can be integrated into the steam cycles of thermal power plants in various configurations. The net power output of a thermal power plant equipped with CCS is:

$$P_{g,t}^{\mathrm{CCS}} = P_{g,t} - P_{g,t}^{\mathrm{capt}} \tag{5.68}$$

where $P_{g,t}$ is the power output of the base power plant and $P_{g,t}^{\mathrm{capt}}$ is the power consumption of the CO_2 capture and compression units. The power consumption of the post-combustion capture plant $P_{g,t}^{\mathrm{capt}}$ is the loss of power from steam extraction and the power required for CO_2 compression and ancillary equipment. This work uses performance data derived from Lucquiaud *et al.* [2009].

This work assumes a train of centrifugal CO_2 compressors with intercooling stages. Dehydration may also be required to limit corrosion. CO_2 compression to around 110 bar is typically required for cost effective CO_2 transportation. Inlet guide vanes in the compressor are used to control the flow of CO_2. However, a minimum CO_2 flow rate and compression load is likely to constrain the operation of the compression system. This is because at low flow rates, a compressor surge can occur and cause significant damage. It is therefore important that any compression system has a sophisticated anti-surge control system [Cato-2, 2013]. These assumptions define the compression, transportation and storage costs.

CO_2 capture variables		
$u_{g,t}^{\text{capt}}$	Unit g CO_2 capture plant binary decision variable at time t	(-)
$P_{g,t}^{\text{capt}}$	Unit g CO_2 capture plant power consumption at time t	(MW_e)
$P_{g,t}^{\text{capt,op}}$	Unit g operating CO_2 capture plant power consumption at time t	(MW_e)
$Y_{g,t}^{\text{capt}}$	Unit g CO_2 capture rate at time t	(-)
$E_{g,t}$	Unit g CO_2 emissions emitted at time t	(tCO_2)
$E_{g,t}^{\text{capt}}$	Unit g CO_2 emissions captured at time t	(tCO_2)
$C_{g,t}^{\text{O\&M,capt}}$	Unit g additional CO_2 capture operating and maintenance cost at time t	(£)
$C_{g,t}^{\text{solv}}$	Unit g solvent make-up cost at time t	(£)
$C_{g,t}^{\text{trans}}$	Unit g CO_2 transport and storage cost at time t	(£)
$C_{g,t}^{\text{CO}_2}$	Unit g CO_2 cost at time t	(£)

Table 5.8: CO_2 capture variables.

Flexible CO_2 capture is achieved by venting a proportion of the CO_2 to the atmosphere or by bypassing the CO_2 capture plant. This reduces the energy requirements for stripping and compressing the CO_2, allowing more power to be generated in the LP turbine [Lucquiaud and Gibbins, 2011]. The amount of steam entering the stripper is reduced and managed to control the CO_2 capture rate. Redirecting steam to the LP turbine can occur very quickly. However, with large amounts of circulating solvent, the capture process can take longer to fully stabilise after a significant load change.

The dynamic control of the PCC plant is an important consideration at partial or zero capture rates. Changes to flue gas input conditions and solvent loading levels will also impact the operational characteristics and transient behaviour of the PCC plant. However, the transient behaviour of the CO_2 capture plant is not considered in this work. This is in order to reduce the complexity of the model and maintain linearity. Further work is required to understand the dynamic behaviour of the CO_2 capture plant and the impacts of load changes and start-up/shut-downs on the CO_2 capture process. Additional parameters could be implemented into the model to characterise the transient behaviour of the CO_2 capture plant.

Flexible capture by venting allows more electricity to be generated and exported at the expense of additional CO_2 emissions. This analysis assumes that the LP turbine has been designed to accommodate the additional steam conditions during bypass and that the electrical generator can export the additional electricity.

Detailed technical analysis of the CO_2 storage, transportation, or compressions systems is beyond the scope of this study. However, it should be noted that in real systems any down-stream changes in operation at the storage, transportation, or compressions stages may limit or constrain the operation of the PCC plant. For example, an injection trip at the storage site may force the PCC plant to reduce the rate of CO_2 capture in order to avoid over pressurising the transportation infrastructure.

One possible solution to increase the operational flexibility of PCC systems is to use solvent storage, which allows the stripper and compression systems to operate more flexibly. However, solvent storage requires additional capital expenditure for the solvent storage tanks and extra solvent, and also requires an over sized stripper and CO_2 compressors that can manage the additional CO_2. The operation of the PCC plant with solvent storage depends on the amount of rich/lean solvent available in the solvent storage tanks. Determining the configuration and optimal operation of PCC with solvent storage is considered beyond the scope of this work. Therefore, it is assumed that real-time flue gases must either be treated or vented.

This implies that the absorption and stripping systems can be modelled using a single decision variable that indicates their operational status. The binary decision variable $u_{g,t}^{\text{capt}}$ is used to represent the operational state of the CO_2 capture plant. This also simplifies the modelling complexity by reducing the number of decision variables.

CO_2 capture parameters		
$P_{g,\min}$	Unit g minimum base power plant output	(MW_e)
$P_{g,\max}$	Unit g maximum base power plant output	(MW_e)
$P_{g,\min}^{\text{capt}}$	Unit g minimum CO_2 capture plant power consumption	(MW_e)
$P_{g,\max}^{\text{capt}}$	Unit g maximum CO_2 capture plant power consumption	(MW_e)
$P_g^{\text{capt,fixed}}$	Unit g fixed CO_2 capture plant power consumption	(MW_e)
$P_{g,\min}^{\text{capt,op}}$	Unit g minimum operating CO_2 capture plant power consumption	(MW_e)
$P_{g,\max}^{\text{capt,op}}$	Unit g maximum operating CO_2 capture plant power consumption	(MW_e)
$Y_{g,\min}^{\text{capt}}$	Unit g minimum CO_2 capture rate	(-)
$Y_{g,\max}^{\text{capt}}$	Unit g maximum CO_2 capture rate	(-)
$\rho_g^{\text{capt,up}}$	Unit g CO_2 capture plant ramp up rate	(MW_e/h)
$\rho_g^{\text{capt,dn}}$	Unit g CO_2 capture plant ramp down rate	(MW_e/h)
$q_g^{\text{capt,op}}$	Unit g energy requirement to capture 1 tonne of CO_2	(MWh_e/tCO_2)
$c_{g,t}^{\text{fuel}}$	Unit g cost of fuel at time t	(£/MWh_{th})
c^{CO_2}	Cost of CO_2	(£/tCO_2)
$c_g^{\text{O\&M,capt}}$	Unit g additional cost of CO_2 capture plant variable operation and maintenance	(£/tCO_2)
c^{solv}	Cost of MEA solvent	(£/kg)
c_g^{trans}	Unit g cost of CO_2 transport and storage	(£/tCO_2)
$e_g^{\text{CO}_2}$	Unit g fuel-specific emission factor	(tCO_2/MWh_{th})
D_g	Unit g total solvent degradation rate	(kg/tCO_2)
D_g^{th}	Unit g solvent degradation rate caused by thermal effects	(kg/tCO_2)
$UT_{g,\min}^{\text{capt}}$	Unit g CO_2 capture plant minimum up time	(h)
$DT_{g,\min}^{\text{capt}}$	Unit g CO_2 capture plant minimum down time	(h)
SU_g^{capt}	Unit g CO_2 capture plant start-up time	(h)
SD_g^{capt}	Unit g CO_2 capture plant shut-down time	(h)

Table 5.9: CO_2 capture parameters.

A flexible CCS unit with venting/bypass capabilities is able to vary the CO_2 capture rate $Y_{g,t}^{\text{capt}}$ between:

$$Y_{g,\min}^{\text{capt}} \leq Y_{g,t}^{\text{capt}} \leq Y_{g,\max}^{\text{capt}} \tag{5.69}$$

where $Y_{g,\min}^{\text{capt}}$ is the minimum design capture rate and $Y_{g,\max}^{\text{capt}}$ is the maximum design capture rate. Figure 5.10 shows the operating range of an illustrative CCS-equipped power plant. The power output $P_{g,t}$ and CO_2 capture rate $Y_{g,t}^{\text{capt}}$ can be varied subject to the base and capture plant technical constraints. A CCS unit is considered inflexible if $Y_{g,t}^{\text{capt}}$ cannot be adjusted and therefore remains constant at the design capture rate.

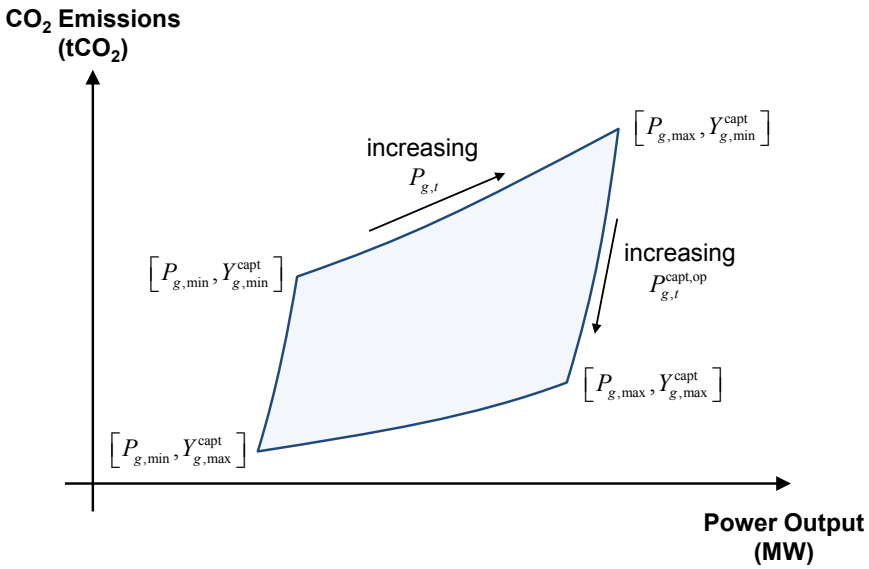

Figure 5.10: The operating range of CCS-equipped power plants. Adapted from Ji *et al.* [2013].

The power consumption of the CO_2 capture plant $P_{g,t}^{\text{capt}}$ is the sum of the fixed power consumption $P_g^{\text{capt,fixed}}$ and the operating power consumption $P_{g,t}^{\text{capt,op}}$, which is assumed to be linearly proportional to the amount of CO_2 being treated $E_{g,t}^{\text{capt}}$ as follows:

$$P_{g,t}^{\text{capt}} = P_g^{\text{capt,fixed}} + P_{g,t}^{\text{capt,op}} = P_g^{\text{capt,fixed}} + q_g^{\text{capt,op}} E_{g,t}^{\text{capt}} \tag{5.70}$$

$$P_{g,t}^{\text{capt}} = P_g^{\text{capt,fixed}} + q_g^{\text{capt,op}} \left(F_{g,t} e_g^{\text{CO}_2} Y_{g,t}^{\text{capt}}\right) \tag{5.71}$$

where $q_g^{\text{capt,op}}$ is the energy requirement to capture 1 tonne of CO_2, $e_g^{\text{CO}_2}$ is the unit-specific CO_2 emission intensity of the base power plant, and $Y_{g,t}^{\text{capt}}$ is the CO_2 capture rate. In reality, the energy requirement of the capture plant $q_g^{\text{capt,op}}$ is likely to vary with time and operating conditions. The maximum and minimum power consumption of the CO_2 capture plant is therefore:

$$P_{g,\min}^{\text{capt}} = P_g^{\text{capt,fixed}} + q_g^{\text{capt,op}} \left(F_{g,t} e_g^{\text{CO}_2} Y_{g,\min}^{\text{capt}}\right) \tag{5.72}$$

$$P_{g,\max}^{\text{capt}} = P_g^{\text{capt,fixed}} + q_g^{\text{capt,op}}\left(F_{g,t} e_g^{\text{CO}_2} Y_{g,\max}^{\text{capt}}\right) \tag{5.73}$$

Equations 5.72 and 5.73 can be rewritten as:

$$P_{g,\min}^{\text{capt}} = P_g^{\text{capt,fixed}} + P_{g,\min}^{\text{capt,op}} \tag{5.74}$$

$$P_{g,\max}^{\text{capt}} = P_g^{\text{capt,fixed}} + P_{g,\max}^{\text{capt,op}} \tag{5.75}$$

where $P_{g,\min}^{\text{capt,op}}$ is the minimum operating CO_2 capture plant power consumption and $P_{g,\max}^{\text{capt,op}}$ is the maximum operating CO_2 capture plant power consumption.

5.9.3 Profit maximisation

An individual flexible CO_2 capture unit seeks to maximise the operating profit $\Pi_{g,t}$ in each time period by adjusting the CO_2 capture rate. The amount of revenue is determined by the net power output of the CCS power plant $P_{g,t}^{\text{CCS}} = P_{g,t} - P_{g,t}^{\text{capt}}$ times the electricity price π_t. The costs include fuel costs and variable O&M costs of the base power plant, CO_2 costs, variable O&M costs, solvent costs and transport costs of the capture plant. The objective function is formulated as:

$$\Pi_{g,t} = \max\left(\left(\overbrace{P_{g,t}^{\text{CCS}} \cdot \pi_t}^{\text{Revenue}}\right) - \left(\overbrace{C_{g,t}^{\text{fuel}} + C_{g,t}^{\text{O\&M}} + C_{g,t}^{\text{ramp}} + C_{g,t}^{\text{O\&M,capt}} + C_{g,t}^{\text{solv}} + C_{g,t}^{\text{trans}} + C_{g,t}^{\text{CO}_2}}^{\text{Costs}}\right)\right) \tag{5.76}$$

where π_t is the simulated electricity price at time t. The operational constraints for thermal power plants in the UCED model are now modified to include the operational characteristics of CO_2 capture plants. Each of the cost components are then described in more detail.

5.9.4 Operational constraints

The operational constraints of conventional power plants was introduced in Section 5.7. These constraints are now modified to include the constraints of CCS-equipped power plants.

Power output constraints

The maximum and minimum power output limits of CCS-equipped power plants are:

$$u_{g,t} P_{g,\min} - u_{g,t}^{\text{capt}} P_{g,\max}^{\text{capt,op}} - P_g^{\text{capt,fixed}} \leq P_{g,t} \leq u_{g,t} P_{g,\max} - P_g^{\text{capt,fixed}} \tag{5.77}$$

$$u_{g,t}^{\text{capt}} P_{g,\max}^{\text{capt,op}} \geq 0 \tag{5.78}$$

$$P_{g,t}^{\text{capt,fixed}} \geq 0 \tag{5.79}$$

where $u_{g,t}^{\text{capt}}$ is a binary decision variable that represents the operational status of the CO_2 capture plant, $P_{g,\max}^{\text{capt,op}}$ is the maximum operating power consumption of the capture plant, and $P_g^{\text{capt,fixed}}$ is the fixed power consumption of the capture plant.

The minimum power output limit considers the minimum power output limit of the base power plant, the fixed power consumption of the CO_2 capture plant and the maximum operating power consumption of the capture plant. The operating range for CCS-equipped power plants are therefore greater than that of conventional thermal power plants.

Ramping constraints

CCS-equipped power plants are able to adjust the power consumption of the CO_2 capture plant up and down independently of the base power plant by varying the amount of steam that is extracted. CCS-equipped power plants can therefore be ramped faster than conventional thermal units by adjusting the power output of the base power plant and the power consumption of the CO_2 capture plant [Ji *et al.*, 2013]. The ramping constraints of the CO_2 capture plant are:

$$P_{g,t}^{\text{capt,op}} \leq P_{g,t-1}^{\text{capt,op}} + u_{g,t}^{\text{capt}} \rho_g^{\text{capt,up}} \tag{5.80}$$

$$P_{g,t}^{\text{capt,op}} \geq P_{g,t-1}^{\text{capt,op}} - u_{g,t}^{\text{capt}} \rho_g^{\text{capt,dn}} \tag{5.81}$$

where $\rho_g^{\text{capt,up}}$ and $\rho_g^{\text{capt,dn}}$ are the up and down ramp rates of the CO_2 capture plant, respectively. Expressed as a ramping ratio these become:

$$\rho_g^{\text{capt,up}} = \alpha_g^{\text{capt,up}} P_{g,\max}^{\text{capt,op}} \tag{5.82}$$

$$\rho_g^{\text{capt,dn}} = \alpha_g^{\text{capt,dn}} P_{g,\max}^{\text{capt,op}} \tag{5.83}$$

where $\alpha_g^{\text{capt,up}}$ and $\alpha_g^{\text{capt,dn}}$ are the maximum upwards/downwards ramping ratios of the CO_2 capture plant, respectively. They represent the maximum rates of change in extracted steam flow.

Reserve constraints

CCS-equipped power plants are able to provide additional spinning reserve by adjusting the CO_2 capture rate and hence the power consumption of the capture plant. The modified reserve constraints for thermal units equipped with CCS are formulated as:

$$R_{g,t}^{\text{SR,up}} \leq \min\{(u_{g,t} P_{g,\max} - P_{g,t}), u_{g,t} \rho_{g,t}^{\text{up}} \Delta t\} + \min\{(P_{g,t}^{\text{capt,op}} - u_{g,t}^{\text{capt}} P_{g,\min}^{\text{capt,op}}), u_{g,t} \rho_{g,t}^{\text{capt,dn}} \Delta t\} \tag{5.84}$$

$$R_{g,t}^{\text{SR,dn}} \leq \min\{(P_{g,t} - u_{g,t} P_{g,\min}), u_{g,t} \rho_{g,t}^{\text{dn}} \Delta t\} + \min\{(u_{g,t}^{\text{capt}} P_{g,\max}^{\text{capt,op}} - P_{g,t}^{\text{capt,op}}), u_{g,t} \rho_{g,t}^{\text{capt,up}} \Delta t\} \tag{5.85}$$

5.9.5 Costs of CO_2 capture

Additional parameters are required to characterise the CO_2 capture, compression, and transportation costs and costs associated with solvent make-up and additional variable O&M. Solvent costs are incurred by the addition of new solvent, which is required to compensate for losses caused by solvent degradation. Volatile and oxidative losses in the absorber, and thermal degradation in the stripper can cause the solvent to degrade over time. A more rigorous formulation would also include the CO_2 capture start-up/shut-down costs, ramping costs, waste costs, reclamation costs, and additional water costs at each time period. However, these cost impacts are assumed to be small and are left to be explored in future.

Efficiency losses during transient operation could be captured by including ramping costs for the CO_2 capture plant. However, these terms have been excluded to preserve linearity and increase computational speed. Each of the additional costs components are described in more detail below.

Variable capture O&M costs

In addition to the base power plant O&M costs are additional O&M costs for the CO_2 capture and compression systems. These additional variable O&M costs are required to represent the additional costs associated with maintaining and operating the PCC plant and compression systems. It is assumed that the variable O&M costs for the PPC system are linearly proportional to the amount of CO_2 being treated as follows:

$$C_{g,t}^{\text{O\&M,capt}} = E_{g,t}^{\text{capt}} c_g^{\text{O\&M,capt}} \tag{5.86}$$

where $c_g^{\text{O\&M,capt}}$ is the variable O&M cost of capture.

Solvent make-up costs

In amine-based PCC systems, solvent can degrade over time which reduces the ability of the system to capture CO_2. In particular, thermal degradation is caused by exposure to high temperatures, predominantly in the stripper and reboiler. MEA-based solvents suffer from oxidative degradation, formation of heat stable salts, and carbamate polymerization [Reynolds *et al.*, 2013]. These thermal effects and a high O_2 content entering the PCC system can negatively impact the solvent degradation rate of MEA-based solvents [IEAGHG, 2012]. Other impurities can also cause amines to degrade at faster rates.

However, the rate and extent of solvent degradation and the type of degradation products formed depends on a large number of factors including the structure of the amine solvent, amine concentration, CO_2 loading, O_2 concentration, and the absorber reaction and solvent regenerator temperatures [CSIRO, 2012]. Other important factors include the presence of SO_X,

NO_X, and particulate matter in the flue gas entering the PCC system and any catalytic effect caused by reaction with plant material.

Additional solvent is therefore required to replenish any solvent that degrades over time. It is assumed that solvent degradation rate caused by thermal effects is constant since solvent is exposed to high temperatures in the stripper for the same period of time regardless of steam extraction rates [Cohen, 2012].

The solvent make-up costs used in this work are formulated as:

$$C^{\text{solv}}_{g,t} = F_{g,\max} e^{\text{CO}_2}_g Y^{\text{capt}}_{g,\max} c^{\text{solv}} \left((D_g - D^{\text{th}}_g) Y^{\text{capt}}_{g,t} + D^{\text{th}} \right) \tag{5.87}$$

where c^{solv} is the cost of solvent (£/kg), D_g is the total solvent degradation rate (kg/tCO_2), and D^{th}_g is the solvent degradation rate caused by thermal effects (kg/tCO_2) for unit g.

The amount of CO_2 that is treated by the capture plant when the base power plant is at full load is $F_{g,\max} e^{\text{CO}_2}_g Y^{\text{capt}}_{g,\max}$. This is used to calculate the amount of solvent that thermally degrades per tonne of CO_2 treated. Other solvent losses that occur are expressed as $D_g - D^{\text{th}}_g$ are and scaled by the CO_2 capture rate.

CO_2 transport and storage costs

Parsons Brinkerhoff [2013a] provide CO_2 transport and storage costs for low, central and high cost scenarios. In the 2012 update, Parsons Brinkerhoff [2012] report the onshore CO_2 transport cost at £5.20 per km per ktCO_2 for onshore pipeline lengths of 5 km, 20 km, and 50 km. Offshore transport costs are reported to be £6.24 per km per ktCO_2 for a length of 70 km. For a typical CCS project in the UK, this gives costs in £/tCO_2 for low, central and high scenarios at £7.43/tCO_2, £11.19/tCO_2, and £16.16/tCO_2, respectively. However, the 2013 update reports that the methodology used in the 2012 update underestimates the central and high costs of CO_2 transport [Parsons Brinkerhoff, 2013a].

The low cost scenario is assumed to utilise some existing transport and injection infrastructure and stores CO_2 in either a depleted oil or gas field [Parsons Brinkerhoff, 2013a]. The central cost scenario assumes new pipeline infrastructure that transports CO_2 to either an offshore depleted oil or gas field. The high cost scenario assumes the storage site is a saline aquifer with a higher delivery pressure.

The 2013 update estimates the costs of CO_2 transport and storage for all CCS technologies to be £8.20/tCO_2, £19.60/tCO_2, and £32.20/tCO_2, for the low, central and high estimates, respectively.

The CO_2 transport and storage costs depend on the amount of CO_2 being treated by the CO_2 capture plant. The transport and storage costs $C^{\text{trans}}_{g,t}$ are then determined by the amount of CO_2

being treated and the cost of CO_2 transport and storage c_g^{trans} (£/tCO_2):

$$C_{g,t}^{\text{trans}} = E_{g,t}^{\text{capt}} c_g^{\text{trans}} \tag{5.88}$$

It is likely that cost of CO_2 transport and storage will vary with time and depend on the location and distance to the storage site, the use of existing infrastructure, and delivery pressure. However, this work assumes that the cost of CO_2 transport and storage is linearly proportional to the amount of CO_2 captured. This simplification preserves model linearity yet still includes some important considerations.

CCS-equipped power plants at part-load will emit more CO_2 per MWh of electricity generated (because of part-load efficiency losses of the base power plant). This will impact the CO_2 emissions captured by the CO_2 capture plant $E_{g,t}^{\text{capt}}$ and therefore impact the CO_2 transport and storage costs $C_{g,t}^{\text{trans}}$. This implies that power plants with more CO_2 intensive fuels will have higher CO_2 transport and storage costs. Varying the CO_2 capture rate will also impact the transport and storage costs $C_{g,t}^{\text{trans}}$.

5.10 Start-up costs

5.10.1 Introduction

In liberalised electricity markets, when electricity prices do not cover the marginal costs of generation, thermal plants seek to minimise the time spent at non-profitable loads. Power plants either shut-down or reduce load if it is not profitable to continue operating in the present state. An increase in VRE capacity is expected to increase power price variation and change the operating regimes and start-up/shut-down schedules of thermal power plants. For mid-merit power plants, an increase in VRE capacity will displace these units and cause them to shut-down for longer periods of time. The next time that these power plants are required to start-up again, they are likely to be colder because they have been shut-down for longer.

This will lead to an increased variation in hot, warm, and cold start-ups as thermal power plants are displaced by VRE, but for irregular and indeterminate periods of time. This will impact the short-term production decisions of plant operators, which are constrained by non-convexities and a temporary irreversibility that reduces flexibility. High start-up and shut-down costs increases the resistance to change states and make frequent start-up/shut-downs more expensive, decreasing flexibility, compared to a 'frictionless' system [Rosnes, 2008].

It is not fully understood how increased cycling operations will change start-up costs into the future or over the expected life of a power plant. Analysis by Kumar *et al.* [2012] gives the start-up fuel and other start-up costs for a number of different thermal power plant unit types. There are also lower and upper bound values reported for capital and maintenance costs in

terms of £/MW for hot, warm, and cold start-ups for each of the different unit types. The data is based on 25 years worth of aggregated North American power plant data and so may not be applicable to GB.

Le *et al.* [1990] model the dispatch errors and economic penalties of using incorrect start-up cost data and express them as a function of the start-up cost. The authors used a unit commitment model and a normal distribution function to quantify the start-up cost error. It is shown that significant errors and cost penalties occur when start-up costs are underestimated. When start-up costs are $\pm$ 50% of the correct costs there is little or no difference. When start-up costs are overestimated there is only a small difference in the economic penalty. The results, therefore showed that it is better to overestimate start-up costs to avoid significant errors and cost penalties.

This implies that it is important to use start-up cost functions that accurately represent the dynamic non-linear costs associated with starting up thermal power plants after a period of cooling, which requires an increasing amount of fuel to reassume operating temperatures.

5.10.2 Fuel input during start-up

The additional fuel consumption required for a start-up (that does not generate any electricity), or the cost of start-up fuel, can be expressed in terms of the number of hours that the power plant would have to operate at full load to consume the same amount of fuel. F-Class CCGTs are reported to consume 0.5 operating hours of fuel during a hot start-up and 1.0 operating hours of fuel during a warm start-up [KEMA, 2008].

IEEE [2013] outline the heat input per start for a number of generation technologies. They report that 16.5 MMBTU of fuel is required for a coal power plant to start-up per MW of capacity. For a large CCGT they report that 2.0 MMBTU is required per MW of capacity. This is approximately 500 MWh_{th} of natural gas per start-up.

The fuel input required for hot/warm/cold start-ups varies considerably. It is therefore important to distinguish between hot, warm, and cold start-ups in unit commitment models by employing time-dependent start-up cost functions. Exponential functions that represent the fuel consumption required to reassume operating temperatures after a shut-down or period of cooling provide a good approximation of start-up costs [Sumbera, 2012].

5.10.3 Start-up cost formulation

Thermal stresses in certain power plant components limit the maximum temperature gradient and therefore increase the start-up time and fuel consumption during start-up. Typically, cold start-ups take longer and require more fuel than hot start-ups. The use of exponential functions to represent the start-up costs of thermal units in unit commitment models is well established. The start-up costs of conventional thermal power plants after a shut-down or period of cooling can be approximated as an exponential function which is given by:

$$C^{\text{start}}_{g,t} = \overbrace{c^{\text{start,fixed}}_{g}}^{\text{fixed}} + \left(\overbrace{F^{\text{start,cold}}_{g} c^{\text{fuel}}_{g,t}}^{\text{fuel}} + \overbrace{F^{\text{start,cold}}_{g} e^{\text{CO}_2}_{g} c^{\text{CO}_2}}^{\text{CO}_2} \right) \cdot \left(\overbrace{1 - e^{(X_{g,t}/\tau^{\text{c}}_{g})}}^{\text{exponential}} \right) \tag{5.89}$$

where $c^{\text{start,fixed}}_{g}$ are the fixed start-up costs (£), $F^{\text{start,cold}}_{g}$ is the fuel consumption during a cold start-up (MWh_{th}), and $X_{g,t}$ is the time period (h) generator g has been online(+)/offline(-) at time t. τ^{c}_{g} is the thermal cooling constant (h) that determines exponential time-dependent profile of a unit's start-up costs, see Figure 5.11.

A counter is used to update $X_{g,t}$ after each time period. If unit g has been offline in period t for 8 hours then $X_{g,t}$ = -8. If unit g starts-up in period $t+1$ then the counter is reset and $X_{g,t+1} = 0$. In period $t+2$ unit g has been online for 1 hour so $X_{g,t+2}$ = 1. Conversely, if the same unit g at time t has been online for 12 hours then $X_{g,t}$ = 12. If unit g shuts-down in period $t+1$ then the counter again is reset and $X_{g,t+1} = 0$. In period $t+2$ unit g has been offline for 1 hour so $X_{g,t+2}$ = -1.

From Equation 5.89, the fuel consumption during start-up is defined as:

$$F^{\text{start}}_{g,t} = F^{\text{start,cold}}_{g} \cdot \left(1 - e^{(X_{g,t}/\tau^{\text{c}}_{g})} \right) \tag{5.90}$$

5.10.4 Start-up and shut-down costs with CO_2 capture

CCS-equipped power plants may be technically capable of capturing a proportion of the CO_2 emissions during start-up and shut-down [IEAGHG, 2012]. However, CO_2 capture plants can only begin stripping CO_2 when steam is available for regeneration. This will depend on the type of start-up, the steam cycle, and the steam conditions required for regeneration. The start-up costs for a CCS-equipped unit that is able to capture a proportion of the CO_2 emissions during start-up is formulated as:

$$C^{\text{start}}_{g,t} = \overbrace{c^{\text{start,fixed}}_{g}}^{\text{fixed}} + \left(\overbrace{F^{\text{start,cold}}_{g} c^{\text{fuel}}_{g,t}}^{\text{fuel}} + \overbrace{F^{\text{start,cold}}_{g} e^{\text{CO}_2}_{g} c^{\text{CO}_2} (1 - Y^{\text{capt}}_{g,t} q^{\text{start,capt}}_{g})}^{\text{CO}_2} \right) \cdot \left(\overbrace{1 - e^{(X_{g,t}/\tau^{\text{c}}_{g})}}^{\text{exponential}} \right) \tag{5.91}$$

where $Y^{\text{capt}}_{g,\text{max}}$ is the maximum CO_2 capture rate and $q^{\text{start,capt}}_{g}$ represents the fraction of CO_2 that can be captured during start-up.

The start-up cost function in Equation 5.91 uses the offline time, where $X_{g,t} < 0$ to calculate the start-up costs and emissions. The start-up costs as a function of the time spent shut-down for different cooling constants is shown in Figure 5.11.

The CO_2 emissions during start-up are therefore:

$$E_{g,t}^{\text{start}} = \left(F_{g,t}^{\text{start,cold}} e_g^{\text{CO}_2} c^{\text{CO}_2} (1 - Y_{g,t}^{\text{capt}} q_g^{\text{start,capt}})\right) \cdot \left(1 - e^{(X_{g,t}/\tau_g^{\text{c}})}\right) \tag{5.92}$$

Both CCGT and USC-PC power plants with PCC could utilise solvent storage tanks to reduce CO_2 emissions during start-up and shut-down. In this configuration, stored lean solvent enters the absorber during start-up and the CO_2 rich solvent from the absorber is stored in a tank [IEAGHG, 2012]. This rich solvent can then be regenerated at a later time assuming the stripper and compressions systems are sized to accommodate the additional rich solvent. This would enable both CCGT and USC-PC power plants with PCC to start-up as quick as a normal power plant without PCC.

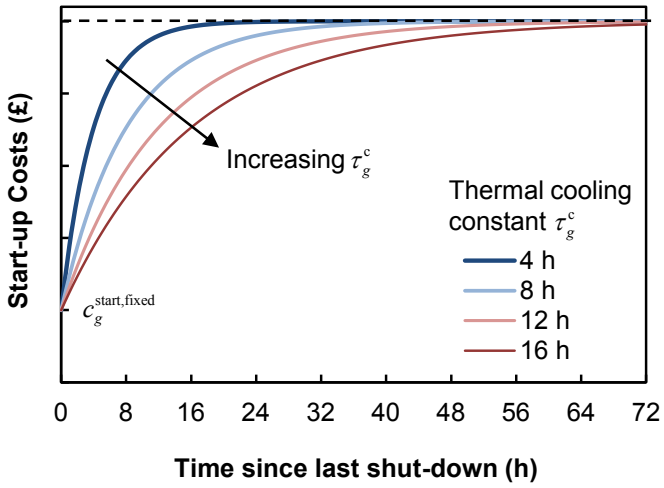

Figure 5.11: Time-dependent exponential start-up costs for different thermal cooling time constants.

The shut-down costs of thermal power plants do not depend on the time units have been online or offline. Therefore shut-down costs of thermal power plants with CCS are expressed mathematically as:

$$C_{g,t}^{\text{shut}} = \overbrace{c_g^{\text{shut,fixed}}}^{\text{fixed costs}} + \overbrace{F_g^{\text{shut}} c_{g,t}^{\text{fuel}}}^{\text{fuel costs}} + \overbrace{F_g^{\text{shut}} e_g^{\text{CO}_2} c^{\text{CO}_2} (1 - Y_{g,t}^{\text{capt}} q_g^{\text{shut,capt}})}^{\text{CO}_2\text{ costs}} \tag{5.93}$$

where $c_g^{\text{shut,fixed}}$ are the fixed shut-down costs (£), F_g^{shut} is the fuel consumption during a shut-down (MWh_{th}), and $q_g^{\text{shut,capt}}$ is the assumed CO_2 capture rate during shut-down.

5.11 IEEE RTS-96 test system

5.11.1 Introduction

The UCED model is validated using a test system. The Institute of Electrical and Electronics Engineers (IEEE) developed an enhanced single-area test system for bulk power system reliability evaluation studies [Grigg *et al.*, 1999]. The IEEE Reliability Test System - 1996 (RTS-96) Grigg *et al.* [1999] was initially developed in 1979 IEEE Reliability Test System Task Force [1979] and later updated in 1989 Allan *et al.* [1986]. The use of the IEEE RTS-96 test system for validating and comparing unit commitment models is well established.

It contains detailed generator information for a total of 32 units including 6 hydro. The 6 hydro units, each 50 MW, are excluded so there is in total 26 thermal power plants with a total installed capacity of 3105 MW. Transmission arrangements are simplified by assuming a single bus network.

5.11.2 Input data assumptions

This analysis uses system and unit-specific data for the unit commitment test case from Wang and Shahidehpour [1993] which includes electricity demand data, generator quadratic cost data, start-up costs, min up/down times, start-up times, up/down ramp rates, and fuel type.

Available in this section are data sources for the IEEE RTS-96 test system. These data sources include:

- power output limits, fuel type and number of generators are provided in Table 5.10;
- demand data is shown in Figure 5.12 and in Table C.1;
- generator data including the minimum up/down times, initial generator statuses, and ramp rates are provided Table 5.11; and
- quadratic cost data for the 26-unit test system is taken from Wang and Shahidehpour [1993] and are shown in Table 5.12.

Available in Appendix C are additional data sources for the IEEE RTS-96 test system. These data sources include:

- electricity demand data is shown in Table C.1;
- start-up costs, thermal cooling constants, and variable O&M costs are shown in Table C.2; and
- fuel costs for each of the generators are obtained from IEEE Reliability Test System Task Force [1979] and are shown in Table C.3.

All costs provided in Wang and Shahidehpour [1993] are in $USD so for the purpose of this test system all costs are provided in $USD.

Unit	Type	Fuel	No.	Max output $P_{g,max}$ (MW)	Min output $P_{g,min}$ (MW)
u12	oil/steam	#6 oil	5	12.00	2.40
u20	oil/CT	#2 oil	4	20.00	4.00
u76	coal/steam	coal	4	76.00	15.20
u100	oil/steam	#6 oil	3	100.00	25.00
u155	coal/steam	coal	4	155.00	54.25
u197	oil/steam	#6 oil	3	197.00	69.00
u350	coal/steam	coal	1	350.00	140.00
u400	nuclear	nuclear	2	400.00	100.00
26-units			26	3105.00	927.80

Table 5.10: Power output and fuel type data for the 26-unit IEEE RTS-96 test system from Wang and Shahidehpour [1993].

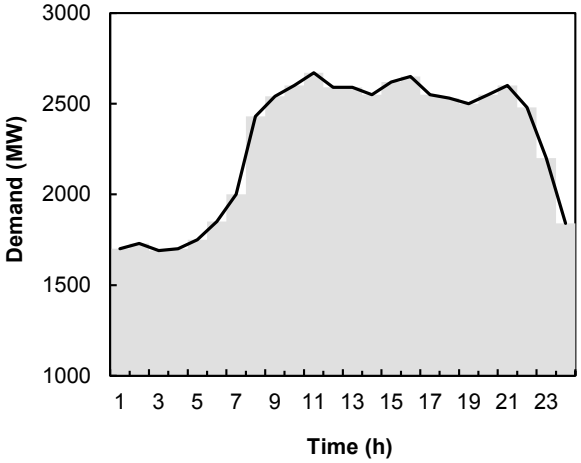

Figure 5.12: Demand data for the 26-unit IEEE RTS-96 test system from Wang and Shahidehpour [1993].

5.11.3 Test results

Ramp rates

Using the demand and generator data outlined above, the commitment schedule for the 26-unit IEEE test system using the proposed model is shown in Figure 5.13. A CO_2 price of \$25/tCO_2 and the spinning reserve requirements are set the same as Lou *et al.* [2015] for benchmarking purposes. This implies that $R_t^{\text{up}} = 400$ MW for all time periods since the largest online generator is unit u400.

Figure 5.13a shows the unit commitment schedule when ramp rates are disabled. Figure 5.13b shows the unit commitment schedule for the same test system but now the ramp rates described in Table 5.11 are enforced. This forces the unit commitment algorithm to commit and part-load more units during hours 1-5 so that there is sufficient upwards ramping capability during the

Unit	Min up time $UT_{g,min}$ (h)	Min down time $DT_{g,min}$ (h)	Initial hours $X_{g,t}$ (h)	Max up ramp rate ρ_g^{up} (MW/h)	Max down ramp rate ρ_g^{dn} (MW/h)
u12	1	1	-1	48.0	60.0
u20	1	1	-1	30.5	70.0
u76	3	2	+3	38.5	80.0
u100	4	2	-3	51.0	74.0
u155	5	3	+5	55.0	78.0
u197	5	4	-4	55.0	99.0
u350	8	5	+10	70.0	120.0
u400	8	4	+10	50.5	100.0

Table 5.11: Min up/down time, initial status, and ramp rate data for the 26-unit IEEE RTS-96 test system from Wang and Shahidehpour [1993].

demand pick-up between hours 7-10.

The total system costs of the IEEE RTS-96 test system with infinite ramp rates is 1.4% lower than for the system with ramp rates enforced. Fuel costs in the system with infinite ramp rates are 3.5% lower. There is a clear saving from increased ramp rates as it reduces part-load efficiency losses and the number of part-load thermal units required to provide ramping services.

This analysis shows the value of improved ramp rates and highlights how ramp rates impact both dispatch schedules and system costs. Improved thermal plant ramp rates can reduce the amount the synchronised thermal units that are required to provide reserve and hence reduce system costs.

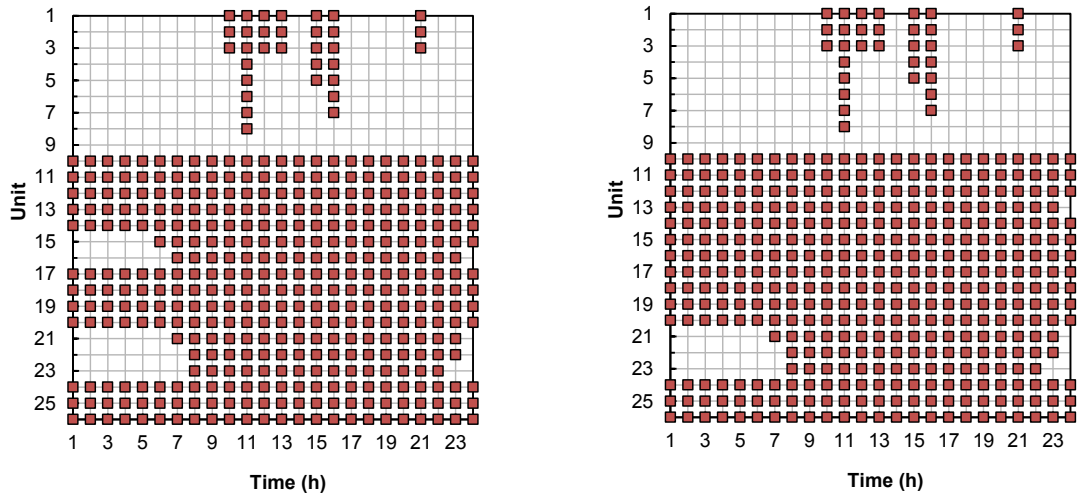

(a) No ramp rates

(b) Ramp rates enforced

Figure 5.13: Unit commitment schedule for the 26-unit IEEE RTS-96 test system.

Unit		Cost coefficient a ($/MW^{2}h)	Cost coefficient b ($/MWh)	Cost coefficient c ($/h)
u12	1	0.0253	25.5472	24.3891
	2	0.0265	25.6753	24.4110
	3	0.0280	25.8027	24.6382
	4	0.0284	25.9318	24.7605
	5	0.0286	26.0611	24.8882
u20	6	0.0120	37.5510	117.7551
	7	0.0126	37.6637	118.1083
	8	0.0136	37.7770	118.4576
	9	0.0143	37.8896	118.8206
u76	10	0.0088	13.3272	81.1364
	11	0.0090	13.3538	81.2980
	12	0.0091	13.3805	81.4641
	13	0.0093	13.4073	81.6259
u100	14	0.0062	18.0000	217.8952
	15	0.0061	18.1000	218.3350
	16	0.0060	18.2000	218.7752
u155	17	0.0046	10.6940	142.7348
	18	0.0047	10.7154	143.0288
	19	0.0048	10.7367	143.3179
	20	0.0049	10.7583	143.5972
u197	21	0.0026	23.0000	259.1310
	22	0.0026	23.1000	259.6490
	23	0.0026	23.2000	260.1760
u350	24	0.0015	10.8616	177.0575
u400	25	0.0019	7.4921	310.0021
	26	0.0020	7.5031	311.9120

Table 5.12: Generator quadratic cost data for the 26-unit IEEE RTS-96 test system from Wang and Shahidehpour [1993].

Parameters for unit type u100		
$P_{g,\min}$	Minimum power output (MW_e)	25.00
$P_{g,\max}$	Maximum power output (MW_e)	100.00
$P_{g,\min}^{\text{capt,op}}$	Minimum operating CO_2 capture plant power consumption (MW_e)	4.42
$P_{g,\max}^{\text{capt,op}}$	Maximum operating CO_2 capture plant power consumption (MW_e)	13.45
ρ_g^{up}	Ramp up rate (MW_e/h)	51.0
ρ_g^{dn}	Ramp down rate (MW_e/h)	74.0
$e_g^{CO_2}$	Emission factor (tCO_2/MWh_{th})	0.2629
$UT_{g,\min}$	Minimum up time (h)	4
$DT_{g,\min}$	Minimum down time (h)	2
$X_{g,t}$	Initial hours (h)	-3
$c_{g,t}^{\text{fuel}}$	Cost of fuel ($/MWh_{th})	7.84

Table 5.13: Unit type u100 parameters for IEEE RTS-96 test system.

Parameters for unit type u155		
$P_{g,\min}$	Minimum power output (MW_e)	54.25
$P_{g,\max}$	Maximum power output (MW_e)	155.00
$P_{g,\min}^{\text{capt,op}}$	Minimum operating CO_2 capture plant power consumption (MW_e)	11.50
$P_{g,\max}^{\text{capt,op}}$	Maximum operating CO_2 capture plant power consumption (MW_e)	28.89
ρ_g^{up}	Ramp up rate (MW_e/h)	55.0
ρ_g^{dn}	Ramp down rate (MW_e/h)	78.0
$e_g^{CO_2}$	Emission factor (tCO_2/MWh_{th})	0.3248
$UT_{g,\min}$	Minimum up time (h)	5
$DT_{g,\min}$	Minimum down time (h)	3
$X_{g,t}$	Initial hours (h)	+4
$c_{g,t}^{\text{fuel}}$	Cost of fuel ($/MWh_{th})	4.09

Table 5.14: Unit type u155 parameters for IEEE RTS-96 test system.

CO_2 capture

This work extends this case study to include flexible CO_2 capture power plants. It is intended to demonstrate how the unit commitment model dispatches thermal power plants to meet demand and reserve requirements with and without flexible CO_2 capture units.

It is assumed that units 14-20 (unit types u100 and u155) are now retrofitted with post-combustion CO_2 capture and compression systems. It is assumed that the efficiency, technical limitations, and cost characteristics of the base power plants remain unchanged. However, the power consumption of the CO_2 capture units reduce the net electrical efficiency of the CCS-equipped units. The technical parameters for unit types u100 and u155 are shown in Tables 5.13 and 5.14, respectively.

Data for the CO_2 capture plants are derived from Lou *et al.* [2015] and shown in Table 5.15. The fixed CO_2 capture plant power consumption $P_g^{\text{capt,fixed}}$ is 3 MW with a maximum CO_2 capture rate $Y_{g,\max}^{\text{capt}}$ of 85%. The power consumption required to capture 1 tonne of CO_2 is assumed to be 0.23 MWh_e/tCO_2. This decreases the maximum power output of units 14-16 (u100) from 100 MW to 83 MW and units 17-20 (u155) from 155 MW to 123 MW. The introduction of CO_2 capture equipment therefore decreases the net power output and minimum power output limits of the CCS-equipped units.

Additional CO_2 capture parameters are shown in Table 5.15. It includes typical values for variable O&M cost of the capture unit, cost of solvent and thermal degradation rate from Cohen [2012]; Cohen and Webber [2012].

CO_2 capture plant parameters		
c^{CO_2}	Cost of CO_2 ($/tCO$_2$)	25
$P_g^{\text{capt,fixed}}$	Fixed CO_2 capture plant power consumption (MW_e)	3
$Y_{g,\min}^{\text{capt}}$	Minimum CO_2 capture rate (-)	0
$Y_{g,\max}^{\text{capt}}$	Maximum CO_2 capture rate (-)	0.85
$q_g^{\text{capt,op}}$	Energy requirement to capture 1 tonne of CO_2 (MWh_e/tCO_2)	0.23
$c_g^{\text{O\&M,capt}}$	CO_2 capture plant variable operation and maintenance ($/tCO$_2$)	0.5
c^{solv}	Cost of MEA solvent ($/kg)	2.5
$c_{g,t}^{\text{trans}}$	CO_2 transport and storage ($/tCO$_2$)	0
D_g	Total solvent degradation rate (kg/tCO$_2$)	1.5
D_g^{th}	Solvent degradation rate caused by thermal effects (kg/tCO$_2$)	0.1

Table 5.15: CO_2 capture plant parameters for IEEE RTS-96 test system.

Figure 5.14 shows the dispatch schedules for the IEEE RTS-96 test system with and without CO_2 capture equipped power plants on unit types u100 and u155. The dispatch schedule shows how the model commits generators to supply demand and upwards spinning reserve.

For the conventional generation portfolio without capture in Figure 5.14a, units types u350 (coal/steam) and u400 (nuclear) run at full load over the time period since their short-run marginal costs are significantly less than other units. Unit types u155 (coal/steam) and u100 (oil/steam) part-load during hours 1-7 in order to meet demand and the upwards spinning reserve requirement.

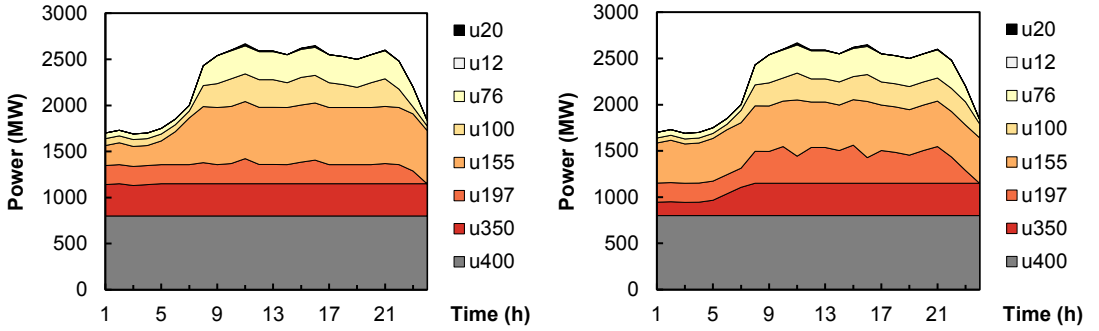

(a) Conventional IEEE RTS-96 test system

(b) IEEE RTS-96 test system with units 14-20 equipped with CCS (unit types u100 and u155)

Figure 5.14: IEEE RTS-96 test system generation dispatch pattern with and without CCS.

Figure 5.14b shows the same system but now unit types u100 and u155 are equipped with CCS. With a CO_2 price of \$25/tCO_2 and the assumed fuel costs, unit type u155 (now with CCS equipment) now has lower short-run marginal costs than u350, since unit type u155 can now capture 85% of the CO_2 emissions, reducing the CO_2 cost penalty. This causes unit type u350 (coal/steam) without CCS to part-load during hours 1-7. Unit type u100 (now with CCS) now also has lower short-run marginal costs as they are able to reduce the costs associated with CO_2.

Figure 5.15 shows how the unit commitment formulation schedules power output and upwards spinning reserve for units 14 and 17 (unit types u100 and u155) before and after flexible CCS equipment is applied. Figures 5.15a and 5.15c show units 14 and 17 without CCS equipment. At hour 8, unit 14 increases power output from 25 MW to 76 MW since its maximum upwards ramp rate is 51 MW/h. This also constrains the amount of upwards spinning reserve that unit 14 can provide within 1 hour. At hour 23, unit 14 ramps down from 100 MW to 26 MW since its maximum downwards ramp rate is 74 MW/h. However, it is only able to provide a maximum of 51 MW/h of upwards spinning reserve since its maximum upwards ramping capability is 51 MW/h. Similarly, unit 17 has a maximum upwards ramp rate of 55 MW/h, constraining the upwards ramping trajectory at hours 5-6 and the upwards spinning reserve contribution.

The minimum and maximum power output of unit 14 (u100) before CCS retrofit is between 25 MW and 100 MW. After the addition of CCS equipment and assuming an 85% CO_2 capture rate, the minimum and maximum power output of unit 14 (u100) is between 18 MW and 84 MW. CCS-equipped units can bypass their CO_2 capture power plants and vent CO_2 to the

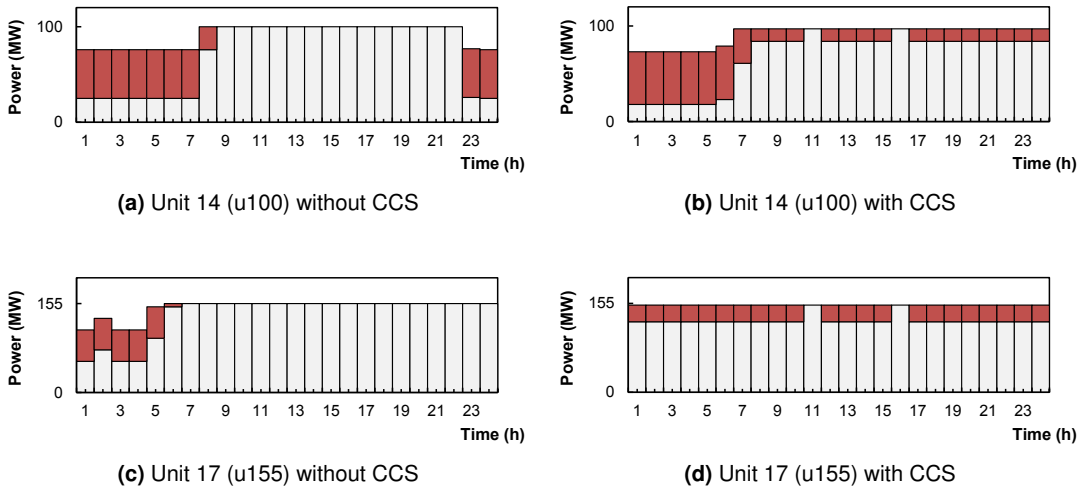

(a) Unit 14 (u100) without CCS

(b) Unit 14 (u100) with CCS

(c) Unit 17 (u155) without CCS

(d) Unit 17 (u155) with CCS

Figure 5.15: Scheduled power outputs (grey) and scheduled upwards spinning reserve (red) for units 14 and 17 (u100 and u155) with and without CCS.

atmosphere when it is economical to do so. This increases the maximum power output of unit 14 from 84 MW (at 85% capture) to 97 MW (zero capture). The maximum power output that can be exported is only 97 MW (not 100 MW) since the CO_2 capture units have a fixed power consumption of 3 MW. This slightly increases the amount of upwards spinning reserve that unit 14 can provide since CCS-equipped units are able to provide upwards spinning reserve equal to the operating power consumption of their capture units plus the normal ramping capability of the base power plant.

The minimum and maximum power output of unit 14 (u100) before CCS retrofit is between 54 MW and 155 MW. This changes to 41 MW and 123 MW with CO_2 capture. Unit 17 can also temporarily decrease the CO_2 capture rate to zero and increase power output to 152 MW.

Figures 5.15b and 5.15d show how the model schedules power and upwards spinning reserve with CCS. At hours 11 and 16, all CCS-equipped capture units bypass their capture systems and reduce their CO_2 capture rates to zero. This is because at hours 11 and 16 electricity prices and demand are high and also peaking units (u12 and u20) are dispatched.

Overall, the total system costs with CCS-equipped power plants for the 24 hour period is \$1.44 million. This compares to the total system costs of \$1.65 million for the conventional system with CO_2 capture. This is a 14.6% reduction in total system costs which is mainly achieved by a reduction in CO_2 costs, in which the price of CO_2 is assumed to be \$25/tCO_2.

This CO_2 capture plant model is able to dispatch CCS-equipped units to provide both energy and reserve requirements for different operating modes of flexible CO_2 capture. The UCED formulation is applicable to any generation portfolio and input data allows any post-combustion capture technology to be characterised for constrained or unconstrained operation. This will

allow later work to provide greater insights into the potential operating regimes of CO_2 capture power plants.

Flexibility

It is possible to quantify the flexibility of individual units within the 26-unit test system using the upwards $\text{flex}_g^{\text{up}}$ and downwards $\text{flex}_g^{\text{dn}}$ flexibility indices:

$$\text{flex}_g^{\text{up}} = \frac{\frac{1}{2}(P_{g,\max} - P_{g,\min}) + \frac{1}{2}(\rho_g^{\text{up}} \cdot \Delta t)}{P_{g,\max}} \tag{5.94}$$

$$\text{flex}_g^{\text{dn}} = \frac{\frac{1}{2}(P_{g,\max} - P_{g,\min}) + \frac{1}{2}(\rho_g^{\text{dn}} \cdot \Delta t)}{P_{g,\max}} \tag{5.95}$$

The flexibility indices for each of the conventional units without CCS are shown in Table 5.16 and Figure 5.16. Units with the highest upwards and downwards flexibility indices have a larger operating range and faster ramp rates. All of the units in the case study have faster downwards ramp rates and so the downwards flexibility indices are all higher.

Unit	Max output $P_{g,max}$ (MW)	Min output $P_{g,min}$ (MW)	Max up ramp rate ρ_g^{up} (MW/h)	Max down ramp rate ρ_g^{dn} (MW/h)	Upwards flex index $flex_g^{up}$ (-)	Downwards flex index $flex_g^{dn}$ (-)
u12	12.00	2.40	48.0	60.0	2.40	2.90
u20	20.00	4.00	30.5	70.0	1.16	2.15
u76	76.00	15.20	38.5	80.0	0.65	0.93
u100*	100.00	25.00	51.0	74.0	*0.69-0.63	0.75
u155*	155.00	54.25	55.0	78.0	*0.56-0.50	0.58
u197	197.00	69.00	55.0	99.0	0.46	0.58
u350	350.00	140.00	70.0	120.0	0.40	0.47
u400	400.00	100.00	50.5	100.0	0.44	0.50
26-units	3105.00	927.80			*0.56-0.55	0.68

*Includes flexibility provision from CO_2 capture plant

Table 5.16: Power output, ramp rates, and upwards/downwards flexibility indices for the 26-unit IEEE RTS-96 test system from Wang and Shahidehpour [1993].

After the addition of CCS to unit types u100 and u155, the upwards flexibility indices also increase. This is because now CCS-equipped units can both potentially increase the power output from the base power plant and decrease the power consumption of the capture plant. For unit type u100 the upwards flexibility index increases from 0.63 to 0.69 and for unit type u155 from 0.50 to 0.56. This slightly increases the overall system upwards flexibility index $\text{FLEX}_g^{\text{up}}$ from 0.55 to 0.56.

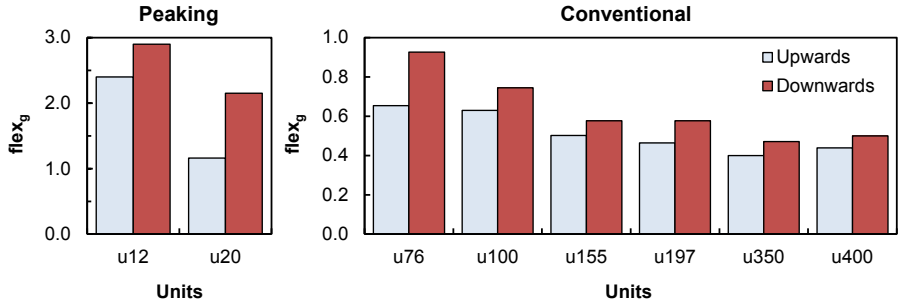

Figure 5.16: Upwards and downwards flexibility indices for the 26-unit IEEE RTS-96 test system.

5.11.4 Summary

This section showed how ramp rates constrained the operation of power plants using the IEEE RTS-96 test system. When ramp rates are assumed to be infinite, the total system costs reduced by 1.4% compared to the same system where ramp rates are enforced. The results demonstrated the clear savings that can be made by increasing ramp rates as they reduce part-load efficiency losses and the number of part-load thermal units that are required to provide ramping services.

The results also demonstrated how flexible CCS can significantly reduce total system costs by reducing the amount CO_2 that is emitted to the atmosphere. In comparison to the conventional IEEE RTS-96 system, the addition of flexible CO_2 capture and storage reduced total system costs by 14.6% with a CO_2 price of \$25/tCO_2.

The implementation of flexible CO_2 capture and storage into a unit commitment model represents a contribution to the literature. The results showed that the UCED formulation is able to dispatch thermal units with and without CO_2 capture to meet demand and reserve requirements, abiding by ramp rate and other unit-specific constraints. Flexible CO_2 capture plants are shown to be capable of providing additional levels of upwards reserve since they are able to bypass their CO_2 capture units.

5.12 Summary

This chapter introduced a UCED model with CCS and energy storage. Section 5.2 outlined the UCED model formulation and objective function. Details about how the model manages large volumes of wind generation are discussed in Section 5.4. A simple electricity pricing model was then introduced that produces an electricity price time-series that is used to optimise the operation of energy storage and flexible CO_2 capture units. The system and unit operating constraints were then outlined in Sections 5.6 and 5.7.

Section 5.8 introduced an energy storage optimisation model intended to be used in-combination with the UCED model. The underlying model assumptions were presented followed by a

detailed formulation of the model. The model uses an electricity price time-series to optimise the operating profits of energy storage units.

Section 5.9 introduced a detailed formulation of the UCED model with CCS-equipped power plants and the unit-specific operating constraints of flexible CCS units. Additional parameters were included to characterise the flexible operation of CO_2 capture units and account for the costs of CO_2 capture, compression, and transportation costs and costs associated with solvent make-up costs and additional variable O&M costs.

Section 5.11 validated the UCED formulation with flexible CCS using the IEEE RTS-96 test system. The results demonstrated the ability of the model to dispatch thermal units to meet demand and spinning reserve requirements. Then, a number of conventional units were retrofitted with flexible CO_2 capture. The results demonstrated how flexible CO_2 capture units provide additional upwards spinning reserve and reduce the minimum power output limits of generators.

The next chapter provides results for a test system of GB across a range of wind capacity scenarios.

Chapter 6

Impacts of variable-output wind

6.1 Introduction

Previous chapters introduced a unit commitment and economic dispatch (UCED) model to analyse power plant operating regimes. The proposed model includes CO_2 capture equipped power plants and energy storage units in systems with large amounts of wind power.

This chapter highlights the importance of including flexibility characteristics in power system models with large amounts of wind. It considers the contributions from energy storage and flexible CO_2 capture power plants to system flexibility and reserve requirements. In particular, the UCED formulation is used to study the impacts on thermal power plant operating regimes, which are evaluated using a number of metrics. The analysis and the UCED model represent a contribution to the literature.

The metrics used in this chapter for analysing the impacts on power plant operation include:

- load factor;
- total GW ramped;
- number, frequency and duration of large upwards/downwards ramps;
- time spent ramping;
- time spent at part-load;
- time spent at max/min power output limits;
- time spent online/offline; and
- number of hot/warm/cold start-ups.

Each of these factors is used to demonstrate how flexibility characteristics of thermal power plants have an important impact on system costs and CO_2 emissions. A comparison is made to highlight the relative impacts of the different flexibility characteristics including:

- part-load efficiencies;
- up/down ramp rates;
- minimum up/down times; and
- start-up/shut-down costs.

Details of the test system are now outlined.

6.2 GB test system

6.2.1 Introduction

To demonstrate the proposed UCED model and the impacts of energy storage and flexible CCS, a test system is developed for GB to examine the performance and outputs of the model. The system is developed to be broadly similar with the expected GB electricity system in 2030, in particular, the Gone Green scenarios for 2030/31 in National Grid [2015c].

The base case scenario does not represent a central projection or an expected scenario in the future. Rather, it is intended to provide a starting point to explore the GB power system with varying levels of wind capacity and flexibility characteristics. The base case scenario is internally consistent with common input parameters assumed across all scenarios unless explicitly stated otherwise.

To simplify the problem the following assumptions have been made:

- non-dispatchable combined heat and power (CHP) units are not modelled;
- miscellaneous other renewable generation technologies are not modelled;
- solar capacity is not modelled;
- transmission constraints and interconnectors are excluded; and
- plant outages are not modelled but reserve is scheduled to cover outages.

This work assumes a simplified generation portfolio of thermal power plants and energy storage units and performs a sensitivity analysis on key variables. This analysis assumes a single-bus transmission network and so does not consider transmission constraints. This is to enable focus on the impacts on generation flexibility requirements of the thermal generation portfolio. Although, it is acknowledged that transmission constraints are an important aspect in power system operation. Solar capacity is also excluded in order to isolate the impacts of variable-output wind power on the power system. Although, it is acknowledged that the impacts of solar PV on the generation requirements is an important area of ongoing research. Also, the effects of emerging electricity-intensive technologies on the electricity demand profile, such as electric vehicles, are not considered and are left for future research.

The UCED model does not consider non-generation costs so power plants that are not utilised do not contribute towards the total system operating cost. This short-term operational analysis does therefore not consider fixed capital or investment costs, such as infrastructure or engineering, procurement and construction (EPC) costs. However, scenarios are compared afterwards using annualised capital costs that are estimated using industry and government data sources, which are then used to estimate the total operating and fixed costs for the scenarios considered.

The base case generation portfolio is designed to meet peak demand and reserve requirements for all wind capacity scenarios. Reserve is scheduled to cover credible plant outages and uncertainty in demand and wind forecasts. This analysis allows the operational costs and CO_2

emissions to be compared on an internally consistent basis, allowing useful comparisons to be made across multiple scenarios. The operating regimes of thermal units are compared to assess the relative impacts of varying ramp rates, start-up/shut-down costs and other flexibility characteristics. The data sources and input data of the UCED model are now outlined.

6.2.2 Input data assumptions

The underlying methodology of this work is to use representative system data and thermal power plant data to examine the potential operating regimes and characteristics of thermal units in an assumed power system.

For leap years 2004 and 2008, the last 24 hours of each time-series are not used. This is to ensure that the time length of each year is 8760 h and not 8784 h for leap years. In other words, only the first 365 days are used in the analysis.

Various cost assumptions and technical data for thermal generation technologies are derived from Parsons Brinkerhoff [2013a], which contains a detailed and comprehensive assessment of GB generation technology costs. The work was commissioned by the Department of Energy and Climate Change (DECC) and so is thought to be a reasonable indicator of future cost estimates for generation technologies in GB. A vast array of data from recent UK and international reference power plants was considered which used both internal confidential information and opinions from experts to produce the technical and cost assumptions.

Details of the assumed thermal plant portfolio and the technical and cost characteristics are now given.

Generation portfolio

The base case scenario is intended to represent a future generation portfolio of low flexibility. This means that the generation portfolio of thermal units is designed with limited flexibility characteristics such as low ramp rates, high start-up/shut-down costs, and long minimum up/down times. The base case scenario is then compared with scenarios that feature more flexible characteristics, which are then analysed using a number of metrics.

The technical parameters of thermal units are not intended to model exact power plants. Rather, they are intended to represent characteristics that provide a realistic representation of the future GB generation technologies. An overview of the base case thermal generation portfolio is shown in Table 6.1.

The generation technologies that are considered in the analysis are briefly described below. A detailed list of technical parameters for each of the generation technologies are available in Appendix D.

Generation Technology (h)	No.	Unit (g)	Efficiency $\eta_{g,t}$ (-)	Max output $P_{g,max}$ (MW)	Total output $\sum P_{g,max}$ (MW)
Nuclear	8	1-8		1650	13200
CCGT+PCC*	4	9-12	0.58 - 0.52*	875 - 795*	3500 - 3180*
CCGT 1-10	10	13-22	0.60 - 0.58	900	9000
CCGT 11-20	10	23-32	0.57 - 0.55	900	9000
CCGT 21-30	10	33-42	0.53 - 0.51	900	9000
CCGT 31-40	10	43-52	0.50 - 0.48	900	9000
OCGT	40	53-92	0.40 - 0.35	565	22600
	92				74980-75300

*Indicates reduced output/efficiency from CCS systems

Table 6.1: Power output, indicative efficiency and generation technology data for GB test system.

Fuel consumption

The quadratic fuel consumption characteristics of thermal units are represented using a piece-wise linear approximation with three segments, Equation 5.14. The linear intercepts and gradients that define the part-load efficiencies of thermal units are provided in Appendix D.

The fuel consumption characteristics and part-load efficiency curves of typical GB thermal units (CCGT and coal) are derived from data provided by a large UK energy company involved in both generation and transmission. These sources are used to define representative functions that define the fuel consumption characteristics of units. Kehlhofer *et al.* [1999] also publishes part-load efficiency data for typical CCGT units. These are used to derive the fuel consumption characteristics of thermal units, see Figure 5.3.

CCGT units 1-20 are intended to represent newer and more efficient F-class CCGTs. Units 21-40 are intended to represent older and less efficient E-class CCGTs. As a result the full and part-load efficiencies of each of the CCGTs are different. This is designed to reflect the possible range in CCGT unit operating efficiencies from best-in-class to mid-range and older units. In other words, thermal units of the same technology are modelled with varying efficiencies and costs to represent units of different ages and part-load efficiencies.

Ramp rates and minimum up/down times

The ramp rates of thermal units that are operating above their minimum power outputs are limited by a number of technical factors. It should be noted that this work assumes that the ramp rates of units are constant when online and operating above their minimum load. This preserves model linearity and therefore decreases computational time. Implementing dynamic ramp rate constraints would likely have impacts on the results but is considered beyond the scope of this work. Ramp rates are tested as a sensitivity to understand the impacts of thermal

plant ramp rates on the metrics listed above. The assumed ramp rates by generation technology for the base case scenario are shown in Table 6.2.

Type	No.	Unit g (-)	Min up time $UT_{g,min}$ (h)	Min down time $DT_{g,min}$ (h)	Initial hours $X_{g,t}$ (h)	Max up ramp rate ρ_g^{up} (MW/h)	Max down ramp rate ρ_g^{dn} (MW/h)
Nuclear	8	1-8	24	24	+8	4950	4950
CCGT+PCC	4	9-12	4	4	+8	300	300
CCGT	40	13-52	4	4	+8	300	300
OCGT	40	53-92	1	1	-24	600	600

Table 6.2: Min up/down time, initial status, and ramp rate data for the 92-unit GB base case scenario.

Nuclear units

Nuclear units are based on the European Pressurised Reactor (EPR) design. It is assumed that these units are capable of light load following cycles between 60% and 100% of rated capacity, ramping at a maximum of 5% of rated capacity per minute [NEA, 2011]. This work also assumes that there are no fuel cycle limitations that prohibit load following duties. Most nuclear units in GB are Advanced Gas-cooled Reactors (AGR) and so provide little or no flexibility services [Pouret and Nuttall, 2007]. The majority of AGRs in the UK are due to be decommissioned in the near future and it is expected that a number of these reactors will be replaced by modern EPRs [National Grid, 2013].

CCGT units

Currently, CCGTs have high efficiencies and provide a mix of baseload and intermediate generation in GB depending on natural gas prices and their relative position in the merit-order.

The typical upwards and downwards ramp rates of CCGTs are around 10 MW/minute with newer units capable of even faster ramp rates [IEA, 2011]. However, for the base case this analysis assumes that CCGT units have upwards and downwards ramp rates of 300 MW/h. For a 900 MW CCGT unit this corresponds to a ramp rate of 5 MW/minute or 0.55% rated capacity per minute. The ramp rates assumed in the base case are later compared with scenarios with faster ramp rates.

The fuel consumption during a cold start-up for a CCGT unit is assumed to be 1500 MWh_{th} [KEMA, 2008; Kumar *et al.*, 2012]. This quantity of start-up fuel is equivalent to operating at full load for approximately 1 hour.

OCGT units

OCGT units are assumed to have upwards and downwards ramp rates of 600 MW/h or 10 MW/minute [IEA, 2011]. An OCGT unit requires 375 MWh_{th} of fuel during a cold start-up which is equivalent to operating at full load for approximately 0.25 h [Kumar *et al.*, 2012].

CCS-equipped units

For the base case scenario, it is assumed that four 900 MW CCGT units are retrofitted with inflexible post-combustion CO_2 capture (PCC). It is assumed that the CO_2 capture rate $Y_{g,\max}^{\text{capt}}$ is constant at 90% [Parsons Brinkerhoff, 2013a]. Table D.5 shows the PCC plant parameters for the base case scenario. The fixed power consumption $P_g^{\text{capt,fixed}}$ of the PCC units is 25 MW. This represents the fixed efficiency reductions and ancillary requirements of the CO_2 capture plant after retrofit. The power consumption required to capture 1 tonne of CO_2 is assumed to be 0.27 MWh_e/tCO_2. This reduces the net power output of the CCS-equipped power plant at full load from 900 MW to 795 MW.

Solvent costs, degradation rates and transport and storage costs are taken from Cohen [2012] and Parsons Brinkerhoff [2013a]. The CO_2 transport and storage costs are based on the assumption that CO_2 is stored offshore in a depleted oil or gas field that utilises some existing infrastructure [Parsons Brinkerhoff, 2013a].

Energy storage units

Energy storage units are not considered in the base case scenario. They are considered separately in order to understand their specific impacts on system operation and costs. Details of the energy storage unit parameters are provided in Table 6.3. The four units are chosen to represent the existing pumped storage capacity in GB. The time-dependent energy losses for pumped storage units are near-zero so they are not considered. In addition, the start-up and shut-down times and the time taken to adjust the charging and discharging rates of energy storage units are assumed to be negligible. The operating costs for energy storage units is typically near-zero and so are not considered in this work. The costs associated with storing energy are dependent on the system electricity price at the time the energy is purchased.

Electricity demand

Demand and wind data between 2002 and 2010 is used in this work as a basis for understanding likely operating regimes of thermal power plants. However, it is likely that in the future demand profiles will change and demand-side flexibility services will increase. This will therefore have implications on the future operating regimes of thermal units and should be studied in future work.

Name	Units (-)	Max charge/ discharge power $P^{c}_{s,max} = P^{d}_{s,max}$ (GW)	Max energy stored $E_{s,max}$ (GWh)	Duration (h)	Round-trip efficiency (%)
Dinorwig	1	1.80	9.1	5.1	80
Foyers	2	0.30	6.3	21.0	80
Cruachan	3	0.40	10.0	25.0	80
Ffestiniog	4	0.36	1.3	3.6	80
Total		2.86	26.7		

Table 6.3: Energy storage device parameters for GB test system.

Historic electricity demand data for GB is taken from National Grid [2015b] and weather-corrected. Electricity demand data is then temporally matched with the derived wind data described in Chapter 4. Since this work utilises wind speed data at hourly resolution, it is not possible to generate higher resolution data without producing interpolation errors, and so hourly demand data is used. Future work should utilise higher resolution data for sub-hourly UCED analysis to improve understanding of short-term operational impacts.

The maximum peak demand for the system is 62.1 GW with a total installed thermal plant capacity of 75.3 GW (excluding wind capacity). Annual electricity demand is approximately 337 TWh but varies between years.

Figure 6.1 shows graphically the installed capacity of each generation technology in the base case scenario and the maximum peak demand level. For a peak demand value of 62.1 GW the capacity margin is 20.7% (excluding wind capacity). Although a capacity margin of 20.7% is historically very high, power plants need to meet both demand and reserve requirements, which will require a number of power plants to part-load. It is a generation portfolio that can meet peak demand and upwards reserve requirements across every wind scenario and assumes that all power plants are available during peak demand periods.

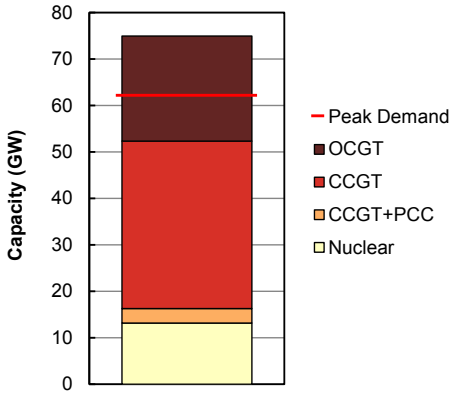

Figure 6.1: Installed capacity of base case thermal generation portfolio.

Fuel prices

Fuel cost data is obtained from the Department of Energy and Climate Change (DECC) central fuel cost projections in DECC [2014b] and converted into £/MWh$_{th}$. Equivalent CO_2 emissions intensities for fuels used in GB electricity generation are obtained from DECC [2012b]. The sensitivity to fuel prices is important if the generation portfolio contains power plants of different fuel types. However, as in the Gone Green scenarios for 2030/31 in National Grid [2015c], this work assumes that all fossil fueled power plants without CCS are gas-fired. Therefore, changes in fuel prices are unlikely to significantly impact the operating regimes of power plants.

CO_2 prices

CO_2 prices are assumed to be £30/tCO_2 for the base case scenario. This is designed to reflect the anticipated carbon floor price of £30/tCO_2 in 2020 [House of Commons, 2014]. However, it has been reported recently that the carbon floor price would be capped at £18/tCO_2 between 2016 to 2020. In order to address CO_2 price uncertainty, the CO_2 price is investigated as a sensitivity.

Reserve requirements

The reserve requirement represents the system's ability to adjust generation output to cover unexpected changes in generation and demand-wind uncertainty within 3.5 standard deviations or 99.95% of events. A reliability standard for security of supply of 3 hours per year, using the Loss of Load Expectation (LOLE) risk metric is assumed [National Grid, 2014a]. This corresponds to a standard deviation of approximately 3.5σ. Reserve must therefore cover any unexpected changes in demand-wind forecast uncertainty within 3.5 standard deviations or 99.95% of events.

Uncertainty in electricity demand is modelled as a normally distributed function with zero-mean with a standard deviation of 1% of current demand [Gross and Galiana, 1987; Bunn, 2000; Silva, 2010]. Uncertainty in wind power is modelled as a normally distributed function with zero-mean with a standard deviation of 10% of forecast wind output 4 hours ahead of real-time, as discussed in Chapter 2. Upwards reserve is also required to cover the largest credible loss in generation, which is expected to be 1800 MW [National Grid, 2011a].

For security reasons, the power system must ensure there is sufficient synchronised thermal generation capacity to meet operating reserve requirements [National Grid, 2011a]. When the minimum output of inflexible thermal power plants and units providing reserve plus the available wind generation exceeds electricity demand then it is necessary to curtail wind output. In the base case scenario, the minimum load level is assumed to be 15000 MW. This is thought to be a reasonable approximation of the minimum load level required to meet the technical

requirements of operating reserve and to limit the rate of change of frequency after a large generation outage [National Grid, 2011a, 2013].

6.3 System impacts

6.3.1 Introduction

To understand the impacts of increasing wind capacity and inter-annual variations in wind output a large number of simulations are performed using the base case generation portfolio.

Using 2010 wind speed and demand data, the UCED model is run for 8760 h for each of the wind capacity scenarios (10 GW, 15 GW, 20 GW, 25 GW, 30 GW, 35 GW, 40 GW, and 45 GW). This is to assess the system impacts of increasing wind capacity on an internally consistent basis i.e. the same electricity demand and wind profiles are used across all scenarios. It is only the spatial distribution of wind turbines and installed wind capacity that changes between these scenarios. The installed wind capacity represents the combined totals of installed onshore and offshore wind capacity, with increasing proportions of offshore wind to represent the growth of the offshore wind fleet in the later scenarios. The year 2010 is selected as it observed the lowest average wind speeds and therefore represents the year with the least contribution from wind and the highest contribution from thermal generation. This results in an enormous amount of output data (122.5 million data points).

Then, using demand and wind data for each year (2002, 2003, 2004, 2005, 2006, 2007, 2008, 2009, and 2010) the UCED model is ran for the 30 GW wind capacity scenario. This produces a further 137.8 million data points. Already this is a large amount of data but it only includes the outputs for the base case generation portfolio. Further simulations are performed later to understand the impacts of key flexibility parameters on operating regimes and system outputs.

For simplicity, the scenarios are referred to by the year that the demand and wind data are taken from, for example the 2002 scenario or 2010 scenario.

Outputs are produced for each unit at each time period and include: generation levels, unit status, upwards/downwards reserve contributions, fuel consumption, CO_2 emitted and CO_2 captured during normal operation, CO_2 emitted and CO_2 captured during start-up/shut-down, time spent shut-down, fuel costs, CO_2 costs, ramping costs, variable O&M costs, etc. In addition, are a number of system related outputs that include demand, net demand, onshore and offshore wind output, wind curtailment, electricity price, upwards/downwards system reserve, upwards/downwards spinning reserve, total fuel consumption, total CO_2 emissions, total CO_2 captured, total system costs, total variable operating costs, total start-up/shut-down costs, total ramping costs, total wind curtailment costs, total fuel costs, total CO_2 costs, total variable O&M costs, etc.

The outputs are generated in a number of spreadsheets which are then analysed to assess operating regimes and system impacts. The results for the base case scenario are now presented.

6.3.2 Wind generation

During periods of high wind output and low net demand, wind curtailment is likely to occur, see Section 5.4. Wind curtailment either occurs because net demand falls below the minimum load level of the system, reserve requirements are not met, or their is insufficient ramping capability provided by committed generators to meet net demand variations. A minimum load level is required to ensure that the power system has sufficient inertia to limit the rate of change of frequency after a large generation outage. Increased levels of wind generation during periods of low net demand is therefore the most likely source of wind curtailment.

Impacts of increasing wind capacity

Figure 6.2 shows the contributions from onshore and offshore wind generation and the amount of wind curtailment for each wind capacity scenario. Wind curtailment increases significantly with installed wind capacities greater than 25 GW which contributes significantly to total system costs, see Table 6.4. It should be noted that 2010 experienced historically low wind speeds and so it is expected that more wind curtailment will occur in the other wind years.

The amount of onshore wind generation peaks in the 30 GW wind capacity scenario. Although the installed capacity of onshore wind increases slightly in the 35 GW, 40 GW, and 45 GW wind capacity scenarios, the amount of onshore wind generation that is realised in these scenarios actually falls because onshore wind is increasingly curtailed to maintain security constraints. The proportions of onshore and offshore wind capacity in each of the scenarios are shown in Table 4.2.

The factors that affect wind curtailment are predominately the minimum load level, which is required to ensure that must-run plants remain operational, system inertia and downwards reserve. Wind is curtailed to ensure that these system requirements are maintained as described in Chapter 5.

Onshore wind is curtailed before offshore wind since it is assumed that in the GB market wind farms are subsidised per MWh of wind generation. This means that the opportunity costs of onshore and offshore wind is negative. For onshore wind, it is assumed that the price paid to curtail output is £50/MWh and offshore is £100/MWh. This is designed to reflect the existing priority of dispatch and anticipated renewable support scheme for wind in GB.

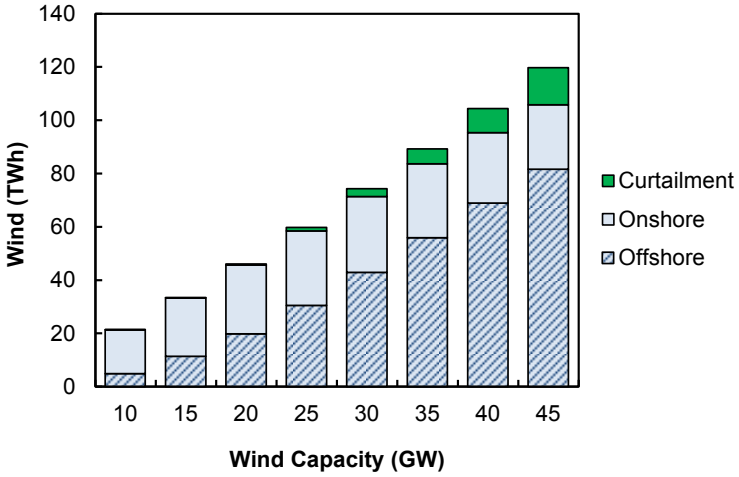

Figure 6.2: Realised onshore and offshore wind output and curtailment for base case generation portfolio with wind capacity between 10 GW and 45 GW using demand and wind data for 2010.

Wind Capacity (GW)	Onshore Wind (TWh)	Offshore Wind (TWh)	Total Wind (TWh)	Curtailment (TWh)	Curtailment (% of total)
10	16.4	4.9	21.4	0.0	0.0
15	22.0	11.4	33.3	0.1	0.3
20	25.8	19.8	45.7	0.4	0.9
25	28.0	30.5	58.5	1.3	2.2
30	28.5	42.8	71.3	3.0	4.0
35	27.8	55.9	83.7	5.5	6.2
40	26.4	68.9	95.3	9.1	8.7
45	24.2	81.6	105.8	14.0	11.7

Table 6.4: Realised onshore and offshore wind generation and curtailment for GB base case scenario using demand and wind data for 2010.

Impacts of inter-annual wind variations

Using wind and demand data for years 2002, 2003, 2004, 2005, 2006, 2007, 2008, 2009 and 2010, Figure 6.3 shows the contributions from onshore and offshore wind generation and the amount of wind curtailment with 30 GW of installed wind capacity. Table 6.5 shows the values for realised onshore and offshore wind generation and curtailment and the costs associated with curtailment (expressed as a percentage of total system costs) for each of the annual scenarios. The average nine year level of curtailment with 30 GW of wind capacity is 3.0 TWh. However, this varies between a minimum of 1.7 TWh and a maximum of 4.7 TWh. This large variation is caused by the underlying patterns in electricity demand and wind output, with large levels of curtailment occurring when low net demand coincides with high wind output.

There is also a large inter-annual variation in the total wind output over the nine year period. For the 2008 annual scenario with 30 GW of wind capacity, the total annual wind generation

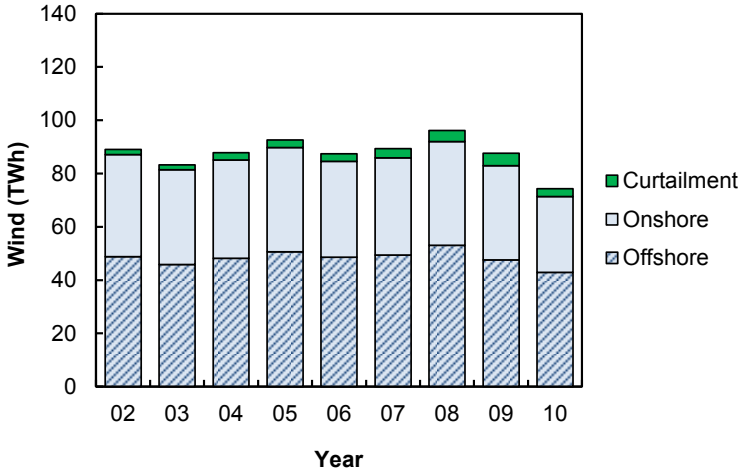

Figure 6.3: Wind output and curtailment for base case generation portfolio with 30 GW of wind capacity using demand and wind data between 2002 and 2010.

is 92.0 TWh. This compares to just 71.3 TWh in the 2010 annual scenario. The range and standard deviation in inter-annual wind output for the 30 GW wind portfolio are 20.7 TWh and 5.6 TWh, respectively. There is a weak negative correlation between net demand and wind curtailment.

Annual Scenario	Onshore Wind (TWh)	Offshore Wind (TWh)	Total Wind (TWh)	Curtailment (TWh)	Curtailment (% of total)
2002	38.3	48.7	87.1	1.9	2.2
2003	35.6	45.9	81.5	1.7	2.1
2004	36.9	48.2	85.1	2.7	3.1
2005	39.1	50.7	89.8	2.8	3.1
2006	36.0	48.6	84.6	2.8	3.2
2007	36.4	49.4	85.8	3.5	4.0
2008	38.9	53.1	92.0	4.1	4.3
2009	35.3	47.6	82.9	4.7	5.4
2010	28.5	42.8	71.3	3.0	4.1
Average	36.1	48.3	84.5	3.0	3.5

Table 6.5: Wind generation and curtailment for GB base case scenario with 30 GW of wind capacity using demand and wind data between 2002 and 2010.

6.3.3 Total system short-run costs

Impacts of increasing wind capacity

The total system short-run costs include variable operating costs (fuel costs, CO_2 costs, ramping costs, variable O&M costs, and variable CO_2 capture related costs), start-up costs, shut-down costs and wind curtailment costs. Figure 6.4a shows the total system costs for each wind scenario using wind and demand data for the year 2010. The variable O&M costs and variable CO_2 capture related costs are labelled as 'other' costs.

With increasing wind capacity the total system costs fall from £13.6 billion with 10 GW of wind capacity to £10.0 billion with 45 GW of wind. Dividing the total system costs for each scenario by the total energy demand (337.2 TWh) gives £40.5/MWh with 10 GW of wind capacity and £29.5/MWh with 45 GW of wind capacity. The total system costs decrease by 27.0% in the 45 GW wind capacity scenario as compared to the 10 GW scenario. However, the fall in total system costs with increasing wind capacity is not linear.

The natural gas price for the base case generation portfolio is 70 p/therm or £23.9/MWh. This is taken from the central fossil fuel price projections in DECC [2014b] and means that fuel costs make up the majority of total system costs across all of the wind scenarios. In comparison, the average natural gas price in 2015 was approximately 40 p/therm.

If we exclude fuel costs, the total non-fuel costs are £3.2 billion with 10 GW of wind capacity and £2.7 billion in the 30 GW and 35 GW scenarios. Adding more wind capacity increases the total non-fuel costs to £3.1 billion in the 45 GW scenario, see Figure 6.4b. In the 45 GW scenario, wind curtailment costs account for 9.2% of total system costs but in the 30 GW and 35 GW wind scenarios wind curtailment costs account for only 1.4% and 3.0% of total system costs. It is the large rise in wind curtailment costs that causes the total non-fuel costs to fall and then increase again with increasing wind capacity.

The majority of the cost savings that occur with increasing wind are due to a reduction in fuel and CO_2 emissions which in turn reduce the total fuel and CO_2 costs. However, this effect is reduced with increasing curtailment costs that are paid to wind generators to reduce output when there is a generation surplus.

Figure 6.5 shows the contribution from each generation technology to total system short-run costs for the 15 GW, 30 GW and 45 GW wind capacity scenarios using 2010 wind and demand data for the base case scenario.

The figures show how increasing wind capacity changes how thermal generation technologies contribute towards total system short-run costs in Figure 6.4a. Increasing wind capacity reduces the relative contribution of OCGT units to start-up/shut-down costs since they are increasingly displaced by wind generation. Conversely, the relative contribution of CCGT units 1-10 to start-up/shut-down costs increases with increasing wind capacity. It should be noted that start-

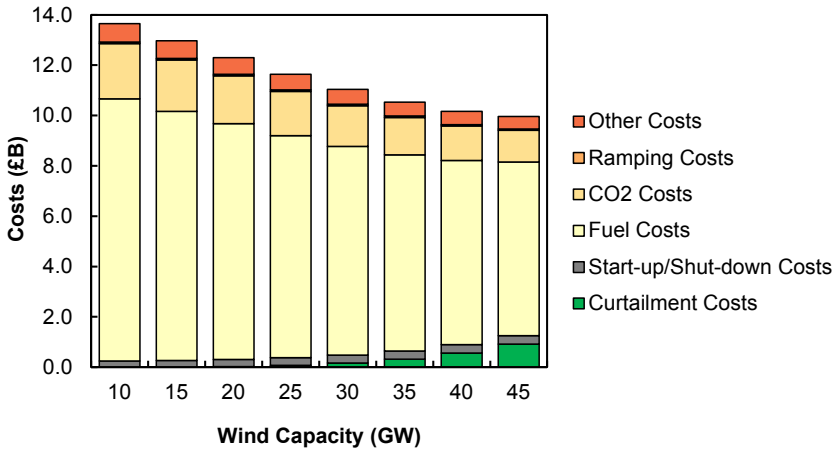

(a) Total system short-run costs

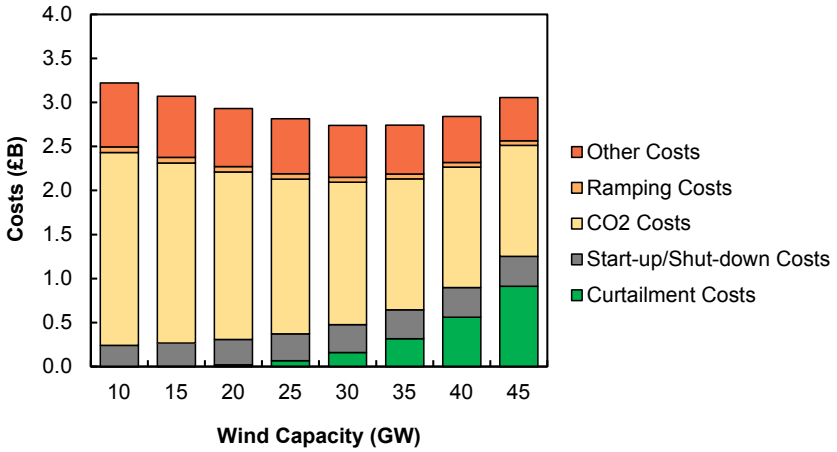

(b) Total system short-run non-fuel costs

Figure 6.4: Total system short-run costs for base case generation portfolio with wind capacity between 10 GW and 45 GW using demand and wind data for 2010.

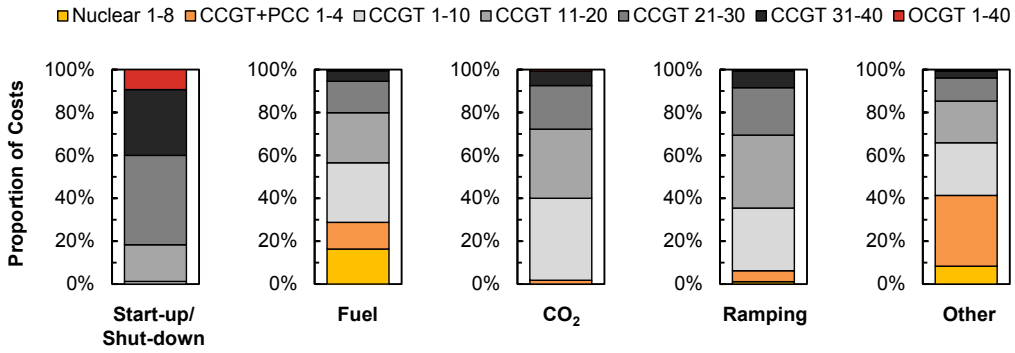

(a) 15 GW wind capacity

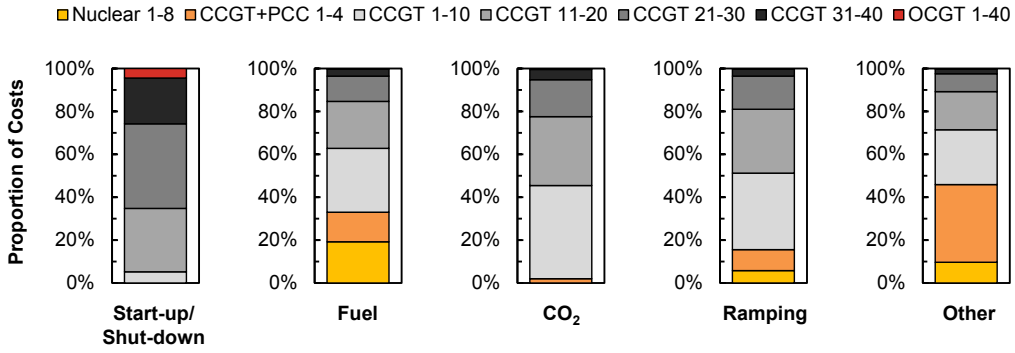

(b) 30 GW wind capacity

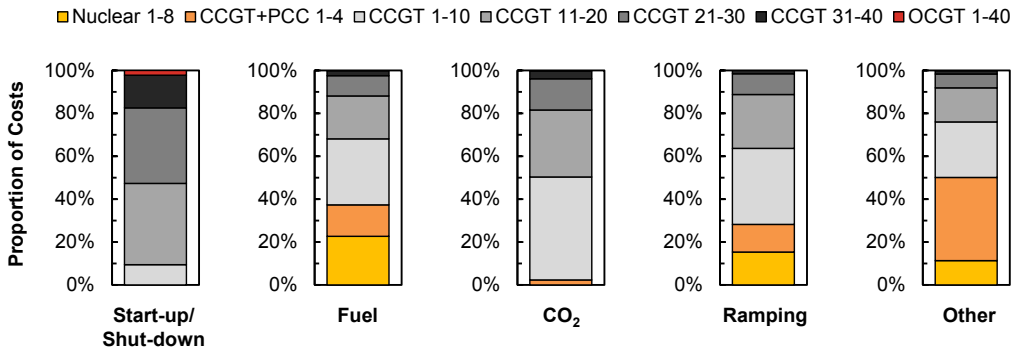

(c) 45 GW wind capacity

Figure 6.5: Contribution of generation technologies to system short-run costs for base case generation portfolio with 15 GW, 30 GW and 45 GW of wind capacity using demand and wind data for 2010.

up/shut-down costs include fixed costs, fuel costs, and CO_2 costs during start-up and shut-down. The fuel and CO_2 costs during start-up and shut-down are considered separately from the fuel and CO_2 costs during normal operation.

Increasing wind capacity also increases the relative contributions of nuclear and CCGT+PCC units to ramping costs as they are increasingly required to provide ramping services. CCGT+PCC units contribute towards the majority of the variable 'other' costs because CO_2 capture units have additional variable O&M costs, solvent costs, solvent degradation costs, and transport and storage costs, as well as the variable O&M costs of the base power plant. For conventional power plants, other costs are simply the variable O&M costs of the base power plants.

The reduction in total fuel costs with increasing wind capacity is also non-linear. There are a number of reasons why this occurs. Wind generation, with near-zero marginal costs, displaces thermal units and forces them to shut-down or reduce output. This reduces both fuel and CO_2 emissions. However, the increase in variable wind generation increases the uncertainty and reserve requirements and so more thermal power plants are required to part-load (at lower marginal efficiencies). This increases the fuel consumption per MWh of electricity generated. It is the displacement of some thermal units and the increased part-loading of residual units that causes the non-linear fall in fuel costs.

Ordering the total hourly system costs starting from the highest then descending to the lowest gives the total system cost duration curve, see Figure 6.6. The area under the curves gives the total system costs over one year for each scenario. The results show clearly the impacts of increasing wind capacity on total system costs. The maximum hourly system costs occur at the annual peak demand when most power plants are operating. In the 15 GW scenario the maximum hourly system costs peaks at £3.31 million. This is the sum of fuel costs, CO_2 costs, ramping costs etc. for the one hour period when hourly system costs are highest.

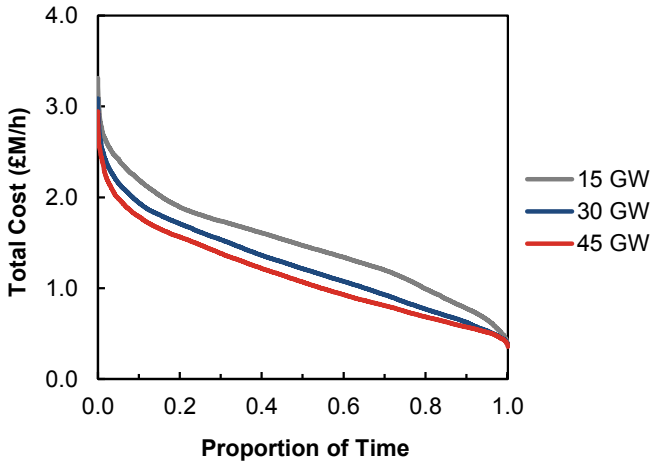

Figure 6.6: Total short-run cost duration curve for base case generation portfolio with wind capacity between 10 GW and 45 GW using demand and wind data for 2010.

It should be noted that costs incurred during a thermal plant start-up (fixed start-up costs, fuel costs, CO_2 costs) are accounted for in the first operational hour (i.e. all of the costs during start-up are summed together and occur in the first hour after the plant has reached its minimum power output limit).

Impacts of inter-annual wind variations

The total system short-run costs and total non-fuel costs for each annual scenario with 30 GW of wind capacity is shown in Figure 6.7. Using 2010 wind and demand data, onshore wind contributed 28.5 TWh and offshore wind 42.8 TWh. The combined total wind generation for the 2010 scenario with 30 GW of wind capacity is 71.3 TWh. The average wind output across all of the 30 GW wind capacity scenarios between 2002 and 2010 is 84.5 TWh. Electricity demand in 2010, however, is much closer to the average between 2002 and 2010. Electricity demand for the 2010 scenario is 337.2 TWh compared to the average of 338.9 TWh between 2002 and 2010. It is the abnormally low wind output in 2010 (compared to the nine year average) that causes the total system costs to be significantly higher than any of the other years. The total system costs for the 2010 scenario are £10.9 billion which is 6.4% higher than the average of £10.2 billion between 2002 and 2010. The least cost annual scenario is 2008 which has a total system cost of £9.9 billion and the highest wind output. The range and standard deviation in the total system costs is £0.99 billion and £0.31 billion, respectively. The range and standard deviation in the total system non-fuel costs is £0.33 billion and £0.08 billion, respectively.

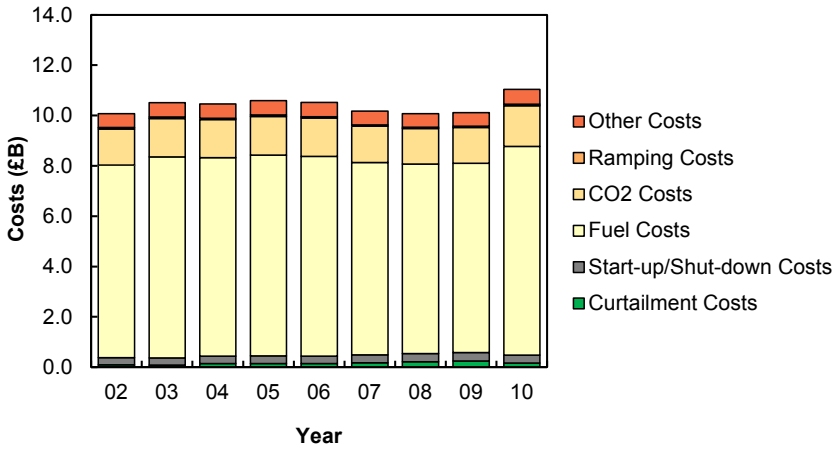

(a) Total system short-run costs

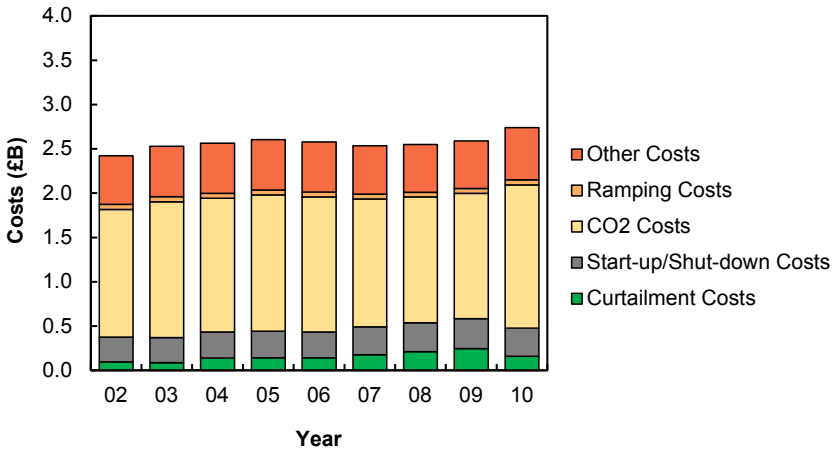

(b) Total system short-run non-fuel costs

Figure 6.7: Total system short-run costs for base case generation portfolio with 30 GW of wind capacity using demand and wind data between 2002 and 2010.

6.3.4 Total CO_2 emissions

Impacts of increasing wind capacity

CO_2 duration curves can be constructed by ordering the hourly CO_2 emissions of the system starting from the highest hourly CO_2 emissions then descending to the lowest. Figure 6.8 shows the CO_2 duration curves for the 15 GW, 30 GW and 45 GW wind scenarios using demand and wind data for 2010. The area under the curves gives the annual CO_2 emissions for each scenario. It includes the CO_2 emissions (emitted to the atmosphere) from thermal power plants (with and without CCS) during normal and part-load operation and during start-up and shut-down.

Figure 6.8 also shows how low CO_2 emissions can fall in certain hours. During low net demand periods, net demand is met by nuclear, wind, and a small amount of thermal generation with CCS. The CO_2 emissions do not fall to zero since CCS units still emit a small fraction (10%) of the CO_2.

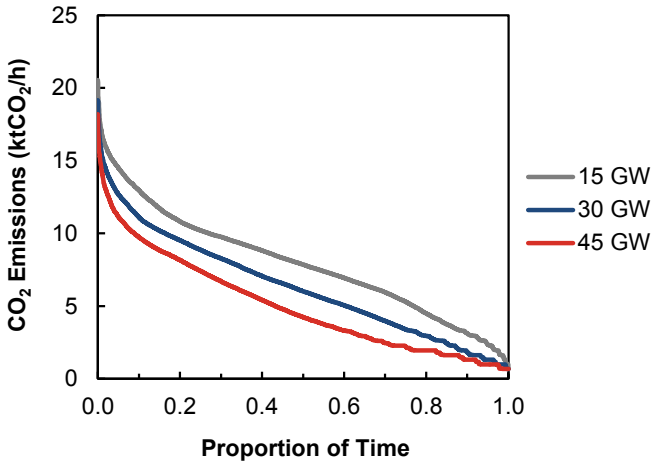

Figure 6.8: CO_2 emissions duration curve for base case generation portfolio with 15 GW, 30 GW, and 45 GW of wind capacity using demand and wind data for 2010.

Figure 6.9 and Table 6.6 show the total annual CO_2 emissions for the base case generation portfolio with increasing wind capacity. The total annual CO_2 emissions fall from 74.4 $MtCO_2$ with 10 GW of wind capacity to 44.0 $MtCO_2$ with 45 GW of wind capacity. Average hourly CO_2 emissions are 8.5 $ktCO_2$[1] with 10 GW of wind and 5.0 $ktCO_2$ with 45 GW of wind. More efficient CCGT units emit less CO_2 per MWh (at full load) but operate for more hours of the year. This is why CCGT units 1-10 emit the largest proportion of CO_2 emissions despite being the most efficient.

The fall in CO_2 emissions with increasing wind capacity is also non-linear. This is because wind generation displaces more expensive and more CO_2 intensive power plants first. Then,

1. 1 thousand tonnes of CO_2 is expressed as 1 $ktCO_2$ and 1 million tonnes of CO_2 is 1 $MtCO_2$.

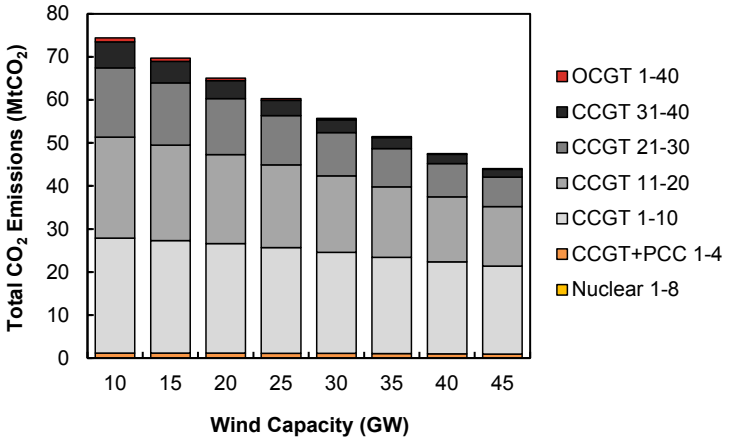

Figure 6.9: Total CO_2 emissions for base case generation portfolio with wind capacity between 10 GW and 45 GW using demand and wind data for 2010.

increasing wind generation does not lead to the same decrease in CO_2 emissions as before. Rather, additional wind generation displaces increasingly more efficient CCGT units and increases the proportion of part-loaded thermal units providing reserve for wind. For example, in the 15 GW wind capacity scenario the CO_2 emissions are 6.3% lower than the 10 GW scenario. But in the 45 GW wind capacity scenario the CO_2 emissions are only 4.0% lower than the 40 GW scenario. Further increases in wind capacity lead to slightly lower decreases in CO_2 emissions.

Table 6.6 also shows how the CO_2 emission intensity of the system expressed as tCO_2 equivalent per MWh of electricity demand varies. In other words this is the annual CO_2 emissions divided by the annual electricity demand. The base case scenario consists of a large amount of low carbon generation technologies. Therefore any increase in wind generation displaces natural gas fired power plants. The CO_2 emission intensity of the system falls from 0.221 tCO_2/MWh with 10 GW of wind capacity to 0.131 tCO_2/MWh with 45 GW of wind capacity.

Wind (GW)	Total CO_2 Emissions ($MtCO_2$)	CO_2 Emissions Intensity (tCO_2/MWh)
10	74.4	0.221
15	69.7	0.207
20	65.0	0.193
25	60.3	0.179
30	55.7	0.165
35	51.5	0.153
40	47.5	0.141
45	44.0	0.131

Table 6.6: Total CO_2 emissions and CO_2 emissions intensity for base case generation portfolio with wind capacity between 10 GW and 45 GW using demand and wind data for 2010.

Impacts of inter-annual wind variations

Figure 6.10 and Table 6.7 show the total CO_2 emissions and the CO_2 emissions intensity for each of the annual scenarios between 2002 and 2010.

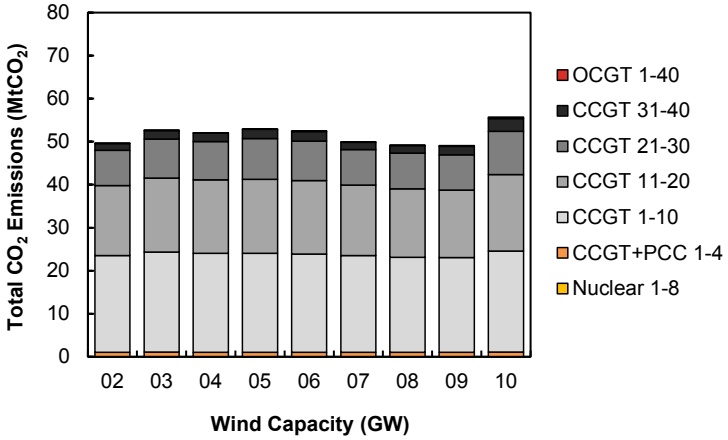

Figure 6.10: Total CO_2 emissions for base case generation portfolio with 30 GW of wind capacity using demand and wind data between 2002 and 2010.

The underlying changes in demand and wind output over the years creates a significant difference between the maximum and minimum observed total CO_2 emissions. Within the space of just one year, the CO_2 emissions increase from 49.1 $MtCO_2$ per year in the 2009 scenario to 55.7 $MtCO_2$ per year in the 2010 scenario. This large change in annual CO_2 emissions is caused by the large variations in annual wind output, which causes 2010 to require significantly more thermal generation. This difference of 6.6 $MtCO_2$ per year is equivalent to the CO_2 emissions of running a 900 MW CCGT unit (with an efficiency of 60%) at full load for approximately 19,000 h or 2.2 years. The measured standard deviation in annual CO_2 emissions is 2.1 $MtCO_2$.

Year	Total CO_2 Emissions ($MtCO_2$)	CO_2 Emissions Intensity (tCO_2/MWh)
2002	49.7	0.147
2003	52.7	0.155
2004	52.0	0.153
2005	52.9	0.152
2006	52.5	0.154
2007	49.9	0.149
2008	49.2	0.145
2009	49.1	0.149
2010	55.7	0.165
Average	51.5	0.152

Table 6.7: Total CO_2 emissions and CO_2 emissions intensity for base case generation portfolio with 30 GW of wind capacity using demand and wind data between 2002 and 2010.

It is clear from the results that inter-annual wind variations can cause significant differences in

annual CO_2 emissions. The annual CO_2 emissions with 2010 data are 8.1% higher than the 9 year average or 13.5% higher than the annual CO_2 emissions with 2009 data.

6.3.5 Marginal CO_2 emissions

Background

The marginal emissions factor (MEF) is a measure of the change in CO_2 emissions caused by a given change in electricity demand. The current MEF of the GB system is estimated to be 0.64 tCO_2/MWh [Hawkes, 2010]. In other words, if electricity demand falls by 1 MWh, then it is expected that the CO_2 emissions of the system would fall by 0.64 tCO_2.

DECC [2014c] calculated historical MEFs for the GB system using several methodologies. Results using balancing mechanism bids from Elexon [2015] were found to give the most credible results. The reported annual MEFs fall between 0.40 - 0.70 tCO_2/MWh depending on the methodology used.

Thomson [2014] analysed the marginal impacts of wind power on CO_2 emissions using historical GB data. The method, originally developed by Hawkes [2010], uses wind and electricity demand data and the historic generation portfolio of thermal power plants to estimate the hourly CO_2 emissions of the system. The marginal displacement factor (MDF) is defined as the reduction in CO_2 emissions due to the displacement of thermal power plants by wind power [Thomson, 2014]. The hourly variations in demand, wind output, and CO_2 emissions can be used to estimate and isolate the impacts of wind power variations on CO_2 emissions.

Figure 6.11 shows the relationship between demand and CO_2 emissions for the base case scenario with 15 GW of wind capacity. The relationship is broadly linear as in Hawkes [2010]. The MEF of the base case scenario with 15 GW of wind capacity is estimated to be 0.442 tCO_2/MWh. This value, however, cannot be compared with the MEF reported by Hawkes [2010] since the assumed thermal generation portfolios are very different. In this work, the base case generation portfolio is made up of nuclear, CCS, and natural gas power plants and so it is expected that in this work the MEF is lower.

It should be noted that these values include the changes in CO_2 emissions that occur from part-loading, starting up and shutting down thermal units in response to a change in wind output or demand.

Thomson [2014] then extended this method to understand how variations in wind output affect the changes in CO_2 emissions. This required using multiple linear regression to isolate the changes in wind output from changes in electricity demand.

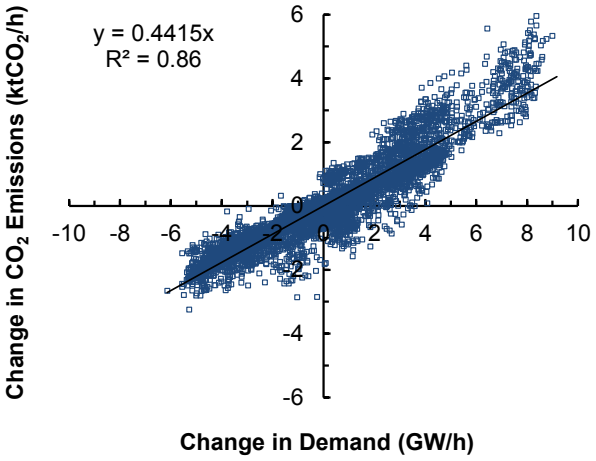

Figure 6.11: Relationship between 1-h changes in electricity demand and CO_2 emissions for base case scenario with 15 GW of wind capacity using demand and wind data for 2010.

Impacts of increasing wind capacity

The 1-h changes in electricity demand ΔD_t, wind output ΔW_t and CO_2 emissions ΔE_t for scenarios with 15 GW, 30 GW and 45 GW of wind capacity are shown in Figure 6.12. The thick black line in the figures shows the three dimensional fit between the points. The figures show how the changes in CO_2 emissions respond to both variations in wind output and electricity demand. With increasing wind capacity the correlation coefficient of the fit reduces.

Figure 6.13 shows the relationship between CO_2 emissions and wind output for each of the 15 GW, 30 GW and 45 GW wind capacity scenarios. The slight negative gradient indicates that an increase in wind output leads to a slight decrease in CO_2 emissions.

The marginal displacement factors (MDFs), a change in CO_2 emissions due to a change in wind output, for the 15 GW, 30 GW, and 45 GW wind capacity scenarios are estimated to be 0.439 tCO_2/MWh, 0.402 tCO_2/MWh, and 0.340 tCO_2/MWh, respectively.

The marginal emissions factors (MEFs), a change in CO_2 emissions due to a change in demand, for the 15 GW, 30 GW, and 45 GW wind capacity scenarios are estimated to be 0.442 tCO_2/MWh, 0.407 tCO_2/MWh, and 0.345 tCO_2/MWh, respectively.

These values are all higher than the average CO_2 emissions intensity of the system which are 0.207 tCO_2/MWh, 0.165 tCO_2/MWh and 0.131 tCO_2/MWh for the 15 GW, 30 GW, and 45 GW wind capacity scenarios, respectively. This shows that marginal changes in wind and demand displace more CO_2 intensive units than the average CO_2 intensity of the system. The MEFs and MDFs are very similar for varying amounts of wind capacity illustrating that changing amounts of wind and demand has a similar impact on CO_2 emissions.

This analysis considers the CO_2 emissions that occur during start-up/shut-down and the addi-

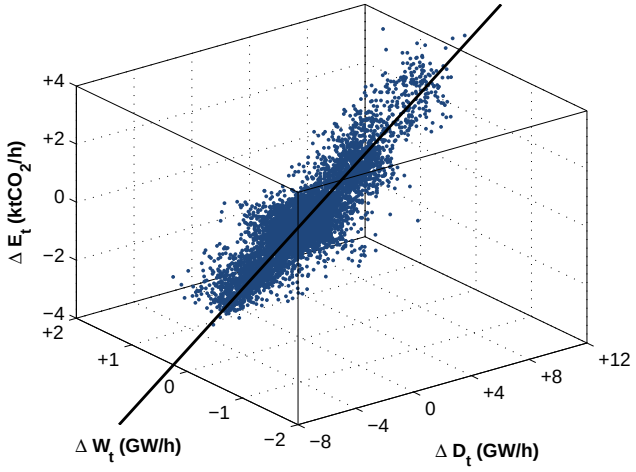

(a) 15 GW

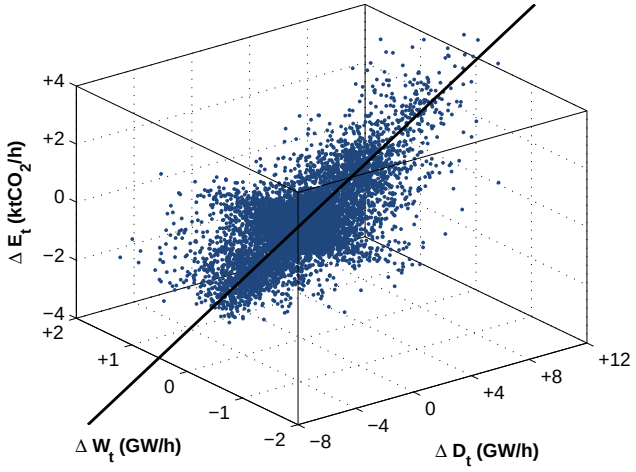

(b) 30 GW

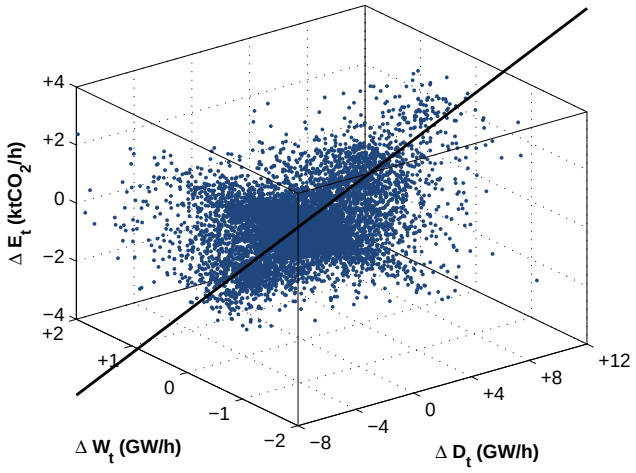

(c) 45 GW

Figure 6.12: Multiple linear regressions shows the relationship between changes in demand, wind, and CO_2 emissions with 15 GW, 30 GW and 45 GW of wind capacity using demand and wind data for 2010.

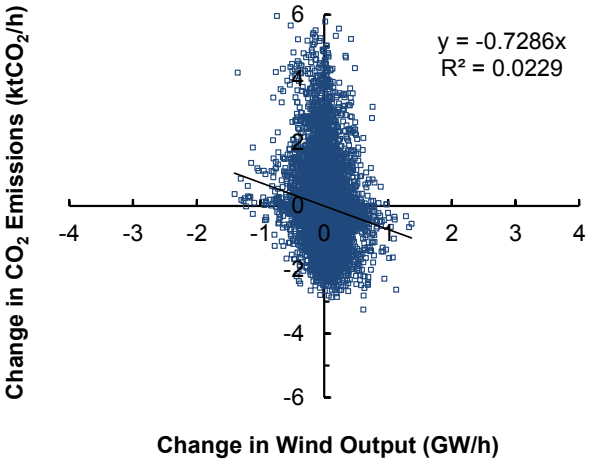

(a) 15 GW

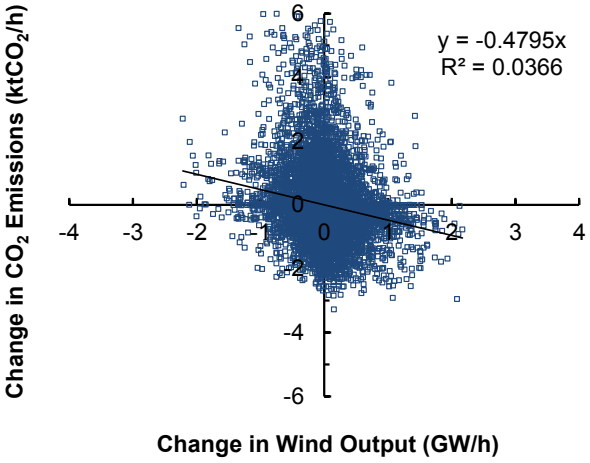

(b) 30 GW

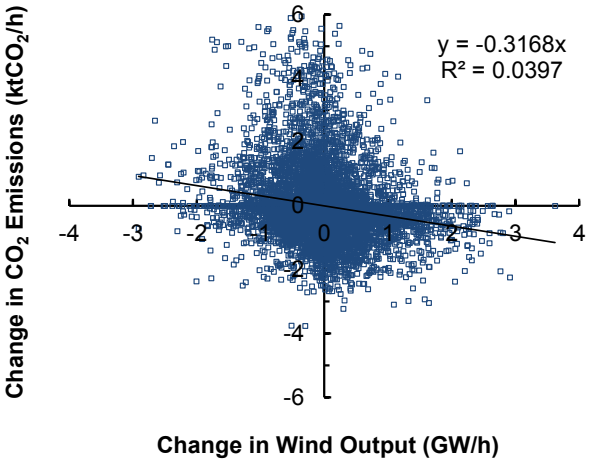

(c) 45 GW

Figure 6.13: Relationship between changes in wind output and CO_2 emissions with 15 GW, 30 GW and 45 GW of wind capacity using demand and wind data for 2010.

tional CO_2 emissions per MWh during part-load operation. It is therefore considered to be a more accurate indicator of the marginal impacts of wind and demand.

6.3.6 System electricity prices

Wind revenue cannibalisation is the process where wind farms reduce or 'cannibalise' their revenue during periods where large amounts of wind generation suppresses prices [Poyry, 2009]. The annual revenue that each wind farm receives is calculated for each year and divided by the annual generation of the wind farm. The annual wind capture price CP_f of wind farm f is the annual revenue divided by the annual generation.

$$CP_f = \frac{\sum_{t=1}^{T} \pi_t \times W_{f,t}}{\sum_{t=1}^{T} W_{f,t}} \tag{6.1}$$

Impacts of increasing wind capacity

The average electricity price in the 15 GW, 30 GW and 45 GW scenarios are £83.9/MWh, £79.6/MWh and £73.0/MWh, respectively. These prices are significantly higher than the electricity prices observed at present since a natural gas price of £23.9/MWh and a CO_2 price of £30/tCO_2 are assumed, in line with the 2020 projections in DECC [2014b]. In 2015, the average wholesale electricity price was £39.9/MWh [APX, 2015] and the natural gas price was approximately 40 p/therm or £13.6/MWh.

Figure 6.14 shows the average electricity price and wind capture price for each wind scenario. The red diamonds show the average electricity price for each wind capacity scenario. The results show that increasing wind capacity drives down the electricity price. However, the capture price that wind farms receive is significantly lower than the electricity price in higher wind capacity scenarios. The black lines show the average capture price of wind farms in each of the scenarios. The spread shows the maximum and minimum capture prices of wind farms. Some wind farms are able to capture significantly higher revenues than others.

The GB wind fleet on average only captures £82.1/MWh, £76.6/MWh and £63.4/MWh for the 15 GW, 30 GW and 45 GW wind scenarios, respectively. The wind capture price is the average annual price that a wind farm would receive if it received the electricity price for every MWh it generated. Wind farms that have a low correlation to the aggregate GB wind fleet typically receive a higher capture price than the average wind farm. In contrast, wind farms that have a high correlation to the aggregate GB wind fleet typically receive a lower capture price than the average wind farm.

Figure 6.15 shows the average capture prices of generation technologies. CCGT units capture more revenue per MWh of electricity generated than the average electricity price. This is

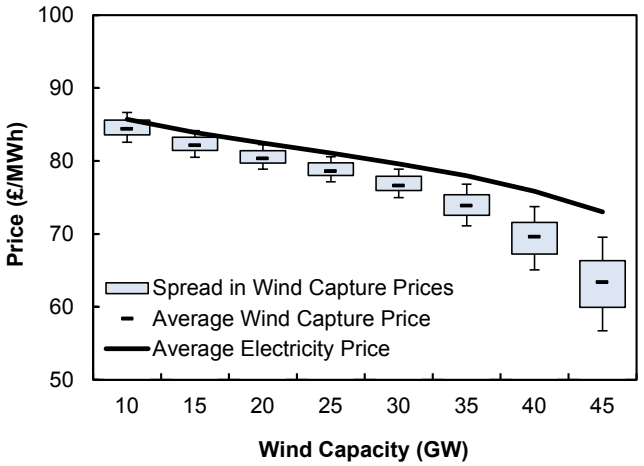

Figure 6.14: Average electricity price and wind capture price for base case generation portfolio with wind capacity between 10 GW and 45 GW using demand and wind data for 2010. The spread shows the maximum and minimum capture prices of wind farms.

because power plants that have higher SRMC require higher electricity prices for them to operate. Since it is only wind generation capacity that is changing between scenarios, the average capture prices for generation technologies falls with increasing wind capacity. The results show clear trends in the average capture prices (and therefore revenues) for generation technologies with increasing wind capacity.

DECC [2013d] provides projected levelised cost of electricity (LCOE) estimates for a number of generation technologies with different discount rates, project start dates etc. For projects starting in 2019, with a discount rate of 10%, the central LCOE projection for an Nth of a kind (NOAK) Nuclear unit is £80/MWh, CCGT unit is £84/MWh, and first of a kind (FOAK) CCGT+PCC is £95/MWh. This analysis assumes average lifetime load factors (net of plant availability) for Nuclear 91%, CCGT 93% and CCGT+PCC 93%, and assumes increasing fuel and CO_2 prices into the future. Therefore direct comparisons cannot be made between the results presented in this work and the analysis by DECC [2013d].

Figure 6.16a shows the variation in monthly electricity prices with increasing wind capacity. In the 15 GW wind scenario, there is a clear seasonal trend with summer months having lower average monthly electricity prices. However, increasing wind capacity reduces the average monthly electricity prices more in those months with large amounts of wind generation. This causes September to have the lowest average monthly electricity price in the 45 GW scenario.

Figure 6.16b shows the hourly variation in average electricity prices with increasing wind capacity. The shape of the daily electricity price profiles do not change significantly, except for a reduction in the evening peak. Electricity prices are suppressed most during peak demand hours between 18:00 and 20:00 but also during early morning hours.

Figure 6.17 shows the normalised wind capture prices of the 45 GW wind portfolio. The wind

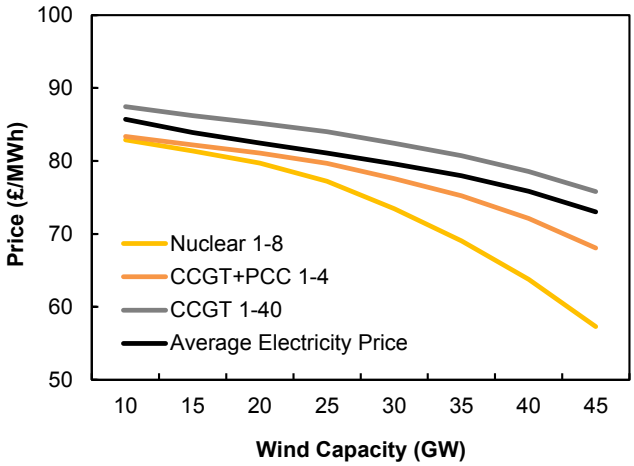

Figure 6.15: Average electricity price and capture prices for generation technologies with wind capacity between 10 GW and 45 GW using demand and wind data for 2010.

capture prices are expressed relative to the average capture price of the portfolio. For example, for the 45 GW wind capacity scenario the average wind capture price of the 45 GW portfolio is £63.4/MWh. If Whitelee wind farm receives an average capture price of £62.8/MWh then the capture price relative to the portfolio is (62.8-63.4)/63.4 = -0.9%. Therefore, relative to the portfolio the average wind capture price of Whitelee wind farm is -0.9%. The wind farms in red receive a higher than average capture price compared to the aggregate wind fleet and the wind farms in blue receive a lower than average capture price. The normalised wind capture prices range from -10% to +10%.

The results show that with an increasing proportion of wind capacity the wind capture prices diverge, with wind farms geographically centered in GB (with a high correlation to the GB wind fleet) capturing the lowest prices on average. It is offshore wind farms with the lowest correlations to the GB wind portfolio that capture the highest prices relative to the wind fleet. This revenue cannibalisation is greatest for onshore wind farms in the centre of GB for larger installed capacities of wind. This provides a first order approximation (without transmission constraints) of the revenues from the market that each wind farm might receive if subsidies or support schemes for onshore and offshore wind were to end. In the 45 GW scenario, certain onshore and offshore wind farms are able to capture up to twice the revenue of centrally located onshore wind farms. This shows that it is both wind speeds and the correlation with the wind fleet that determine the average capture price.

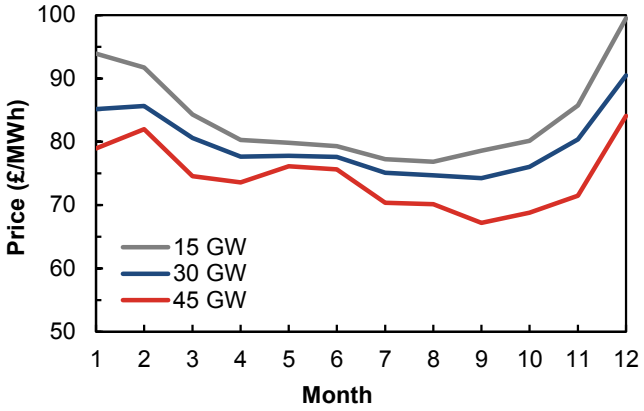

(a) By month

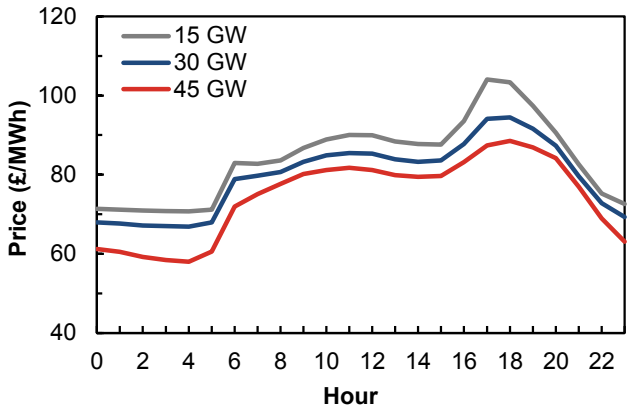

(b) By hour

Figure 6.16: Average electricity prices by month and hour for base case generation portfolio with wind capacity between 15 GW, 30 GW and 45 GW using demand and wind data for 2010.

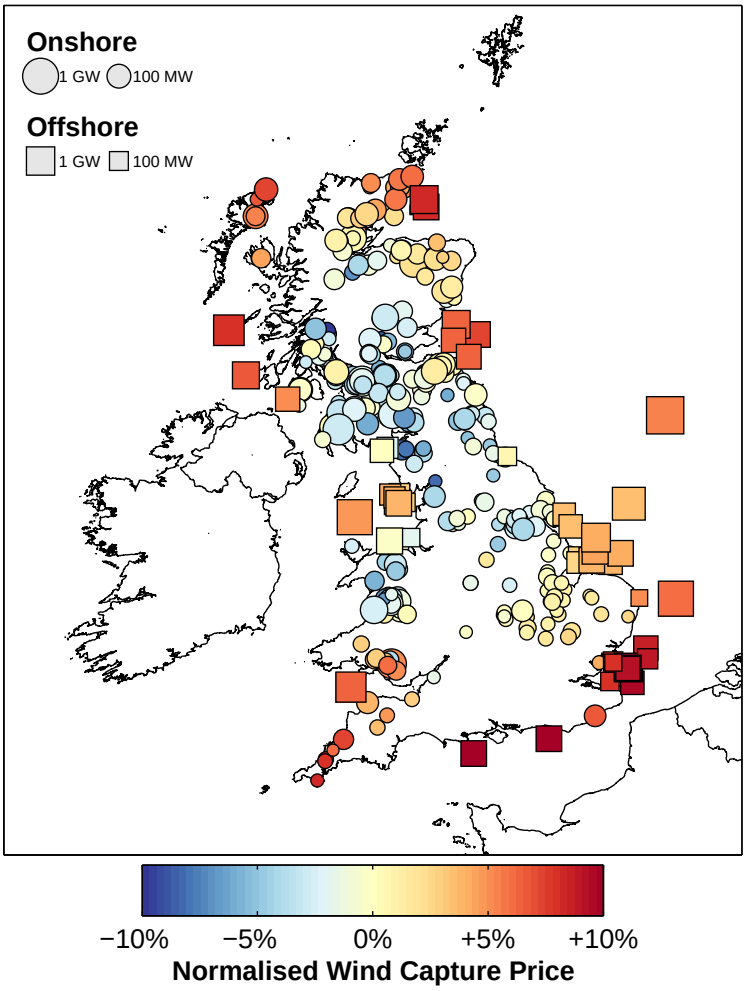

Figure 6.17: Normalised wind capture price with 45 GW of wind capacity using demand and wind data for 2010.

Impacts of inter-annual wind variations

Figure 6.18a shows the price duration curves for each year between 2002 and 2010 with 30 GW of installed wind capacity. The shape of the price durations curves are all very similar, especially during 'normal' periods. This is because fuel and CO_2 costs remain constant between scenarios. However, peak electricity prices do change across scenarios as wind generation contributes varying amounts during peak hours, see Figure 6.18b. This causes the capacity margin to be smaller during certain years (i.e. 2010 and 2005) which increases the price mark-up. Similarly, during years where wind generation exceeds demand, electricity prices can fall below zero. One negative price event occurred for 4 h in the 2009 scenario.

Figure 6.18c shows the monthly variations in average electricity prices between the annual scenarios with 30 GW of wind capacity. There is a significant variation in the average electricity prices, particularly in winter months when wind output fluctuates more.

Month 12 (December) for the 2010 scenario is significantly higher than other months. This is because December 2010 was historically the coldest December since Met Office records began in 1910 [Met Office, 2015]. This causes higher than average electricity demand and causes the significantly higher average monthly electricity price in December 2010. The results show that the simple electricity pricing model is able to capture detailed seasonal trends in electricity demand.

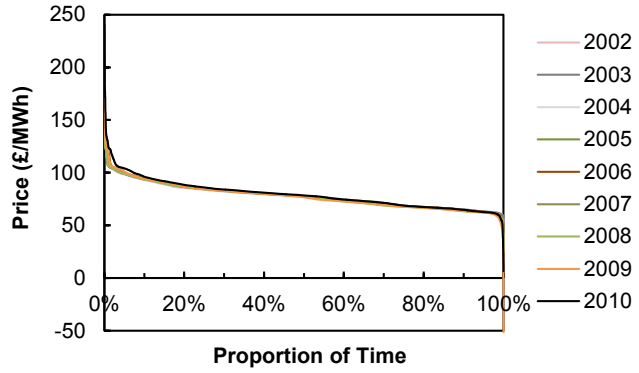

(a) Price duration curves

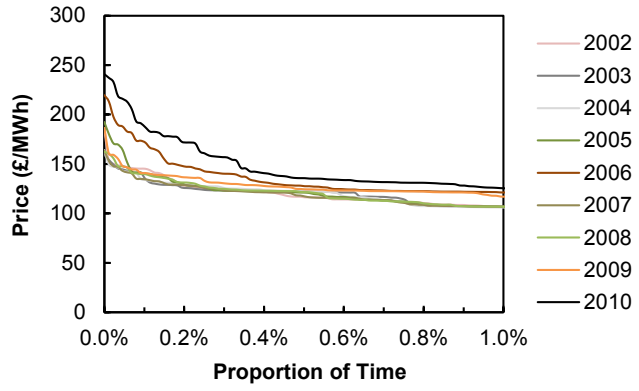

(b) Peak electricity prices

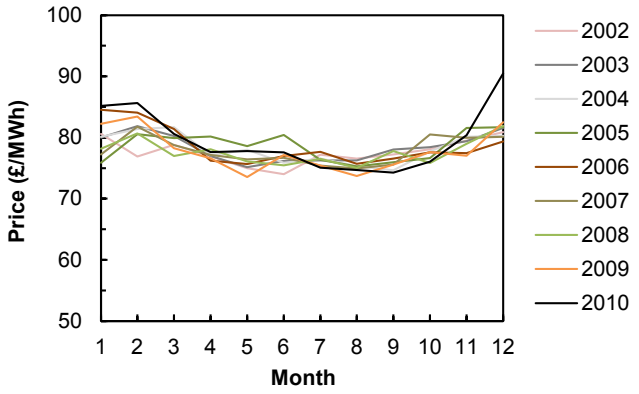

(c) Average monthly electricity prices

Figure 6.18: Simulated price duration curves with 30 GW of wind capacity between 2002 and 2010.

6.4 Impacts on power plant operating regimes

The impacts of wind generation on power plant operating regimes is assessed using a number of metrics. These metrics include the load factors of thermal generation technologies; the time spent shut-down, at minimum load, at part-load and at full load; the start-up requirements; and the ramping requirements. The methodology used to assess each of the metrics is also outlined.

6.4.1 Load factors

Methodology used to assess load factors

A set is defined to represent each generation technology. As described in Section **??**, G is the set of all thermal units $g = \{1,2,3,...,G\}$. H is the set of generation technologies $h = \{1,2,3,...,H\}$.

With increasing amounts of wind capacity the load factors of thermal units decrease, as expected. This occurs more for mid-merit power plants than for peaking plant or baseload power plant. The load factor of each unit g is defined as:

$$LF_g = \frac{\sum_{t=1}^{T} P_{g,t}}{P_{g,\max} \times T} \tag{6.2}$$

where T is the number of hours in each year i.e. 8760 h. For each generation technology h, the average load factor LF_h is then calculated.

Impacts of increasing wind capacity

Figure 6.19a shows how the load factors of thermal generation technologies change with increasing amounts of wind capacity for the base case scenario. There is a gradual fall in the load factors, for example, the load factors of CCGT+PCCs falls from 97.5% with 10 GW of wind capacity to 75.8% with 45 GW of wind capacity. This affects the volume of CO_2 that is treated by the PCC plant and the amount of CO_2 that is compressed, transported and stored.

The most severe fall in load factors occurs to mid-merit thermal power plants such as CCGT units 11-20. For these units, the average load factors fall from 73.0% to 39.6% with 10 GW and 45 GW of wind capacity, respectively. Similarly, the average load factors of CCGT units 21-30 fall from 42.5% to 16.2% with 10 GW and 45 GW of wind capacity, respectively.

The largest percentage point fall in load factors is for CCGT units 11-20 which drops by 33.4 percentage points between the 10 GW and 45 GW wind capacity scenarios and the load factors of CCGT+PCC units 1-4 fall by 21.8 percentage points. This fall in load factors is illustrated in Figure 6.19b which shows the reduction in load factors in percentage points (PP) compared to the 10 GW wind capacity scenario. The change in load factors are expressed in

percentage points i.e. if the load factor falls from 60% to 40% then the fall in load factor is 20 percentage points. Increasing the amount of wind capacity causes the load factors of thermal generation technologies to fall at different rates. For example, the shape of the curves that describe the fall in load factors with increasing wind capacity is different for CCGT units 31-40 and CCGT+PCC units 1-4. In other words, increasing the amount of wind capacity increasingly reduces the load factors of CCGT+PCC units 1-4, but decreasingly reduces the load factors of CCGT units 31-40. This is due to their relative positions within the merit-order. CCGT+PCC units 1-4 have significantly lower SRMC than CCGT units 31-40 and so operate for more hours of the year.

The results show that large volumes of wind significantly impact the load factors of thermal power plants and that the fall in load factors is not symmetric for generation technologies. Mid-merit thermal power plants suffer the most from increased wind capacity, observing the highest fall in load factors. Thermal generation technologies that are high in the merit-order (cheapest SRMC) see load factors fall increasingly with more wind capacity. In the higher wind capacity scenarios, wind generation starts to displace other low-carbon generation technologies such as nuclear and CCS. This causes the load factors of these 'traditional' baseload thermal units to fall more with each incremental wind capacity addition.

	Load Factor (%)						
Wind Capacity (GW)	**Nuclear 1-8**	**CCGT +PCC 1-4**	**CCGT 1-10**	**CCGT 11-20**	**CCGT 21-30**	**CCGT 31-40**	**OCGT 1-40**
10	100.0	97.5	88.3	73.0	42.5	14.1	0.9
15	99.9	95.9	86.3	68.3	37.8	11.5	0.6
20	99.7	93.6	83.7	63.1	33.4	9.4	0.5
25	99.3	90.9	80.5	57.9	28.9	7.7	0.4
30	98.9	87.7	76.5	52.9	25.0	6.4	0.3
35	98.3	83.6	72.3	48.1	21.7	5.4	0.2
40	97.5	79.6	68.5	43.8	18.7	4.4	0.2
45	96.8	75.8	65.0	39.6	16.2	3.7	0.1

Table 6.8: Average load factors for base case generation portfolio with wind capacity between 10 GW and 45 GW using demand and wind data for 2010.

Figure 6.20 shows the load factors of CCGT+PCC units 1-4 with 15 GW, 30 GW, and 45 GW of wind capacity. The temporal distributions show the load factors by month and time of day. With 15 GW of wind capacity, the average load factor of CCGT+PCC units 1-4 is 95.9%, which drops to 87.7% with 30 GW and to 75.8% with 45 GW of wind capacity. Load factors drop mainly during overnight periods in the summer when demand is typically low. However, the temporal distributions show that in the 45 GW wind capacity scenario that load factors can fall to low levels even during winter months during the day when demand is typically high. Moreover, high levels of wind can persist for several days, causing the load factors of CCGT+PCC units 1-4 to remain at low levels for lengthier periods of time. This has important

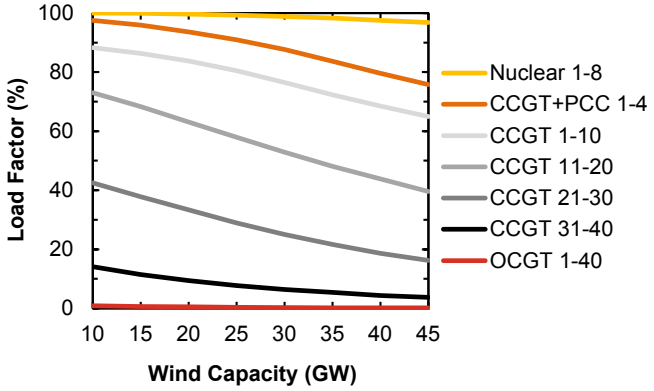

(a) Load factors (%)

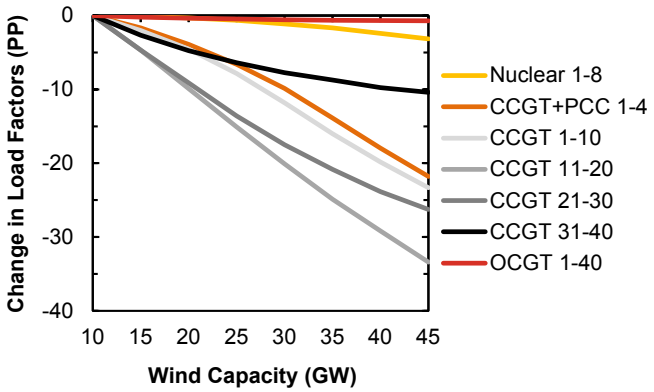

(b) Change in load factors compared to 10 GW scenario (percentage points)

Figure 6.19: Load factors for base case generation portfolio with wind capacity between 10 GW and 45 GW using demand and wind data for 2010.

implications for the rest of the CO_2 transportation and storage infrastructure. The quantity and variability of captured CO_2 becomes increasingly dependent on wind output.

Impacts of inter-annual wind variations

Figure 6.21 and Table 6.9 show how the load factors of thermal generation technologies changes between years. The load factors of generation technologies for each annual scenario are compared to the nine year average between 2002 and 2010. These are then used to calculate the change in load factors in percentage points (compared to the nine year average).

The standard deviations in load factors also provide an indication of how sensitive each generation technology is to changes in demand and wind output between years. The standard deviations in load factors for thermal generation technologies are shown in Table 6.9.

The results show that the load factors of CCGT units 11-20 are most sensitive to inter-annual variations in demand and wind output since these load factors vary the most between annual

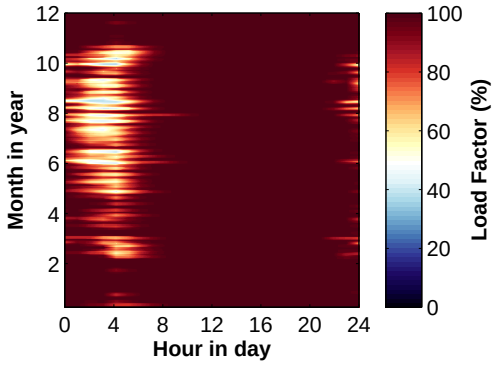

(a) 15 GW wind capacity

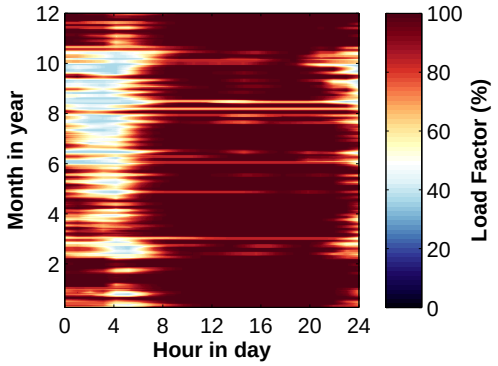

(b) 30 GW wind capacity

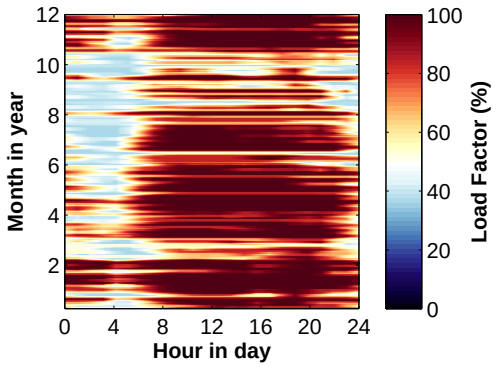

(c) 45 GW wind capacity

Figure 6.20: Temporal distributions showing the load factors by month and time of day for CCGT+PCC units 1-4 with 15 GW, 30 GW and 45 GW of wind capacity using demand and wind data for 2010.

scenarios. For example, the average load factor of CCGT units 11-20 in the 2010 annual scenario is 52.9% yet in the 2009 annual scenario the average load factor is just 45.7%. This is a significant difference in annual load factor and again shows that mid-merit CCGT units are the most volatile and influenced by changes in net demand between years. This is likely to heavily influence annual profits between years.

	Load Factor (%)						
Year	Nuclear 1-8	CCGT +PCC 1-4	CCGT 1-10	CCGT 11-20	CCGT 21-30	CCGT 31-40	OCGT 1-40
2002	98.2	85.6	72.8	47.3	19.7	3.2	0.1
2003	98.5	86.9	75.6	50.7	22.0	4.1	0.1
2004	98.2	85.8	74.7	50.2	21.5	3.9	0.1
2005	98.2	86.0	74.5	50.7	23.0	4.4	0.1
2006	98.3	85.6	73.9	50.4	22.3	4.7	0.1
2007	98.1	84.3	72.7	47.9	19.6	3.4	0.1
2008	97.8	82.1	71.3	46.3	19.8	3.5	0.1
2009	98.1	82.5	71.0	45.7	19.8	4.1	0.1
2010	98.9	87.7	76.5	52.9	25.0	6.4	0.3
Average	98.3	85.2	73.7	49.1	21.4	4.2	0.1
Std Dev	0.29	1.75	1.76	2.28	1.77	0.90	0.07

Table 6.9: Average load factors for base case generation portfolio with 30 GW wind capacity using demand and wind data between 2002 and 2010.

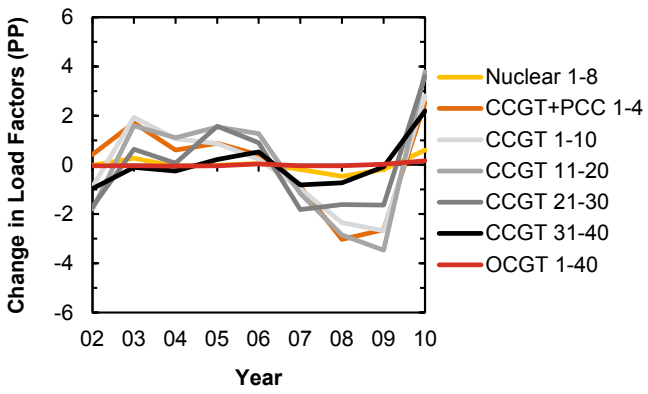

Figure 6.21: Change in load factors compared to nine year average between 2002 and 2010 in percentage points (PP) for base case generation portfolio with 30 GW of wind capacity using demand and wind data between 2002 and 2010.

6.4.2 Time spent at different loads

Methodology to assess loading requirements

Analysing the time that power plants spend at different loads gives an indicator of the various impacts of wind generation on power plant operating regimes. Power plants are either shut-down (when $P_{g,t} < P_{g,\min}$), at minimum load (when $P_{g,t} = P_{g,\min}$), at part-load (when $P_{g,\max} > P_{g,t} > P_{g,\min}$), or at full load (when $P_{g,t} = P_{g,\max}$). The analysis here differentiates between time spent at minimum load and at part-load when $P_{g,\max} > P_{g,t} > P_{g,\min}$.

The number of hours each year that each power plant operates at these loads is counted and used to illustrate the impacts of increasing wind capacity and inter-annual variations in wind output. The average time spent at different loads is then averaged for each generation technology.

Impacts of increasing wind capacity

Figure 6.22 shows for each generation technology the time spent at different loads. The results show clearly the impacts of incremental additions of wind capacity on the operating levels of thermal power plants. In general, with increasing wind capacity, power plants spend less time at full load and more time shut-down.

Power plants at part-load (i.e. with power outputs between $P_{g,\max} > P_{g,t} > P_{g,\min}$), are likely to be either ramping (either increasing or decreasing output), providing upwards/downwards reserve or they are the marginal generator.

Nuclear power plants undergo a transformation where the time spent at full load decreases from 99.3% with 10 GW of wind capacity to 71.3% with 45 GW of wind capacity. Nuclear units have to increasingly part-load to accommodate large volumes of wind during low net demand periods. Similarly, the time spent at full load for CCGT+PCC units decrease as these units reduce output to accommodate increasing volumes of wind generation. CCGT+PCC units do not shut-down since they are assumed to operate all the time to ensure a minimum flow rate of captured CO_2. At minimum power output limits with a 90% CO_2 capture rate, CCGT+PCC units capture approximately 145 tCO_2/h. The time spent at part-load increases from 6.2% of the time in the 10 GW wind capacity scenario to 16.8% of the time in the 45 GW wind capacity scenario.

CCGT units 1-10 also spend significantly less time at full load with increasing proportions of wind capacity. The time spent at full load falls from 75.2% in the 10 GW wind capacity scenario to 39.4% the 45 GW wind capacity scenario. This decrease in the time spent at full load is matched by a similar increase in the time spent at minimum load which increases from 13.5% in the 10 GW wind capacity scenario to 43.8% in the 45 GW wind capacity scenario.

Figure 6.23 shows how the time spent at part-load changes for each of the generation technologies with increasing wind capacity. Interestingly, the time spent at part-load does not increase

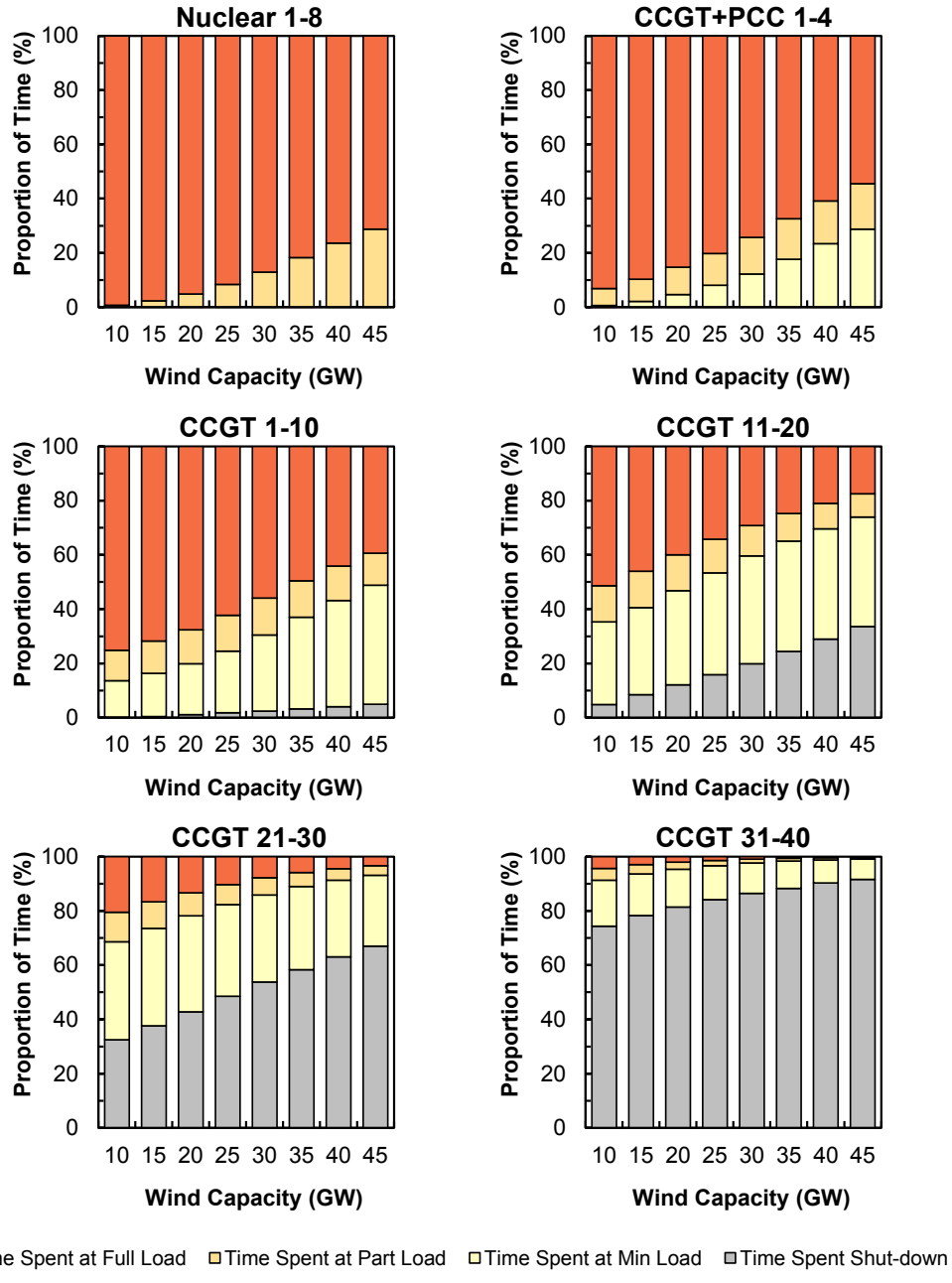

Figure 6.22: Proportion of time that thermal units spend shut-down, at minimum load, at part-load and at full load for thermal generation technologies with wind capacity between 10 GW and 45 GW using demand and wind data for 2010.

for all generation technologies. With larger installed wind capacities, nuclear and CCGT+PCC units increasingly part-load to accommodate wind generation while CCGT units 11-40 spend less time part-loading.

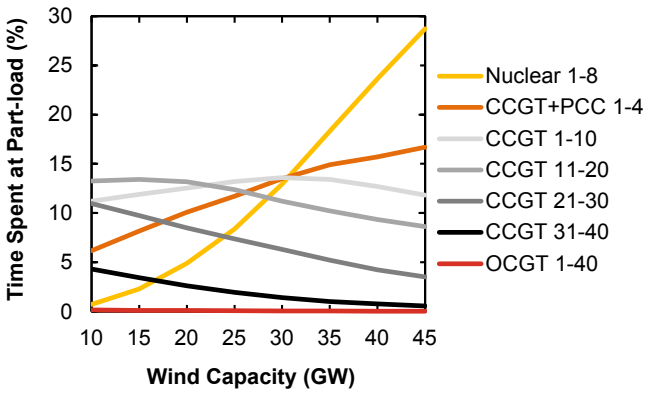

Figure 6.23: Time spent at part-load (excluding minimum load) for base case generation portfolio with wind capacity between 10 GW and 45 GW using demand and wind data for 2010.

Impacts of inter-annual wind variations

Figure 6.24 shows for each generation technology the time spent at different loads for the 30 GW wind capacity scenario using wind and demand data for years between 2002 and 2010.

In general, for low wind years (i.e. 2010) power plants spend more time at full load and less time shut-down and for baseload units (i.e. nuclear and CCGT+PCC units) less time is spent at minimum load and part-load compared to the average wind year. For example, using 2010 wind and demand data with 30 GW wind capacity, CCGT+PCC units spend 12.2% and 13.5% of the time at minimum load and at part-load, respectively. Yet, with 2008 wind and demand data, the same units spend 19.8% and 15.5% of the time at minimum load and at part-load, respectively. For peaking and mid-merit plant during low wind years, more time is spent at minimum load and at part-load compared to average.

The results show clearly that varying amounts of wind generation between years can significantly affect the time power plants spend at different loads. This in turn impacts the average efficiency and CO_2 emission intensity of units and has important implications on maintenance. For example, with 30 GW of wind capacity the average efficiency of CCGT units 1-10 using 2010 data is 58.4%. The average efficiency drops to 57.9% using 2008 data since 2008 was historically a high wind year. The increased wind generation in 2008 causes CCGT units to increasingly part-load which reduces the average efficiency of units.

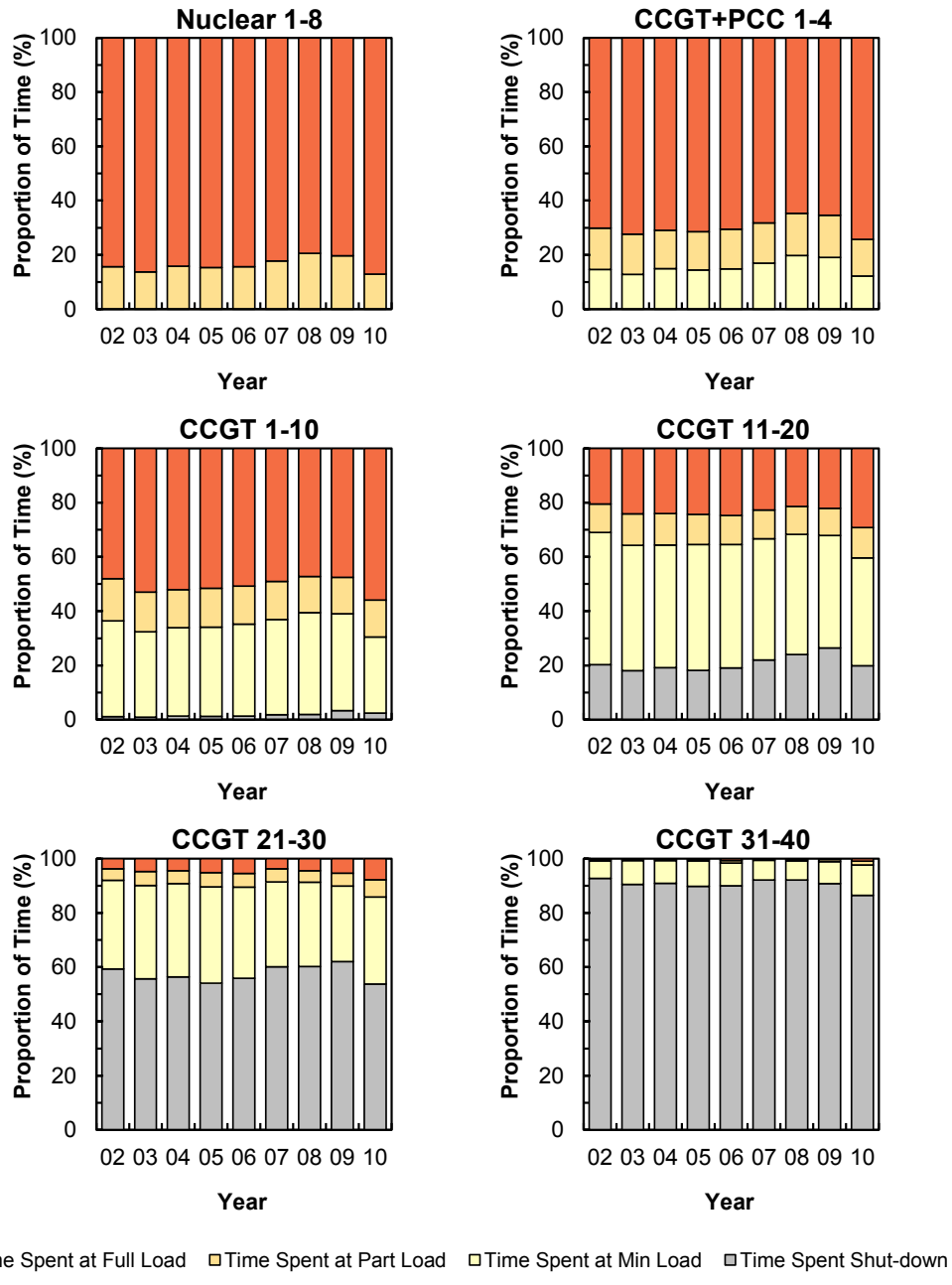

Figure 6.24: Proportion of time that thermal units spend shut-down, at minimum load, at part-load and at full load for thermal generation technologies with 30 GW of wind capacity using demand and wind data between 2002 and 2010.

6.4.3 Start-up requirements

Methodology to assess thermal plant start-up requirements

The start-up requirements of thermal power plants is an important indicator to understanding operating regimes. For each power plant, the number of hours that the power plant spends shut-down before it starts up is counted. For example, if a power plant has been shut-down for 8 hours before the power plant starts up, $X_{g,t}$ = - 8. The negative sign is used to indicate that the power plant has been offline[2]. For each thermal plant start-up, the time spent shut-down is logged.

This is then used to categorise each start-up as either hot ($-X_t \leq$ 12 h), warm (12 h < $-X_t \leq$ 72 h), or cold ($-X_t >$ 72 h). The speed at which power plants cool down after a shut-down is determined by their thermal cooling constants τ_g^{c}. Understanding this is important since increasing wind generation will alter how long thermal power plants spend shut-down. This will affect the start-up fuel that is required to increase temperatures back up to normal operating temperatures and therefore effect start-up costs and CO_2 emissions. This is also important for power system flexibility since if a plant has been shut-down for a longer period of time, it will take longer to start-up and respond to an unexpected increase in net demand.

The start-up costs, fuel and CO_2 emissions during start-up are modelled using a time-dependent exponential function:

$$C_{g,t}^{\mathrm{start}} = \overbrace{c_g^{\mathrm{start,fixed}}}^{\text{fixed}} + \left(\overbrace{F_g^{\mathrm{start,cold}} c_{g,t}^{\mathrm{fuel}}}^{\text{fuel}} + \overbrace{F_g^{\mathrm{start,cold}} e_g^{\mathrm{CO_2}} c^{\mathrm{CO_2}}}^{\mathrm{CO_2}} \right) \cdot \left(\overbrace{1 - e^{(X_{g,t}/\tau_g^{\mathrm{c}})}}^{\text{exponential}} \right) \tag{6.3}$$

For further details about the start-up costs of thermal power plants see Section 5.10.

Using this equation and the start-up characteristics described in Section 6.2.2, the start-up costs from cold ($-X_t$ = 72 h) for a CCGT unit are approximately £56,000; from warm ($-X_t$ = 24 h) the start-up cost are approximately £50,000; and from hot ($-X_t$ = 8 h) £32,000. The start-up costs for conventional and CCS-equipped power plants are outlined in Section 5.10 in Equations 5.89 and 5.91. The distribution and type of start-up has a significant impact on the total start-up costs and CO_2 emissions.

This work also assumes that thermal power plants do not have restrictions on the number of start-ups that they can perform annually. However, in reality certain units may have limitations on the number of cold start-ups that they can perform between each maintenance cycle. It is therefore essential that the hot/warm/cold start-up requirements are understood to inform the future operating characteristics of thermal power plants.

---

2. $X_{g,t}$ is a variable that counts the number of hours that each power plant has been online(+) or offline(-).

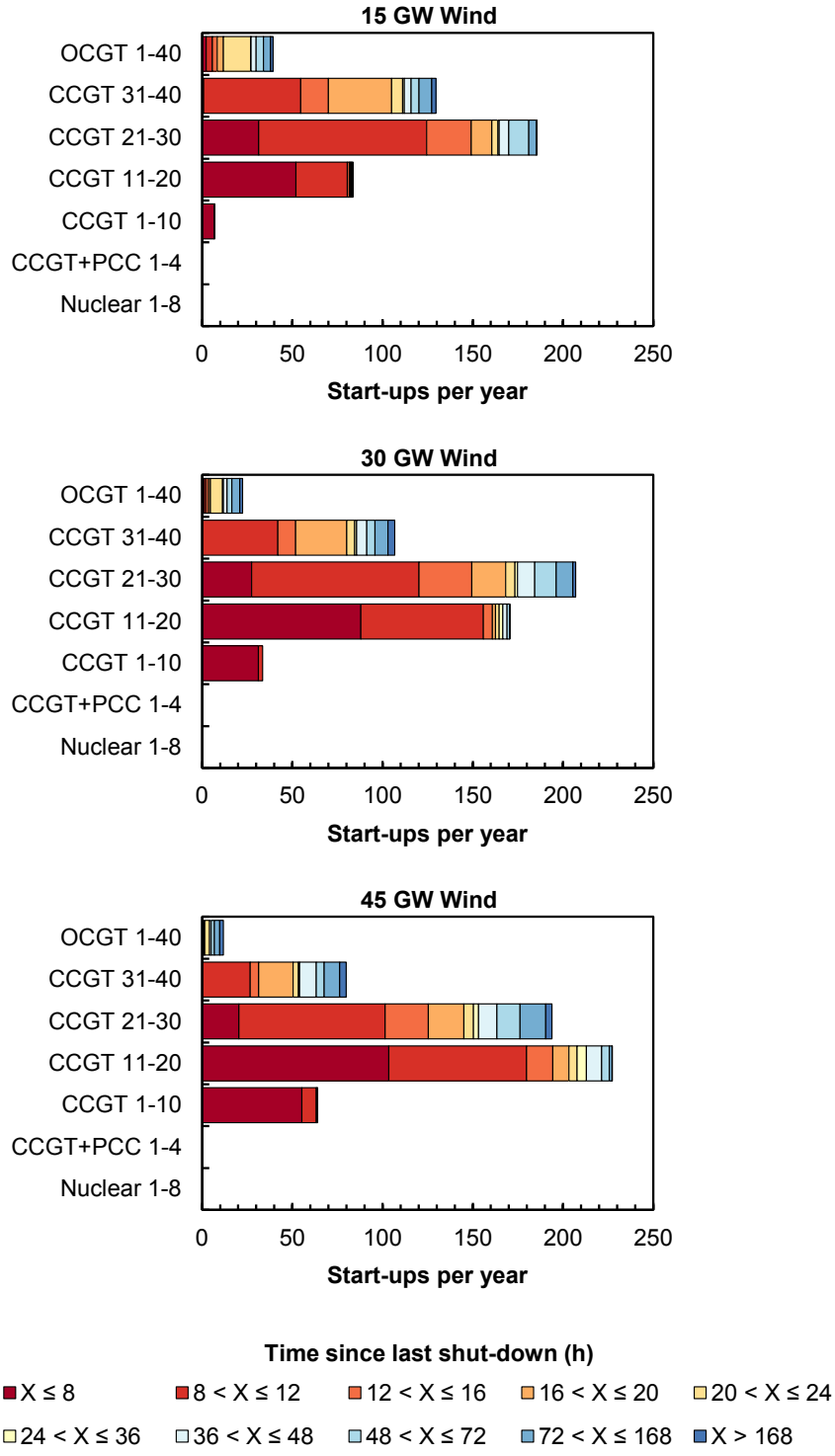

Figure 6.25: Number of start-ups per year categorised by time since last shut-down for thermal generation technologies for 15 GW, 30 GW and 45 GW of wind capacity using demand and wind data for 2010.

Impacts of increasing wind capacity

Figure 6.25 shows the distribution of hot/warm/cold start-ups for thermal generation technologies in the base case scenario with 15 GW, 30 GW and 45 GW of wind capacity. With 15 GW of wind capacity, CCGT units 21-30 perform on average the most start-ups per year at 186. This is split into 124 hot start-ups, 57 warm start-ups, and 5 cold start-ups. In the 45 GW wind capacity scenario, CCGT units 21-30 perform on average 194 start-ups per year, with 101 hot start-ups, 75 warm start-ups, and 18 cold start-ups. This is a large increase in the number of cold start-ups where the time spent shut-down is 72 hours or greater.

CCGT units 1-10 perform just 7 start-ups per year in the 15 GW wind capacity scenario. This increases to 64 start-ups per year with 45 GW of wind capacity. The sharp rise in the number of hot start-ups occurs because wind generation starts to increasingly displace and interrupt the operation of these 'traditional' baseload units. CCGT units 1-10 are then forced to shut-down for short periods of time to accommodate the large volumes of wind generation.

Figure 6.26 shows the change in the number of start-ups per year between the 45 GW and 15 GW wind capacity scenarios. A positive change on the x-axis shows an increase in the number of start-ups in the 45 GW wind capacity scenario compared to the 15 GW scenario. This figure shows the dramatic shift in start-up requirements that occurs because of increasing wind capacity. The 45 GW wind capacity scenario requires CCGT units 11-20 to start-up on average an additional 144 times per year compared to the 15 GW scenario. CCGT units 21-30 in the 45 GW wind capacity scenario are required to perform more colder start-ups and fewer hotter start-ups compared to the 15 GW scenario.

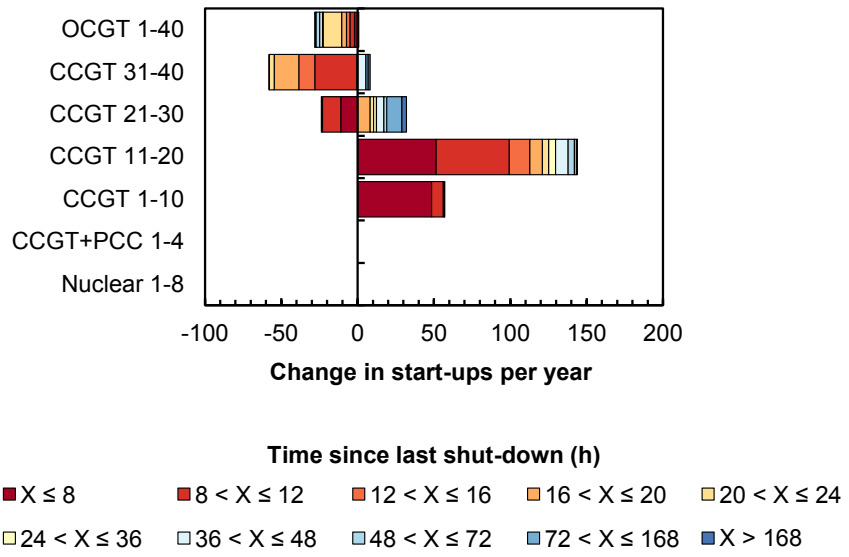

Figure 6.26: Change in the number of start-ups per year categorised by time since last shut-down for thermal generation technologies between the 45 GW and 15 GW wind capacity scenarios using demand and wind data for 2010.

6.4.4 Ramping requirements

Methodology to assess ramping requirements

The bulk of power system flexibility is provided by thermal power plants adjusting their output by ramping up or down to meet changes in net demand. Therefore, the ramping requirements of thermal power plants provides insights on the changing flexibility requirements of power systems.

For each power plant g, the power output time-series is first used to produce the ramping time-series.

$$\Delta P_{g,t} = u_{g,t}\left(P_{g,t} - P_{g,t-1}\right) \tag{6.4}$$

where $\Delta P_{g,t}$ is the change in power output of unit g at time t. The power output time-series only considers the power outputs of units that are online and operating between $P_{g,\max}$ and $P_{g,\min}$. The change in power output during start-up/shut-down between zero and $P_{g,\min}$ is not considered. This is to understand the ramping duties of power plants that are online and committed.

The ramping time-series for each generation technology h is then calculated.

$$\Delta P_{h,t} = \sum_{g \in h}^{H} \Delta P_{g,t} \tag{6.5}$$

The ramping time-series' can be ordered from the highest value in the time-series to the lowest value to produce ramping duration curves which illustrate the magnitude and time spent ramping.

The upwards and downwards ramping time-series' for each unit g can be calculated as follows:

$$\Delta P^{\text{up}}_{g,t} = \Delta P_{g,t} \quad \text{for} \quad P_{g,t} - P_{g,t-1} > 0 \tag{6.6}$$

$$\Delta P^{\text{dn}}_{g,t} = \Delta P_{g,t} \quad \text{for} \quad P_{g,t} - P_{g,t-1} < 0 \tag{6.7}$$

The total ramping performed over the time period (8760 h) is found by adding the absolute values of all of the upwards and downwards ramps.

Impacts of increasing wind capacity

Figure 6.27 shows the total ramping requirements of the thermal generation portfolio with wind capacities between 10 GW and 45 GW. The values on the y-axis show the number of GW that the average unit (within a generation technology class) ramps over 1 year. The total GW ramped illustrates the number of GW that each power plant (of a given generation technology) ramps.

Increasing the wind capacity increases the total ramping requirements for nuclear units 1-8 and CCGT+PCC units 1-4. This is because increasing volumes of wind creates deeper net demand variations by displacing less efficient and more expensive SRMC plant first. This increases the ramping requirements of thermal units higher in the merit-order.

The ramping requirements of CCGT units 1-10 increases between 10 GW and 30 GW of wind capacity. On average, each of the CCGT units 1-10 performs 407 GW of ramping per year in the 30 GW wind capacity scenario. The ramping requirements then gradually fall again in the 45 GW wind capacity scenario.

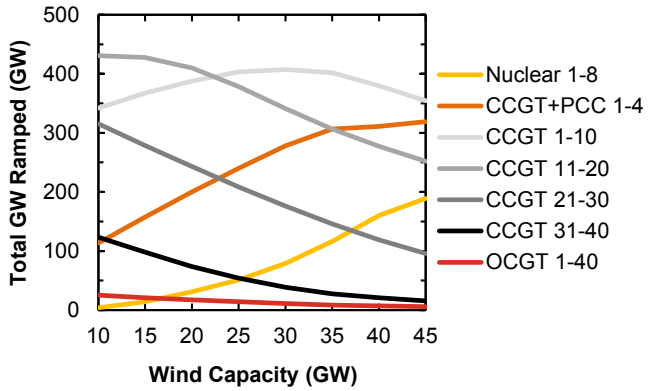

(a) Total GW ramped (upwards and downwards ramps)

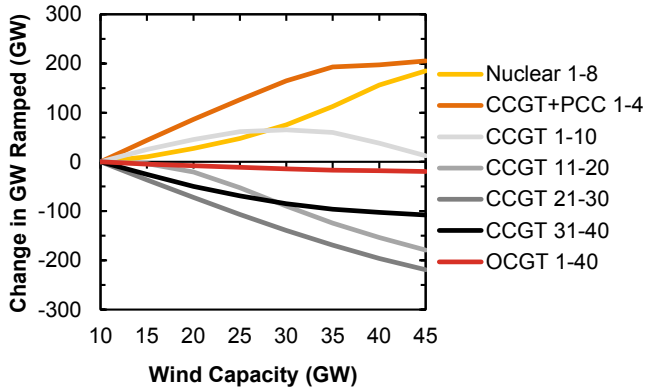

(b) Change in GW ramped compared to 10 GW wind capacity scenario

Figure 6.27: Average ramping requirements for each generation technology with wind capacities between 10 GW and 45 GW using demand and wind data for 2010.

Figure 6.28 shows the ramping duration curves for each thermal generation technology. The ramping time-series for each generation technology is normalised between -1 and +1 so the ramping requirements of thermal generation technologies can be compared side-by-side. For example, if CCGT units 1-10 have a normalised ramp rate of +1 this means that all 10 units are ramping at their maximum upwards ramp rate of 300 MW/h.

For most of the year ($\approx$ 60%) thermal power plants are not ramping (their power output

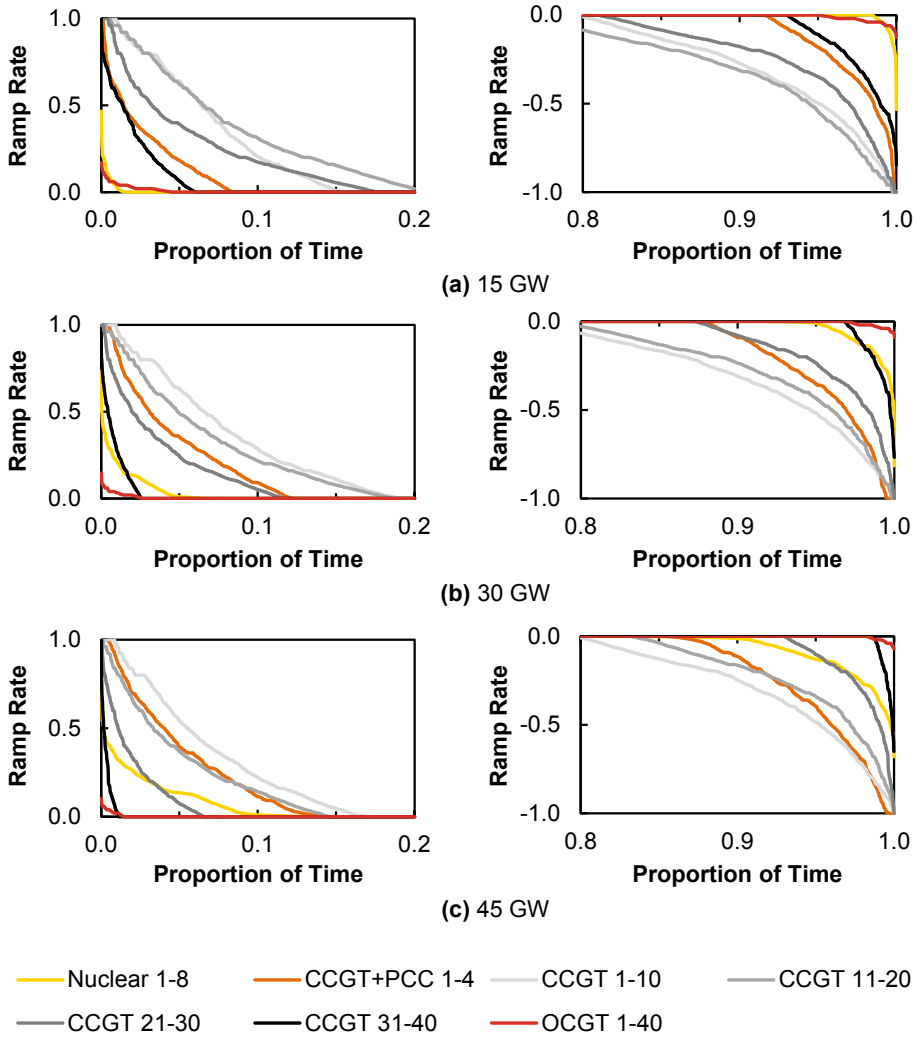

Figure 6.28: Normalised ramping duration curves for thermal generation technologies with 15 GW, 30 GW and 45 GW of wind capacity using demand and wind data for 2010.

is not changing between time periods). The area under the curves gives the total ramping requirements for each generation technology. The area between the positive curves and the x-axis gives the total upwards ramping requirements and the area between the negative curves and the x-axis gives the total downwards ramping requirements.

Figure 6.29 shows the hourly ramping requirements of CCGT units 1-40 for 15 GW, 30 GW and 45 GW wind capacity scenarios for the first two working weeks in January 2010. Each generation technology class (i.e. CCGT units 1-10, 11-20, 21-30, and 31-40) consists of ten CCGT units each with a rated capacity of 900 MW. The upwards and downwards ramp rate limits for each CCGT unit is 300 MW/h. This means that for each generation technology class the maximum upwards and downwards ramp rate is 3000 MW/h. This would imply that all ten CCGT units within that class are ramping at their maximum ramp rate of 300 MW/h.

The results show that increasing wind capacity typically decreases the ramping requirements for the average CCGT unit. This is because increasing volumes of wind displaces large amounts of CCGT generation and so less units are online providing ramping services. However, the ramping requirements of CCGT units 1-10 increases from 96 GW (upwards and downwards) in the 15 GW scenario to 141 GW and 131 GW in the 30 GW and 45 GW scenarios, respectively.

Figure 6.30 shows the ramping requirements for CCGT units with 15 GW, 30 GW and 45 GW of wind capacity. The temporal distributions show the impacts of increasing wind capacity on the ramping requirements of different CCGT units. The colour axis shows the ramping intensity. A value of +1 (shown in red) illustrates that the ten CCGT units are ramping at +3000 MW/h. A value of zero (shown in white) illustrates that the net ramping intensity of the CCGT units at that time period is zero. A value of -1 (shown in blue) illustrates that the net ramping intensity is -3000 MW/h.

Figure 6.30a shows the ramping requirements for CCGT units 1-10 with 15 GW of wind capacity. The ramping requirements are very periodic and predictable with CCGT units 1-10 increasing their power outputs in the morning between 06:00 - 08:00. The reduced ramping requirements during morning hours at weekends can be observed also. In general the ramping requirements are very orderly with a shift by +1 hour occurring in summer months because of daylight savings time.

Figure 6.30c shows the ramping requirements for CCGT units 1-10 but now with 45 GW of wind capacity. The temporal distributions are significantly altered as CCGT units 1-10 adjust output more frequently and irregularly to manage wind imbalances.

The remaining figures in Figure 6.30 show a similar pattern of increasing irregularity with increasing levels of installed wind capacity. The ramping requirements of CCGT units 21-30 reduces significantly with additional wind capacity as these units are displaced by wind and therefore not required to ramp to meet demand variations.

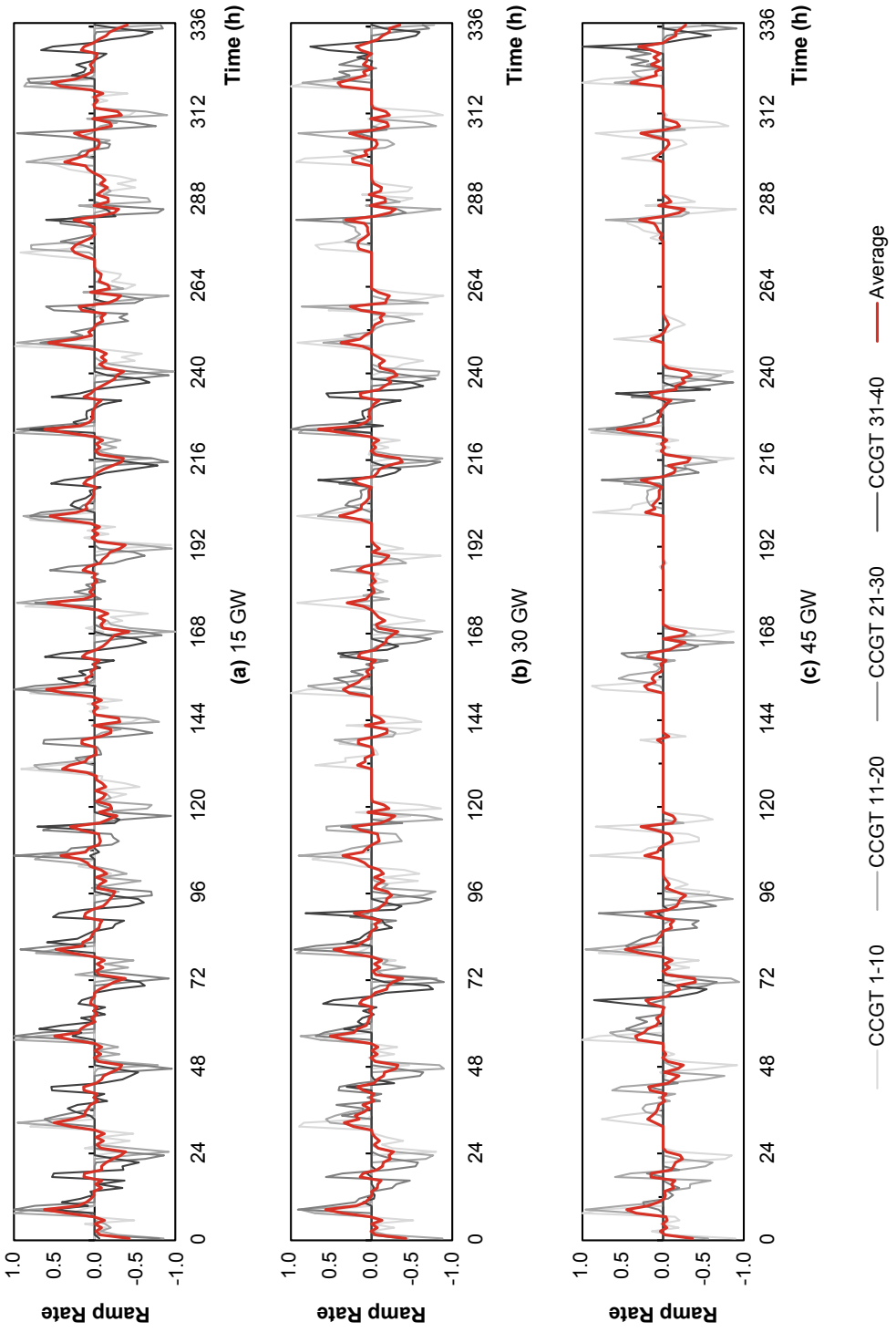

Figure 6.29: Normalised ramping requirements for CCGT units with 15 GW, 30 GW and 45 GW of wind capacity using demand and wind data for the first two working weeks in January 2010.

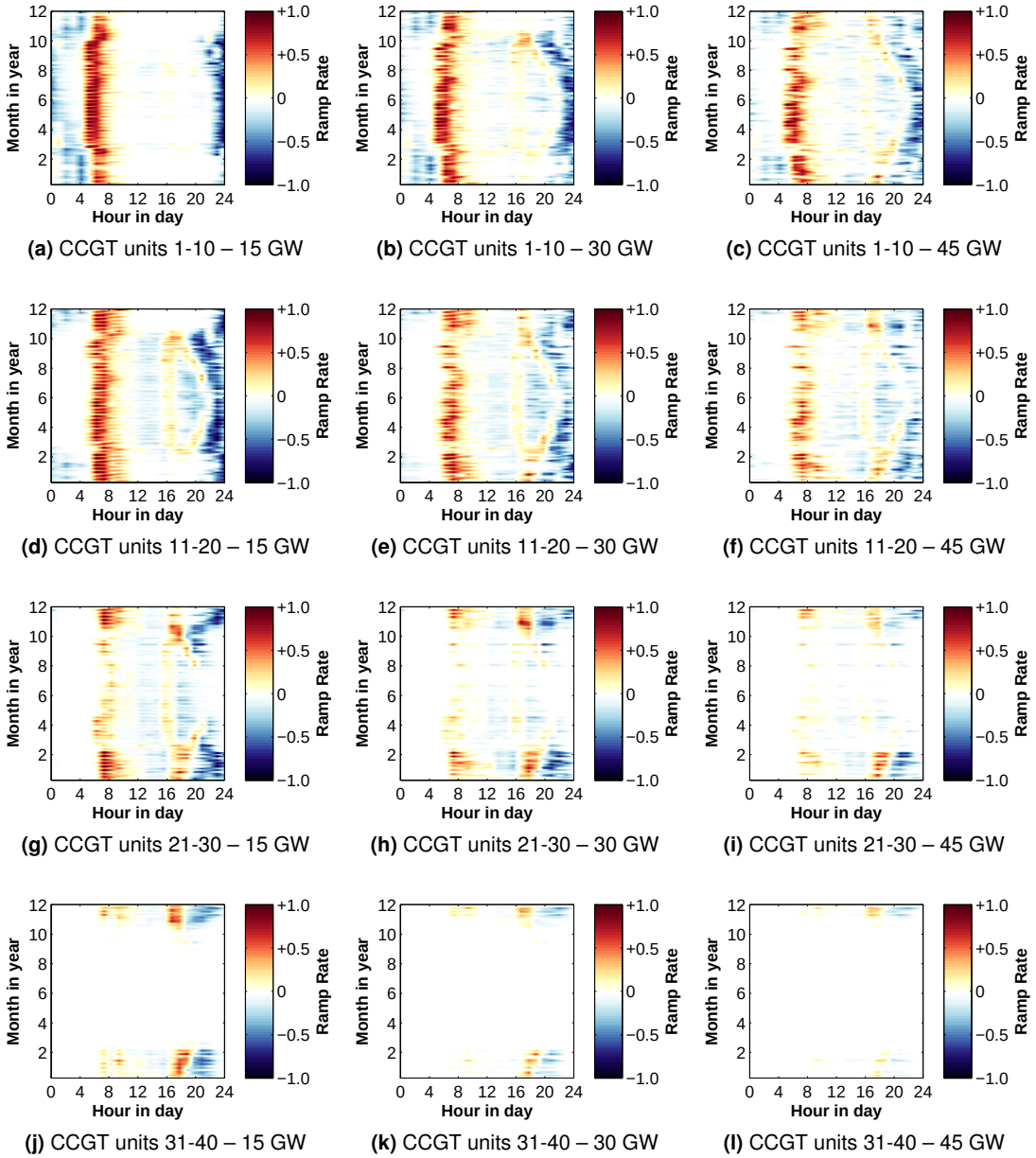

(a) CCGT units 1-10 – 15 GW **(b)** CCGT units 1-10 – 30 GW **(c)** CCGT units 1-10 – 45 GW

(d) CCGT units 11-20 – 15 GW **(e)** CCGT units 11-20 – 30 GW **(f)** CCGT units 11-20 – 45 GW

(g) CCGT units 21-30 – 15 GW **(h)** CCGT units 21-30 – 30 GW **(i)** CCGT units 21-30 – 45 GW

(j) CCGT units 31-40 – 15 GW **(k)** CCGT units 31-40 – 30 GW **(l)** CCGT units 31-40 – 45 GW

Figure 6.30: Temporal distributions showing the ramping requirements by month and time of day for CCGT units 1-40 with 15 GW, 30 GW and 45 GW of wind capacity using demand and wind data for 2010.

6.4.5 Correlation with wind output

Methodology to assess correlation coefficients

The Pearson product-moment correlation coefficient r measures the strength of a linear association between two variables. An r-value of +1 indicates a perfect positive correlation between the two variables. In contrast, an r-value of -1 indicates a perfect negative correlation. An r-value of 0 indicates there is no correlation between the two variables. The correlation coefficients between wind output and power plant output are computed with increasing wind capacity.

Equation 6.8 shows the equation to calculate the correlation coefficient between wind output W_t and the power output of each generation technology $P_{h,t}$:

$$r(W_t, P_{h,t}) = \frac{\sum_{t=1}^{T}(W_t - \overline{W})(P_{h,t} - \overline{P_h})}{\sqrt{\sum_{t=1}^{T}(W_t - \overline{W})^2}\sqrt{\sum_{t=1}^{T}(P_{h,t} - \overline{P_h})^2}} \tag{6.8}$$

where $\overline{W} = \frac{1}{T}\sum_{t=1}^{T} W_t$ and $\overline{P_h} = \frac{1}{T}\sum_{t=1}^{T} P_{h,t}$ are the mean values of W_t and $P_{h,t}$ over time period T, respectively.

Equation 6.9 shows the equation to calculate the correlation coefficient between the 1-h change in wind output ΔW_t and the 1-h change in the power output of generation technology $\Delta P_{h,t}$:

$$r(\Delta W_t, \Delta P_{h,t}) = \frac{\sum_{t=1}^{T}(\Delta W_t - \overline{\Delta W})(\Delta P_{h,t} - \overline{\Delta P_h})}{\sqrt{\sum_{t=1}^{T}(\Delta W_t - \overline{\Delta W})^2}\sqrt{\sum_{t=1}^{T}(\Delta P_{h,t} - \overline{\Delta P_h})^2}} \tag{6.9}$$

where $\overline{\Delta W} = \frac{1}{T}\sum_{t=1}^{T} \Delta W_t$ and $\overline{\Delta P_h} = \frac{1}{T}\sum_{t=1}^{T} \Delta P_{h,t}$ are the mean values of ΔW_t and $\Delta P_{h,t}$ over time period T, respectively.

These correlation coefficients are intended to illustrate the changing relationship between wind output and the power outputs of thermal generation technologies with increasing wind capacity.

Impacts of increasing wind capacity

Figure 6.31 shows the correlation coefficients of wind output and the power outputs for each generation technology class with increasing wind capacity.

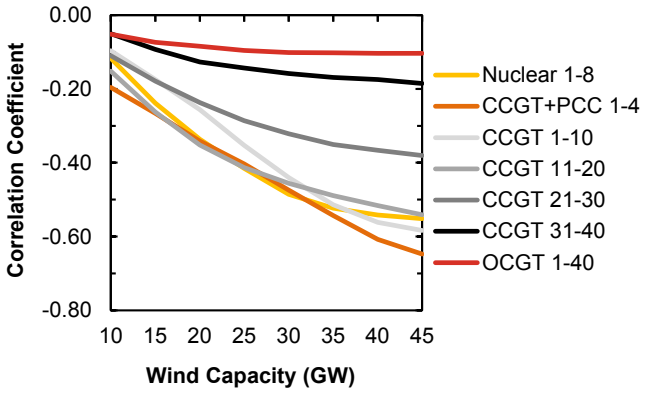

Figure 6.31: Correlation coefficients for generation technologies with wind capacity between 10 GW and 45 GW using demand and wind data for 2010.

The power outputs of thermal power plants become increasingly negatively correlated with wind output with increasing wind capacity. In other words, when wind output increases, the power outputs of thermal power plants decrease. This is expected since the SRMC of thermal power plants are higher than for wind generation. The change in correlation coefficients shows the sensitivity of each generation technology to increases in wind capacity. Interestingly, the correlation coefficient is strongest for CCGT+PCC units 1-4 in the 45 GW scenario with an r-value of -0.648 (r^2 = 0.419). This illustrates that there exists a moderate negative correlation between the power outputs of CCS-equipped units and wind output.

Figure 6.32 shows the correlation coefficients of 1-h changes in wind output and the 1-h changes in the power outputs of thermal generation technologies.

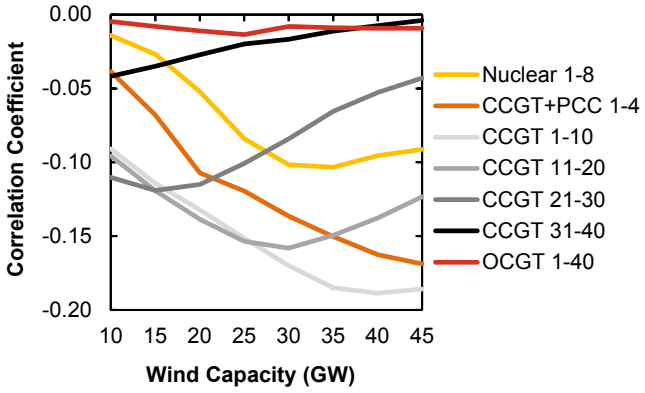

Figure 6.32: Correlation coefficients of 1-h wind output variations ΔW_t and the 1-h power output variations for each generation technology $\Delta P_{h,t}$ with wind capacity between 10 GW and 45 GW using demand and wind data for 2010.

This figure shows the relationship between hourly changes in wind output and the hourly changes in power plant output. There is a weak negative correlation between the hourly changes in wind output and thermal power plant outputs.

6.5 Sensitivity analysis

6.5.1 Introduction

Power plant operating regimes, system short-run costs and CO_2 emissions may be sensitive to changes in minimum up/down times and part-load efficiencies of thermal power plants. To investigate this, several case studies are presented which are compared to the base case generation portfolio to assess the sensitivity of power plant load factors, system short-run costs and CO_2 emissions to changes in thermal power plant characteristics. The results also demonstrate the importance of accounting for minimum up/down times and part-load efficiency losses in energy systems models.

6.5.2 Impacts of part-load efficiency losses

Introduction

Thermal power plants are typically less efficient when they operate at loads lower than their rated capacity. This is caused by a number of technical factors that reduce the efficiency when operating below design output.

To explore the sensitivity of total system short-run costs to part-load (PL) losses, the UCED model is run for the base case generation portfolio without part-load efficiency losses included to understand how this impacts total system short-run costs. In other words, power plants can reduce output without incurring additional part-load efficiency losses (i.e. the efficiency of the power plant remains constant at the full load efficiency). This is to understand how part-load efficiency losses impact the power plant dispatch and the fuel consumption and CO_2 emissions of power plants at part-load and the difference this makes to overall total system costs and CO_2 emissions.

Figure 6.33 shows the part-load efficiency curve for a 900 MW CCGT unit with a full load efficiency of 60%. When part-load efficiency losses are excluded the efficiency stays constant at 60%. This impacts the fuel consumption at part-load.

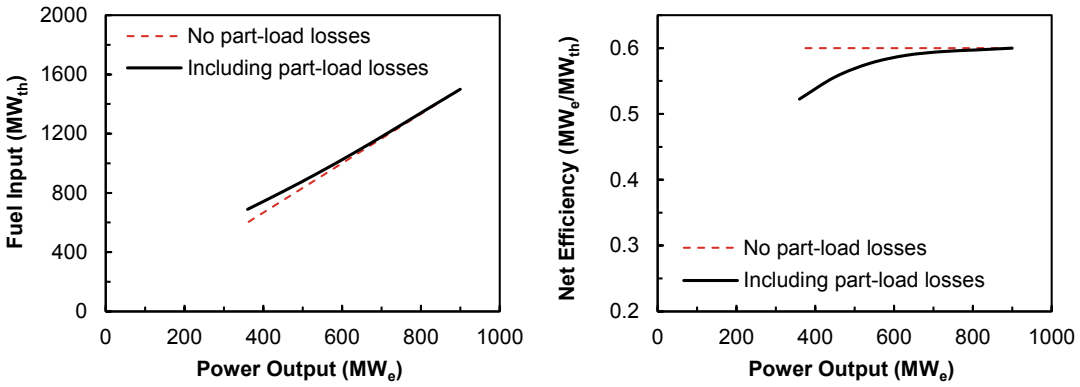

(a) Fuel input **(b)** Net efficiency

Figure 6.33: Input-output and efficiency curves for a 900 MW CCGT unit with a full load efficiency of 60%.

Impacts on system costs

Figure 6.34 shows the change in total system short-run costs between the base case scenario where part-load efficiency losses are included and the scenario when they are excluded. When part-load losses are excluded, the results underestimate total system short-run costs by approximately £0.4-0.5 billion. For example, the total system cost of the 45 GW scenario without part-load losses is £9.26 billion. This compares to £9.74 billion when part-load efficiency losses are included. In other words, by excluding or not modelling the part-load efficiency losses of thermal power plants the total system costs are significantly underestimated.

The costs associated with part-load efficiency losses increase as a percentage of total system costs from 3.7% with 10 GW of wind capacity to 5.2% with 45 GW of wind capacity. This is because total system costs fall with increasing wind capacity. However, the fuel costs associated with part-load efficiency losses does increase. This is because increasing wind generation increases the amount of part-loaded thermal units that are required to provide reserve requirements. This increases the losses associated with generating at part-load.

Not including part-load efficiency losses underestimates the fuel consumption and CO_2 emissions of power plants at part-load, especially when modelling systems with larger proportions of wind. This also impacts the costs associated with CO_2 capture since it affects the amount of CO_2 being treated by the CO_2 capture plant. It is likely that this effect will become stronger with more CCS-equipped power plants installed. Incorporating part-load losses into unit commitment models with CCS is therefore very important for accurately simulating fuel consumption and CO_2 emissions and therefore the flows of captured CO_2.

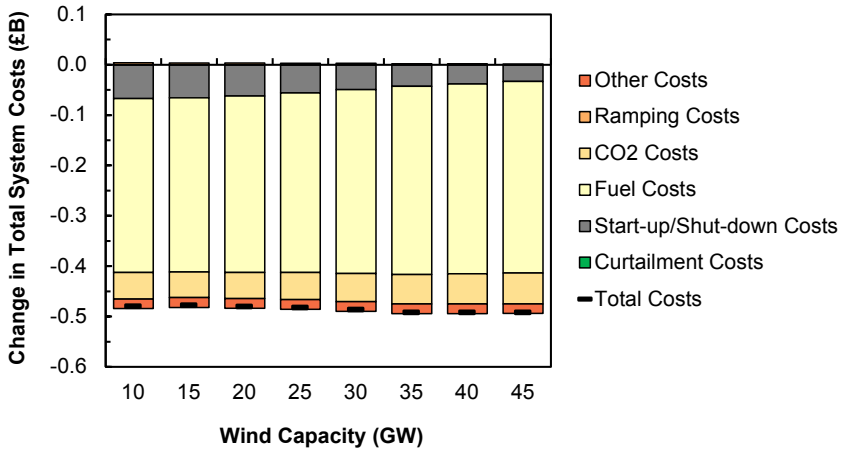

Figure 6.34: Change in total system short-run costs for base case generation portfolio when excluding part-load efficiency losses with wind capacity between 10 GW and 45 GW using demand and wind data for 2010.

Impacts on CO_2 emissions

The CO_2 emissions for the base case scenario and the scenario with no part-load (PL) efficiency losses for the 10 GW to 45 GW wind capacity scenarios using 2010 wind and demand data are shown in Table 6.10.

Wind Capacity (GW)	Base Case Total CO_2 Emissions ($MtCO_2$)	No PL losses Total CO_2 Emissions ($MtCO_2$)	Change in CO_2 Emissions (% of total)
10	74.4	72.2	-2.89
15	69.7	67.6	-3.00
20	65.0	62.9	-3.23
25	60.3	58.2	-3.52
30	55.7	53.6	-3.85
35	51.5	49.2	-4.30
40	47.5	45.3	-4.67
45	44.0	41.8	-5.07

Table 6.10: Total CO_2 emissions for the base case scenario with part-load losses and the scenario without part-load losses included and the change in CO_2 emissions expressed as a percentage of the total base case CO_2 emissions with wind capacity between 10 GW and 45 GW using demand and wind data for 2010.

The results show that CO_2 emissions are lower when part-load efficiency losses are excluded. Excluding part-load efficiency losses reduces the total annual CO_2 emissions by approximately 2.2 $MtCO_2$ per year. This is equivalent to the CO_2 emissions of running a 900 MW CCGT unit (with an efficiency of 60%) at full load for over 6000 hours. After excluding part-load losses, CO_2 emissions reduce by 2.89% in the 10 GW wind capacity scenario and reduce by 5.07% in the 45 GW scenario. The results show that increasing wind capacity significantly increases

part-load efficiency losses and therefore the additional CO_2 emissions that occur from operating at part-load.

Part-loaded thermal power plants typically have lower thermal efficiencies and therefore emit more CO_2 per MWh of electricity generated than when at full output. This affects all thermal power plants except nuclear units which are assumed to have negligible part-load efficiency losses and do not emit CO_2.

Impacts on load factors

Figure 6.35 shows how the load factors of thermal generation technologies changes when part-load efficiency losses are excluded for wind capacity scenarios between 10 GW and 45 GW using demand and wind data for 2010.

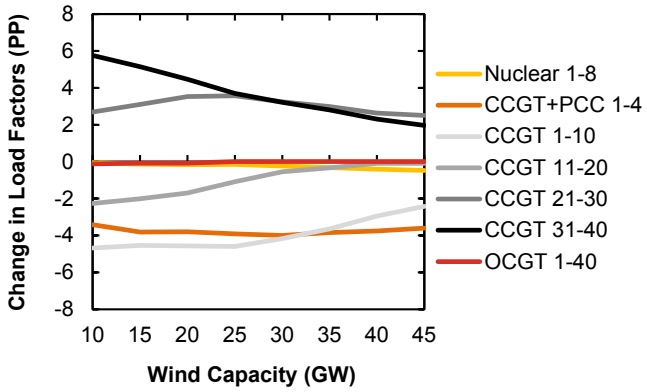

Figure 6.35: Change in the load factors for thermal generation technologies without part-load losses included compared to the base case scenario with wind capacity between 10 GW and 45 GW using demand and wind data for 2010.

This analysis demonstrates the changes that occur to the load factors of thermal generation technologies when part-load losses are excluded. This is to understand the impact of assuming incorrect part-load efficiency characteristics or even excluding part-load efficiency losses from power system studies.

The load factors of baseload units, in particular CCGT+PCC units 1-4 and CCGT units 1-10, decrease significantly when part-load efficiency losses are excluded. This is because without part-load losses it costs the same per MWh of electricity generated to operate thermal power plants at part-load (since no additional losses are incurred). The UCED model therefore dispatches more thermal units to operate at part-load and for longer periods of time since there is no additional cost per MWh. This generally decreases the load factors of baseload units and improves the load factors of peaking plant.

In the base case scenario, it is more expensive to operate thermal units at part-load so the UCED model dispatches units to either operate at higher efficiencies or shuts them down (to avoid increased costs from operating at part-load).

The error in the average annual load factor is as high as 5.8 percentage points i.e. when part-load losses are included the load factors of CCGT units 31-40 are on average 13.0% and after excluding part-load losses the load factors increase to 18.8%. This highlights the importance of using accurate part-load efficiency curves for thermal power plants to reduce dispatch errors.

Impacts on start-up requirements

Figure 6.36 shows how the start-up requirements of the thermal generation portfolio changes when part-load losses are excluded compared to the base case scenario with 30 GW of wind capacity. When part-load efficiency losses are excluded, it is cheaper to operate thermal power plants at part-load for extended periods of time instead of shutting down. This generally reduces the start-up requirements and the number of hot and warm start-ups for CCGT units.

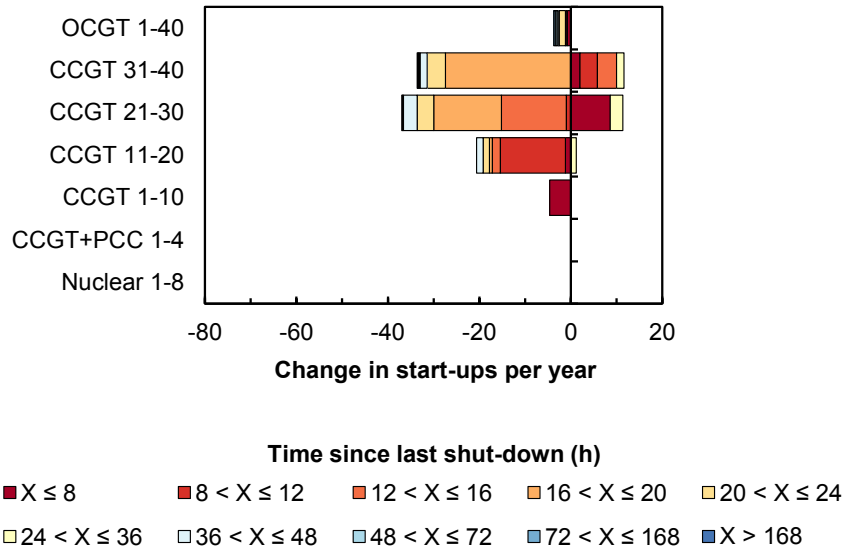

Figure 6.36: Change in the number of start-ups per year categorised by time since last shut-down compared to the base case scenario for thermal generation technologies when part-load losses are excluded with 30 GW wind capacity using demand and wind data for 2010.

6.5.3 Impacts of increased ramp rates

Introduction

Typically, faster ramp rates benefit power plants with a larger operating range. Power plants with slower ramp rates will have higher operating costs since they are not able to operate at their economic optimal load [Haynes, 1987]. Power plants with faster ramp rates, on the other hand, are able to immediately adjust their output to their economic optimal load. This should reduce the impacts of dispatch errors and improve fuel efficiency. In addition, power plants with infinite ramp rates can provide more of their capacity as reserve. This should decrease the

number of part-loaded thermal units providing reserve requirements and lead to further fuel and CO_2 savings. However, power plants with faster ramp rates are also able to start-up and shut-down faster. This should increase the number of start-ups and possibly increase start-up and shut-down costs. To explore this, a case study where thermal power plants have infinite ramp rates is assessed.

The base case scenario, where power plants are limited by the ramp rates detailed in Table 6.2, is compared to the same system but where power plants have infinite ramp rates. In other words, power plants can now rapidly adjust their power outputs in response to wind imbalances or variations in net demand between their minimum an maximum power output limits. The base case scenario represents a system with limited ramping capability where most units have modest maximum upwards/downwards ramp rate limits of 5 MW/min. It should be noted that power plants still incur ramping costs when changing power output. The only difference is that now all power plants can ramp faster. This is to understand the value of faster ramp rates to power systems with increasing proportions of wind capacity.

Impacts on system costs

Figure 6.37 shows the change in total system short-run costs between the base case scenario, where ramp rates are included, and the scenario where both upwards and downwards ramp rates are infinite. A positive increase on the y-axis describes an increase in costs compared to the base case scenario i.e. where increased ramp rates increase system costs. A decrease on the y-axis represents a decrease in costs or a saving in costs compared to the base case scenario.

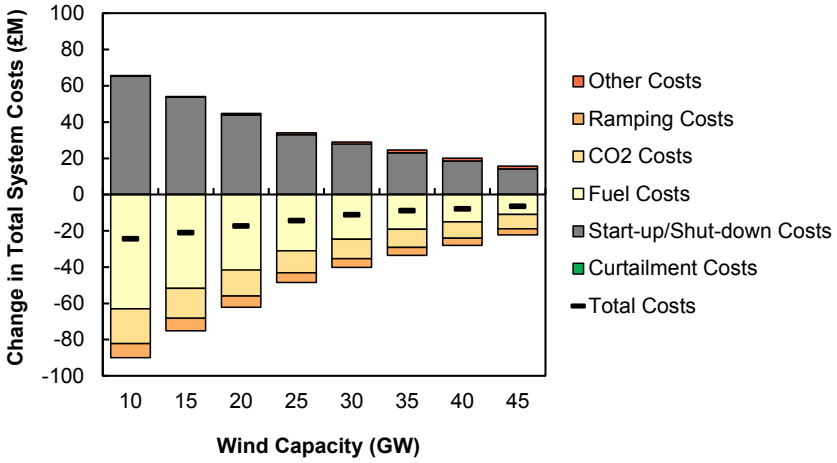

Figure 6.37: Change in total system short-run costs for base case generation portfolio with infinite ramp rates with wind capacity between 10 GW and 45 GW using demand and wind data for 2010.

For each wind capacity scenario, there is a small decrease in fuel, CO_2 and ramping costs. This is caused by an increase in the utilisation of more efficient and less expensive power plants

such as CCGT+PCC units 1-4 and CCGT units 1-10 and a decrease in the utilisation of less efficient and more expensive power plants such as CCGT units 21-40.

A power system with infinite ramp rates utilises baseload and efficient units slightly more, which decreases the energy and ramping requirements of less efficient and more expensive thermal units lower in the merit-order. Increased ramp rates also allow power plants to rapidly adjust power output to meet changes in net demand. When net demand falls, more expensive power plants reduce output and shut-down to reduce costs. However, this increases the number of start-ups for less efficient power plants lower in the merit-order, increasing start-up/shut-down costs.

Overall, the total cost savings are very small. For example, with the 10 GW wind capacity scenario, the total system costs decrease by £24.4 million per year, just 0.18% of total system costs. With 45 GW of wind capacity the cost savings reduce to £6.5 million or 0.07% of total system costs. Since fuel and CO_2 costs are generally lower with larger amounts of wind, the reduction in fuel and CO_2 costs is also smaller.

The ability of thermal power plants to provide reserve is limited by its ramp rate over a given time period, see Equations 5.84 and 5.85. For thermal units without ramp rate limitations, the upwards and downwards spinning reserve contributions become:

$$R_{g,t}^{\mathrm{SR,up}} \leq u_{g,t} P_{g,\max} - P_{g,t} \tag{6.10}$$

$$R_{g,t}^{\mathrm{SR,dn}} \leq P_{g,t} - u_{g,t} P_{g,\min} \tag{6.11}$$

Increased ramp rates therefore allow power plants to provide additional amounts of their capacity as reserve, reducing the number of part-loaded units that are required to provide reserve services. This cost saving is reflected in Figure 6.37.

The results show that increased ramp rates increase the utilisation of more efficient units which improves fuel efficiency and leads to fuel and CO_2 cost savings, but also reduce the energy requirements of less efficient units, forcing them to shut-down more frequently. This is explored below in more detail by analysing the change in load factors between scenarios of increasing wind capacity.

Impacts on CO_2 emissions

The CO_2 emissions of the system with infinite ramp rates is between 0.19-0.26 $MtCO_2$ lower than the CO_2 emissions of the base case scenario with ramp rates enforced for wind capacities between 10 GW and 45 GW. This corresponds to a reduction of approximately 0.35-0.42% of the total system CO_2 emissions of the base case scenario. The results show that increased ramp rates reduces CO_2 emissions across all wind capacity scenarios. This is to be expected since increasing power plant ramp rates allows units to operate at their economic optimal loads.

Table 6.11 shows how the CO_2 emissions change with increasing wind capacity for the scenarios with infinite and normal ramp rates.

Wind Capacity (GW)	Base Case Total CO_2 Emissions ($MtCO_2$)	Inf RR Total CO_2 Emissions ($MtCO_2$)	Change in CO_2 Emissions (% of total)
10	74.39	74.13	-0.356
15	69.68	69.44	-0.343
20	65.03	64.80	-0.355
25	60.31	60.10	-0.356
30	55.71	55.52	-0.357
35	51.46	51.25	-0.394
40	47.53	47.33	-0.418
45	44.05	43.86	-0.424

Table 6.11: Total CO_2 emissions for base case and infinite ramp rate (RR) scenarios and the change in CO_2 emissions expressed as a percentage of the total base case CO_2 emissions with wind capacity between 10 GW and 45 GW using demand and wind data for 2010.

Impacts on load factors

The change in load factors of thermal power plants with infinite ramp rates compared to the base case scenario is shown in Figure 6.38. With low levels of installed wind capacity, the load factors of more efficient thermal power plants, such as CCGT units 1-20, increase and the load factors of less efficient and more expensive thermal power plants decrease. For example, in the 10 GW wind capacity scenario, for a system with infinite thermal plant ramp rates, the load factors of CCGT units 1-20 are approximately 1.8 percentage points higher than for a system with the ramp rates detailed in Table 6.2. The average load factor for CCGT units 1-10 with infinite ramp rates is 91.9% but when ramp rates are enforced the average load factor drops to 90.1%.

The results show that increasing the ramp rates of all thermal units changes the load factors of thermal power plants in different ways depending on the level of installed wind capacity.

They also demonstrate the sensitivity of system costs and thermal plant load factors to changes in ramp rates. Additionally, this work highlights the importance of using accurate ramp rates when modelling thermal power plants as this can lead to dispatch errors and changes in load factors. However, there is only a small decrease in total system costs when the ramp rates of thermal power plants are increased.

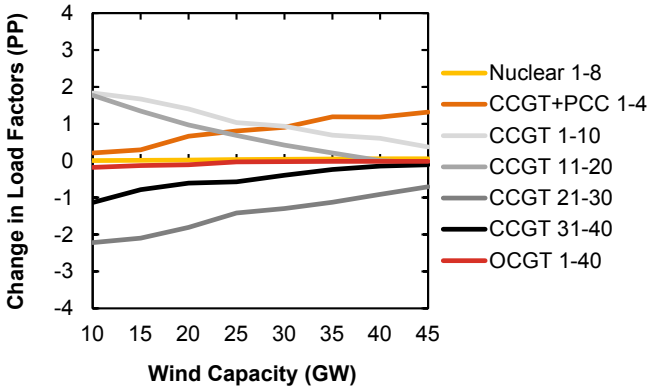

Figure 6.38: Change in the load factors for thermal generation technologies with infinite ramp rates compared to the base case scenario with wind capacity between 10 GW and 45 GW using demand and wind data for 2010.

Impacts on start-up requirements

Figure 6.39 shows how the start-up requirements of the thermal generation portfolio changes when ramp rates are increased compared to the base case scenario with 30 GW of wind capacity. With infinite ramp rates, CCGT units 21-30 perform nearly 50 additional start-ups per year when ramp rates are increased. As discussed previously, more efficient power plants higher in the merit-order, such as CCGT units 1-20, are able to rapidly adjust output to meet net demand variations and provide increasing amounts of their capacity as reserve. Increasing the ramp rates of baseload and less expensive power plants reduces the energy and ramping requirements of more expensive CCGT units 21-40. More expensive power plants can also rapidly reduce power output when net demand falls and shut-down to reduce costs. However, when net demand increases, these power plants are required to then start-up again. This increases the start-up requirements for these units.

In the infinite ramp rate scenario, the start-up requirements of OCGT units reduces compared to the base case scenario. This is because in the base case scenario, with limited upwards/downwards flexibility, OCGT units are required at certain times to provide ramping and reserve services to meet unexpected variations in net demand. When ramp rates are infinite, there is a reduced need for OCGT units to provide flexibility.

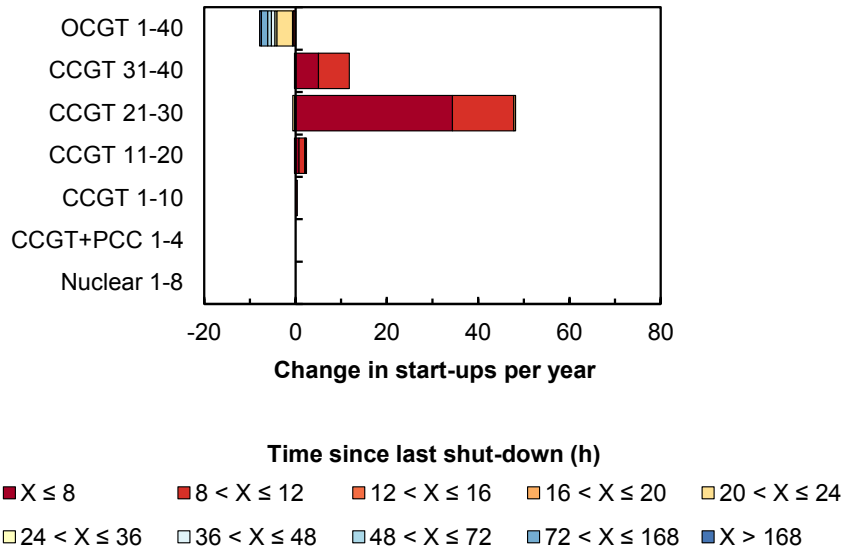

Figure 6.39: Change in the number of start-ups per year categorised by time since last shut-down compared to the base case scenario for thermal generation technologies with infinite ramp rates compared to the base case scenario with 30 GW wind capacity using demand and wind data for 2010.

6.5.4 Impacts of reduced minimum up/down times

Introduction

Thermal power plants have minimum up and down times which ensures they remain online or offline for a minimum number of hours. Power plants with lower minimum up/down times are expected to have more flexible operating regimes since they are not committed to remain in the same state for a minimum number of hours. This will allow power plants to change states more frequently and hence improve the operational flexibility of the system and reduce costs.

The base case scenario, where power plants are limited by the minimum up/down times detailed in Table 6.2, is compared to the same system but where minimum up/down times are set to 1 hour. Whilst this is unrealistic for a large CCGT power plant, the purpose of this exercise is to estimate the upper bound of cost savings that could be achieved if power plants were not limited by minimum up/down times.

Impacts on system costs

Figure 6.40 shows the change in total system short-run costs compared to the base case scenario assuming 30 GW of wind capacity scenario. Minimum up/down times for all units are set to 1 h. However, this only affects CCGT units since OCGT units already have minimum up/down times of 1 h and nuclear and CCGT+PCC units are assumed to be must run. Therefore, the reduction in total system costs is attributed to the savings from reducing the minimum up/down times of CCGT units from 4 h to 1 h. The cost savings are, however, very small compared to inter-annual changes in wind output.

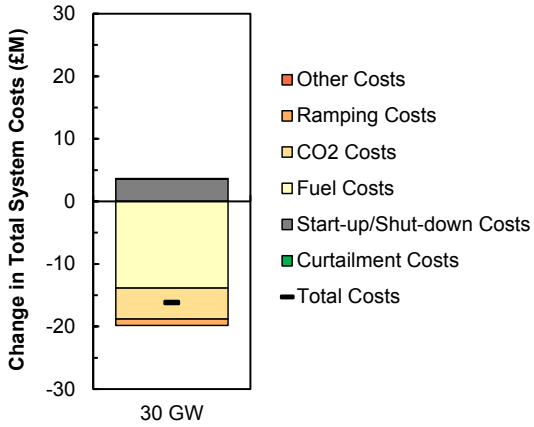

Figure 6.40: Change in total system short-run costs compared to base case generation portfolio when minimum up/down times are 1 h with 30 GW of wind capacity using demand and wind data for 2010.

6.5.5 Impacts of reduced start-up and shut-down costs

Introduction

Reducing start-up and shut-down costs decreases the resistance to change states and makes frequent start-up/shut-downs less expensive, increasing flexibility, compared to a system with high start-up and shut-down costs [Rosnes, 2008].

The base case scenario, with high start-up and shut-down costs, is compared to the same scenario but now start-up and shut-down costs for thermal units are lower. This is to understand the impacts of reduced start-up and shut-down costs on power system operation.

In the base case scenario, CCGT units have fixed start-up costs $c_g^{\text{start,fixed}}$ = £10000 per start and start-up fuel $F_g^{\text{start,cold}}$ = 1500 MWh_{th} for cold start-ups. In the low start-up and shut-down cost scenario, $c_g^{\text{start,fixed}}$ = £5000 per start and $F_g^{\text{start,cold}}$ = 750 MWh_{th}.

Impacts on system costs

Figure 6.41 shows the change in system short-run costs compared to the base case scenario when start-up and shut-down costs are reduced by a factor of two for thermal power plants. The most obvious feature is that start-up and shut-costs are lower than the base case scenario. However, there are also lower fuel, CO_2 and ramping costs as power plants are more likely to shut-down instead of remaining at minimum load. The analysis shows that reduced start-up and shut-down costs produces fuel and CO_2 savings in the order of £52 million per year. Decreasing power plant start-up and shut-down costs increases operational flexibility as power plants are able to change states with less resistance.

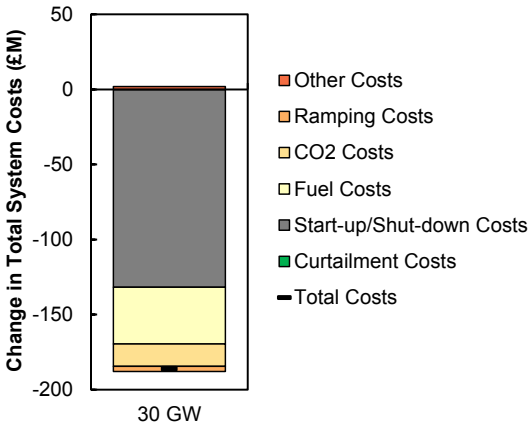

Figure 6.41: Change in total system short-run costs compared to base case generation portfolio when start-up/shut-down costs are reduced by a factor of two with 30 GW of wind capacity using demand and wind data for 2010.

Impacts on start-up requirements

Figure 6.42 shows how the start-up requirements of the thermal generation portfolio changes when start-up and shut-down costs are reduced compared to the base case scenario with 30 GW of wind capacity. Decreasing the start-up costs by a factor of two increases the number of start-ups for CCGT units 1-40 and OCGT units. Most of the increase in start-ups are hot start-ups where the power plant shuts down for a period of less than 8 h.

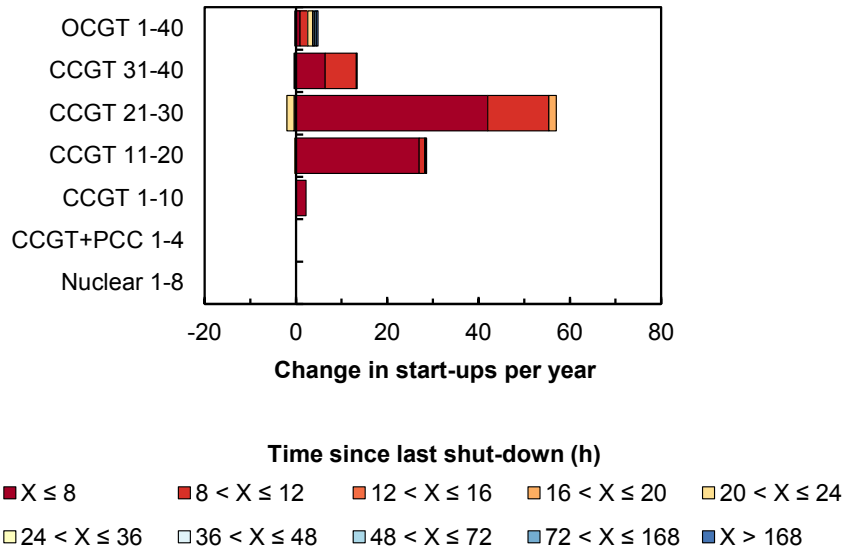

Figure 6.42: Change in the number of start-ups per year categorised by time since last shut-down compared to the base case scenario for thermal generation technologies when start-up/shut-down costs are reduced by a factor of two with 30 GW wind capacity using demand and wind data for 2010.

6.5.6 Summary

This section analysed a number of key sensitivities such as the part-load losses of thermal power plants, ramp rates, minimum up/down times, and start-up/shut-down costs. The results show that system costs, CO_2 emissions and power plant load factors change when part-load losses are excluded. This highlights the importance of modelling part-load efficiency losses in unit commitment studies.

The results also show that power plant operating regimes are sensitive to changes in ramp rates, minimum up/down times and start-up/shut-down costs. Compared to the base case scenario, total system costs fall very slightly when ramp rates are infinite. CO_2 emissions also fall by approximately 0.35-0.42% compared to the base case scenario with infinite ramp rates. Load factors of thermal units are also sensitive to changes in ramp rates. The load factors of less expensive units increase and the load factors of more expensive units decrease with lower installed wind capacities (i.e. 10 GW wind capacity).

Reducing the start-up and shut-down costs of thermal units decreases total system costs. Power plants are able to shut-down more economically and so spend less time at minimum load. This results in fuel and CO_2 cost savings compared to the base case scenario.

6.6 Flexible CO_2 capture and energy storage case study

6.6.1 Introduction

A case study is introduced to highlight some important interactions that occur between energy storage and flexible CO_2 capture. The UCED model is tested using wind and demand data for the first working week (168 h) in January 2010. Figure 6.43 shows the time-series of demand data and onshore/offshore wind data used in the case study. A large number of additional tests are also performed with various fuel prices, CO_2 prices and demand-wind input data to ensure the model produces credible results across a range of system conditions and to improve model robustness.

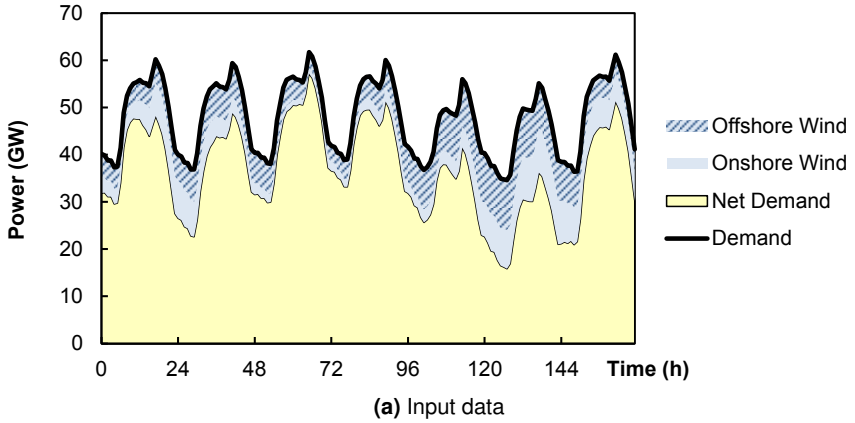

Figure 6.43: Input demand and wind profiles for the case study with 30 GW of wind capacity for the first week in January 2010.

This illustrative case study is developed to demonstrate the operation of four energy storage units and four 900 MW CCGT power plants equipped with flexible CO_2 capture units. The thermal generation portfolio and energy storage units are scheduled to meet electricity demand and provide reserve and flexibility requirements. The technical and cost characteristics of CO_2 capture units are outlined in Table D.5. The scenarios use wind and demand data from 2010 and assume 15 GW, 30 GW and 45 GW of installed wind capacity. The case study assumes a CO_2 price of £50/tCO_2 to understand the impacts of high CO_2 prices on the operation of CO_2 capture plants. The natural gas price is assumed to be £23.9/MWh. The electricity price is simulated for each time step and is used to optimise the charge/discharge profiles for each energy storage unit and flexible CO_2 capture plant. The results are presented at delivery time after power plants have been re-dispatched to meet realised net demand.

6.6.2 Case study results

Electricity prices

Figure 6.44 shows the simulated electricity price for the case study with 30 GW of wind. The simulated electricity price includes the marginal cost of the marginal 'price-setting' generator, the time-weighted start-up/shut-down cost, and price mark-up/mark-down functions to account for an under/over supply of electricity.

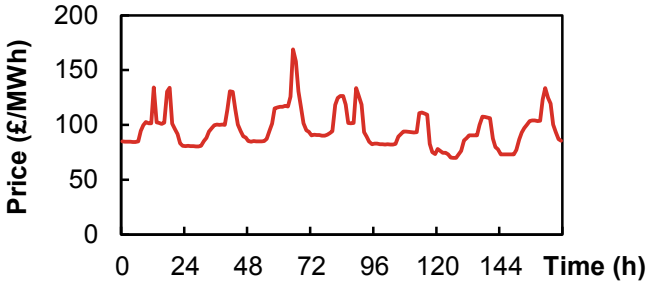

(a) Electricity price (£/MWh)

Figure 6.44: Simulated electricity price for the illustrative case study with 30 GW of wind capacity using data for the first working week in January 2010.

Generation dispatch patterns

Figure 6.45 displays the power outputs for each generation technology over the time horizon. Nuclear power plants are continuously operated at their maximum power output limits. CCGT units provide the majority of intermediate generation with OCGT units only operating when there is a large unexpected change in wind output or when electricity demand is high.

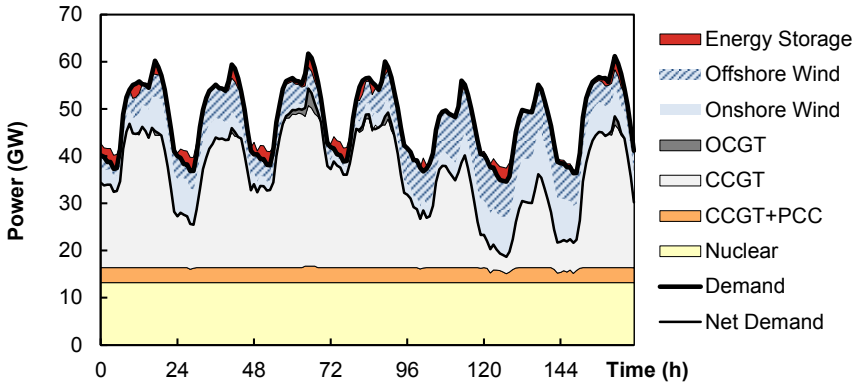

(a) Power outputs by generation technology (GW)

Figure 6.45: Power outputs by generation technology for the illustrative case study with 30 GW of wind capacity using data for the first working week in January 2010.

For a CO_2 price of £50/tCO_2, the SRMC of CCGT+PCC units is lower than the SRMC of efficient CCGTs so CCGT+PCC units operate higher in the merit-order. During periods of

high wind output and low demand, CCGT+PCC units part-load to accommodate more wind generation. During periods when electricity prices are very high, CCGT+PCC units bypass their capture plants and vent CO_2.

CCS-equipped power plant operation

Figure 6.46a shows the power outputs of CCGT+PCC units 1-4 over the time period. During periods when the electricity price is very high, it is more profitable for CCGT+PCC units to bypass capture and vent CO_2 to the atmosphere. This incurs additional CO_2 costs but if the revenue gained from selling the additional electricity is more than the increase in costs then CO_2 capture plants are bypassed. During times when net demand is low, CCGT+PCC units reduce load. This impacts the total CO_2 emissions that are captured by the four PCC units, as shown in Figure 6.46b.

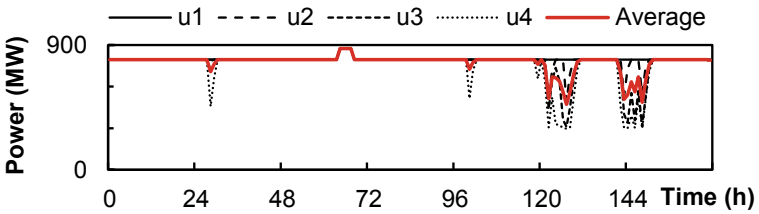

(a) Power outputs of CCGT+PCC units 1-4 (MW)

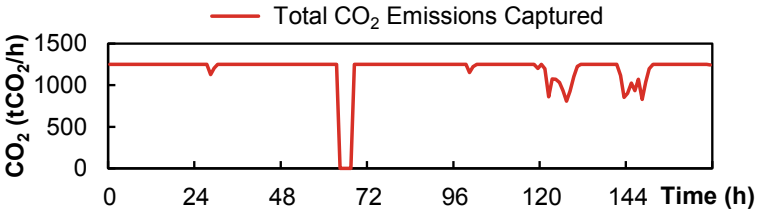

(b) Total CO_2 emissions captured by CCGT+PCC units 1-4 (tCO_2/h)

Figure 6.46: Power outputs and captured CO_2 emissions for CCGT+PCC units 1-4 for the illustrative case study with 30 GW of wind capacity using data for the first working week in January 2010.

Flexible CO_2 capture power plants ramp up with the base power plant and turn off when electricity prices are very high. One bypass event occurs that lasts for four hours. Bypass events coincide with OCGT and energy storage output when electricity prices are very high. Capture plant bypass reduces the need for peaking plant to come online for short periods of time, reducing start-up and energy requirements. During periods of low net demand, the base CCGT power plant reduces power output with the PCC units reducing load equivalent to the CO_2 emissions of the base power plant. Flexible CO_2 capture systems also provide upwards reserve when capture rates are at 90% since they have the capability to reduce the capture rate to zero and increase power output.

It is likely that enabling capture plant bypass would reduce the need for additional peaking plant generation and reduce the number of peaking plant start-ups. The interactions between peaking plant, energy storage and flexible CO_2 capture systems with bypass capability should be further explored.

CCS-equipped power plant revenue

Figure 6.47 shows the revenues of CCGT+PCC units 1-4 over the time period with flexible capture (FC) and for the base case (BC) scenario without flexible CO_2 capture. This illustrative case study shows that enabling flexible CO_2 capture slightly increases the revenue from the sale of electricity. Bypassing the CO_2 capture plant increases the amount of electricity that can be exported and so increases revenue.

Increasing wind generation over the time period suppresses the electricity price and therefore reduces the revenue available for CCGT+PCC units. This effect is most noticeable between 30 GW and 45 GW of wind capacity.

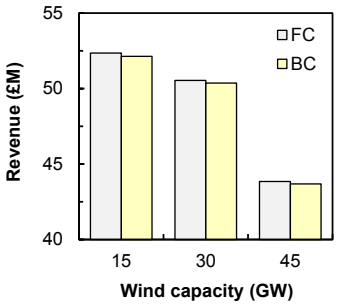

(a) Revenue (£M)

Figure 6.47: Total revenues for CCGT+PCC units 1-4 for the illustrative case study with flexible capture (FC) and for the base case (BC) scenario without flexible CO_2 capture with 15 GW, 30 GW, and 45 GW of wind capacity using data for the first working week in January 2010.

Energy storage operation

The optimal charge/discharge profiles for each of the energy storage units are shown in Figure 6.48a. The positive values on the y-axis are the power outputs that are generated by the discharging of energy from the storage units. The negative values on the y-axis are the power inputs that are consumed by energy storage units that are charging. The total output of all four units is shown in red. The aggregate profile of the portfolio of energy storage units is smoothed but is heavily influenced by storage unit s_1 since it is by far the largest.

Energy storage units are utilised least with 45 GW of wind capacity (compared to scenarios with 15 GW and 30 GW of wind capacity) since larger amounts of wind generation displaces

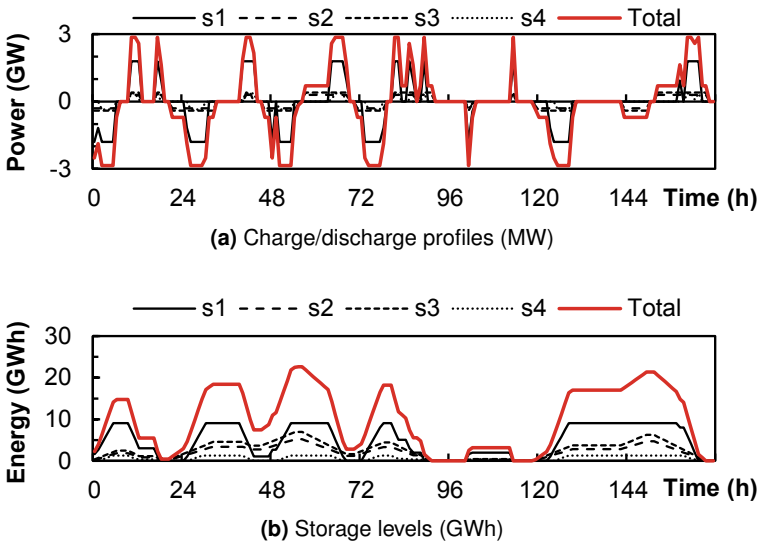

Figure 6.48: Energy storage charge/discharge profiles and storage levels for the illustrative case study with 30 GW of wind capacity using data for the first working week in January 2010.

marginal price-setting thermal units and suppress the electricity price. This reduces the opportunities for price arbitrage and hence reduces the utilisation of price-sensitive energy storage units.

Figure 6.48b shows the storage level for each of the energy storage units over the optimisation period. Each of the units behaves differently when exposed to the same electricity price time-series. Unit s_4 has the most diurnal charge/discharge cycle because of its low maximum storage level of 1.3 GWh. In addition, unit s_1 has a short storage durations and so also observes a typical daily charge/discharge cycle.

Energy storage model convergence

In the case above, the algorithm converges on the optimal solution to 99% accuracy within 47000 iterations and 99.9% within 73000 iterations, see Figure 6.49. It takes approximately 8 s for the algorithm to compute 100000 iterations for each energy storage unit. The algorithm is performed once at the UC stage (for each energy storage device) and once again at the ED stage.

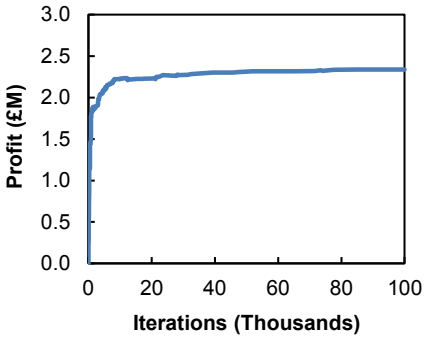

Figure 6.49: Energy storage optimisation algorithm convergences on upper boundary of the operating profit available as a result of time-shifting energy for unit s_1 with 30 GW of wind.

Energy storage profit

The total profits from arbitrage opportunities for energy storage units are shown in Figure 6.50a. Unit s_1 is the largest in terms of installed charging/discharging capacity so it gains a larger profit over the time period. The profit that each storage unit receives as a result of time-shifting energy is observed to fall with increasing wind capacity. The fall in energy storage operating profits occurs because thermal generation capacity remains constant as wind capacity rises. This is also explained by the fact that increased wind generation displaces the more expensive price-setting thermal power plants and so reduces the system marginal price. This makes it cheaper for energy storage devices to purchase energy but also reduces the periods where electricity prices are high.

The fall in operating profits between the 15 GW and 30 GW wind capacity scenarios is roughly the same for each storage unit. However, storage units with shorter storage durations observe larger decreases in operating profits with increasing wind capacity. For example, storage units s_1 and s_4, with storage durations of 5.1 h and 3.6 h, observe the largest fall in operating profits, yet storage units s_2 and s_3, with storage durations of 21.0 h and 25.0 h, observe a slightly smaller fall in operating profits.

Figure 6.50b shows the profits from time-shifting energy for each of the units as a function of the maximum charge/discharge power (MW). In this case, units s_2 and s_3 receive the largest profits as a function of the maximum charge/discharge power.

Figure 6.50c shows the operating profits as a function of the maximum storage volume (MWh). Storage units with larger stores are shown to have lower profits per MWh.

Figure 6.51 shows the average storage levels of the four storage devices with increasing wind capacity. The storage units with longer storage durations take more hours charging at full capacity to fill up their stores. This means that on average their storage levels are lower. With increasing wind capacity, the storage devices with longer storage durations utilise their stores more.

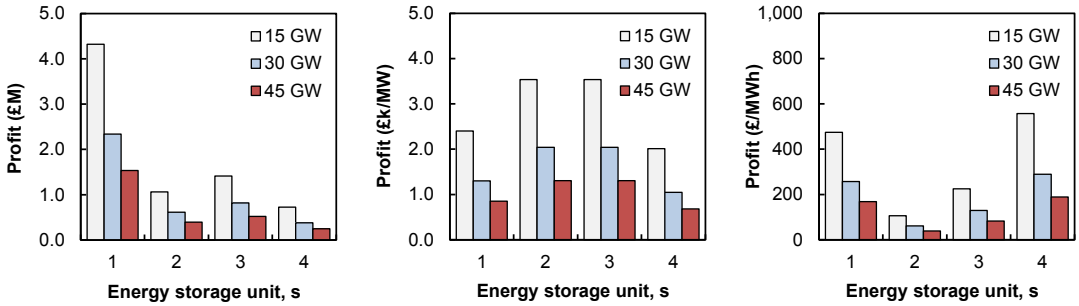

(a) Total profit **(b)** Profit per MW **(c)** Profit per MWh

Figure 6.50: Operating profit as a function of the maximum charge/discharge power and maximum storage volume for the four energy storage units described in Table 6.3 using demand-wind data for the first week in January 2010.

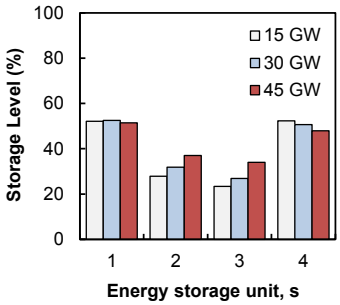

(a) Storage level (%)

Figure 6.51: Average energy storage levels for the four energy storage units described in Table 6.3 using demand-wind data for the first week in January 2010.

The results demonstrate that the energy storage and UCED models are able to capture significant details about the operation of energy storage units in response to varying electricity prices. Interesting trends in profit are revealed with regards to the sizes and volumes of energy storage devices. Further work should expand on this simple case study to understand the annual impacts of increasing wind capacity on energy storage profitability and operation. Developing the energy storage portfolio to include additional energy storage units and technologies with varying characteristics, such as round-trip efficiency, would also be of interest.

6.7 Impacts of CO_2 capture plant bypass

6.7.1 Introduction

The base case generation portfolio contains four CCGT units retrofitted with integrated post-combustion CO_2 capture (PCC). The work in Sections 6.3, 6.4, and 6.5, however, assumed that these units cannot bypass their CO_2 capture units or adjust their CO_2 capture rates. This means that the CCGT+PCC units in the base case scenario have a constant CO_2 capture rate of 90%. However, it is likely that thermal power plants equipped with PCC may bypass their CO_2 capture systems and vent CO_2 to the atmosphere. It is likely that this will occur when demand for electricity is high and the price of CO_2 is low.

This simple case study investigates the impacts of flexible CO_2 capture units that can bypass their CO_2 capture systems and vent CO_2 to the atmosphere. This is done for a range of CO_2 prices and transport and storage costs to understand the sensitivity of CCS-equipped power plant operation to CO_2 and electricity prices.

6.7.2 Flexible CO_2 capture

Chalmers and Gibbins [2007] introduced the concept of decision diagrams that illustrate the choice between capturing CO_2 or bypassing. Chalmers [2010]; Chalmers *et al.* [2012] then extended this concept for a broader range of input assumptions and operating modes for pulverised coal power plants.

Figure 6.52 shows the decision diagrams for the CCGT+PCC units with bypass capability with increasing fuel costs. The technical parameters and costs of these units are provided in Section 6.2.2 and Table D.5. CCS-equipped power plants can now bypass their CO_2 capture units and vent CO_2 to the atmosphere when it is profitable for them to do so.

The objective function of flexible CO_2 capture units is to maximise the operating profit by adjusting the CO_2 capture between zero and 90%:

$$\Pi_{g,t} = \max\left(\left(\overbrace{(P_{g,t} - P_{g,t}^{\text{capt}}) \cdot \pi_t}^{\text{Revenue}} \right) - \left(\overbrace{C_{g,t}^{\text{fuel}} + C_{g,t}^{\text{O\&M}} + C_{g,t}^{\text{ramp}} + C_{g,t}^{\text{O\&M,capt}} + C_{g,t}^{\text{solv}} + C_{g,t}^{\text{trans}} + C_{g,t}^{\text{CO}_2}}^{\text{Costs}} \right) \right) \tag{6.12}$$

where $\Pi_{g,t}$ is the operating profit in each time period, π_t is the simulated electricity price, $P_{g,t}$ is the power output of the base power plant and $P_{g,t}^{\text{capt}}$ is the power consumption of the CO_2 capture plant. Operating costs include fuel costs and variable O&M costs of the base power plant; and CO_2 costs, variable O&M costs, solvent costs and transport costs of the CO_2 capture plant. Flexible CO_2 capture units are able to reduce their CO_2 capture rates to zero if it increases their operating profits.

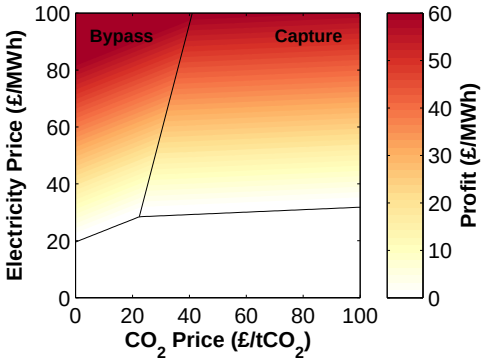

(a) Natural gas price – £10/MWh

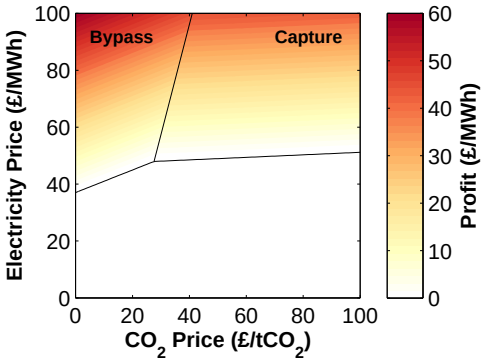

(b) Natural gas price – £20/MWh

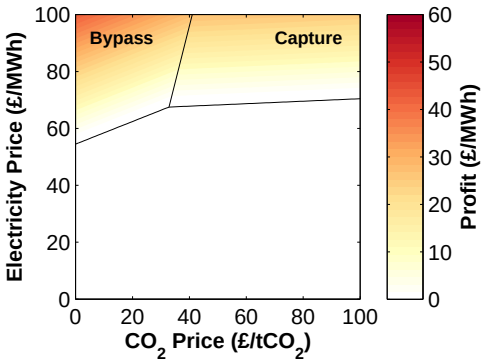

(c) Natural gas price – £30/MWh

Figure 6.52: Decision diagrams for CCGT+PCC units that can either bypass the CO_2 capture systems or capture CO_2 at 90%.

The lines in Figure 6.52 show the boundaries between areas where it is either more profitable to capture CO_2 or to bypass. There is also a region where the CCGT+PCC unit would not operate at all because the electricity price is not enough to cover its short-run marginal costs.

Figure 6.53 shows the sensitivity of CCGT+PCC units to changes in the CO_2 transport and storage costs. When CO_2 transport and storage costs are increased from £10/tCO_2 (base case) to £20/tCO_2 the profitable operating space decreases. CCS-equipped units require increasing CO_2 prices in order to capture CO_2.

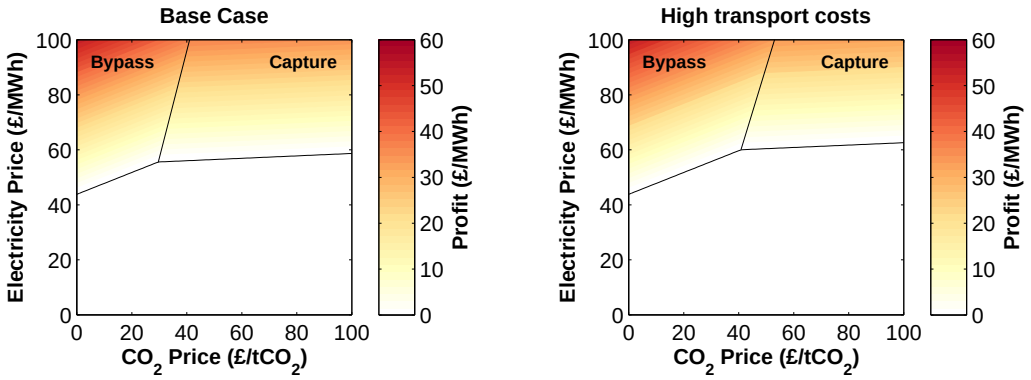

(a) CO_2 transport and storage cost – £10/tCO_2 **(b)** CO_2 transport and storage cost – £20/tCO_2

Figure 6.53: Decision diagrams with varying CO_2 transport and storage costs where CCGT+PCC units can either bypass the CO_2 capture plant or capture 90% of the CO_2. The natural gas price is £23.9/MWh.

A linear optimisation technique is used to calculate the optimal CO_2 capture rate between 90% and 0% that maximises the operating profit in Equation 6.12. This case study example assumes that the optimal design point for CO_2 capture is 90%. In reality, PCC plants may operate at CO_2 capture rates higher than their design point if CO_2 abatement is more valuable [Errey *et al.*, 2014]. However, for the purpose of this work the maximum CO_2 capture rate is assumed to be 90%.

A preliminary investigation found that for a range of CO_2 prices and fuel costs there are very few instances where the optimal CO_2 capture rate is between 90% and 0%. The findings showed that either it is more profitable to operate at 90% capture rate or it is optimal to operate at 0% capture rate. Therefore, to simplify the optimisation problem and increase the computational speed, this case study assumes that the CO_2 capture rate $Y_{g,t}^{\text{capt}}$ is either zero or 90%.

A plant operator has the decision to either capture CO_2 at 90% or bypass the CO_2 capture unit, in effect reducing the CO_2 capture rate to zero. If the PCC unit is bypassed and CO_2 is vented to the atmosphere, the CCGT+PCC unit is able to increase net power output from 795 MW (90% capture rate) to 875 MW (zero capture rate). The maximum power output that can be exported is 875 MW (not 900 MW) since the CO_2 capture unit is assumed to have a fixed power consumption of 25 MW.

It may be financially beneficial to fully bypass the residual ancillary power consumption of the CO_2 capture plant (25 MW) during certain periods (i.e. where electricity prices are very high). However, this work assumes that at least some ancillary CO_2 capture plant equipment is required during bypass to enable faster start-ups after bypass [Errey *et al.*, 2014].

The system impacts of flexible CO_2 capture plant bypass with increasing CO_2 costs is now presented.

6.7.3 System impacts

In the base case (BC) scenario, CO_2 capture units must capture 90% of the CO_2 from the base power plant. They do not have the option to bypass their CO_2 capture systems. In the flexible capture (FC) scenario, CO_2 capture units can bypass or capture at 90% depending on whether it is more profitable to do so.

Figure 6.53a shows the decision diagram for CCGT+PCC units 1-4 in the base case scenario. With a natural gas price of £23.9/MWh and a CO_2 price of £30/tCO_2, it is almost always profitable to bypass capture and vent CO_2. When the CO_2 price increases to £40/tCO_2, the electricity price must exceed approximately £97/MWh for it to be profitable for the CO_2 capture unit to bypass. The gradient of the line that determines the decision to bypass/capture is very steep. A small increase in the CO_2 price will result in significantly fewer instances where bypass is profitable.

Figure 6.54 shows the system short-run costs in the BC and FC scenarios with CO_2 prices ranging from £30/tCO_2 to £50/tCO_2. The natural gas price is constant between scenarios at £23.9/MWh. For a CO_2 price of £30/tCO_2, as previously discussed, it is more profitable for CO_2 capture units to bypass in the FC scenario. The total costs with a CO_2 price of £30/tCO_2 are almost identical between the two scenarios. Total fuel costs in the base case scenario with a CO_2 price of £30/tCO_2 are £8.30 billion, which decreases to £8.19 billion when flexible capture is enabled. Fuel costs decrease because the electricity output penalty of CCS-equipped units is reduced. However, CO_2 costs increase from £1.62 billion in the base case scenario to £1.87 billion when flexible capture and CCGT+PCC units bypass. This example illustrates a period where the CO_2 price is not high enough to encourage CO_2 capture.

With an increasing CO_2 price, bypass events become less likely because CO_2 abatement is more valuable. With a CO_2 price of £50/tCO_2 the total system short-run costs in the BC scenario are £11.99 billion and reduce to £11.96 billion in the FC scenario. This simple case study illustrates the system short-run cost savings that occur with CO_2 prices higher than £30/tCO_2 when flexible CO_2 capture plant bypass is allowed.

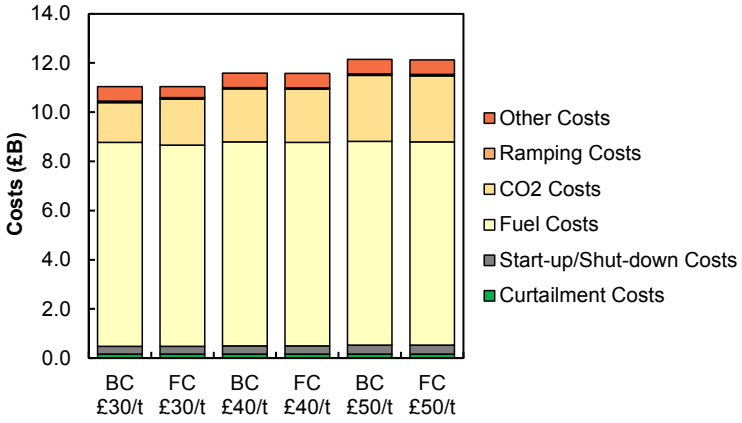

(a) Total system short-run costs

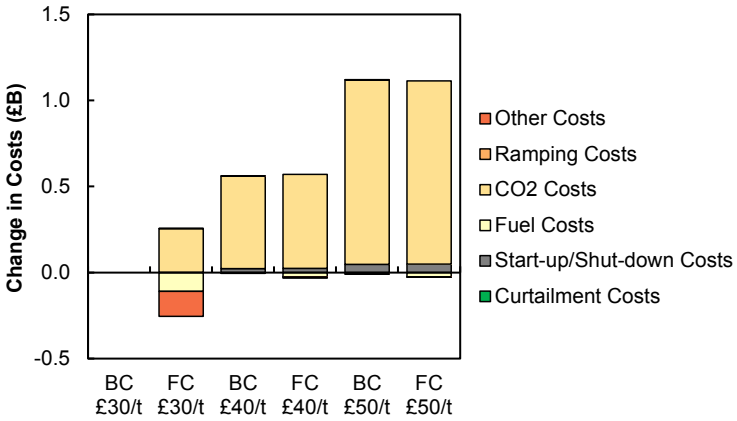

(b) Change in total system short-run costs compared to base case with £30/tCO_2

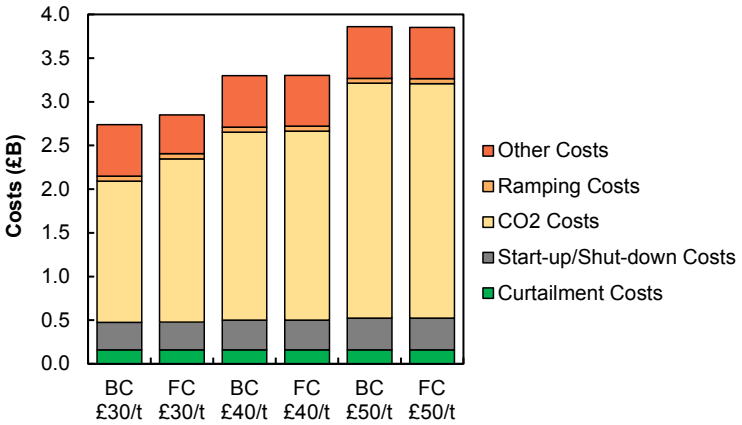

(c) Total system short-run non-fuel costs

Figure 6.54: Total system short-run costs with increasing CO_2 prices for the base case (BC) scenario and flexible capture (FC) scenario with 30 GW of wind capacity using demand and wind data for 2010. In the BC scenario, CCGT+PCC units have a constant CO_2 capture rate of 90% and in the FC scenario CCGT+PCC units can bypass their CO_2 capture units if it is profitable.

6.8 Summary

This chapter presents results for an illustrative thermal generation portfolio with varying proportions of wind capacity. The amount of realised onshore and offshore wind generation and curtailed wind is reported for each wind capacity scenario. Total system costs are then analysed for the base case scenario with increasing wind capacity and inter-annual variations in demand and wind output. The results show that there is a non-linear relationship between total system costs and increasing wind capacity. Certain annual scenarios with low wind output result in higher annual system costs and CO_2 emissions, since more thermal generation is required.

CO_2 duration curves are used to illustrate the changes to the distribution of CO_2 emissions with increasing wind capacity and the marginal CO_2 emissions of the system are analysed. System electricity prices are observed to fall with increasing wind capacity as additional wind generation displaces marginal power plants and suppresses prices.

The load factors of thermal power plants are shown to fall with increasing wind capacity, with certain generation technologies suffering greater reductions in load factors. The load factors of mid-merit generation technologies are most sensitive to inter-annual demand-wind variations. The time that power plants spend online/offline and at minimum load, part-load and full load is then analysed. Less expensive power plants, higher in the merit-order, spend an increasing amount of time either at part-load or at minimum load with increasing amounts of wind capacity.

The start-up requirements of the thermal generation portfolio is analysed with increasing wind capacity. The distribution in hot/warm/cold start-ups changes for different thermal generation technologies. Increasing wind capacity increases the number of start-ups for less expensive and more efficient CCGT units and generally decreases the number of start-ups for more expensive and less efficient thermal units. Ramping duration curves illustrate the magnitude and frequency of ramp events and temporal distributions highlight the seasonal and diurnal ramping requirements of conventional power plants.

The analysis also highlights the importance of accounting for the part-load efficiency of thermal units in energy systems models. The analysis shows that CO_2 emissions are particularly sensitive to changes in part-load efficiency, where annual system CO_2 emissions can be up to 5% lower when part-load efficiency losses are excluded. Excluding or underestimating part-load efficiency losses can therefore underestimate system costs and CO_2 emissions. The results also highlight the value of improved minimum up/down times and reduced start-up and shut-down costs to power systems with large proportions of wind capacity.

Chapter 7

Conclusions

7.1 Thesis summary

This thesis aims to improve understanding of power plant operating regimes in power systems with variable renewable generation, in particular onshore and offshore wind power in GB.

Chapter 2 provides an overview of power system flexibility and reserve requirements. The potential generation flexibility of CCS-equipped thermal power plants is then critically discussed and the work highlights the possible downstream flexibility issues that may affect the operation of CO_2 capture plants. The importance of flexible CCS-equipped units to manage increased flexibility and reserve requirements is also outlined. Chapter 2 also provides an up-to-date literature review of power system integration studies and methods to study power system operation.

Chapter 3 introduces a high-resolution wind resource dataset and an aggregate power curve approach to generate onshore and offshore wind capacity factors. The dataset includes 386 onshore and offshore GB wind farms at existing and proposed wind locations. This is used to represent the expected spatial distribution of onshore and offshore wind turbines to allow analysis of future wind capacity scenarios without knowing the exact timing of new wind installations. The simulated hourly wind capacity factors for operational wind sites are compared with published data, demonstrating that the aggregate power curve approach can produce credible production profiles for onshore and offshore wind in GB.

Chapter 4 presents a detailed analysis of the wind resource dataset to understand wind variability over operational timescales for various future wind scenarios. The work shows that increased wind capacity does not substantially increase wind ramp events as the offshore wind that is installed at later stages in future scenarios is geographically dispersed. It is expected that stakeholders may be able to use the temporally-matched dataset of weather-corrected demand and wind data to investigate additional scenarios and case studies.

Chapter 5 presents a unit commitment and economic dispatch (UCED) model that includes flexible CO_2 capture power plants and energy storage units. A simple electricity pricing model is developed that accounts for the marginal costs of power plants and the time-weighted start-up and shut-down costs. The electricity pricing model also includes a price mark-up and mark-

down function to account for periods where the capacity margin is low and where there are very large proportions of wind generation.

The UCED model balances the requirement for low computational time (several hours to run an 8760 h simulation) and the need to consider all of the key system and unit operating constraints such as ramp rates, minimum and maximum power output limits, start-up times, and minimum up/down times etc. A piece-wise linear approximation of power plant fuel consumption is utilised to represent the part-load efficiency of thermal units and maintain fast solution times. This accurately models the behaviour of part-loaded thermal units, which are increasingly required to provide reserve requirements for wind power. The UCED formulation is adapted and modified to include new decision variables and parameters to include flexible CO_2 capture power plants. The IEEE RTS-96 test system is introduced and used to demonstrate the ability of the UCED model to dispatch conventional thermal power plants and CCS-equipped units to meet demand and provide reserve requirements.

Chapter 6 shows that significant and fundamental changes are likely to occur to power plant operating regimes with increased wind capacity. A number of metrics are used to evaluate power plant operating regimes and the ramping and start-up requirements of thermal power plants for increasing amounts of wind capacity. The start-up requirements change significantly with wind capacity additions, reducing the start-up requirements for thermal power plants lower in the merit-order.

The results also quantify the impacts of inter-annual variations in wind output on system costs, CO_2 emissions and thermal power plant load factors. The work highlights how flexible CO_2 capture systems can contribute towards reserve requirements and provide additional output during peak demand periods. A case study is developed to demonstrate the capability of the UCED model to optimise the operation of energy storage units and flexible CO_2 capture units to maximise operating profit.

This thesis also provides extended insights on the likely operating patterns of CCS-equipped power plants with flexible CO_2 capture units. A sensitivity analysis explores the impacts of increasing CO_2 prices on system costs and capture plant bypass events.

7.2 Contributions

A key contribution of this work is the development of a unit commitment and economic dispatch model and the assessment and analysis of system costs and thermal power plant operating regimes across a range of scenarios that consider increasing amounts of wind, CO_2 prices and thermal power plant operating characteristics. The main contributions of this work are now summarised.

- A series of representative wind deployment scenarios are developed for GB with increasing wind capacity to reflect the expected spatial distribution of onshore and offshore wind capacity in the future. This work quantifies the contributions from onshore and offshore wind to electricity demand and estimates the amount of wind curtailment that occurs across a range of scenarios. An assessment of wind and net demand variability at hourly, daily, seasonal and annual time-scales highlights the changing generation flexibility requirements.
- A dataset is created that consists of temporally-matched weather-corrected electricity demand and simulated wind power outputs over a period of nine years (2002 - 2010). It is hoped that this dataset can be made publicly available and accessible to enable future research efforts to extend the analysis presented in this thesis.
- A novel UCED model is developed with flexible CO_2 capture power plants and energy storage units. Key reserve and flexibility requirements are represented and unit-specific operating constraints such as up/down ramp rates, maximum and minimum power output limits, start-up times, minimum up/down times, and reserve contributions are included to study thermal power plant operating regimes with large proportions of wind.
- CO_2 emissions are analysed for an assumed thermal generation portfolio and the concept of CO_2 emission duration curves are developed to evaluate the impacts of increasing amounts of wind capacity on the distribution of CO_2 emissions.
- A multiple linear regression illustrates the marginal impacts of wind and demand on CO_2 emissions across a range of future UK wind scenarios. This CO_2 emissions analysis considers the marginal impacts resulting from part-load efficiency losses, start-up/shut-down events, and increased reserve requirements for larger amounts of wind.
- Methodology is developed to assess power plant start-up and ramping requirements. The start-up/shut-down costs and number of hot/warm/cold start-ups are quantified for various wind capacity scenarios and ramping duration curves are employed to highlight the changes in ramping requirements for thermal power plants resulting from increased wind generation capacity.

7.3 Key findings and conclusions

The work in this thesis is mainly focused on the impacts of wind on an assumed thermal generation portfolio with CCS. The main conclusions are summarised below.

- Annual wind capacity factors vary significantly between years with a strong seasonal variation observed for the onshore wind fleet, with capacity factors lowest in summer months. A slight diurnal variation is also observed for the onshore wind fleet and for offshore wind farms close to the coastal boundary.
- Increasing amounts of offshore wind capacity smooths wind output variability and reduces the magnitude of wind ramp events. Onshore wind ramp events are more extreme

than offshore wind ramps since the majority of onshore wind capacity is geographically concentrated in the centre of GB. There is also observable inter-annual variations in wind ramp events, with some years experiencing more extreme upwards and downwards ramps. Both upwards and downwards onshore wind ramp events are more extreme in winter months.

- There is a non-linear relationship between increasing wind capacity and fuel and CO_2 costs. Increasing amounts of wind capacity increases the proportion of thermal units required to provide reserve. This increases part-load efficiency losses and the additional fuel and CO_2 costs associated with operating at part-load.
- A sensitivity analysis examines the impacts of part-load efficiency losses on power plant load factors, system costs and CO_2 emissions. Scenarios that include and exclude part-load efficiency losses are compared side-by-side to highlight the importance of modelling the part-load efficiency of power plants. Excluding part-load efficiency losses causes dispatch errors and underestimates costs and CO_2 emissions.
- An illustrative case study investigates the impacts of ramp rates, minimum up/down times, and start-up/shut-down costs of thermal power plants as a sensitivity to understand the impacts of these parameters on power plant operating regimes. Changing these parameters causes dispatch errors and impacts operational flexibility.
- The operating profits for energy storage units, as a result of time-shifting energy, decrease with increasing wind capacity. Increasing wind generation suppresses electricity prices and therefore increases the opportunities for energy storage units to purchase electricity at lower prices. However, this also reduces the opportunities for energy storage units to sell electricity at higher prices, reducing overall operating profits. Energy storage units with shorter storage durations observe larger decreases in operating profits with increasing wind capacity.

7.4 Future work

This work provides extended insights on the impacts of wind variability to power plant operating regimes. However, there are a number of opportunities to improve and extend the work presented in this thesis. This section presents suggestions for future research.

This thesis considered a large number of wind capacity scenarios using temporally-matched demand and wind data. However, there are other scenarios and generation technologies that have not been explored that may improve understanding of power plant operating regimes. For example, CCGT power plants are considered with post-combustion CO_2 capture with amine scrubbing. Future work could examine other power generation technologies, such as coal or biomass, with different integration options and CO_2 capture technologies. The UCED model developed in this thesis can be adapted to consider other technologies and configurations by modifying the operating constraints of the base and CO_2 capture power plants.

This analysis assumed a portfolio of large-scale pumped storage units. Future work should analyse the impacts of different energy storage technologies and energy storage for heat applications. In addition, this work assumed that energy storage units operate through arbitrage opportunities. Future work should also explore the potential impacts of reserve and response provision and transmission constraint management as well as considering different sizes of energy storage such as distribution-scale energy storage units.

It is also likely that demand-side management will become increasingly important in future power systems. Future work should examine the impacts of changing demand profiles and demand-side flexibility services on power plant operating regimes.

Future work should include the transmission constraints of the power system. Developing a unit commitment model with transmission constraints would enable a more thorough investigation of security-constrained power system operation.

This work assumes that fuel and CO_2 prices are deterministic parameters that do not vary with time. This is to ensure that scenarios are compared on an internally consistent basis and to isolate the impacts of wind. Further work could explore the impacts of seasonal or time-varying fuel and CO_2 prices on the thermal generation portfolio.

This work utilises wind speed data at hourly resolution and so it is not possible to generate higher resolution data without producing interpolation errors. Increasing the temporal resolution of the UCED model would increase the computational requirements but would capture sub-hourly power plant cycling operations. Future work should utilise higher resolution data for sub-hourly UCED analysis to improve understanding of short-term operational impacts.

The simple electricity pricing model used in this thesis uses the marginal costs and time-weighted start-up/shut-down costs of the marginal 'price-setting' generator to simulate the system marginal price for each time step. A price mark-down function is used to represent electricity price behaviour during periods of high wind output and low demand for electricity. However, there are very limited historical observations of negative price events. Therefore, future work should seek to improve the electricity pricing model.

The analysis presented in this thesis assumes large proportions of onshore and offshore wind capacity. Including additional renewable energy sources such as solar, wave, and tidal power into the UCED analysis should be performed in future work as they are likely to contribute increasing amounts towards electricity demand.

This work did not consider CO_2 flow rate constraints of the CO_2 transportation network. Analysing geographical CO_2 flow rates with velocity management and accounting for injection and storage constraints should be considered in future work. Variable CO_2 capture rates between 0% and 95% should also be considered with the possibility of solvent storage. This would vastly increase the complexity of the model, but would allow for an improved understanding of electricity and CO_2 transportation systems.

References

Adams, S. A. and Keith, D. W. Are global wind power resource estimates overstated? *Environmental Research Letters*, 8, 2013.

Ali, M., Matevosyan, J., and Milanovic, J. V. Probabilistic assessment of wind farm annual energy production. *Electric Power Systems Research*, 89:70–79, 2012.

Alie, C. A generalized framework for scheduling the operation of power plants incorporating CO2 capture. In *International Test Network for CO2 Capture: Report on 8th Workshop*. 2005.

Allan, R. N., Billinton, R., and Abdel-Gawad, N. M. K. The IEEE reliability test system - extensions to and evaluation of the generating system. *IEEE Transactions on Power Systems*, 1(4):1–7, 1986.

AMEC. A carbon capture and storage network for Yorkshire and Humber - An introduction to understanding the transportation of CO2 from Yorkshire and Humber emitters into offshore storage sites, 2008. URL `http://www.ccsassociation.org/docs/2008/Yorkshire%20Forward%20-%20A%20Carbon%20Capture%20and%20Storage%20Network%20for%20Yorkshire%20and%20Humber%20June%2008.pdf`.

Antoniou, I. and Pedersen, S. M. Influence of turbulence, wind shear and low-level jets on the power curve and the AEP of a wind turbine. *Eurpean Wind Energy Conference*, 2009.

APX. APX Power UK, 2015. URL `https://www.apxgroup.com/trading-clearing/apx-power-uk/`.

Arce, A., MacDowell, N., Shah, N., and Vega, L. F. Flexible operation of solvent regeneration systems for CO2 capture processes using advanced control techniques: Towards operational cost minimisation. *International Journal of Greenhouse Gas Control*, 11:236–250, 2012.

Atkinson, N., Harman, K., Lynn, M., Schwarz, A., and Tindal, A. Long-term wind speed trends in Northwestern Europe, 2009. URL `http://www.gl-garradhassan.com/assets/downloads/Long_term_wind_speed_trends_in_northwestern_Europe.pdf`.

Baldick, R. The Generalized Unit Commitment Problem. *IEEE Transactions on Power Systems*, 10(1):465–475, Feb 1995.

Balling, L. Fast cycling and rapid start-up: new generation of plants achieves impressive results, 2011. URL `http://www.energy.siemens.com/br/pool/hq/power-generation/power-plants/gas-fired-power-plants/combined-cycle-powerplants/Fast_cycling_and_rapid_start-up_US.pdf`.

Barbour, E. *An Investigation into the potential of Energy Storage to tackle Intermittency in Renewable Energy Generation*. PhD thesis, University of Edinburgh, 2013.

Barbour, E., Wilson, I. A. G., Bryden, I. G., McGregor, P. G., Mulheran, P. A., and Hall, P. J. Towards an objective method to compare energy storage technologies: development and validation of a model to determine the upper boundary of revenue available from electrical price arbitrage. *Energy & Environmental Science*, 5:5425–5436, 2012.

Baringa. Negative pricing in the GB wholesale electricity market. *DECC*, 2015.

Barthelmie, R., Larsen, G., Pryor, S., Jorgensen, H., Bergstrom, H., Schlez, W., Rados, K., Lange, B., Volund, P., Neckelmann, S., Mogensen, S., Schepers, G., Hegberg, T., Folkerts, L., and Magnusson, M. ENDOW (efficient development of offshore wind farms): modelling wake and boundary layer interactions. *Wind Energy*, 7(3):225–245, 2004.

Barthelmie, R. J. and Jensen, L. E. Evaluation of wind farm efficiency and wind turbine wakes at the Nysted offshore wind farm. *Wind Energy*, 13:573–586, 2010.

Bhardwaj, A., Kamboj, V. K., Shukla, V. K., Singh, B., and Khurana, P. Unit Commitment in Electrical Power System - A Literature Review. *2012 IEEE International Power Engineering and Optimization Conference*, 2012.

Bibby, B. M., Skovgaard, I. M., and Sorensen, M. Diffusion-type models with given marginal distribution and autocorrelation function. *Bernoulli Journal*, 11:191–220, 2005.

Black, M. and Strbac, G. The Role of Storage in Integrating Wind Energy. In *Future Power Systems, 2005 International Conference on*, pages 1–6, 2005.

Black, M. and Strbac, G. Value of Bulk Energy Storage for Managing Wind Power Fluctuations. *IEEE Transactions on Energy Conversion*, 22(1):197–205, 2007.

Breeze, P. *Power Generation Technologies*. Elsevier, 2005.

Brouwer, A. S., van den Broek, M., Seebregts, A., and Faaij, A. P. C. The flexibility requirements for power plants with CCS in a future energy system with a large share of intermittent renewable energy sources. *Energy Procedia GHGT-11*, 37:2657–2664, 2013.

Bruce, A. R. W., Harrison, G. P., Gibbins, J., and Chalmers, H. Assessing operating regimes of CCS power plants in high wind and energy storage scenarios. *Energy Procedia GHGT-12*, 63:7529 – 7540, 2014.

Bunn, D. W. Forecasting loads and prices in competitive power markets. *Proceedings of the IEEE*, 88(2):163–169, 2000.

Burton, T., Jenkins, N., Sharpe, D., and Bossanyi, E. *Wind Energy Handbook*. Wiley, 2nd edition, 2011.

Cannon, D. J., Brayshaw, D. J., Methven, J., Coker, P. J., and Lenaghan, D. Using reanalysis data to quantify extreme wind power generation statistics: A 33 year case study in Great Britain. *Renewable Energy*, 75:767–778, 2015.

Carbon Trust. Offshore wind power: big challenge, big opportunity - Maximising the environmental, economic and security benefits, 2008. URL `http://www.carbontrust.com/media/42162/ctc743-offshore-wind-power.pdf`.

Cardinal, M. and Miller, N. Grid Friendly Wind Plant Controls: WindCONTROL - Field Test Results. *WindPower June 6, 2006 Pittsburgh, PA*, 2006.

Carrillo, C., Montano, A. F. O., Cidras, J., and Diaz-Dorado, E. Review of power curve modelling for wind turbines. *Renewable and Sustainable Energy Reviews*, 21:572–581, 2013.

Cato-2. Anti-surge system for CO2 compressor. *CATO-2 Deliverable WP 2.1-D15C*, 2013.

CCSA. CCS Cost Reduction Taskforce: Final Report, May 2013. URL `https://www.gov.uk/government/uploads/system/uploads/attachment_data/file/201021/CCS_Cost_Reduction_Taskforce_-_Final_Report_-_May_2013.pdf`.

Chalmers, H. *Flexible operation of coal-fired power plants with post-combustion capture of carbon dioxide*. PhD thesis, University of Surrey, 2010.

Chalmers, H. and Gibbins, J. Initial evaluation of the impact of post-combustion capture of carbon dioxide on supercritical pulverised coal power plant part load performance. *Fuel*, 86 (14):2109 – 2123, 2007.

Chalmers, H., Gibbins, J., and Leach, M. Valuing power plant flexibility with CCS: the case of post-combustion capture retrofits. *Mitigation and Adaptation Strategies for Global Change*, 17(6):621–649, 2012. doi: doi:10.1007/s11027-011-9327-5.

Chamorro, L. P. and Porte-Agel, F. A Wind-Tunnel Investigation of Wind-Turbine Wakes: Boundary-Layer Turbulence Effects. *Boundary-Layer Meteorology*, 132(1):129–149, 2009.

Cohen, G. T. R., S. M. and Webber, M. E. Optimizing post-combustion CO2 capture in response to volatile electricity prices. *International Journal of Greenhouse Gas Control*, 8:180–195, 2012.

Cohen, S. M. *A Techno-economic Plant- and Grid-Level Assessment of Flexible CO2 Capture*. PhD thesis, The University of Texas at Austin, 2012.

Colmenar-Santos, A., Campinez-Romero, S., Enriquez-Garcia, L. A., and Perez-Molina, C. Simplified Analysis of the Electric Power Losses for On-Shore Wind Farms Considering Weibull Distribution Parameters. *Energies*, 7:6856–6885, 2014.

Conroy, N., Deane, J. P., and Gallachoir, B. P. O. Wind turbine availability: Should it be time or energy based? - A case study in Ireland. *Renewable Energy*, 36:2967–2971, 2011.

Crown Estate. Offshore wind operational report 2014, 2014. URL http://www.thecrownestate.co.uk/media/5462/ei-operational-wind-report-2014.pdf.

CSIRO. Activity 3: Process Modelling for Amine-based Post Combustion Capture Plant. Technical report, CSIRO - Australian National Low Emissions Coal Research and Development, 2012.

Daly, P., Flynn, D., and Cunniffe, N. Inertia Considerations within Unit Commitment and Economic Dispatch for Systems with High Non-Synchronous Penetrations. *Conference Paper Eindhoven, The Netherlands, 29 June - 2 July 2015*, 2015.

DECC. UK Renewable Energy Roadmap, 2011. URL https://www.gov.uk/government/uploads/system/uploads/attachment_data/file/48128/2167-uk-renewable-energy-roadmap.pdf.

DECC. UK Renewable Energy Roadmap Update 2012, 2012a. URL https://www.gov.uk/government/uploads/system/uploads/attachment_data/file/80246/11-02-13_UK_Renewable_Energy_Roadmap_Update_FINAL_DRAFT.pdf.

DECC. 2012 Guidelines to Defra / DECC's GHG Conversion Factors for Company Reporting, May 2012b. URL https://www.gov.uk/government/uploads/system/uploads/attachment_data/file/69554/pb13773-ghg-conversion-factors-2012.pdf.

DECC. CCS Roadmap - Storage Strategy. April 2012c.

DECC. UK Renewable Energy Roadmap Update 2013, 2013a. URL https://www.gov.uk/government/uploads/system/uploads/attachment_data/file/255182/UK_Renewable_Energy_Roadmap_-_5_November_-_FINAL_DOCUMENT_FOR_PUBLICATIO___.pdf.

DECC. 2013 Government GHG Conversion Factors for Company Reporting: Methodology Paper for Emission Factors, July 2013b. URL https://www.gov.uk/government/uploads/system/uploads/attachment_data/file/224437/pb13988-emission-factor-methodology-130719.pdf.

DECC. Electricity Market Reform Delivery Plan, Dec 2013c. URL https://www.gov.uk/government/uploads/system/uploads/attachment_data/file/268221/181213_2013_EMR_Delivery_Plan_FINAL.pdf.

DECC. Electricity Generation Costs (December 2013). 2013d.

DECC. 2014 Government GHG Conversion Factors for Company Reporting: Methodology Paper for Emission Factors FINAL, July 2014a. URL http://www.ukconversionfactorscarbonsmart.co.uk/documents/2014%20Emission%20Factor%20Methodology%20Paper_FINAL-4Jul14.pdf.

DECC. DECC Fossil Fuel Price Projections. September 2014b.

DECC. Analysis of the Marginal Emission Factor (MEF), 2014c. URL https://www.gov.uk/government/uploads/system/uploads/attachment_data/file/357753/MEF_Analysis_-_Report_FINAL.pdf.

Domenichini, R., Mancuso, L., Ferrari, N., and Davison, J. Operating Flexibility of Power Plants with Carbon Capture and Storage (CCS). *Energy Procedia GHGT-11*, 37:2727 – 2737, 2013.

Doquet, M. Use of stochastic process to sample wind power curves in planning studies. *Power Tech, 2007 IEEE Lausanne*, pages 663 – 670, 2007.

Eager, D. *Dynamic Modelling of Generation Capacity Investment in Electricity Markets with High Wind Penetration.* PhD thesis, University of Edinburgh, 2011.

EC. Directive 2009/72/EC of the European Parliament, Aug 2009. URL http://eur-lex.europa.eu.

El-Hajj, A. and Kabalan, K. The use of spreadsheets to calculate the convolution sum of two finite sequences. *International Journal of Engineering Education*, 20:867–871, 2004.

Ela, E., Milligan, M., Kirby, B., Lannoye, E., Flynn, D., O'Malley, M., and Zavadil, B. Evolution of Operating Reserve Determination in Wind Power Integration Studies. *2010 IEEE Power & Energy Society General Meeting, Minneapolis, Minnesota, July 25-29, 2010*, 2011.

Electricity Capacity Regulations. The Electricity Capacity Regulations 2014. *Acts of Parliament*, 2014.

Elexon. The Balancing and Settlement Code. 2001.

Elexon. The New Electricity Trading Arrangements, 2015. URL http://www.bmreports.com/.

Energy Act. Energy Act 2013. *Acts of Parliament*, 2013.

Energy Research Partnership. The future role for energy storage in the UK Main Report. *June 2011 Energy Research Partnership Technology Report*, 2011.

Erinmez, I. A., Bickers, D. O., Wood, G. F., and Hung, W. W. NGC experience with frequency control in England and Wales - provision of frequency response by generators. *Proceedings of Power Engineering Society 1999 Winter Meeting, IEEE*, 1999.

Errey, O., Chalmers, H., Lucquiaud, M., and Gibbins, J. Valuing responsive operation of post-combustion CCS power plants in low carbon electricity markets. *Energy Procedia GHGT-12*, 63:7471 – 7484, 2014.

ETI. Carbon capture and storage Building the UK carbon capture and storage sector by 2030 - Scenarios and actions, 2015. URL `http://www.eti.co.uk/wp-content/uploads/2015/03/CCS-Building-the-UK-carbon-capture-and-storage-sector-by-2013.pdf`.

EU. Directive 2009/28/EC of the European Parliament and of the Council of 23 April 2009 on the promotion of the use of energy from renewable sources and amending and subsequently repealing Directives 2001/77/EC and 2003/30/EC. *Official Journal of the European Union*, 2009.

Feng, Y., Tavner, P. J., and Long, H. Early experiences with UK round 1 offshore wind farms. *Proceedings of the ICE - Energy*, 2010.

GE Energy. Analysis of wind generation inmpact on ERCOT ancillary services requirements, 2008. URL `http://www.uwig.org/attchb-ercot_a-s_study_final_report.pdf`.

Ghosh, T. K. and Prelas, M. A. *Energy Resources and Systems: Volume 1: Fundamentals and Non-Renewable Resources*. Springer Science & Business Media, 2009.

Green, J., Bowen, A., Fingersh, L. J., and Wan, Y. Electrical Collection and Transmission Systems for Offshore Wind Power. In *2007 Offshore Technology Conference Houston, Texas*, 2007.

Green, R. and Staffell, I. The Impact of Government Interventions on Investment in the GB Electricity Market, Nov 2013. URL `http://ec.europa.eu/competition/state_aid/studies_reports/green_staffell_en.pdf`.

Green, R. and Vasilakos, N. The Long-term Impact of Wind Power on Electricity Prices and Generating Capacity. Technical report, University of Birmingham, 2007.

Green, R. and Vasilakos, N. Market behaviour with large amounts of intermittent generation. *Energy Policy*, 38:3211–3220, 2010.

Green, R. and Yatchew, A. Support Schemes for Renewable Energy: An Economic Analysis. *Economics of Energy and Environmental Policy*, 1(2):83–98, 2012.

Green, R., Staffell, I., and Vasilakos, N. Divide and Conquer? k-Means Clustering of Demand Data Allows Rapid and Accurate Simulations of the British Electricity System. *IEEE Transactions on Engineering Management*, 61(2):251–260, May 2014.

Greenacre, P. UKERC Technology and Policy Assessment Cost Methodologies Project: Offshore Wind Case Study, 2012.

Greenacre, P., Gross, R., and Heptonstall, P. Great Expectations: The cost of offshore wind in UK waters - understanding the past and projecting the future, 2010.

Grigg, C., Wong, P., Albrecht, P., Allan, R., Bhavaraju, M., Billinton, R., Chen, Q., Fong, C., Haddad, S., Kuruganty, S., Li, W., Mukerji, R., Patton, D., Rau, N., D. Reppen A. Schneider, M. S., and Singh., C. The IEEE reliability test system-1996: A report prepared by the reliability test system task force of the application of probability methods subcommittee. *IEEE Transactions on Power Systems*, 14(3):1010ï£¡1020, August 1999.

Gross, G. and Galiana, F. D. Short-term load forecasting. *Proceedings of the IEEE*, 75(12): 1558–1573, 1987.

Grunewald, P. Electricity storage in future GB networks - a market failure? *BIEE 9th Accademic Conference, Oxford, 19-20 Sep 2012*, 2012.

Haines, M. R. and Davison, J. Enhancing dynamic response of power plant with postcombustion capture using "Stripper stop". *International Journal of Greenhouse Gas Control*, 20: 49–56, 2013.

Harman, K. How does the real world performance of wind turbines compare with sales power curves?, 2012. URL `http://www.ewea.org/events/workshops/wp-content/uploads/proceedings/Analysis_of_Operating_Wind_farms/EWEA%20Workshop%20Lyon%20-%205-4%20Keir%20Harman%20GLGH.pdf`.

Hassan, U. A wind tunnel investigation of the wake structure within small wind turbine farms. Technical report, UK Department of Energy, ETSU., 1992.

Hawkes, A. Estimating marginal CO2 emissions rates for national electricity systems. *Energy Policy*, 38(10):5977–5987, 2010.

Hawkins, S. *A High Resolution Reanalysis of Wind Speeds over the British Isles forWind Energy Integration.* PhD thesis, The University of Edinburgh, 2012.

Hawkins, S., Eager, D., and Harrison, G. P. Characterising the reliability of production from future British offshore wind fleets. In *Renewable Power Generation (RPG 2011)*, 2011.

Hayes, B., Ilie, I., Porpodas, A., and Djokic, S. Equivalent Power Curve Model of a Wind Farm Based on Field Measurement Data. *Supergen Networks*, pages 1–7, 2010.

Haynes, C. J. How to determine a unit ramp rate (MW/min) for lowest total production cost. 1987.

Holton, J. R. and Hakim, G. J. *An Introduction to Dynamic Meteorology*. Elsevier, 5th edition, 2013.

Holttinen, H., Milligan, M., Kirby, B., Acker, T., Neimane, V., and Molinski, T. Using Standard Deviation as a Measure of Increased Operational Reserve Requirement for Wind Power. *Wind Engineering*, 32(4), 2008.

House of Commons. Carbon Price Floor: Reform, May 2014. URL `https://www.gov.uk/government/publications/carbon-price-floor-reform`.

HSE. Hazards arising from the conveyance and use of gas from Non-Conventional Sources (NCS), 2011. URL `http://www.hse.gov.uk/research/rrpdf/rr882.pdf`.

Huber, M., Dimkova, D., and Hamacher, T. Integration of wind and solar power in Europe: Assessment of flexibility requirements. *Energy*, 69:236–246, 2014.

Ibrahim, T. K. and Rahman, M. M. Thermal Impact of Operating Conditions on the Performance of a Combined Cycle Gas Turbine. *Journal of Applied Research and Technology*, 10: 567–577, 2012.

IEA. Harnessing variable renewables: A guide to the balancing challenge, 2011. URL `http://www.iea.org/publications/freepublications/publication/Harnessing_Variable_Renewables2011.pdf`.

IEAGHG. Retrofitting CO2 capture to existing power plants 2011/2 May 2011, May 2011. URL `http://ieaghg.org/docs/General_Docs/Reports/2011-02.pdf`.

IEAGHG. Operating Flexibility of Power Plants with CCS. *Report: 2012/6*, 2012.

IEEE. Finding Flexibility, Dec 2013. URL `http://magazine.ieee-pes.org/files/2013/10/2013nov-lew.pdf`.

IEEE Reliability Test System Task Force. IEEE reliability test system. *IEEE Transactions on Power Apparatus and Systems*, pages 2047 – 2054, 1979.

IMechE. Energy Storage: The missing link in the UK's energy commitments, April 2014. URL `http://www.imeche.org/docs/default-source/reports/imeche-energy-storage-report.pdf?sfvrsn=4`.

Ji, Z., Kang, C., Chen, Q., Xia, Q., Jiang, C., Chen, Z., and Xin, J. Low-Carbon Power System Dispatch Incorporating Carbon Capture Power Plants. *IEEE Transactions on Power Systems*, 28(4):4615–4623, Nov 2013.

Johnson, C., Graves, A., Tindal, A., Cox, S. D., Schlez, W., and Neubert, A. New developments in wake models for large wind farms. In *AWEA windpower conference. Chicago, USA*. GL Garrad Hassan, 2009.

Kaiser, K., Langreder, W., Hohlen, H., and Hojstrup, J. *Wind Energy*, chapter Turbulence Correction for Power Curves, pages 159–162. Springer, 2007.

Kaldellis, J. K. and Zafirakis, D. The influence of technical availability on the energy performance of wind farms: Overview of critical factors and development of a proxy prediction model. *Journal of Wind Engineering and Industrial Aerodynamics*, 115:65–81, 2013.

Kehlhofer, R., Warner, J., Nielsen, H., and Bachmann, R. *Combined-cycle gas & steam turbine power plants*. PennWell Publishing Company, Tulsa, Oklahoma, 2nd edition, 1999.

KEMA. Review of the LRMC costs of CCGT electricity generation in Singapore to establish the technical parameters for setting the Vesting Price for the period 1 January 2009 to 31 December 2010, November 2008. URL `https://www.ema.gov.sg/cmsmedia/Licensees/CCGT_RMC_Calcs.pdf`.

Kirschen, D. S., Ma, J., Silva, V., and Belhomme, R. Optimizing the Flexibility of a Portfolio of Generating Plants to Deal with Wind Generation. In *Power and Energy Society General Meeting, 2011 IEEE*, pages 1–7, 2011.

Kiss, P., Vargo, L., and Janosi, I. M. Comparison of wind power estimates from the ECMWF reanalyses with direct turbine measurements. *Journal of Renewable and Sustainable Energy*, 1, 2009.

Klemp, J. B., Gill, D. O., Barker, D. M., Duda, M. G., Wang, W., and Powers, J. G. A Description of the Advanced Research WRF Version 3. 2008.

Kohl, A. L. and Riesenfeld, F. C. *Gas Purification*. Gulf Publishing Company, Houston, Texas, second edition, 1974.

Kooijman, H. J. Power Curves for Different Ambient Conditions: GEs perspective on extreme inflow conditions. 2012.

Kubrik, M., Brayshaw, D., and Coker, P. Reanalysis: an improved data set for simulating wind generation? In *WREF 2012*, 2012.

Kumar, N., Besuner, P., Lefton, S., Agan, D., and Hilleman, D. Power Plant Cycling Costs. Technical report, Intertek APTECH, 2012.

Lannoye, E., Flynn, D., and O'Malley, M. Power System Flexibility Assessment - State of the Art. In *Power and Energy Society General Meeting, 2012 IEEE, 22-26 July 2012*, pages 1 – 6, 2012.

Lawal, A., Wang, M., Stephenson, P., Koumpouras, G., and Yeung, H. Dynamic Modelling and Analysis of Post-Combustion CO2 Chemical Absorption Process for Coal-fired Power Plants. *Fuel*, 89(10):2791–2801, Oct 2010.

Le, K. D., Jackups, R. R., Feinstein, J., Thompson, H. H., Wolf, H. M., Stein, E. C., Gorski, A. D., and Griffith, J. S. Operational aspects of generation cycling. *IEEE Transactions on Power Systems*, 5(4):1194–1203, 1990.

Li, J., Wen, J., and Han, X. Low-carbon unit commitment with intensive wind power generation and carbon capture power plant. *Journal of Modern Power Systems and Clean Energy*, 3(1): 63–71, January 2015.

Licari, J., Ekanayake, J., and Moore, I. Inertia response from full-power converter-based permanent magnet wind generators. *Journal of Modern Power Systems and Clean Energy*, 1 (1):26–33, 2013.

Liu, X., Wu., J., Jenkins, N., and Bagdanavicius, A. Combined analysis of electricity and heat networks. *Applied Energy*, 162:1238–1250, 2015.

Lou, S., Lu, S., Wu, Y., and Kirschen, D. S. Optimizing Spinning Reserve Requirement of Power System With Carbon Capture Plants. *IEEE Transactions on Power Systems*, 30(2): 1056–1063, March 2015.

Lucquiaud, M. and Gibbins, J. On the integration of CO2 capture with coal-fired power plants: A methodology to assess and optimise solvent-based postcombustion capture systems. *Chemical Engineering Research and Design*, 89:1553 – 1571, 2011.

Lucquiaud, M., Patel, P., Chalmers, H., and Gibbins, J. Retrofitting CO2 capture ready fossil plants with post-combustion capture. Part 2: requirements for natural gas combined cycle plants using solvent-based flue gas scrubbing. *Proceedings of the Institution of Mechanical Engineers, Part A: Journal of Power and Energy*, 223(3):227–238, 2009.

Ludig, S., Haller, M., and Bauer, N. Tackling long-term climate change together: the case of flexible CCS and fluctuating renewable energy. In *10th International Conference on Greenhouse Gas Technologies Amsterdam, The Netherlands: Elsevier*, 2010.

Ma, J. *Evaluating and Planning Flexibility in a Sustainable Power System with Large Wind Penetration*. PhD thesis, The University of Manchester, 2012.

Ma, J., Silva, V., Belhomme, R., Kirschen, D. S., and Ochoa, L. F. Evaluating and Planning Flexibility in Sustainable Power Systems. *IEEE Transactions on Sustainable Energy*, 4(1): 200–209, 2011.

Ma, J., Silva, V., Ochoa, L. F., Kirschen, D. S., and Belhomme, R. Evaluating the profitability of flexibility. In *Power and Energy Society General Meeting, 2012 IEEE*, pages 1–8, 2012.

Makarov, Y. V., Loutan, C., Ma, J., and de Mello, P. Operational Impacts of Wind Generation on California Power Systems. *IEEE Transactions on Power Systems*, 24(2):1039–1050, 2009.

Manwell, J. F., McGowan, J. G., and Rogers, A. L. *Wind Energy Explained: Theory, Design and Application*. Wiley-Blackwell, 2009.

Martens, P., Delarue, E., and D'haeseleer, W. A Mixed Integer Linear Programming Model for a Pulverized Coal Plant With Post-Combustion Carbon Capture. *IEEE Transactions on Power Systems*, 27(2):741–751, May 2012.

Martin-Martinez, S., Vigueras-Rodriguez, A., Gomez-Lazaro, E., Molina-Garcia, A., Muljadi, E., and Milligan, M. *Advances in Wind Power*, chapter 12. Intech, 2012.

Martinez de Alegria, I., Andreu, J., J. L. Martin, a. P. I., Villate, J. L., and Camblong, H. Connection requirements for wind farms: A survey on technical requierements and regulation. *Renewable and Sustainable Energy Reviews*, 11:1858ï£¡1872, 2007.

Met Office. Winter 2010/11, 2015. URL `http://www.metoffice.gov.uk/climate/uk/summaries/2011/winter`.

Milligan, M., Donohoo, P., Lew, D., Ela, E., Kirby, B., Holttinen, H., Lannoye, E., Flynn, D., O'Malley, M., Miller, N., Eriksen, P. B., Gottig, A., Rawn, B., Gibescu, M., Lazaro, E. G., Robitaille, A., and Kamwa, I. Operating Reserves and Wind Power Integration: An International Comparison. *The 9th Annual International Workshop on Large-Scale Integration of Wind Power into Power Systems as well as on Transmission Networks for Offshore Wind Power Plants Conference Quebec, Canada, October 18-19, 2010*, 2010.

Muljadi, E., Gevorgian, V., Singh, M., and Santoso, S. Understanding Inertial and Frequency Response of Wind Power Plants. *IEEE Symposium on Power Electronics and Machines in Wind Applications, Denver, Colorado, July 16-18, 2012*, 2012.

National Grid. Operating the Electricity Transmission Networks in 2020, June 2011a. URL `http://www.nationalgrid.com/NR/rdonlyres/DF928C19-9210-4629-AB78-BBAA7AD8B89D/47178/Operatingin2020_finalversion0806_final.pdf`.

National Grid. National Electricity Transmission System Seven Year Statement. 2011b.

National Grid. 2013 Electricity Ten Year Statement. 2013.

National Grid. UK Future Energy Scenarios. 2014a.

National Grid. Winter Outlook 2014/15, 2014b. URL `http://www2.nationalgrid.com/media/Resources/PDFs/reports/WinterOutlookReport2014.pdf`.

National Grid. The Grid Code, 2015a. URL http://www2.nationalgrid.com/uk/industry-information/electricity-codes/grid-code/the-grid-code/.

National Grid. Metered half-hourly electricity demands, 2015b. URL http://www.nationalgrid.com/uk/electricity/data/demand+data/.

National Grid. Future Energy Scenarios. Jul 2015c.

NCAR. WRF ARW Version 3 Modeling System User's Guide. *National Center for Atmospheric Research*, 2008.

NCAR. WRF ARW Version 3 Modeling System User's Guide. *National Center for Atmospheric Research*, 2014.

NEA. Technical and economic aspects of load following with nuclear power plants. *Nuclear Energy Agency*, 2011.

NERC. Flexibility Requirements and Metrics for Variable Generation: Implications for System Planning Studies, August 2010. URL http://www.nerc.com/files/IVGTF_Task_1_4_Final.pdf.

Nickell, B. M. Wind Dispatchability and Storage Interconnected Grid Perspective. 2008.

Norgaard, P. and Holttinen, H. A multi-turbine power curve approach. *Nordic Wind Power Conference, 1-2 March 2004*, pages 1–5, 2004.

Nosair, H. and Bouffard, F. Flexibility Envelopes for Power System Operational Planning. *IEEE Transactions on Sustainable Energy*, 6(3):800–809, Jul 2015.

NREL. Renewable Electricity Futures Study (Entire Report), 2012.

O'Dwyer, C. and Flynn, D. Using Energy Storage to Manage High Net Load Variability at Sub-Hourly Time-Scales. *IEEE Transactions on Power Systems*, PP(PP):1–10, 2014.

Ofgem. Electricity Capacity Assessment. 2012.

Ofgem. Electricity Capacity Assessment Report 2014. 2014a.

Ofgem. Renewables Obligation (RO), 2014b. URL https://www.ofgem.gov.uk/environmental-programmes/renewables-obligation-ro.

Oldenburg, C. M. Joule-Thomson cooling due to CO2 injection into natural gas reservoirs. *Proceedings, Tough Symposium 2006*, 2006.

Ouyang, Z. and Shahidehpour, S. M. Heuristic multi-area unit commitment with economic dispatch. *IEE Proceedings C - Generation, Transmission and Distribution*, 138(3):242–252, May 1991.

Palmintier, B. S. *Incorportating operation flexibility into electric generation planning: Impacts and methods for system design and policy analysis.* PhD thesis, Massachusetts Institute of Technology, 2013.

Parsons Brinkerhoff. Electricity Generation Cost Model - 2012 Update of Non Renewable Technologies. 2012.

Parsons Brinkerhoff. Electricity Generation Cost Model - 2013 Update of non-renewable technologies. April 2013a.

Parsons Brinkerhoff. Electricity Generation Cost Model - 2013 Update of renewable technologies. June 2013b.

Parsons Brinkerhoff. Technical Assessment of the Operation of Coal & Gas Fired Plants. *DECC*, 2014.

Perez-Arriaga, I. and Batlle, C. Impacts of intermittent renewables on electricity generation system operation. *Economics of Energy and Environmental Policy*, 1:3–17, 2012.

Pfenninger, S. and Keirstead, J. Renewables, nuclear, or fossil fuels? Scenarios for Great Britain's power system considering costs, emissions and energy security. *Applied Energy*, 152:83–93, 2015.

Phillips, J. L., Cox, S. D., Henderson, A. R., and Gill, J. P. Wake effects within and between large wind projects: the challenge of scale, density and neighbours - onshore and offshore. In *EWEC conference. Warsaw, Poland.* GL Garrad Hassan, 2010.

Pinson, P., H. Nielsen, a. H. M., Lange, M., and Kariniotakis, G. Methods for the Estimation of the Uncertainty of Wind Power Forecasts. *ANEMOS project, Technical University of Denmark, Lyngby, Denmark*, 2007.

Pouret, L. and Nuttall, W. J. Can Nuclear Power Be Flexible? *EPRG Draft Working Paper, Judge Business School, University of Cambridge*, 2007.

Poyry. Implications of Intermittency. 2009.

Poyry. Wind Energy and Electricity Prices - Exploring the 'merit-order effect'. 2010.

Poyry. The challenges of intermittency in North West European power markets, 2011. URL `http://www.poyry.com/sites/default/files/imce/files/intermittency_-_march_2011_-_energy.pdf`.

Poyry. Valuing Flexibility, May 2014. URL `http://www.elforsk.se/Documents/Market%20Design/seminars/DAM/2_Poyry.pdf`.

Qadrdan, M., Abeysekera, M., Chaudry, M., Wu, J., and Jenkins, N. Role of power-to-gas in an integrated gas and electricity system in Great Britain. *International Journal of Hydrogen Energy*, 40(17):5763–5775, 2015.

Quarton, D. and Ainslie, J. Turbulence in wind turbine wakes. *Wind Engineering*, 14:15–23, 1989.

RAENG. Wind Energy: Implications of large-scale deployment on the GB electricity system, 2014. URL `http://www.raeng.org.uk/publications/reports/wind-energy-implications-of-large-scale-deployment`.

Rareshide, E., Tindal, A., Johnson, C., Graves, A., Simpson, E., Bleeg, J., Harris, T., and Schoborg, D. Effects of complex wind regimes on turbine performance. In *AWEA Windpower Conference,Chicago, Illinois, USA.*, 2009.

Renewable UK. Offshore Wind Project Timelines, 2014. URL `http://www.renewableuk.com/en/publications/reports.cfm/Offshore-Wind-Project-Timelines`.

Renewable UK. UK Wind Energy Database (UKWED), 2015. URL `http://www.renewableuk.com/en/renewable-energy/wind-energy/uk-wind-energy-database/`.

Reynolds, A. J., Verheyen, T. V., Adeloju, S. B., Meuleman, E., Chaffee, A., Cottrell, A. J., and Feron, P. Chemical Characterization of MEA Degradation in PCC pilot plants operating in Australia. *Energy Procedia GHGT-11*, 37:877–882, 2013.

Rosnes, O. The Impact of Climate Policies on the Operation of a Thermal Power Plant. *The Energy Journal*, 29:1–22, 2008.

Rosso, A., Ma, J., Kirschen, D. S., and Ochoa, L. F. Assessing the Contribution of Demand Side Management to Power System Flexibility. In *2011 50th IEEE Conference on Decision and Control and European Control Conference (CDC-ECC) Orlando, FL, USA, December 12-15*, 2011.

Schallenberg-Rodriguez, J. A methodological review to estimate techno-economical wind energy. *Renewable and Sustainable Energy Reviews*, 21:272–287, 2013.

ScottMadden. Fast Response Energy Storage Devices: Technology Descriptions and Overview. 2009.

Seyedi, M. and Bollen, M. The utilization of synthetic inertia from wind farms and its impact on existing speed governors and system performance. 2013.

Sharma, S., Huang, S. H., and Sarma, N. D. R. System Inertial Frequency Response Estimation and Impact of Renewable Resources in ERCOT Interconnection. *Power and Energy Society General Meeting, 2011 IEEE*, pages 1–6, 2011.

Sheble, G. B. and Fahd, G. N. Unit commitment literature synopsis. *IEEE Transactions on Power Systems*, 9(1):128–135, Feb 1994.

Silva, V. L. F. P. *Value of flexibility in systems with large wind penetration*. PhD thesis, Imperial College London, 2010.

Sinden, G. Characteristics of the UK wind resource: Long-term patterns and relationship to electricity demand. *Energy Policy*, 35:112–127, 2007.

Solomon, S., Qin, D., Manning, M., Chen, Z., Marquis, M., Averyt, K. B., Tignor, M., and Miller, H. L. IPCC Fourth Assessment Report (AR4): Climate Change 2007: The Physical Science Basis. Technical report, IPCC, 2007.

Sorensen, T., Nielsen, P., and Thogersen, M. L. Recalibrating Wind Turbine Wake Model Parameters - Validating the Wake Model Performance for Large Offshore Wind Farms. 2006.

Sorensen, T., Nielsen, P., and Thogersen, M. L. Adapting and calibration of existing wake models to meet the conditions inside offshore wind farms. 2008.

Staffell, I. and Green, R. How does wind farm performance decline with age? *Renewable Energy*, 66:775–786, 2014.

Staffell, I. and Green, R. Is there still merit in the merit order stack? The impact of dynamic constraints on optimal plant mix. *IEEE Transactions on Power Systems*, 31:43–53, 2016. URL `http://www.biee.org/wpcms/wp-content/uploads/Staffell-Merit-in-the-Merit-Order-Stack.pdf`.

Strbac, G., Aunedi, M., Pudjianto, D., Djapic, P., Gammons, S., and Druce, R. Understanding the Balancing Challenge. 2012.

Stull, R. B. *An Introduction to Boundary Layer Meteorology*. Springer, 1988.

Sumbera, J. Modelling generator constraints for the self-scheduling problem, 2012. URL `http://energyexemplar.com/wp-content/uploads/publications/Modelling-generator-constraints-for-the-self-scheduling-problem.pdf`.

Thiringer, T. and Petersson, A. Control of a Variable-Speed Pitch-Regulated Wind Turbine, 2005.

Thomson, R. C. *Carbon and Energy Payback of Variable Renewable Generation*. PhD thesis, University of Edinburgh, 2014.

Tielens, P. and Hertem, D. V. Grid Inertia and Frequency Control in Power Systems with High Penetration of Renewables. *Young Researchers Symposium in Electrical Power Engineering, Delft, The Netherlands 16-17 April 2012*, 2012.

Tindal, A., Johnson, C., LeBlanc, M., Harman, K., Rareshide, E., and Graves, A. Site-specific adjustments to wind turbine power curves. In *AWEA Windpower Conference, Houston, Texas, USA.*, 2008.

Ulbig, A. and Andersson, G. On Operational Flexibility in Power Systems. In *Power and Energy Society General Meeting, 2012 IEEE*, 2012.

Ulbig, A. and Andersson, G. Analyzing Operational Flexibility of Electric Power Systems, 2014. URL `http://arxiv.org/pdf/1312.7618v2.pdf`.

Ummels, B. *Wind Integration: Power System Operation with Large-Scale Wind Power in Liberalised Environments.* PhD thesis, Technische Universiteit Delft, 2009.

Van der Hoven, I. Power spectrum of horizontal wind speed in the frequency range from 0.0007 to 900 cycles per hour. *Journal of Meteorology*, 14:160–164, 1957.

Veltin, J. and Belfroid, S. CATO-2 Deliverable WP 2.1-D15B Flow assurance studies for CO2 transport. Technical report, CATO 2, 2013.

Wan, Y., Ela, E., and Orwig, K. Development of an Equivalent Wind Plant Power-Curve. In *WindPower 2010, Dallas, USA*. NREL, 2010.

Wang, C. and Shahidehpour, S. M. Effects of ramp-rate limits on unit commitment and economic dispatch. *IEEE Transactions on Power Systems*, 8(3):1341–1350, Aug 1993.

Wen, Y., Guo, C., Pandzic, H., and Kirschen, D. S. Enhanced Security-Constrained Unit Commitment With Emerging Utility-Scale Energy Storage. *IEEE Transactions on Power Systems*, PP(99):1–11, 2015.

Wetterzentrale. Archiv, 2015. URL `http://www.wetterzentrale.de/topkarten/tkfaxbraar.htm`.

Wood, A. J. and Wollenberg, B. F. *Power generation, operation and control.* John Wiley & Sons, 2nd edition, 1996.

Wu, L. and Infield, D. Wind Plant Contributions to Power System Frequency Response. In *European Wind Energy Association Annual Conference (EWEA2012), Copenhagen, Denmark, 2012.*, 2012.

Zhang, D. *Ultra-Supercritical Coal Power Plants: Materials, Technologies and Optimisation.* Elsevier, 2013.

Zhang, Y., Bank, J., Wan, Y. H., Muljadi, E., and Corbus, D. Synchrophasor Measurement Based Wind Plant Inertia Estimation. In *IEEE Green Technologies Conference*, Denver, Colorado, April 2013.

Zhao, H., Feng, Y., Zhang, X. Q., and Ren, Z. Hydro-thermal unit commitment considering pumped storage stations. *1998 IEEE International Conference on Power System Technology - (POWERCON 2012)*, 1:576–580, 1998.

Appendix A

Wind sites

A complete list of the onshore and offshore wind sites available in the wind reanalysis dataset from Hawkins [2012] is provided in Table A.1.

Site I.D.	Site Name	Location	Region	Latitude	Longitude
Onshore					
100001	Conisholme Fen Re-submission	Lincolnshire	EE	53.43	-0.08
100003	Beinn Tharsuinn	Highland	NES	57.80	-4.33
100005	Calliachar	Perth & Kinross	NES	56.57	-3.83
100006	Tangy	Argyll & Bute	NWS	55.49	-5.68
100009	Deucheran Hill	Argyll & Bute	NWS	55.63	-5.56
100010	Beinn Mhor	Western Isles	NWS	56.07	-5.04
100013	Den Brook	Devon	SWE	50.80	-3.90
100014	North Pickenham Wind Farm	Norfolk	EA	52.63	0.75
100018	Rothes	Moray	NES	57.54	-3.37
100020	Mynydd Clogau	Powys	NWA	52.58	-3.43
100022	Clyde Wind Farm	South Lanarkshire	SS	55.47	-3.65
100023	Dorenell	Moray	NES	57.35	-3.12
100024	Tir Mostyn & Foel Goch	Denbighshire	NWA	53.11	-3.49
100026	Black Hill	Scottish Borders	SS	55.80	-2.43
100029	Llanbadarn Fynydd	Powys	NWA	52.40	-3.33
100030	Novar	Highland	NES	57.71	-4.43
100034	Beinn an Tuirc	Argyll & Bute	NWS	55.57	-5.57
100037	Hill of Towie	Moray	NES	57.49	-3.03
100038	Westfield Lane	West Yorkshire	EE	53.67	-1.28
100039	Pen Y Cymoedd	South Wales	SWA	51.70	-3.59
100040	Llandinam Repowering	Powys	NWA	52.44	-3.41
100041	Langham	Lincolnshire	EM	53.26	0.28
100043	Fairburn Estate	Highland	NES	57.53	-4.65
100044	Mark Hill	South Ayrshire	SS	54.99	-4.93
100046	Wansbeck Blyth Harbour	Northumberland	NEE	55.12	-1.49
100049	Tappaghan Mountain	Co Fermanagh	NI	54.55	-7.55
100050	Garrane	Co Fermanagh	NI	54.30	-7.23
100053	Broadmeadows	Scottish Borders	SS	55.57	-2.93
100057	Teeswind North	North Yorkshire	NEE	54.62	-1.13
100058	Kiln Pit Hill	Northumberland	NEE	54.89	-1.94

Continued on next page

Table A.1 – *Continued from previous page*

Site I.D.	Site Name	Location	Region	Latitude	Longitude
100061	Harelaw Renewable Energy Park	East Ayrshire	SS	55.74	-4.43
100063	Burnfoot Hill	Stirling	SS	56.21	-3.77
100068	Ovenden Moor Repowering	West Yorkshire	EE	53.78	-1.94
100070	Whitelee Phase II Extension	East Renfrewshire	SS	55.69	-4.23
100071	Batsworthy Cross	Devon	SWE	50.97	-3.69
100072	Griffin Forrest	Perth & Kinross	NES	56.59	-3.73
100074	Hunter's Hill	Co Tyrone	NI	54.45	-7.31
100077	Shira	Argyll & Bute	NWS	56.36	-4.98
100078	Coal Clough Repowering	Lancashire	NWE	53.75	-2.17
100079	Whiteside Hill	Dumfries & Galloway	SS	55.32	-4.02
100080	Corriemoillie Forest	Highland	NES	57.66	-4.75
100082	Glass Moor	Cambridgeshire	EM	52.57	-0.11
100083	Barmoor South Moor	Northumberland	NEE	55.66	-2.03
100085	Whitelee	East Renfrewshire	SS	55.69	-4.23
100086	Butterwick Moor	County Durham	NEE	54.67	-1.39
100089	Kelburn	North Ayrshire	SS	55.76	-4.80
100092	Green Rigg	Northumberland	NEE	55.13	-2.15
100093	Crystal Rig	Scottish Borders	SS	55.90	-2.51
100095	Ora More	Co Fermanagh	NI	54.33	-7.89
100096	Bradwell on Sea	Essex	EA	51.72	0.91
100097	Slieve Divena Extension	Co Tyrone	NI	54.51	-7.11
100099	Wester Dod Aikengall Extension	East Lothian	SS	55.93	-2.46
100100	Gruig	Co Antrim	NI	55.03	-6.25
100104	Mynydd Clogau Extension	Powys	NWA	52.58	-3.43
100107	Green Knowes	Perth & Kinross	NES	56.25	-3.67
100110	Llandinam P&L	Powys	NWA	52.44	-3.41
100112	Grise	Cumbria	NWE	54.74	-2.90
100118	Goole Fields	Humberside	EE	53.67	-0.89
100119	Hagshaw Hill	South Lanarkshire	SS	55.55	-3.92
100120	Millennium Extention	Highland	NES	57.13	-4.83
100121	Yelvertoft Wind Farm	Northamptonshire	EM	52.37	-1.15
100123	Grange (Flixborough)	Lincolnshire	EE	53.63	-0.70
100127	Wryde Croft Re-submission	Cambridgeshire	EM	52.64	-0.06
100128	Afton	East Ayrshire	SS	55.31	-4.17
100129	Burton Wold Wind Farm	Northamptonshire	EM	52.36	-0.65
100131	Llanbrynmair	Powys	NWA	52.64	-3.56
100139	Tom Nan Clach Re-submission	Highland	NES	57.39	-3.90
100140	Pates Hill	West Lothian	SS	55.83	-3.65
100142	Wryde Croft	Cambridgeshire	EM	52.64	-0.06
100143	Callagheen Extension	Co Fermanagh	NI	54.43	-8.01
100144	Chalmerston	East Ayrshire	NWE	54.53	-3.10
100145	Blackcraig, Glenkens	Dumfries & Galloway	SS	55.09	-4.11
100146	Dunbeath	Highland	NES	58.26	-3.50
100148	Long Mountain	Co Antrim	NI	54.97	-6.44
100150	Black Law 1 Construction Phase I	South Lanarkshire	SS	55.77	-3.74
100151	Arecleoch	South Ayrshire	SS	55.05	-4.88

Continued on next page

Table A.1 – *Continued from previous page*

Site I.D.	Site Name	Location	Region	Latitude	Longitude
100153	Carno Phase I Extension	Powys	NWA	52.55	-3.60
100156	Wingates	Northumberland	NEE	55.25	-1.87
100159	Sunderland Re-submission	Yorkshire	EE	53.75	-0.07
100160	Haswell Moor	Durham	NEE	54.78	-1.46
100163	Beinn an Tuirc Extension	Argyll & Bute	NWS	55.57	-5.57
100164	Hare Hill Extension	East Ayrshire	SS	55.35	-4.13
100165	Aire and Calder Wind Farm	Humberside	EE	53.69	-1.03
100166	Beinn Mhor Secondary Application	Western Isles	NES	58.02	-3.54
100167	Tievenameenta	Co Tyrone	NI	54.67	-7.68
100168	Breaker Hill	South Ayrshire	SS	55.16	-4.86
100170	Tallentire Hill	Cumbria	NWE	54.72	-3.37
100171	Castlecraig	Co Tyrone	NI	55.04	-7.96
100172	Crystal Rig 2	Scottish Borders	SS	55.90	-2.54
100173	Hagshaw Hill Extension	North Lanarkshire	SS	55.56	-3.90
100176	Llyn Alaw	Anglesey	NWA	53.36	-4.45
100177	Strathy North	Highland	NES	58.49	-4.04
100179	Nun Wood	Northamptonshire	EM	52.21	-0.65
100183	Whitelee Phase I Extension	East Renfrewshire	SS	55.69	-4.23
100184	Glens of Foudland	Aberdeenshire	NES	57.42	-2.64
100185	Walkway, High Swainston	County Durham	NEE	54.67	-1.38
100187	Crook Hill Re-submission	Lancashire	NWE	53.68	-2.13
100188	Smulgedon	Co Londonderry	NI	54.98	-6.15
100190	Boyndie Airfield	Aberdeenshire	NES	57.65	-2.61
100192	Langhope Rig	Scottish Borders	SS	55.47	-2.94
100193	Black Law 1 Construction Phase III	South Lanarkshire	SS	55.77	-3.74
100195	Swaffham	Norfolk	EA	52.66	0.70
100198	Wether Hill	Dumfries & Galloway	SS	55.22	-4.04
100200	Garreg Lwyd Hill	Powys	NWA	52.41	-3.27
100201	Alltwalis (formerly Blaengwen)	Carmarthenshire	SWA	51.98	-4.25
100203	Scout Moor	Lancashire	NWE	53.67	-2.27
100204	Minsca Farm	Dumfries & Galloway	SS	55.11	-3.22
100205	Muirhall	South Lanarkshire	SS	55.77	-3.59
100207	Braes O'Doune	Stirling	SS	56.28	-4.06
100208	Carscreugh Renewable Energy Park	Dumfries & Galloway	SS	54.92	-4.77
100210	Davidstow Community Wind Farm	Cornwall	SWE	50.63	-4.63
100212	Paul's Hill	Moray	NES	57.45	-3.48
100214	Auchencorth Moss	Midlothian	SS	56.45	-3.25
100216	Fferm Wynt Llaithddu	Powys	NWA	52.62	-3.72
100217	Goonhilly Repowering	Cornwall	SWE	50.05	-5.20
100218	Bowbeat	Scottish Borders	SS	55.72	-3.14
100219	Gordonbush	Highland	NES	58.11	-3.94
100220	Wardlaw Wood	North Ayrshire	SS	55.71	-4.72
100221	Bicker Fen	Lincolnshire	EM	52.93	-0.22
100223	Park Head	Northumberland	NEE	55.23	-1.84
100226	Minnygap Re-submission	Dumfries & Galloway	SS	55.25	-3.53
100229	Llyn Brenig	Denbighshire	NWA	53.10	-3.51

Continued on next page

Table A.1 – *Continued from previous page*

Site I.D.	Site Name	Location	Region	Latitude	Longitude
100235	Swinford	Leicestershire	EM	52.43	-1.15
100241	Slieve Kirk	Co Londonderry	NI	54.84	-7.17
100243	Keadby	Lincolnshire	EE	53.60	-0.74
100246	Edinbane	Highland	NWS	57.43	-6.42
100248	Cefn Croes	Ceredigion	NWA	52.41	-3.75
100249	Caton Moor Repowering	Lancashire	NWE	54.06	-2.66
100252	Hadyard Hill, Barr	South Ayrshire	SS	55.25	-4.72
100254	ECOCAS	Powys	NWA	52.59	-3.49
100256	Mynydd Waun Fawr	Powys	NWA	52.64	-3.46
100260	Meikle Carewe Re-submission	Aberdeenshire	NES	57.02	-2.29
100261	Waun Garno	Powys	NWA	52.87	-3.96
100264	Holbeach Marsh	Lincolnshire	EM	52.84	0.09
100265	Knoweside	South Ayrshire	SS	55.38	-4.74
100266	Artfield Fell	Dumfries & Galloway	SS	54.97	-4.77
100268	Tween Bridge Moor	South Yorkshire	EE	53.61	-0.91
100269	An Suidhe	Argyll & Bute	NWS	56.22	-5.22
100270	Gordonstown	Aberdeenshire	NES	57.44	-2.48
100271	West Hinkley Re-submission	Somerset	SWE	51.20	-3.15
100274	New Albion	Northamptonshire	EM	52.45	-0.76
100275	Berry Burn	Moray	NES	57.61	-3.62
100277	Lochluichart	Highland	NES	57.68	-4.79
100281	Altahullion Phase III Extension	Co Londonderry	NI	54.96	-7.03
100287	Pentland Road	Western Isles	NWS	58.26	-6.51
100290	Carraig Gheal (Loch Awe)	Argyll & Bute	NWS	56.43	-5.24
100291	Dummuie	Aberdeenshire	NES	57.42	-2.74
100295	Heckington Fen	Lincolnshire	EM	53.00	-0.21
100296	West Ancroft	Northumberland	NEE	55.70	-2.04
100298	Harestanes	Dumfries & Galloway	SS	55.22	-3.57
100299	Fallago Rig	Scottish Borders	SS	55.83	-2.66
100300	Black Law Phase I Extension	West Lothian	SS	55.77	-3.74
100302	Cemmaes	Powys	NWA	52.64	-3.68
100305	Ben Aketil	Highland	NWS	57.43	-6.46
100306	Crystal Rig 2 Extension	Scottish Borders	SS	55.91	-2.55
100310	Strathy South	Highland	NES	58.43	-4.07
100311	Dalswinton, Pennyland Moor	Dumfries & Galloway	SS	55.17	-3.67
100312	Lamonby	Cumbria	NWE	54.72	-2.94
100314	Tormywheel	West Lothian	SS	55.90	-2.26
100315	Sixpenny Wood	Yorkshire	EE	53.74	-0.80
100317	Novar Extension	Highland	NES	57.71	-4.43
100319	Cruach Mhor	Argyll & Bute	NWS	56.04	-5.16
100322	Deeping St Nicholas	Lincolnshire	EM	52.73	-0.22
100323	Nutsgrove Farm	Cambridgeshire	EM	52.64	-0.04
100325	Long Park	Scottish Borders	SS	55.67	-2.84
100327	Hirfynydd	Neath Port Talbot	SWA	51.74	-3.72
100328	Earlsburn	Stirling	SS	56.08	-4.08
100335	Park Estate (Pairc)	Western Isles	NWS	58.40	-6.31

Continued on next page

Table A.1 – *Continued from previous page*

Site I.D.	Site Name	Location	Region	Latitude	Longitude
100338	Dun Law Extension	Scottish Borders	SS	55.81	-2.86
100340	Bagot's Park	Staffordshire	WM	52.84	-1.88
100341	Dungavel Hill Wind Farm	South Lanarkshire	SS	55.60	-4.08
100347	Hare Hill	East Ayrshire	SS	55.35	-4.12
100348	Cambusmore	Highland	NES	57.99	-4.27
100349	Millour Hill	North Ayrshire	SS	55.74	-4.78
100350	Carno A & B Extension	Powys	NWA	52.55	-3.60
100352	Tullinoid	Co Fermanagh	NI	54.42	-7.82
100353	Crook Hill	Lancashire	NWE	53.68	-2.13
100356	Nant Bach Re-submission	Conwy	NWA	53.01	-3.50
100357	Black Law 1 Construction Phase II	South Lanarkshire	SS	55.77	-3.74
100360	Coldham	Cambridgeshire	EM	52.58	-0.15
100364	Rothes Extension	Moray	NES	57.54	-3.38
100365	Upper Holton	Suffolk	EA	52.36	1.54
100366	Rosehall Woods	Highland	NES	58.00	-4.55
100368	Camster	Highland	NES	58.40	-3.30
100370	Cowans Law	East Ayrshire	SS	55.65	-4.34
100373	Dunmaglass	Highland	NES	57.33	-4.31
100374	Ray Estate	Northumberland	NEE	55.16	-2.01
100375	Dun Law	Scottish Borders	SS	55.81	-2.86
100378	Mid Hill 1	Aberdeenshire	NES	56.96	-2.46
100379	St Breock Repowering	Cornwall	SWE	50.48	-4.86
100381	Slieve Rushen Repowering	Co Fermanagh	NI	54.16	-7.62
100383	Altahullion Phase I Extension	Co Londonderry	NI	54.96	-7.03
100384	Durran Mains	Caithness	NES	58.54	-3.42
100385	Fullabrook Down	Devon	SWE	51.15	-4.11
100386	Windy Standard Extension	Dumfries & Galloway	SS	55.29	-4.40
100388	Cemmaes 2	Powys	NWA	52.66	-3.66
100389	Mynydd y Betws	Carmarthenshire	SWA	51.78	-3.92
100390	Garves Mountain	Co Antrim	NI	55.15	-6.46
100392	Tirgwynt	Montgomeryshire	NWA	52.59	-3.49
100396	Earlshaugh	Scottish Borders	SS	55.44	-3.44
100398	Bishopwood	North Yorkshire	EE	53.78	-1.14
100399	St John's Hill Extension	Aberdeenshire	NES	56.87	-2.24
100402	Little Raith	Fife	NES	56.11	-3.30
100404	Kilgallioch	Dumfries & Galloway	SS	55.01	-4.74
100406	Cushnie	Aberdeenshire	NES	57.17	-2.86
100408	Milton Keynes	Buckinghamshire	EM	52.14	-0.66
100410	Stags Holt	Cambridgeshire	EM	52.58	-0.15
100411	Corriegarth Estate	Highland	NES	57.23	-4.44
100415	Gedney Marsh (Red House)	Lincolnshire	EM	52.84	-0.11
100420	Alcan Aluminium Smelter	Northumberland	NEE	55.20	-1.56
100422	Farr Windfarm	Highland	NES	57.33	-4.09
100424	Lissett Airfield	Yorkshire	EE	54.01	-0.25
100425	Windy Standard	Dumfries & Galloway	SS	55.29	-4.21
100426	Carn Hill	Co Antrim	NI	54.72	-5.92

Continued on next page

Table A.1 – *Continued from previous page*

Site I.D.	Site Name	Location	Region	Latitude	Longitude
100427	Bagmoor	Lincolnshire	EE	53.64	-0.63
100429	Hill of Ochiltree	Dumfries & Galloway	SS	55.04	-4.61
100430	Crystal Rig 1 Extension	Scottish Borders	SS	55.90	-2.51
100431	Kilbraur Extension	Highland	NES	58.05	-4.13
100438	Tullo	Aberdeenshire	NES	56.84	-2.40
100440	Moel Maelogen Extension	Conwy	NWA	53.14	-3.72
100443	Glenkerie Wind Farm	Scottish Borders	SS	55.54	-3.46
100444	Curryfree	Co Londonderry	NI	54.93	-7.31
100446	Knabs Ridge, Felliscliffe	North Yorkshire	EE	54.00	-1.64
100450	West Durham	County Durham	NEE	54.77	-1.82
100451	Kilbraur	Highland	NES	58.05	-4.13
100453	Kelmarsh	Northamptonshire	EA	52.40	0.95
100455	Waterhead Moor	North Ayrshire	SS	55.82	-4.79
100456	Ewe Hill	Dumfries & Galloway	SS	55.18	-3.12
100457	Toddleburn	Scottish Borders	SS	55.77	-2.81
100459	Hyndburn	Lancashire	NWE	53.71	-2.38
100464	Achany Estate	Highland	NES	58.00	-4.53
100467	Hall Farm	North Yorkshire	EE	53.87	-0.36
100468	Berrier Hill	Cumbria	NWE	54.67	-2.90
100470	Carnedd Wen	Powys	NWA	52.68	-3.59
100472	Rusholme	North Yorkshire	EE	53.73	-0.92
100473	Mynydd Gorddu	Ceredigion	NWA	52.46	-3.97
100475	Ardrossan	North Ayrshire	SS	55.69	-4.81
100477	Ardkinglass/Clachan Flats	Argyll & Bute	NWS	56.29	-4.95
100479	Altahullion Phase II Extension	Co Londonderry	NI	54.96	-7.03
100480	Muirhall Re-submission	South Lanarkshire	SS	55.76	-3.58
100481	Slieve Divena 1	Co Tyrone	NI	54.51	-7.11
100485	Fforch Nest Wind Farm	Bridgend	SWA	51.60	-3.49
100486	Dersalloch	East Ayrshire	SS	55.32	-4.40
100488	Callagheen	Co Fermanagh	NI	54.43	-8.01
100489	Maesgwyn	Neath Port Talbot	SWA	51.76	-3.62
100495	Red Tile	Cambridgeshire	EM	52.45	-0.01
100496	A'Chruach	Argyll & Bute	NWS	56.14	-5.34
100498	Baillie Wind Farm	Highland	NES	58.05	-4.13
100499	Bracco	North Lanarkshire	SS	55.87	-3.86
100500	Millennium	Highland	NES	57.13	-4.83
100501	Minch Moor	Scottish Borders	SS	56.11	-3.30
100502	Causeymire	Highland	NES	58.43	-3.51
100504	Wharrels Hill	Cumbria	NWE	54.73	-3.28
100507	Earlsburn extension	Stirling	SS	56.08	-4.08
100508	Carland Cross Repowering	Cornwall	SWE	50.35	-5.02
100509	Stacain	Argyll & Bute	NWS	56.40	-4.99
100510	Bullamoor	Yorkshire	EE	54.36	-1.39
100514	Drone Hill	Scottish Borders	SS	55.90	-2.26
100516	Glenconway	Co Londonderry	NI	54.84	-6.84
100520	Aikengall	East Lothian	SS	55.93	-2.46

Continued on next page

Table A.1 – *Continued from previous page*

Site I.D.	Site Name	Location	Region	Latitude	Longitude
100521	Drumderg	Perth & Kinross	NES	56.68	-3.36
100522	Matlock Moor	Derbyshire	EM	53.17	-1.53
100523	Withernwick Re-submission	Humberside	EE	53.85	-0.16
100525	Halsary	Highland	NES	58.43	-3.41
100528	Methlick Farmers Wind Farm	Aberdeenshire	NES	57.39	-2.30
100532	Hunters Hill	Co Tyrone	NI	54.45	-7.31
100533	Craigengelt Hill	Stirling	SS	56.06	-4.05
100534	Biggleswade	Bedfordshire	EM	52.05	-0.25
100535	Bristol Sewage Treatment Works	Gloucestershire	SWE	51.51	-2.67
100538	Calder Water	South Lanarkshire	SS	55.64	-4.21
100542	Gortfinbar	Omagh	NI	54.54	-7.03
100550	Slatbeg	Co Tyrone	NI	54.36	-7.21
100561	Standingfauld Farm	Perth & Kinross	NES	56.30	-3.82
100563	Bagot's Park Re-submission	Staffordshire	WM	52.84	-1.88
100565	Cregganconroe	Co Tyrone	NI	54.61	-6.97
100569	Rowan Tree	Scottish Borders	SS	55.74	-2.86
100571	Muirpark	Stirling	SS	56.06	-4.03
100576	Andershaw	South Lanarkshire	SS	55.52	-3.87
100577	Middlemoor	Northumberland	NEE	55.50	-1.77
100578	Old Dalby	Leicestershire	EM	52.81	-1.03
100579	Spaldington Common	Yorkshire	EE	53.79	-0.82
100586	Ewe Hill	Dumfries & Galloway	SS	55.18	-3.12
100587	Linton	Cambridgeshire	EM	52.08	0.24
100588	Harrington	Northamptonshire	EM	52.39	0.03
100591	Muaitheabhal Re-submission	Western Isles	NWS	58.02	-6.54
100593	Baumber	Lincolnshire	EM	53.24	-0.19
100594	Solway Bank	Dumfries & Galloway	SS	55.11	-3.10
100596	Truthan Barton	Cornwall	SWE	50.32	-5.03
100597	Burton Wold Wind Farm Extension	Northamptonshire	EM	52.36	-0.66
100601	Elginny Hill	Co Antrim	NI	54.87	-6.18
100604	Middleton	East Renfrewshire	SS	55.75	-4.41
100607	Wandylaw Moor	Northumberland	NEE	55.52	-1.80
100614	Spireslack	East Ayrshire	SS	55.53	-4.03
100620	Saxby Wold	Yorkshire	EE	53.64	-0.47
100622	Screggagh	Co Tyrone	NI	54.45	-7.34
100626	Sober Hill	Yorkshire	EE	53.84	-0.61
100627	Boulfruich	Highland	NES	58.30	-3.43
100628	Penny Hill	South Yorkshire	EE	53.39	-1.28
100630	Seegronan	Co Tyrone	NI	54.65	-7.70
100634	Inishative	Omagh	NI	54.57	-6.98
100635	Watford Lodge	Northamptonshire	EM	52.33	-1.11
100636	Hirddywell	Powys	NWA	52.61	-3.75
100639	Twin Rivers Wind Farm	Yorkshire	EE	53.70	-0.87
100645	Woodlane	North Yorkshire	EE	53.98	-1.57
100647	Lenchwick	Worcestershire	WM	52.15	-1.98
100649	Muaitheabhal	Western Isles	NWS	58.02	-6.54

Continued on next page

Table A.1 – *Continued from previous page*

Site I.D.	Site Name	Location	Region	Latitude	Longitude
100651	Gronan	Co Tyrone	NI	54.65	-7.70
100658	Threapland Lees	Cumbria	NWE	54.73	-3.30
100660	Cotton Farm	Cambridgeshire	EM	52.26	-0.20
100661	Carno Phase II Extension	Powys	NWA	52.54	-3.60
100662	Whitton	Scottish Borders	SS	55.49	-2.38
100663	Carno A & B	Powys	NWA	52.55	-3.60
100669	Little Cheyne Court	Kent	SEE	50.96	0.82
100671	Kildrummy	Aberdeenshire	NES	57.27	-2.97
100674	Coldham Extension	Cambridgeshire	EM	52.60	0.13
100677	Allt Dearg	Argyll & Bute	NWS	55.96	-5.45
100679	Dunbeg	Co Londonderry	NI	55.09	-6.82
100683	Ffynnon Oer	Neath Port Talbot	SWA	51.68	-3.67
100685	St John's Hill	Aberdeenshire	NES	56.87	-2.24
100687	Kirkharle Wind Farm	Northumberland	NEE	55.12	-2.01
100689	Altgolan	Co Tyrone	NI	54.63	-7.67
100690	Spittal Hill	Highland	NES	58.46	-3.43
100692	The Grange	Northumberland	EM	52.75	0.17
100695	Lilibourne Wind Farm	Northamptonshire	EM	52.39	-1.16
100701	Armistead	Cumbria	NWE	54.28	-2.64
100702	North Rhins	Dumfries & Galloway	SS	54.87	-5.09
100709	Teiges	Co Fermanagh	NI	54.30	-7.34
100710	Bryngydfa	Powys	NWA	52.40	-3.26
100714	Kilchattan	Argyll & Bute	NWS	55.35	-5.60
100717	Hill of Stroupster	Highland	NES	58.58	-3.15
100719	Red Gap Farm	County Durham	NEE	54.65	-1.32
100724	Cleek Hall	Yorkshire	EE	53.78	-1.02
100725	Newfield Wind Farm	Dumfries & Galloway	SS	55.18	-3.32
100728	Wadlow Wind Farm	Cambridgeshire	EM	52.16	0.31
100729	Derwydd Bach	Denbighshire	NWA	53.04	-3.45
100732	Mynydd y Gwair	Swansea	SWA	51.76	-3.96
100740	Cowans Law Re-submission	East Ayrshire	SS	55.64	-4.39
Offshore					
100025	Lincs	Norfolk	HU	53.19	0.49
100032	Kentish Flats	Kent	TH	51.45	1.14
100036	Lynn & Inner Dowsing	Lincolnshire	HU	53.13	0.44
100056	Sheringham Shoal	Norfolk	HU	53.13	1.15
100062	Beatrice	North Sea	CRO	58.11	-3.09
100088	Gunfleet Sands I	Essex	TH	51.73	1.21
100094	Teesside	County Durham	TD	54.63	-1.08
100102	Westernmost Rough	Yorkshire	HU	53.81	0.15
100103	Firth of Forth	Firth of Forth	FRT	56.35	-1.73
100113	Thanet	Thames	TH	51.43	1.63
100141	Greater Gabbard - Inner	East Anglia	TH	51.92	1.92
100147	Norfolk	Norfolk	TH	52.62	2.57

Continued on next page

Table A.1 – *Continued from previous page*

Site I.D.	Site Name	Location	Region	Latitude	Longitude
100194	Dogger Bank	Dogger Bank	TD	55.21	2.34
100199	London Array	Thames	TH	51.65	1.54
100206	Irish Sea	Irish Sea	IRS	53.77	-4.39
100209	Hastings	Norfolk	ECH	50.64	-0.18
100236	North Hoyle	Denbighshire	IRS	53.43	-3.40
100237	Rhyl Flats	Conwy	IRS	53.37	-3.65
100285	West Duddon	Irish Sea	IRS	53.99	-3.47
100307	Dudgeon	Norfolk	HU	53.26	1.37
100308	Humber Gateway	Humberside	HU	53.64	0.29
100332	Hornsea	Yorkshire	HU	53.96	1.55
100336	Docking Shoal	Norfolk	HU	53.16	0.75
100344	Scroby Sands	Norfolk	TH	52.63	1.78
100361	Ormonde	Cumbria	IRS	54.10	-3.42
100376	Moray Firth	Moray Firth	CRO	58.15	-2.84
100423	Walney II	Irish Sea	IRS	54.09	-3.62
100441	Barrow	Cumbria	IRS	53.98	-3.28
100462	Walney I	Irish Sea	IRS	54.05	-3.53
100466	Burbo Bank	Merseyside	IRS	53.48	-3.18
100474	West Isle of Wight	Isle of Wight	ECH	50.43	-1.81
100476	Race Bank	Norfolk	HU	53.29	0.82
100482	Robin Rigg	Solway	IRS	54.75	-3.68
100493	Greater Gabbard	East Anglia	TH	51.77	1.96
100513	Triton Knoll	East Anglia	HU	53.48	0.84
100517	Bristol Channel	Bristol Channel	LUN	51.37	-4.47
100552	London Array I	Thames	TH	51.63	1.53
100590	West of Duddon Sands	Cumbria	IRS	53.97	-3.43
100610	London Array II	Thames	TH	51.63	1.53
100640	Gwynt y Mor	Conwy	IRS	53.43	-3.63
100684	Gunfleet Sands II	Essex	TH	51.72	1.21
100800	Solway Firth	Solway	IRS	54.71	-3.80
100802	Islay	West coast	MAL	55.77	-6.75
100803	Argyll Array	West coast	MAL	56.41	-7.12
100804	Kintyre	West coast	MAL	55.44	-5.84
100805	Beatrice	Morray Firth	CRO	58.26	-2.89
100806	Inch Cape	Forth Estuary	FRT	56.49	-2.19
100807	Neart na Gaoithe	Forth Estuary	FRT	56.27	-2.25
100808	Forth Array	Forth Estuary	FRT	56.04	-1.92

Table A.1: Onshore and offshore wind farms available in the wind resource model from Hawkins [2012].

Appendix B

Wind temporal distributions

B.1 Capacity factors

The temporal distributions of capacity factors for the onshore and offshore wind portfolios are shown in Figure B.1.

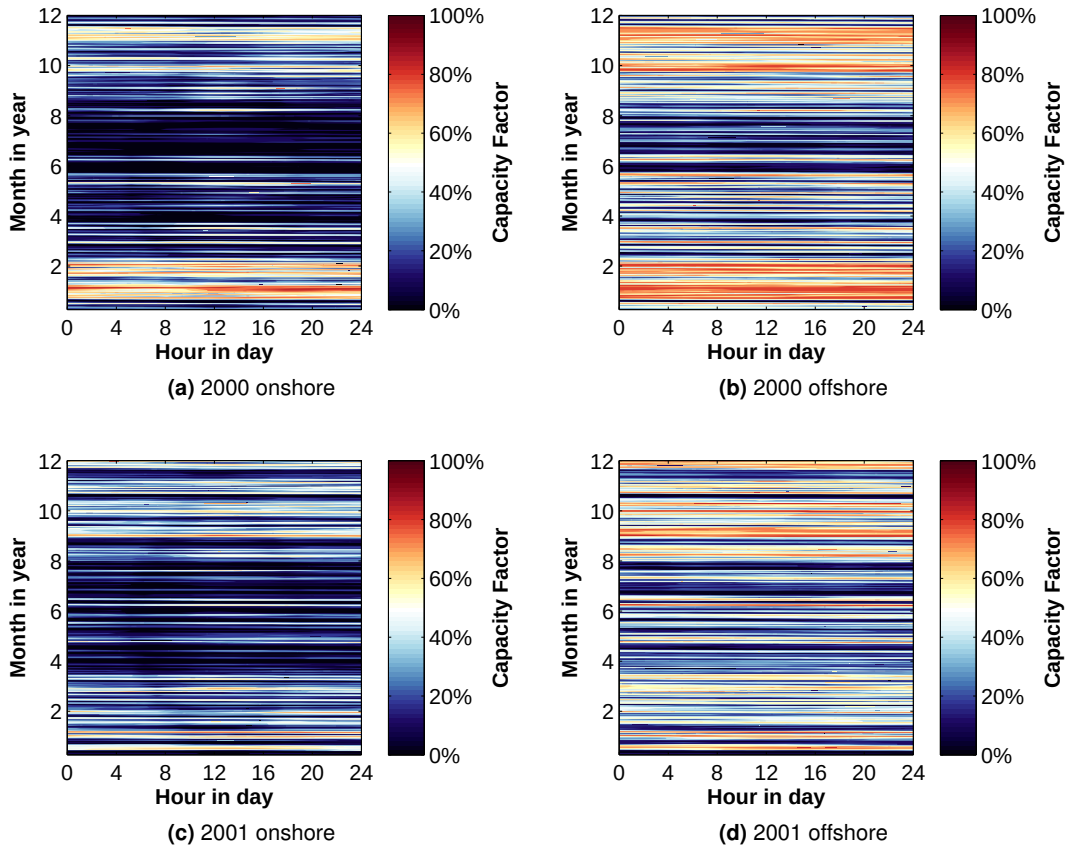

Figure B.1: Temporal distributions for onshore and offshore capacity factors by year. *Continued on next page*

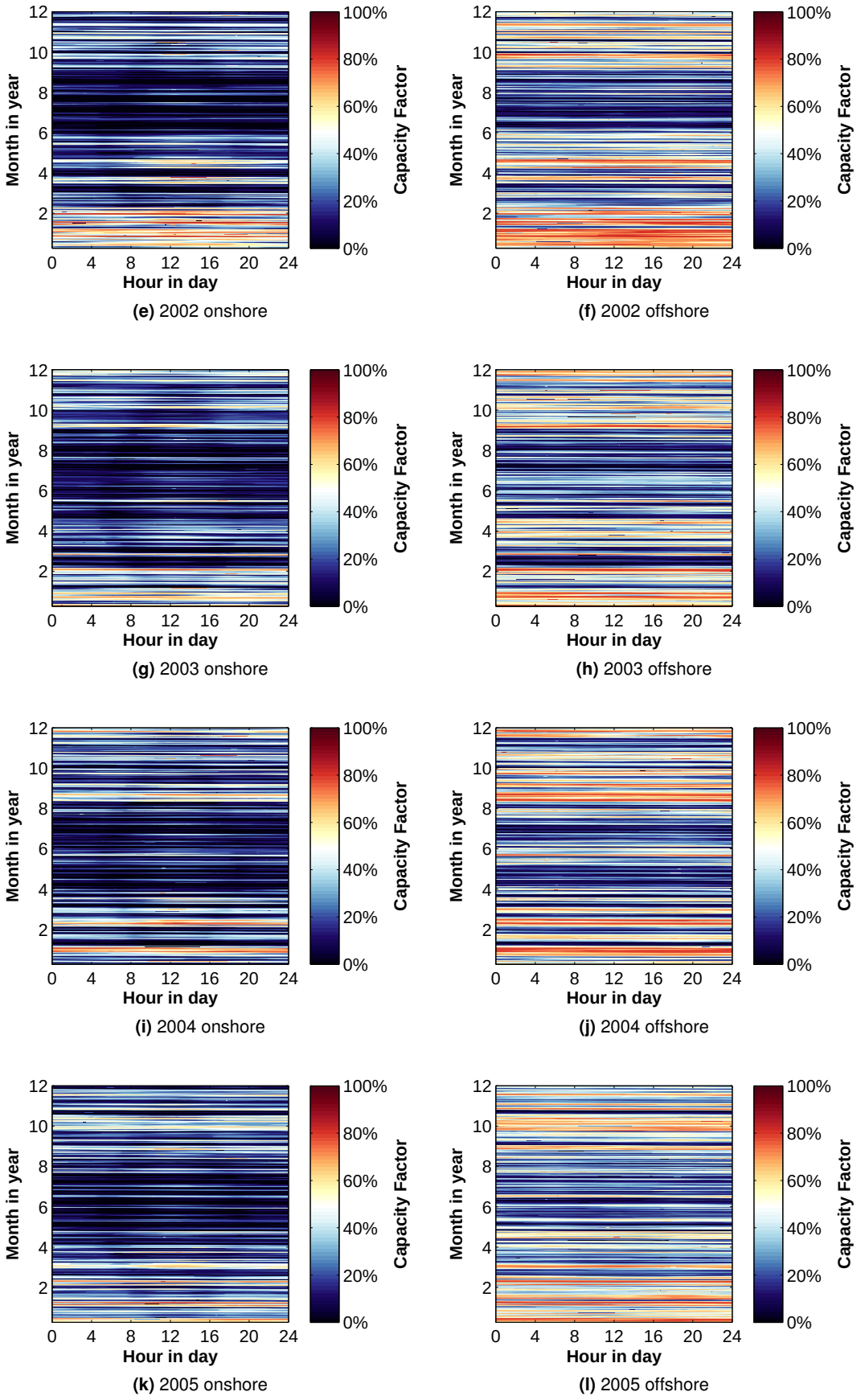

(e) 2002 onshore

(f) 2002 offshore

(g) 2003 onshore

(h) 2003 offshore

(i) 2004 onshore

(j) 2004 offshore

(k) 2005 onshore

(l) 2005 offshore

Figure B.1: Temporal distributions for onshore and offshore capacity factors by year. *Continued on next page*

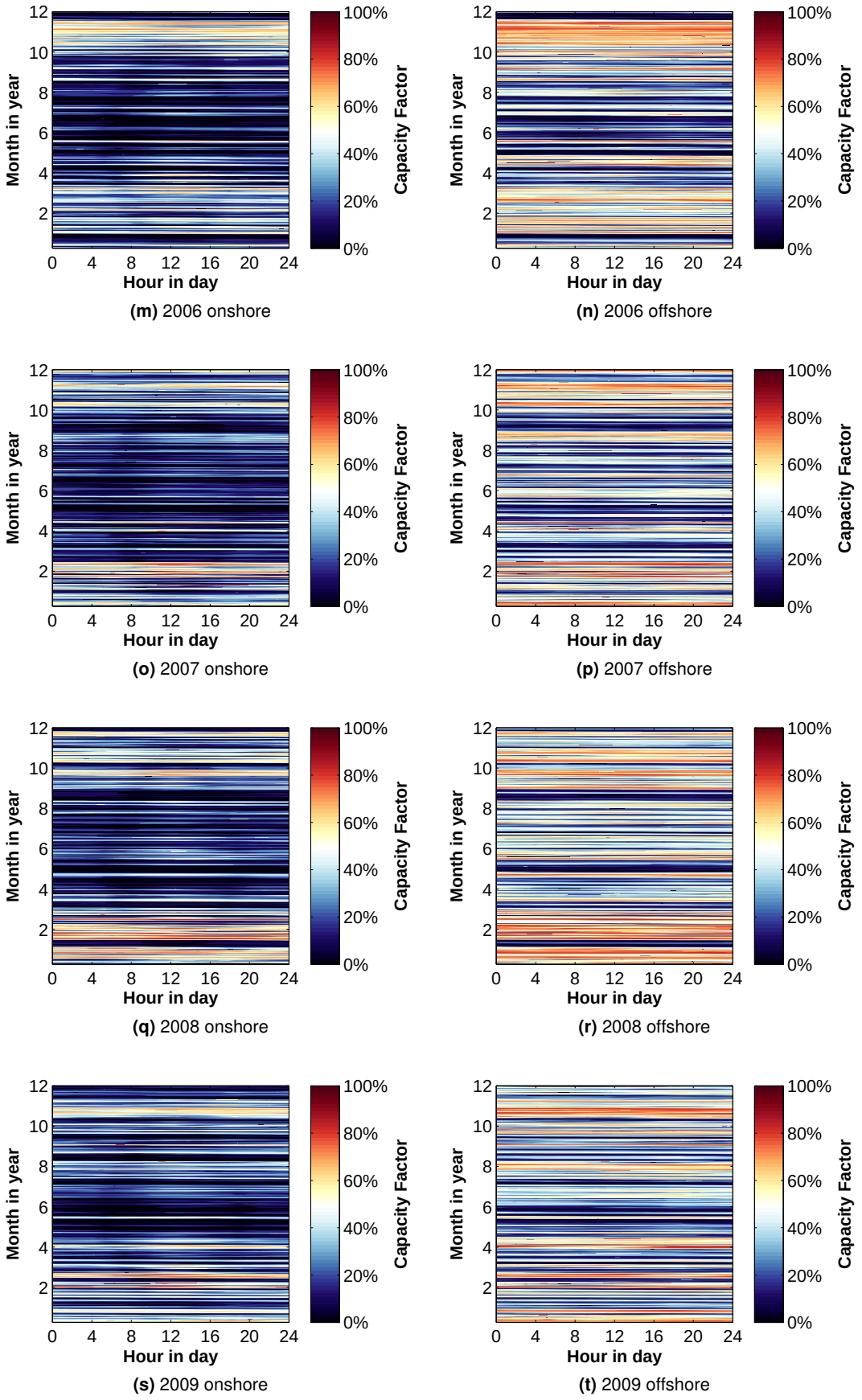

(m) 2006 onshore **(n)** 2006 offshore

(o) 2007 onshore **(p)** 2007 offshore

(q) 2008 onshore **(r)** 2008 offshore

(s) 2009 onshore **(t)** 2009 offshore

Figure B.1: Temporal distributions for onshore and offshore capacity factors by year. *Continued on next page*

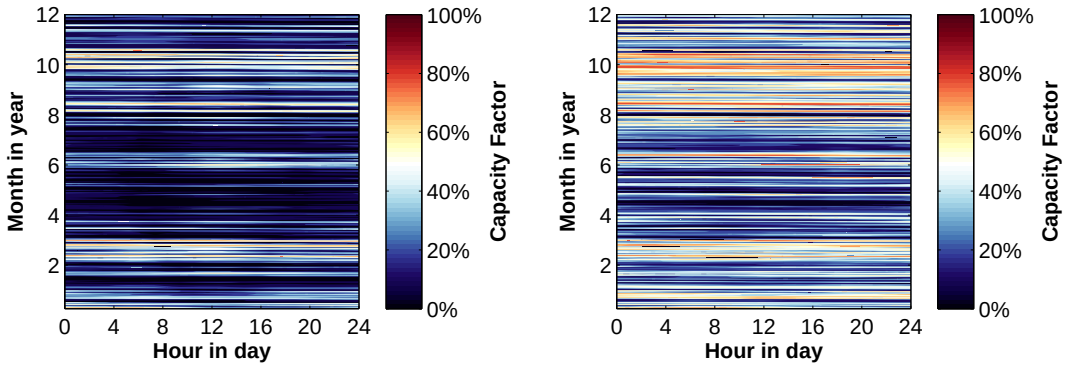

(u) 2010 onshore **(v)** 2010 offshore

Figure B.1: Temporal distributions for onshore and offshore capacity factors by year.

B.2 Wind ramps

The temporal distributions of 1-h wind ramp events for the onshore and offshore wind portfolios are shown in Figure B.2.

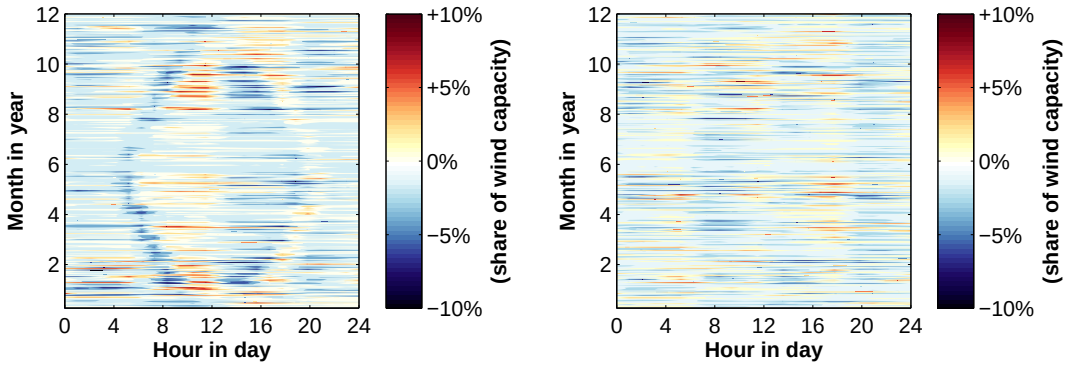

(a) 2000 onshore **(b)** 2000 offshore

Figure B.2: Temporal distributions for 1-h onshore and offshore wind ramp events by year.
Continued on next page

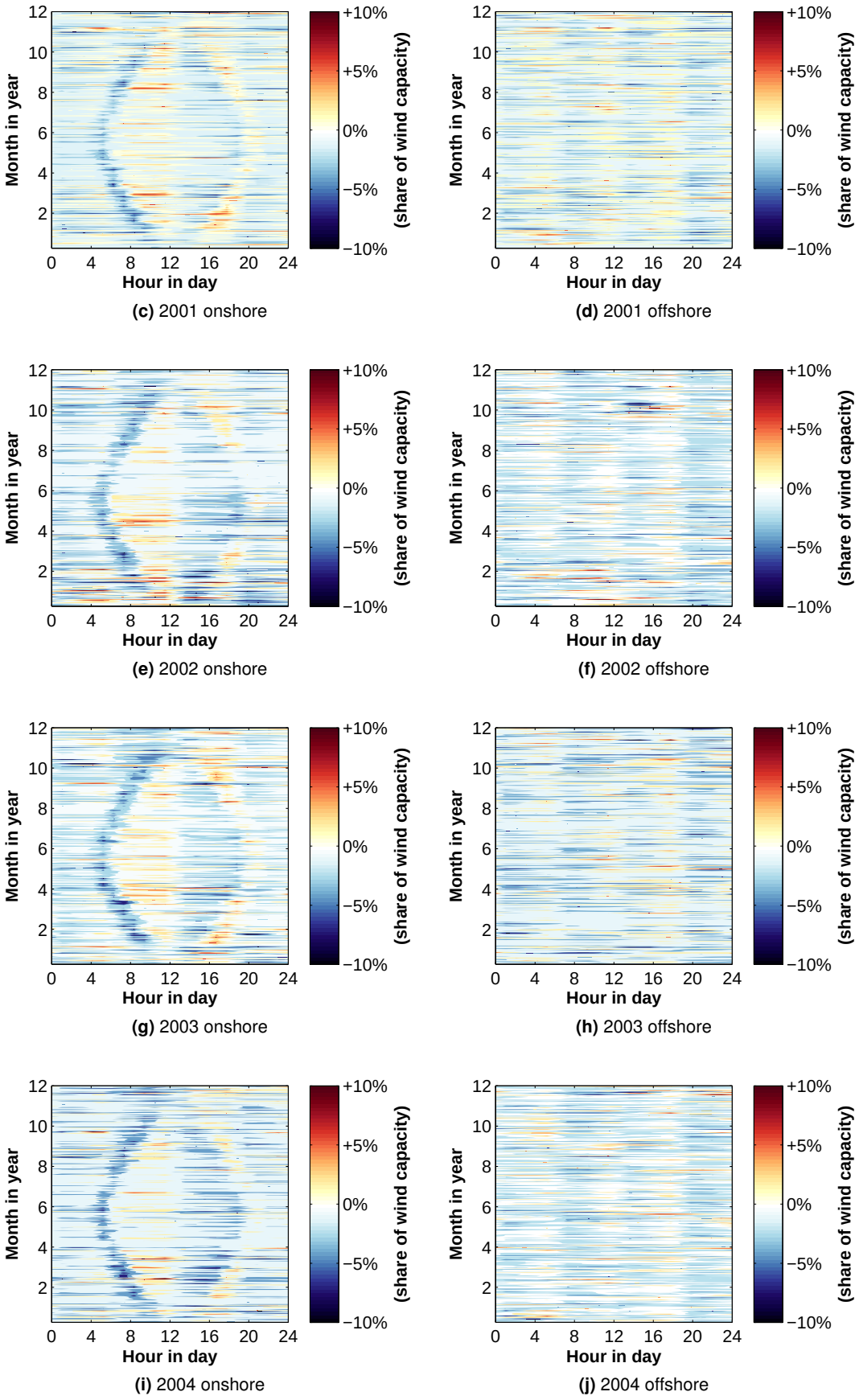

(c) 2001 onshore **(d)** 2001 offshore

(e) 2002 onshore **(f)** 2002 offshore

(g) 2003 onshore **(h)** 2003 offshore

(i) 2004 onshore **(j)** 2004 offshore

Figure B.2: Temporal distributions for 1-h onshore and offshore wind ramp events by year.
Continued on next page

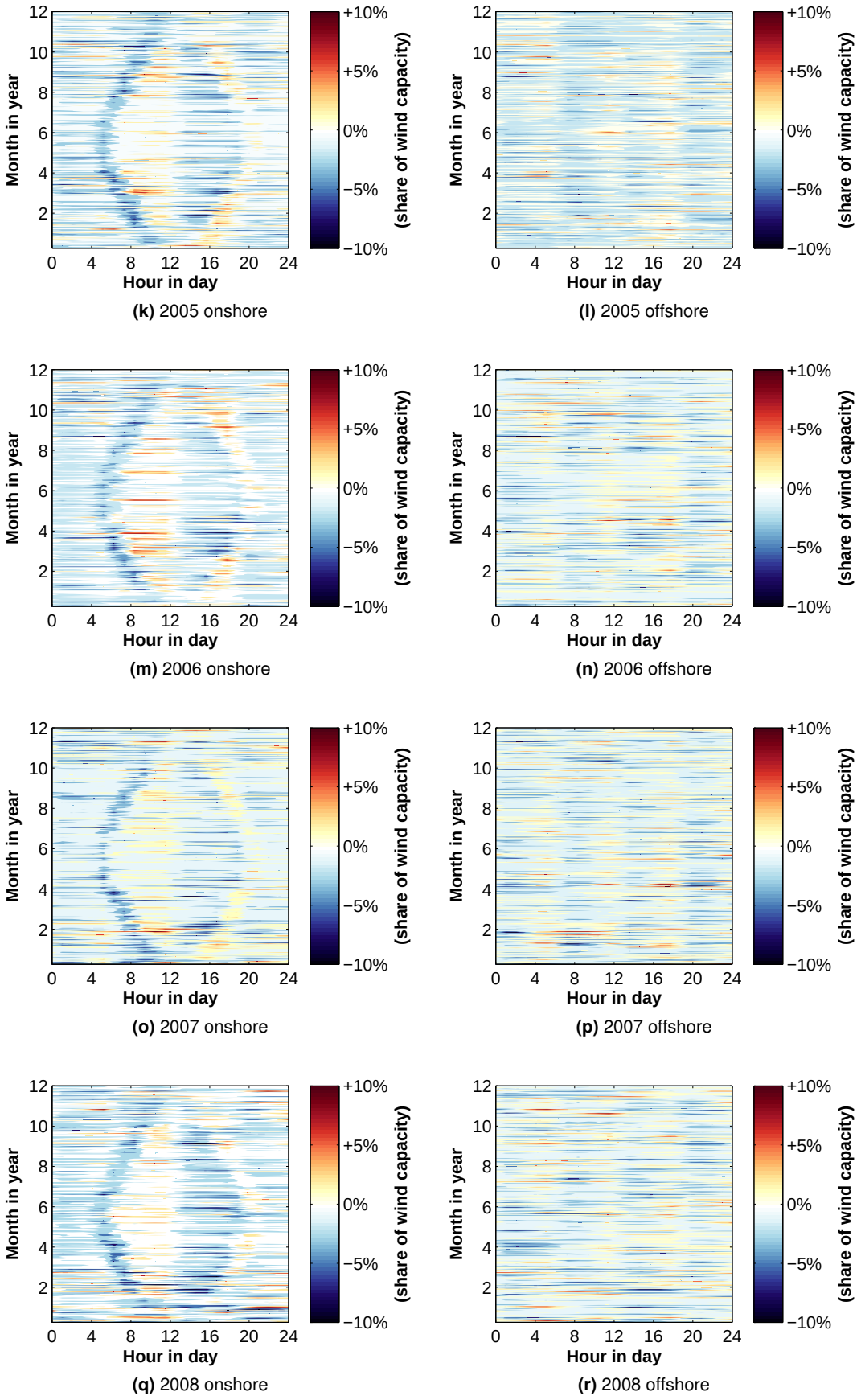

Figure B.2: Temporal distributions for 1-h onshore and offshore wind ramp events by year.
Continued on next page

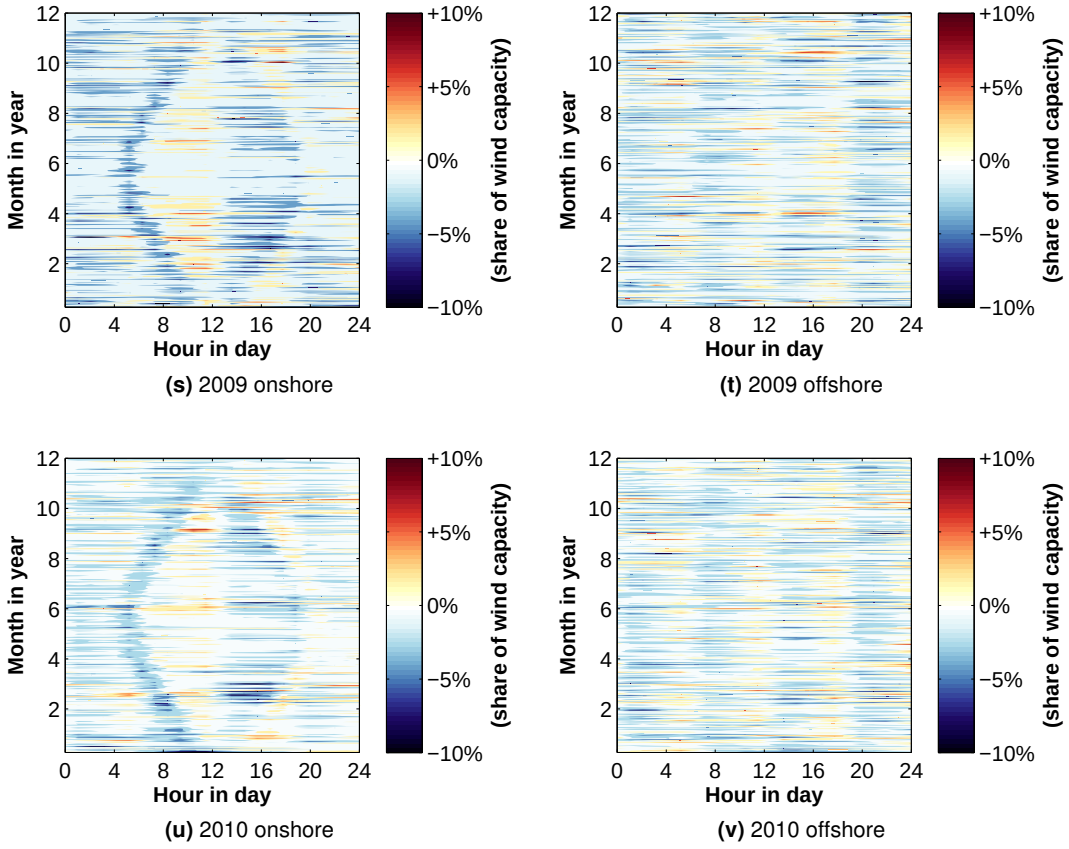

Figure B.2: Temporal distributions for 1-h onshore and offshore wind ramp events by year.

Appendix C

Test System Data – IEEE RTS-96

C.1 IEEE RTS-96 test system data

The IEEE RTS-96 single-area test system is used to validate the unit commitment model. Data for the 26-unit test system is taken from Wang and Shahidehpour [1993]; Grigg *et al.* [1999]. The Institute of Electrical and Electronics Engineers (IEEE) developed an enhanced single-area test system for bulk power system reliability evaluation studies [Grigg *et al.*, 1999]. Transmission arrangements are simplified by assuming a single bus network. The IEEE Reliability Test System - 1996 (RTS-96) Grigg *et al.* [1999] was initially developed in 1979 IEEE Reliability Test System Task Force [1979] and later updated in 1986 Allan *et al.* [1986]. It contains detailed generator information for a total of 32 units including 6 hydro. The 6 hydro units, each 50 MW, are excluded so there is in total 26 thermal power plants with a total installed capacity of 3105 MW. Electricity demand data for the test system is shown in Table C.1.

Available in the section are additional data sources for the IEEE RTS-96 test system used in Chapter 5. These include:

- electricity demand data is shown in Table C.1;
- start-up costs, thermal cooling constants, and variable O&M costs are shown in Table C.2; and
- fuel costs for each of the generators are obtained from IEEE Reliability Test System Task Force [1979] and are shown in Table C.3.

Start-up cost data for the 26-unit system in Wang and Shahidehpour [1993] are taken from Ouyang and Shahidehpour [1991], which is shown in Table C.2 and is implemented in the form:

$$C_{g,t}^{\text{start}} = \overbrace{A_g}^{\text{fixed}} + \overbrace{B_g}^{\text{fuel}} \left(\overbrace{1 - e^{(X_{g,t}/\tau_g^c)}}^{\text{exponential}} \right) \tag{C.1}$$

where A_g are the fixed costs (\$), B_g are the fuel costs incurred during start-up (\$), $X_{g,t}$ is the time period (h) generator g has been online(+)/offline(-) at time t, and τ_g^c is the thermal cooling constant (h) that determines the exponential time-dependent profile of a unit's start-up costs. The start-up cost formulation in Ouyang and Shahidehpour [1991] is the same as the start-up

Time t (h)	Demand D_t (MW)	Time t (h)	Demand D_t (MW)
1	1700	13	2590
2	1730	14	2550
3	1690	15	2620
4	1700	16	2650
5	1750	17	2550
6	1850	18	2530
7	2000	19	2500
8	2430	20	2550
9	2540	21	2600
10	2600	22	2480
11	2670	23	2200
12	2590	24	1840

Table C.1: Demand data for the 26-unit IEEE RTS-96 test system from Wang and Shahidehpour [1993].

Unit	Fixed start-up costs A_g ($)	Fuel start-up costs B_g ($)	Thermal cooling constant τ_g^c (h)	Variable O&M costs $c_g^{O\&M}$ ($/MWh$_e$)
u12	0	0	1	0.90
u20	20	20	2	5.00
u76	50	50	3	0.90
u100	70	70	4	0.80
u155	150	150	6	0.80
u197	200	200	8	0.70
u350	300	200	8	0.70
u400	500	500	10	0.30

Table C.2: Start-up cost data for the 26-unit IEEE RTS-96 test system from Wang and Shahidehpour [1993] and Ouyang and Shahidehpour [1991].

Fuel	Fuel cost ($/MWh$_{th}$)	Fuel cost ($/MBTU$_{th}$)	CO_2 emission intensity (tCO_2/MWh$_{th}$)
Oil #6	7.85	2.30	0.2629
Oil #2	10.24	3.00	0.2474
Coal	4.09	1.20	0.3248
Nuclear	2.05	0.60	-

Table C.3: Fuel cost data and CO_2 emissions factors for the 26-unit IEEE RTS-96 test system from IEEE Reliability Test System Task Force [1979].

cost formulation proposed in this thesis without CO_2 costs and CO_2 capture equipment. The start-up cost data for the 26-units are implemented using the equation:

$$C_{g,t}^{\text{start}} = \overbrace{c_g^{\text{start,fixed}}}^{\text{fixed}} + \left(\overbrace{F_g^{\text{start,cold}} c_{g,t}^{\text{fuel}}}^{\text{fuel}} \right) \cdot \left(\overbrace{1 - e^{(X_{g,t}/\tau_g^{\text{c}})}}^{\text{exponential}} \right) \tag{C.2}$$

where $c_g^{\text{start,fixed}}$ are the fixed start-up costs (£), and $F_g^{\text{start,cold}}$ is the fuel consumption during a cold start-up (MWh_{th}). This implies that A_g in Equation C.1 is equal to $c_g^{\text{start,fixed}}$ and B_g is equal to $F_g^{\text{start,cold}} c_{g,t}^{\text{fuel}}$. Including CO_2 costs and CO_2 capture equipment the start-up cost function becomes:

$$C_{g,t}^{\text{start}} = \overbrace{c_g^{\text{start,fixed}}}^{\text{fixed}} + \left(\overbrace{F_g^{\text{start,cold}} c_{g,t}^{\text{fuel}}}^{\text{fuel}} + \overbrace{F_g^{\text{start,cold}} e_g^{\text{CO}_2} c_t^{\text{CO}_2} (1 - Y_{g,t}^{\text{capt}})}^{\text{CO}_2} \right) \cdot \left(\overbrace{1 - e^{(X_{g,t}/\tau_g^{\text{c}})}}^{\text{exponential}} \right) \tag{C.3}$$

where $Y_{g,t}^{\text{capt}}$ is the CO_2 capture rate during start-up and $e_g^{\text{CO}_2}$ is the fuel-specific emission factor.

Appendix D

Test System Data – GB

D.1 GB test system data

This section includes system data used in Chapter 6. It contains data for typical GB generation technologies and unit-specific fuel consumption data. The three linear segments in Table D.1 are equally spaced between the minimum and maximum power output limits of units.

		Segment 1		**Segment 2**		**Segment 3**	
		$\beta_{g,1}$	$\alpha_{g,1}$	$\beta_{g,2}$	$\alpha_{g,2}$	$\beta_{g,3}$	$\alpha_{g,3}$
Type	**No.**	MW_{th}/MW_e	MW_{th}	MW_{th}/MW_e	MW_{th}	MW_{th}/MW_e	MW_{th}
Nuclear	1	2.7265	0.0000	2.7265	0.0000	2.7265	0.0000
	2	2.7265	0.0000	2.7265	0.0000	2.7265	0.0000
	3	2.7265	0.0000	2.7265	0.0000	2.7265	0.0000
	4	2.7265	0.0000	2.7265	0.0000	2.7265	0.0000
	5	2.7265	0.0000	2.7265	0.0000	2.7265	0.0000
	6	2.7265	0.0000	2.7265	0.0000	2.7265	0.0000
	7	2.7265	0.0000	2.7265	0.0000	2.7265	0.0000
	8	2.7265	0.0000	2.7265	0.0000	2.7265	0.0000
CCGT+PCC	9	1.3977	199.3173	1.5589	112.2566	1.6384	55.0061
	10	1.4001	199.6609	1.5616	112.4502	1.6412	55.1010
	11	1.4025	200.0046	1.5643	112.6437	1.6440	55.1958
	12	1.4049	200.3482	1.5669	112.8373	1.6469	55.2906
CCGT	13	1.3495	192.4442	1.5051	108.3857	1.5819	53.1094
	14	1.3555	193.3034	1.5118	108.8696	1.5890	53.3465
	15	1.3615	194.1625	1.5186	109.3535	1.5960	53.5836
	16	1.3675	195.0216	1.5253	109.8373	1.6031	53.8206
	17	1.3736	195.8808	1.5320	110.3212	1.6101	54.0577
	18	1.3796	196.7399	1.5387	110.8051	1.6172	54.2948
	19	1.3856	197.5990	1.5454	111.2889	1.6243	54.5319
	20	1.3916	198.4581	1.5522	111.7728	1.6313	54.7690
	21	1.3977	199.3173	1.5589	112.2566	1.6384	55.0061
	22	1.4037	200.1764	1.5656	112.7405	1.6455	55.2432
	23	1.4097	201.0355	1.5723	113.2244	1.6525	55.4803
	24	1.4157	201.8946	1.5790	113.7082	1.6596	55.7174
	25	1.4218	202.7538	1.5858	114.1921	1.6666	55.9545
	26	1.4278	203.6129	1.5925	114.6760	1.6737	56.1916

Continued on next page

Table D.1 – *Continued from previous page*

		Segment 1		Segment 2		Segment 3	
		$\beta_{g,1}$	$\alpha_{g,1}$	$\beta_{g,2}$	$\alpha_{g,2}$	$\beta_{g,3}$	$\alpha_{g,3}$
Type	**No.**	MW_{th}/MW_e	MW_{th}	MW_{th}/MW_e	MW_{th}	MW_{th}/MW_e	MW_{th}
	27	1.4338	204.4720	1.5992	115.1598	1.6808	56.4287
	28	1.4398	205.3311	1.6059	115.6437	1.6878	56.6658
	29	1.4458	206.1903	1.6126	116.1276	1.6949	56.9029
	30	1.4519	207.0494	1.6194	116.6114	1.7019	57.1400
	31	1.4579	207.9085	1.6261	117.0953	1.7090	57.3771
	32	1.4639	208.7676	1.6328	117.5792	1.7161	57.6142
	33	1.4699	209.6268	1.6395	118.0630	1.7231	57.8513
	34	1.4760	210.4859	1.6462	118.5469	1.7302	58.0884
	35	1.4820	211.3450	1.6529	119.0308	1.7373	58.3255
	36	1.4880	212.2041	1.6597	119.5146	1.7443	58.5626
	37	1.4940	213.0633	1.6664	119.9985	1.7514	58.7997
	38	1.5001	213.9224	1.6731	120.4824	1.7584	59.0367
	39	1.5061	214.7815	1.6798	120.9662	1.7655	59.2738
	40	1.5121	215.6407	1.6865	121.4501	1.7726	59.5109
	41	1.5181	216.4998	1.6933	121.9339	1.7796	59.7480
	42	1.5242	217.3589	1.7000	122.4178	1.7867	59.9851
	43	1.5302	218.2180	1.7067	122.9017	1.7938	60.2222
	44	1.5362	219.0772	1.7134	123.3855	1.8008	60.4593
	45	1.5422	219.9363	1.7201	123.8694	1.8079	60.6964
	46	1.5483	220.7954	1.7269	124.3533	1.8149	60.9335
	47	1.5543	221.6545	1.7336	124.8371	1.8220	61.1706
	48	1.5603	222.5137	1.7403	125.3210	1.8291	61.4077
	49	1.5663	223.3728	1.7470	125.8049	1.8361	61.6448
	50	1.5724	224.2319	1.7537	126.2887	1.8432	61.8819
	51	1.5784	225.0910	1.7605	126.7726	1.8503	62.1190
	52	1.5844	225.9502	1.7672	127.2565	1.8573	62.3561
OCGT	53	2.0362	182.2970	2.2711	102.6707	2.3870	50.3090
	54	2.0483	183.3757	2.2846	103.2783	2.4011	50.6067
	55	2.0603	184.4544	2.2980	103.8858	2.4152	50.9044
	56	2.0724	185.5331	2.3114	104.4933	2.4293	51.2021
	57	2.0844	186.6117	2.3249	105.1008	2.4435	51.4997
	58	2.0965	187.6904	2.3383	105.7083	2.4576	51.7974
	59	2.1085	188.7691	2.3518	106.3159	2.4717	52.0951
	60	2.1206	189.8478	2.3652	106.9234	2.4858	52.3928
	61	2.1326	190.9265	2.3786	107.5309	2.5000	52.6905
	62	2.1447	192.0051	2.3921	108.1384	2.5141	52.9882
	63	2.1567	193.0838	2.4055	108.7459	2.5282	53.2859
	64	2.1688	194.1625	2.4189	109.3535	2.5423	53.5836
	65	2.1808	195.2412	2.4324	109.9610	2.5565	53.8812
	66	2.1929	196.3199	2.4458	110.5685	2.5706	54.1789
	67	2.2049	197.3985	2.4593	111.1760	2.5847	54.4766
	68	2.2170	198.4772	2.4727	111.7835	2.5988	54.7743
	69	2.2290	199.5559	2.4861	112.3911	2.6130	55.0720
	70	2.2411	200.6346	2.4996	112.9986	2.6271	55.3697

Continued on next page

Table D.1 – *Continued from previous page*

		Segment 1		Segment 2		Segment 3	
		$\beta_{g,1}$	$\alpha_{g,1}$	$\beta_{g,2}$	$\alpha_{g,2}$	$\beta_{g,3}$	$\alpha_{g,3}$
Type	**No.**	MW_{th}/MW_e	MW_{th}	MW_{th}/MW_e	MW_{th}	MW_{th}/MW_e	MW_{th}
	71	2.2531	201.7133	2.5130	113.6061	2.6412	55.6674
	72	2.2652	202.7919	2.5265	114.2136	2.6553	55.9650
	73	2.2772	203.8706	2.5399	114.8211	2.6694	56.2627
	74	2.2893	204.9493	2.5533	115.4287	2.6836	56.5604
	75	2.3013	206.0280	2.5668	116.0362	2.6977	56.8581
	76	2.3134	207.1067	2.5802	116.6437	2.7118	57.1558
	77	2.3254	208.1853	2.5936	117.2512	2.7259	57.4535
	78	2.3375	209.2640	2.6071	117.8587	2.7401	57.7512
	79	2.3495	210.3427	2.6205	118.4662	2.7542	58.0488
	80	2.3616	211.4214	2.6340	119.0738	2.7683	58.3465
	81	2.3736	212.5001	2.6474	119.6813	2.7824	58.6442
	82	2.3856	213.5787	2.6608	120.2888	2.7966	58.9419
	83	2.3977	214.6574	2.6743	120.8963	2.8107	59.2396
	84	2.4097	215.7361	2.6877	121.5038	2.8248	59.5373
	85	2.4218	216.8148	2.7012	122.1114	2.8389	59.8350
	86	2.4338	217.8935	2.7146	122.7189	2.8531	60.1327
	87	2.4459	218.9722	2.7280	123.3264	2.8672	60.4303
	88	2.4579	220.0508	2.7415	123.9339	2.8813	60.7280
	89	2.4700	221.1295	2.7549	124.5414	2.8954	61.0257
	90	2.4820	222.2082	2.7683	125.1490	2.9096	61.3234
	91	2.4941	223.2869	2.7818	125.7565	2.9237	61.6211
	92	2.5061	224.3656	2.7952	126.3640	2.9378	61.9188

Table D.1: Generator quadratic cost data for the 92-unit GB test system.

Nuclear plant parameters		
$P_{g,\min}$	Minimum power output (MW_e)	990
$P_{g,\max}$	Maximum power output (MW_e)	1650
ρ_g^{up}	Ramp up rate (MW_e/h)	4950
ρ_g^{dn}	Ramp down rate (MW_e/h)	4950
α_g^{up}	Upwards ramping ratio (-)	3.00
α_g^{dn}	Downwards ramping ratio (-)	3.00
$UT_{g,\min}$	Minimum up time (h)	24
$DT_{g,\min}$	Minimum down time (h)	24
$X_{g,t}$	Initial hours (h)	+8
$c_{g,t}^{\text{fuel}}$	Cost of fuel (£/MWh_{th})	5.1
$e_g^{CO_2}$	Emission factor (tCO_2/MWh_{th})	0
$c_g^{\text{O\&M}}$	Variable O&M cost ($£/MWh_e$)	0.5
$c_g^{\text{ramp,up}}$	Upwards ramping cost ($£/MW_e$)	5.0
$c_g^{\text{ramp,dn}}$	Downwards ramping cost ($£/MW_e$)	5.0
$c_g^{\text{start,fixed}}$	Fixed start-up cost (£)	100000
$F_g^{\text{start,cold}}$	Fuel consumption during cold start-up (MWh_{th})	5000
τ_g^{c}	Thermal cooling constant (h)	8
$c_g^{\text{shut,fixed}}$	Fixed shut-down cost (£)	25000
F_g^{shut}	Fuel consumption during shut-down (MWh_{th})	1250

Table D.2: Nuclear plant parameters.

CCGT plant parameters		
$P_{g,\min}$	Minimum power output (MW_e)	360
$P_{g,\max}$	Maximum power output (MW_e)	900
ρ_g^{up}	Ramp up rate (MW_e/h)	300
ρ_g^{dn}	Ramp down rate (MW_e/h)	300
α_g^{up}	Upwards ramping ratio (-)	0.33
α_g^{dn}	Downwards ramping ratio (-)	0.33
$UT_{g,\min}$	Minimum up time (h)	4
$DT_{g,\min}$	Minimum down time (h)	4
$X_{g,t}$	Initial hours (h)	+8
$c_{g,t}^{\text{fuel}}$	Cost of fuel (£/MWh_{th})	23.9
$e_g^{CO_2}$	Emission factor (tCO_2/MWh_{th})	0.2267
$c_g^{\text{O\&M}}$	Variable O&M cost (£/MWh_e)	2.5
$c_g^{\text{ramp,up}}$	Upwards ramping cost (£/MW_e)	5.0
$c_g^{\text{ramp,dn}}$	Downwards ramping cost (£/MW_e)	5.0
$c_g^{\text{start,fixed}}$	Fixed start-up cost (£)	10000
$F_g^{\text{start,cold}}$	Fuel consumption during cold start-up (MWh_{th})	1500
τ_g^{c}	Thermal cooling constant (h)	12
$c_g^{\text{shut,fixed}}$	Fixed shut-down cost (£)	2500
F_g^{shut}	Fuel consumption during shut-down (MWh_{th})	375

Table D.3: CCGT plant parameters.

OCGT plant parameters		
$P_{g,\min}$	Minimum power output (MW_e)	225
$P_{g,\max}$	Maximum power output (MW_e)	565
ρ_g^{up}	Ramp up rate (MW_e/h)	600
ρ_g^{dn}	Ramp down rate (MW_e/h)	600
α_g^{up}	Upwards ramping ratio (-)	1.06
α_g^{dn}	Downwards ramping ratio (-)	1.06
$UT_{g,\min}$	Minimum up time (h)	1
$DT_{g,\min}$	Minimum down time (h)	1
$X_{g,t}$	Initial hours (h)	-8
$c_{g,t}^{\text{fuel}}$	Cost of fuel (£/MWh_{th})	23.9
$e_g^{\text{CO}_2}$	Emission factor (tCO_2/MWh_{th})	0.2267
$c_g^{\text{O\&M}}$	Variable O&M cost (£/MWh_e)	5.0
$c_g^{\text{ramp,up}}$	Upwards ramping cost (£/MW_e)	5.0
$c_g^{\text{ramp,dn}}$	Downwards ramping cost (£/MW_e)	5.0
$c_g^{\text{start,fixed}}$	Fixed start-up cost (£)	5000
$F_g^{\text{start,cold}}$	Fuel consumption during cold start-up (MWh_{th})	400
τ_g^{c}	Thermal cooling constant (h)	24
$c_g^{\text{shut,fixed}}$	Fixed shut-down cost (£)	12500
F_g^{shut}	Fuel consumption during shut-down (MWh_{th})	100

Table D.4: OCGT plant parameters.

Post-combustion capture plant parameters		
$P_g^{\text{capt,fixed}}$	Fixed CO_2 capture plant power consumption (MW_e)	25
$Y_{g,\text{min}}^{\text{capt}}$	Minimum CO_2 capture rate (-)	0
$Y_{g,\text{max}}^{\text{capt}}$	Maximum CO_2 capture rate (-)	0.90
$q_g^{\text{capt,op}}$	Energy requirement to capture 1 tonne of CO_2 (MWh_e/tCO_2)	0.27
$c_g^{\text{O\&M,capt}}$	CO_2 capture plant variable operation and maintenance (£/tCO_2)	1.5
c^{solv}	Cost of MEA solvent (£/kg)	2.0
$c_{g,t}^{\text{trans}}$	CO_2 transport and storage (£/tCO_2)	10.0
D_g	Total solvent degradation rate (kg/tCO_2)	1.5
D_g^{th}	Solvent degradation rate caused by thermal effects (kg/tCO_2)	0.1

Table D.5: Post-combustion capture plant parameters.

Appendix E

List of symbols

E.1 List of symbols

c^{CO_2}	Cost of CO_2	(£/tCO_2)
$c^{fuel}_{g,t}$	Unit g cost of fuel at time t	(£/MWh$_{th}$)
$c^{O\&M}_{g}$	Unit g cost of variable O&M for base power plant	(£/MWh$_e$)
$c^{on,curt}$	Cost of onshore wind curtailment	(£/MWh$_e$)
$c^{of,curt}$	Cost of offshore wind curtailment	(£/MWh$_e$)
$c^{ramp,up}_{g}$	Unit g upwards ramping cost	(£/MW$_e$)
$c^{ramp,dn}_{g}$	Unit g downwards ramping cost	(£/MW$_e$)
$c^{shut,fixed}_{g}$	Unit g fixed shut-down cost	(£)
$c^{start,fixed}_{g}$	Unit g fixed start-up cost	(£)
$C_{g,t}$	Unit g variable operating cost at time t	(£)
$C^{CO_2}_{g,t}$	Unit g CO_2 cost at time t	(£)
C^{curt}_{t}	Cost of wind curtailment at time t	(£)
$C^{fuel}_{g,t}$	Unit g fuel cost at time t	(£)
$C^{O\&M}_{g,t}$	Unit g variable O&M cost at time t	(£)
$C^{O\&M,capt}_{g,t}$	Unit g additional CO_2 variable O&M cost at time t	(£)
$C^{ramp}_{g,t}$	Unit g ramping cost at time t	(£)
$C^{shut}_{g,t}$	Unit g shut-down cost at time t	(£)
$C^{start}_{g,t}$	Unit g start-up cost at time t	(£)
$C^{solv}_{g,t}$	Unit g solvent cost at time t	(£)
$C^{trans}_{g,t}$	Unit g CO_2 transport and storage cost at time t	(£)
C^{total}	Total system costs	(£)
CF_t	Capacity factor at time t	(-)
D_g	Unit g total solvent degradation rate	(kg/tCO_2)
D^{th}_{g}	Unit g solvent degradation rate caused by thermal effects	(kg/tCO_2)
D_t	Electricity demand at time t	(MW$_e$)
$D_{t,min}$	Minimum load level at time t	(MW$_e$)
D^{ACS}_{t}	Average Cold Spell (ACS) winter peak demand at time t	(MW$_e$)
D^{net}_{t}	Net demand at time t	(MW$_e$)

D_t^{peak}	Peak demand at time t	(MW_e)
$DT_{g,\min}$	Unit g minimum down time	(h)
$DT_{g,\min}^{\text{capt}}$	Unit g CO_2 capture plant minimum down time	(h)
$e_g^{CO_2}$	Unit g fuel-specific emission factor	(tCO_2/MWh_{th})
E^{total}	Total system CO_2 emissions	(tCO_2)
$E_{g,t}$	Unit g CO_2 emissions emitted at time t	(tCO_2)
$E_{g,t}^{\text{capt}}$	Unit g CO_2 emissions captured at time t	(tCO_2)
$E_{g,t}^{\text{shut}}$	Unit g shut-down emissions at time t	(tCO_2)
$E_{g,t}^{\text{start}}$	Unit g start-up emissions at time t	(tCO_2)
$E_{s,t}$	Unit s energy stored at time t	(MWh_e)
$E_{s,\max}$	Unit s maximum energy stored	(MWh_e)
$F_{g,\max}$	Unit g maximum fuel consumption	(MW_{th})
$F_{g,\min}$	Unit g minimum fuel consumption	(MW_{th})
F_g^{shut}	Unit g fuel consumption during shut-down	(MWh_{th})
$F_g^{\text{start,cold}}$	Unit g fuel consumption during cold start-up	(MWh_{th})
$F_{g,t}$	Unit g fuel consumption at time t	(MW_{th})
$F_{g,t}^{\text{shut}}$	Unit g shut-down fuel consumption at time t	(MW_{th})
$F_{g,t}^{\text{start}}$	Unit g start-up fuel consumption at time t	(MW_{th})
g	Generating unit index	(-)
h	Thermal generation technology index	(-)
h_g^{a}	Unit g quadratic fuel consumption parameter	(MW_{th})
h_g^{b}	Unit g quadratic fuel consumption parameter	(MW_{th}/MW_e)
h_g^{c}	Unit g quadratic fuel consumption parameter	(MW_{th}/MW_e^2)
I	Turbulence intensity	(-)
k	Linear segment index	(-)
$P_{g,\max}$	Unit g maximum power output of base power plant	(MW_e)
$P_{g,\min}$	Unit g minimum power output of base power plant	(MW_e)
$P_{g,\max}^{\text{capt}}$	Unit g maximum power output of CO_2 capture plant	(MW_e)
$P_{g,\min}^{\text{capt}}$	Unit g minimum power output of CO_2 capture plant	(MW_e)
$P_{g,t}$	Unit g power output at time t	(MW_e)
$P_{g,t}^{\text{capt}}$	Unit g CO_2 capture plant power consumption at time t	(MW_e)
$P_{g,\max}^{\text{capt}}$	Unit g maximum CO_2 capture plant power consumption	(MW_e)
$P_{g,\min}^{\text{capt}}$	Unit g minimum CO_2 capture plant power consumption	(MW_e)
$P_g^{\text{capt,fixed}}$	Unit g fixed CO_2 capture plant power consumption	(MW_e)
$P_{g,t}^{\text{capt,op}}$	Unit g operating capture plant power consumption at time t	(MW_e)
$P_{g,\max}^{\text{capt,op}}$	Unit g maximum operating capture plant power consumption	(MW_e)
$P_{g,\min}^{\text{capt,op}}$	Unit g minimum operating capture plant power consumption	(MW_e)
$P_{g,t}^{\text{CCS}}$	Unit g net power output equipped with CCS at time t	(MW_e)
$P_{h,t}$	Generation technology h power output at time t	(MW_e)

$P^{\mathrm{c}}_{s,\max}$	Unit s maximum power input	($\mathrm{MW_e}$)
$P^{\mathrm{d}}_{s,\max}$	Unit s maximum power output	($\mathrm{MW_e}$)
$P^{\mathrm{c}}_{s,t}$	Unit s charging power input at time t	($\mathrm{MW_e}$)
$P^{\mathrm{d}}_{s,t}$	Unit s discharging power output at time t	($\mathrm{MW_e}$)
P_t	Power output at time t	($\mathrm{MW_e}$)
$q^{\mathrm{capt,op}}_g$	Unit g energy requirement to capture 1 tonne of $\mathrm{CO_2}$	($\mathrm{MWh_e/tCO_2}$)
$R^{\mathrm{SR,dn}}_{g,t}$	Unit g downwards spinning reserve contribution at time t	($\mathrm{MW_e}$)
$R^{\mathrm{SR,up}}_{g,t}$	Unit g upwards spinning reserve contribution at time t	($\mathrm{MW_e}$)
$R^{\mathrm{StR,dn}}_{g,t}$	Unit g downwards standing reserve contribution at time t	($\mathrm{MW_e}$)
$R^{\mathrm{StR,up}}_{g,t}$	Unit g upwards standing reserve contribution at time t	($\mathrm{MW_e}$)
R^{dn}_t	Downwards reserve requirement at time t	($\mathrm{MW_e}$)
R^{up}_t	Upwards reserve requirement at time t	($\mathrm{MW_e}$)
$R^{\mathrm{SR,dn}}_t$	Downwards reserve requirement at time t	($\mathrm{MW_e}$)
$R^{\mathrm{SR,up}}_t$	Upwards spinning reserve requirement at time t	($\mathrm{MW_e}$)
$R^{\mathrm{StR,dn}}_t$	Downwards standing reserve requirement at time t	($\mathrm{MW_e}$)
$R^{\mathrm{StR,up}}_t$	Upwards standing reserve requirement at time t	($\mathrm{MW_e}$)
s	Energy storage unit index	(-)
SD_g	Unit g shut-down time	(h)
SD^{capt}_g	Unit g $\mathrm{CO_2}$ capture plant shut-down time	(h)
SMP_t	System marginal price at time t	(£/$\mathrm{MWh_e}$)
SU_g	Unit g start-up time	(h)
SU^{capt}_g	Unit g $\mathrm{CO_2}$ capture plant start-up time	(h)
t	Time interval index	(h)
$u_{g,t}$	Unit g base power plant binary decision variable at time t	(-)
$u^{\mathrm{capt}}_{g,t}$	Unit g $\mathrm{CO_2}$ capture plant binary decision variable at time t	(-)
U_t	Wind speed at time t	(m/s)
$U^{\text{cut-in}}$	Cut-in wind speed	(m/s)
$U^{\text{cut-out}}$	Cut-out wind speed	(m/s)
U^{rated}	Rated wind speed	(m/s)
$\overline{U}$	Mean wind speed	(m/s)
$UT_{g,\min}$	Unit g minimum up time	(h)
$UT^{\mathrm{capt}}_{g,\min}$	Unit g $\mathrm{CO_2}$ capture plant minimum up time	(h)
w^{dn}_t	Price mark-down at time t	(£/$\mathrm{MWh_e}$)
w^{exp}_t	Exponential price mark-up at time t	(£/$\mathrm{MWh_e}$)
w^{hyp}_t	Hyperbolic price mark-up at time t	(£/$\mathrm{MWh_e}$)
w^{up}_t	Price mark-up at time t	(£/$\mathrm{MWh_e}$)
W_t	Wind power output at time t	($\mathrm{MW_e}$)
W^{curt}_t	Total wind power curtailed at time t	($\mathrm{MW_e}$)
W^{of}_t	Offshore wind power output at time t	($\mathrm{MW_e}$)

W_t^{on}	Onshore wind power output at time t	(MW_e)
$W_t^{\text{of,curt}}$	Offshore wind power curtailed at time t	(MW_e)
$W_t^{\text{on,curt}}$	Offshore wind power curtailed at time t	(MW_e)
$\overline{W}$	Mean wind output	(MW_e)
$X_{g,t}$	Unit g time period online(+)/offline(-) at time t	(h)
$Y_{g,t}^{\text{capt}}$	Unit g CO_2 capture rate at time t	(-)
$Y_{g,\text{max}}^{\text{capt}}$	Unit g maximum CO_2 capture rate	(-)
$Y_{g,\text{min}}^{\text{capt}}$	Unit g minimum CO_2 capture rate	(-)
$\alpha_{g,k}$	Unit g fuel consumption at zero load for linear segment k	(MW_th)
$\alpha_{g,k}^{\text{tan}}$	Unit g fuel consumption at zero load for tangent k	(MW_th)
$\beta_{g,k}$	Unit g heat rate for linear segment k	($\text{MW}_\text{th}/\text{MW}_\text{e}$)
$\beta_{g,k}^{\text{tan}}$	Unit g heat rate for tangent k	($\text{MW}_\text{th}/\text{MW}_\text{e}$)
ΔCF_t	Change in capacity factor at time t	(-)
ΔD_t	Change in demand at time t	(MW_e)
ΔD_t^{net}	Change in net demand at time t	(MW_e)
ΔE_t	Change in CO_2 emissions at time t	(tCO_2)
$\Delta P_{g,t}$	Unit g change in power output at time t	(MW_e)
Δt	Time interval	(h)
ΔW_t	Change in wind power output at time t	(MW_e)
$\eta_{g,t}$	Unit g real-time efficiency at time t	($\text{MW}_\text{e}/\text{MW}_\text{th}$)
η_s^{c}	Unit s charging efficiency	(-)
η_s^{d}	Unit s discharging efficiency	(-)
η_s^{rt}	Unit s round-trip efficiency at time t	(-)
μ_t^{dn}	Downwards reserve for largest credible loss in demand	(MW_e)
μ_t^{up}	Upwards reserve for largest credible loss in generation	(MW_e)
π_t	Electricity price at time t	(£/MWh_e)
Π_s	Unit s profit	(£)
$\Pi_{g,t}$	Unit g profit at time t	(£)
ρ_g^{dn}	Unit g ramp down rate	(MW_e/h)
ρ_g^{up}	Unit g ramp up rate	(MW_e/h)
$\rho_g^{\text{capt,dn}}$	Unit g CO_2 capture plant ramp down rate	(MW_e/h)
$\rho_g^{\text{capt,up}}$	Unit g CO_2 capture plant ramp up rate	(MW_e/h)
σ_U	Standard deviation in the horizontal wind speed	(m/s)
τ_g^{c}	Unit g thermal cooling constant	(h)
τ_s^{e}	Unit s rate of leakage	(% per hour)

Table E.1: List of symbols.